

Reactivities of biologically active small molecules:
Kinetic assessment of electrophilic enones and characterization of
a photoactive phosphoantigen probe



Zur Erlangung des
DOKTORGRADES DER NATURWISSENSCHAFTEN
(Dr. rer. nat.)
der Fakultät für Chemie und Pharmazie
der Universität Regensburg

DISSERTATION

vorgelegt von Monika Enzinger
aus Regensburg
Mai 2019

Die vorliegende Arbeit wurde unter der Leitung von PD Dr. Sabine Amslinger in der Zeit von November 2014 bis April 2019 angefertigt.

Promotionsgesuch eingereicht am: 03.05.2019

Eidesstattliche Erklärung

Ich erkläre hiermit an Eides statt, dass ich die vorliegende Arbeit ohne unzulässige Hilfe Dritter und ohne Benutzung anderer als der angegebenen Hilfsmittel angefertigt habe. Die aus anderen Quellen direkt oder indirekt übernommenen Daten und Konzepte sind unter Angabe des Literaturzitats gekennzeichnet.

Monika Enzinger

Content

ABBREVIATIONS	VI
A ELECTROPHILES OF THE ENONE-TYPE AND THE INVESTIGATION OF THEIR REACTIVITY AND BIOLOGICAL ACTIVITY	1
A 1 Introduction	1
A 1.1 Signal transduction pathways and their role in inflammation	1
A 1.2 Enones as electrophilic, covalently binding inflammation mediators	3
A 1.3 In-vitro cell assays to determine the toxicity and anti-inflammatory activity of compounds	6
A 1.4 General methodological access to kinetic measurements for the determination of the reactivity of compounds	8
A 1.5 The Kinetic Thiol Assay for electrophiles and its application in the determination of the reactivity of chalcone derivatives	10
A 1.6 α -X-Hydroxychalcones (α -X-HCs)	14
A 1.7 Synthesis of oxadiazoline enones (OXEs): a library of new electrophilic substances with an enone unit	16
A 1.8 Synthesis of further electrophiles in the Amslinger work group	22
A 1.9 Further development of the kinetic thiol assay towards the investigation of colorless electrophiles	25
A 1.10 Aim of the present work	29
A 2 Results and Discussion I: Synthesis, kinetic and biological evaluation of oxadiazoline enones (OXEs): a library of new anti-inflammatory electrophilic compounds	31
A 2.1 Synthesis	32
A 2.2 UV-Vis spectral properties of OXEs and OXE analogues	37
A 2.3 Kinetic evaluation of OXE and OXE analogues	40
A 2.4 Biological evaluation of the OXE and OXE analogues substance library	56
A 3 Results and Discussion II: Reactivity assessment of further electrophiles by the kinetic thiol assay	63
A 3.1 Reactivity modification of phenylacrylamide derivatives as reactive units in drug development	63
A 3.2 Juglone and juglone derivatives and their reactivity towards cysteamine	66
A 3.3 α -Nitro-hydroxychalcone (α -NO ₂ -HC) as part of the α -X-hydroxychalcone (α -X-HC) substance library	75
A 4 Results and Discussion III: Investigations for a further development of the kinetic thiol assay towards the use of colorless enones as test substances	79
A 4.1 Syntheses	79
A 4.2 Fluorescence investigations of Michael addition reactions	85
A 5 Summary of Chapter A	88
A 6 Experimental	90
	IV

A 6.1	General synthesis information	90
A 6.2	Syntheses of OXEs, OXE analogues and their precursors	90
A 6.3	Synthesis of NO ₂ -flavanone and precursors	99
A 6.4	Synthesis of fluorescent aromatic thiol dyes	102
A 6.5	Kinetic evaluation of electrophiles	108
A 6.6	In-vitro cell assays	111
 B CHARACTERIZATION OF A NEW PHOTOACTIVE PROTEIN PROBE FOR THE LABELING OF BTN3A4		 113
B 1	Introduction	113
B 1.1	The immune modulator role of HMBPP	113
B 1.2	BioBP-HMBPP as a new photoactive protein probe for the labeling of BTN3A4	115
B 1.3	Aim of this work	116
B 2	Results and Discussion	117
B 2.1	Photochemical and UV-Vis evaluation, handling of proteins and probe solutions	117
B 2.2	Stimulation of $\gamma\delta$ T cells by BioBP-HMBPP (103)	120
B 2.3	Labeling of the B30.2 domain of the protein BTN3A1 by BioBP-HMBPP (103) in the absence and presence of HMBPP (102)	123
B 2.4	Labeling of a BTN3A1-B30.2 charge transfer mutant	128
B 2.5	Determination of labeling efficiency by BioBP-HMBPP	129
B 3	Summary of Chapter B	130
B 4	Experimental	131
B 4.1	General information	131
B 4.2	Photochemical labeling of proteins with BioBP-HMBPP and Western Blot analysis of biotinylated proteins	131
C	LITERATURE	133
D	APPENDIX	139
D 1	NMR spectra of synthesized compounds	139
D 2	Pre-kinetic UV-Vis spectra of OXEs	162
D 3	Additional figures for the kinetic evaluation of OXEs and OXE analogues	167
D 4	LC-MS data of juglone derivatives in kinetic assay buffer	177
D 5	Additional figures for protein labeling experiments	190
D 6	PhD thesis figures	Fehler! Textmarke nicht definiert.

Abbreviations

15d-PGJ2	15-Deoxy- Δ 12,14-prostaglandine J2
A	Absorbance
α -X-TMC	α -X-Substituted 2',3,4',4-tetramethoxychalcones
α -X-HC	α -X-Substituted 2'-hydroxy, 3,4',4-trimethoxychalcones
B30.2	Domain of the protein BTN3A1
BioBP-HMBPP	Biotin-Benzophenone-HMBPP
BP-HMBPP	(<i>E</i>)-4-((4-Benzoyl-benzoyl)oxy)-3-methylbut-2-en-1-yl diphosphate, Benzo-Phenone-HMBPP
BSA	Bovine serum albumin
BTN3A1	Butyrophilin 3A1
CPS	Counts per second
c	Concentration [mol/l], [M]
CD69	Cluster of differentiation 69
CDCl ₃	Deuterated chloroform
COX-2	Cyclooxygenase 2
CuI3	Cullin 3
δ	Chemical shift
DCM	Dichloromethane
DCY	Dansyl cysteamine
DCYA	Dansyl cysteamine assay
DIPEA	Diisopropylethylamine
DMAPP	Dimethylallyl diphosphate (formerly: pyrophosphate)
DMF	Dimethylformamide
DMSO/DMSO-d ₆	Dimethyl sulfoxide/deuterated dimethyl sulfoxide
DOXP	1-Deoxy-D-xylulose 5-phosphate
E	Electrophile
EC ₅₀	Effective concentration
EGFR	Epidermal growth factor receptor
EDTA	Ethylendiamintetraacetic acid
EG	Ethylene glycol
EGF	Epidermal growth factor
EI-MS	Electron impact mass spectrometry
ESI-MS	Electrospray ionization mass spectrometry
EtOAc	Ethyl acetate
EtOH	Ethanol
eq.	Equivalents

FITR	Fourier-transform infrared spectroscopy
FPPS	Farnesyl diphosphate synthase
GSH	Glutathione
HEPES	4-(2-Hydroxyethyl)-1-piperazineethanesulfonic acid
HMBPP	(<i>E</i>)-4-Hydroxy-3-methylbut-2-enyl diphosphate
HO-1	Heme oxygenase 1
HOAc	Acetic acid
HRPO	Horseradish peroxidase
HTS	High throughput screening
HV	High vacuum
Hz	Hertz
I κ B α	Inhibitory κ B-protein α
IC ₅₀ /IC ₂₀	Inhibitory concentration
IKK	Inhibitory κ B-protein kinase
IL	Interleukin
iNOS	Inducible NO-Synthase
IPP	Isopentenyl diphosphate
IR	Infrared
k	Reaction rate constant
Keap1	Kelch-like ECH-associated protein 1
λ	Wavelength
LC-MS	Liquid chromatography Mass spectrometry
LPS	Lipopolysaccharide
LR-MS	Low-resolution Mass spectrometry
M	Molar mass [g/mol]
[value] M	Concentration [mol/l]
<i>m/z</i>	Mass per charge number
mCPBA	Metachloroperbenzoic acid
Me	Methyl
MeO	Methoxy
MeOH	Methanol
MS	Mass spectrometry
MSTI	(<i>E</i>)-2-(4-Mercaptostyryl)-1,3,3-trimethyl-3 <i>H</i> -indol-1-ium iodide
MTT	3-(4,5-Dimethylthiazol-2-yl)-2,5-diphenyltetrazolium bromide
NBD	7-Nitrobenzo[c][1,2,5]-oxadiazol-4-thiol
<i>n</i> -BuLi	<i>n</i> -Buthyllithium

NED	<i>N</i> -(1-Naphthyl)ethylenediamine
NF- κ B	Nuclear factor kappa-light-chain-enhancer of activated B cells
nm	Nanometer
NMR	Nuclear magnetic resonance-spectroscopy
Nrf2	Nuclear factor-erythroid-2-related factor
NOS	NO-synthase
OXAc	Acyl-substituted oxadiazoline
OXCE	Oxadiazoline cyclohexane enone
OXE	Oxadiazoline enone
OXEp	Oxadiazoline epoxide
OXTE	Oxadiazol thioester
PAg	Phosphoantigen
PBMCs	Peripheral blood mononuclear cells
PBS	Phosphate-buffered saline
<i>p</i> -BZ-C-C5-OPP	(<i>E</i>)-4-((4-Benzoyl-benzoyl)oxy)-3-methylbut-2-en-1-yl diphosphate
Ponceau S	3-Hydroxy-4-(2-sulfo-4-[4-sulfophenylazo]phenylazo)-2,7-naphthalenedisulfonic acid sodium salt
PP	Diphosphate
ppm	Parts per million
PVDF	Polyvinylidene difluoride
R _f	Retention factor
RPMI medium	Roswell Park Memorial Institute medium
rt	Room temperature
SD	Standard deviation
SDS-PAGE	Sodium dodecyl sulfate polyacrylamide gel electrophoresis
T cell	Thymus-derived lymphocyte
TBS-T	Tris-buffered saline with 0.1% Tween
TCR	T cell receptor
TFA	Trifluoroacetic acid
TLC	Thin layer chromatography
TMC	Tetramethoxychalcone
TNF	Tumor necrosis factor
Tris-HCl	Tris(hydroxymethyl)aminomethane
UV-VIS	Ultraviolet-visible-light-spectroscopy
v	Reaction rate

A Electrophiles of the enone-type and the investigation of their reactivity and biological activity

A 1 Introduction

A 1.1 Signal transduction pathways and their role in inflammation

The biochemical reaction of organisms to external stimuli of all kinds is controlled by a complex signal transduction network in which biomolecules interact extra- and intracellularly. If a cell is activated from the outside by the binding of a signal molecule to a membrane receptor, this is the beginning of a multitude of possible intracellular information transmission pathways. Numerous proteins regulate gene expression and subsequent production of proteins and enzymes via signaling cascades (Figure 1).

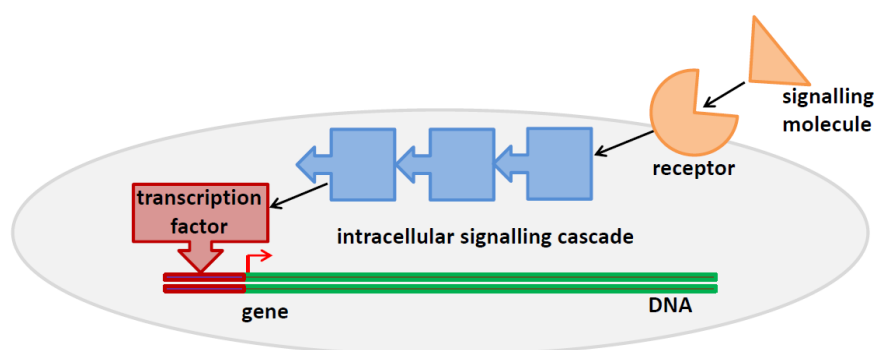


Figure 1: Principle of intracellular signal cascades under the influence of external stimuli.

Inflammation is a well-studied biochemical process as it is the cause and/or symptom of many diseases. Various signal transduction pathways have been identified as mechanisms for the development of inflammation, for example the NF- κ B pathway. NF- κ B (nuclear factor kappa-B) is a transcription factor that, when bound to its target structures on the DNA, triggers the biosynthesis of pro-inflammatory proteins^[1] such as TNF (tumor necrosis factors), COX-2 (cyclooxygenase 2) and iNOS (inducible nitrite oxide synthase). In the cytosol, NF- κ B is present in its inactive form, bound to the inhibitor protein I κ B α (inhibitory κ B protein α). External stimuli activate protein kinases such as IKK (inhibitory κ B protein kinase) that phosphorylate the inhibitor protein, which leads to its ubiquitination and degradation and activates NF- κ B by release (Figure 2).^[2]

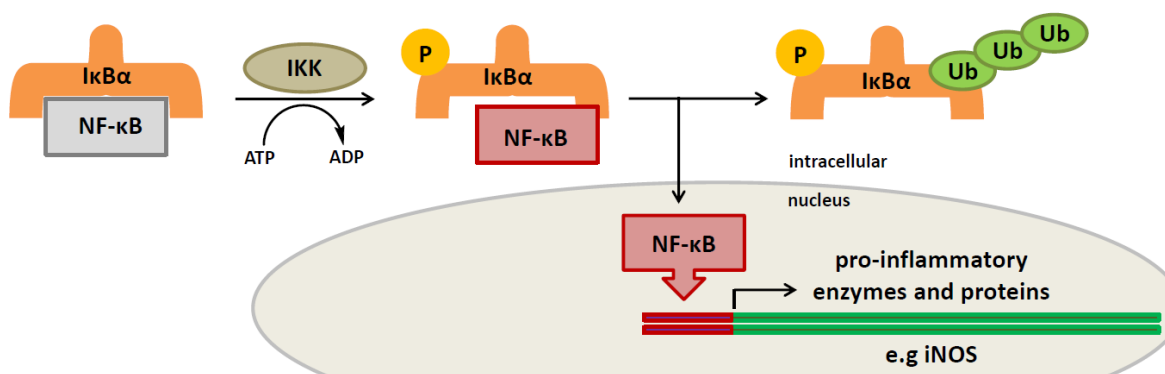
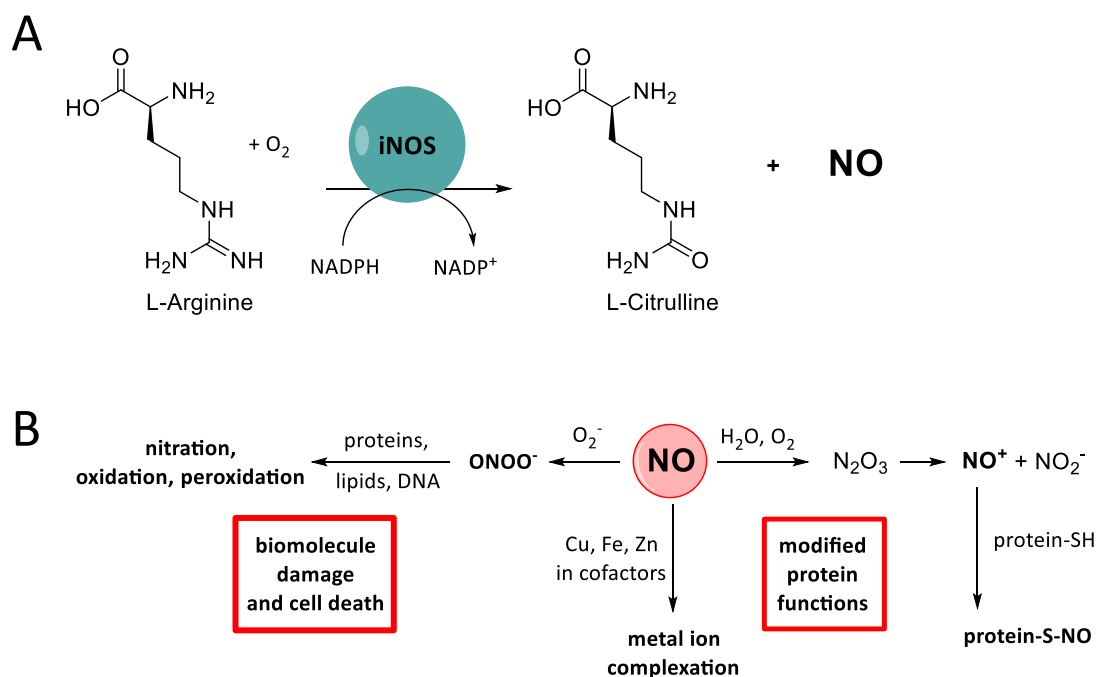


Figure 2: Schematic mechanism of the NF- κ B signal transduction pathway. NF- κ B: nuclear factor kappa B, IKK: I κ B kinase, I κ B α : kappa-B inhibitor, Ub-Ub-Ub: ubiquitination, iNOS: inducible NO synthase.

One of the pro-inflammatory enzymes produced by the influence of NF- κ B is iNOS. This enzyme is one of three NOS isoforms, heme dioxygenases that cause the conversion of L-arginine to citrulline and the gaseous signaling molecule nitric oxide, NO^[3] (see Scheme 1A). NO in general has multiple functions in the human body, depending on its concentration and the tissue of release. For example, in the neural system and in endothelia it is synthesized by nNOS (neuronal NOS) and eNOS (endothelial NOS), respectively, and acts as a neurotransmitter, causing for example vaso- and bronchodilatation in the latter. These functions are regulated in such way that NO is present in low concentrations and its activity is short-lasting.^[4]

However, this is different in iNOS-containing cells. iNOS is found in the cytosol of macrophages^[5] in a basic amount, but its synthesis is up-regulated by external stimuli such as bacterial lipopolysaccharides (LPS) or pro-inflammatory cytokines (e.g. TNF and interleukins, ILs) in inflamed tissues, tumor tissue or by microbial infections via the NF- κ B pathway as described in Figure 2. Here, NO acts as an important mediator of inflammation and un-specific immune response by different mechanisms of action, depending on its chemical form, summarized in Scheme 1B.^[4] NO can directly act as ligand to metal ions in cofactors, such as iron in heme proteins, and coordination leads to increased activation or inhibition of those enzymes. Furthermore, NO is oxidized by oxygen O₂ to NO⁺, the nitrosyl cation, which is able to react with nucleophiles in amino acid residues of enzymes, transcription factors and ion channels. In fact this leads to the nitrosylation of cysteine thiols, which modifies the activity of these proteins.^[6] Then, NO reacts also very quickly with the superoxide radical anion O₂⁻, which leads to the formation of ONOO⁻, peroxonitrite. This high-potency cellular toxin performs nitration and oxidation in biomolecules, leading to protein de-functionalization, DNA damage and strand breaks^[7] or peroxidation of lipids^[8] and causing overall necrosis and apoptosis.^[9]



Scheme 1: **A:** Biosynthesis of NO by iNOS; **B:** effects of NO towards biomolecules in immune response and as a trigger of inflammation.

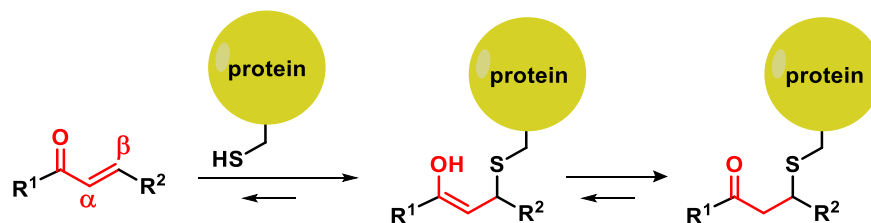
Based on these descriptions, one can imagine that, despite the positive role of NO in the fight against infections and tumors, uncontrolled overexpression of iNOS and subsequent increased NO synthesis also damages healthy cells, leading to several diseases described as NO-induced via the NF- κ B pathway.^{[10] [11]} Asthma, arthritis and various forms of bowel diseases (intestinal inflammation) are amongst them. These pathological mechanisms raise the question which biochemical measures can be taken to intervene in the development of inflammation. If these biochemical connections are known, the course of associated diseases can be influenced.

A 1.2 Enones as electrophilic, covalently binding inflammation mediators

For pharmacologically active substances it is possible to intervene at certain points of signal transduction by covalent or non-covalent binding. If these biologically active compounds are electrophiles, covalent binding plays a particularly important role as they can react with biomolecular nucleophiles. These interactions can for example influence the activity of proteins in general and enzymes in particular, leading to a positive influence on many diseases. This has been well investigated and proven for a large number of biologically active electrophilic natural compounds of various chemical structures and target proteins.^[12]

Cysteine residues on the surface of proteins are an important target. The nucleophilic properties of their terminal thiol group (sulfhydryl group) enable them to form covalent bonds

with electrophilic compounds. Organic molecules that have a carbonyl function in the immediate vicinity of a carbon-carbon double bond (α,β -unsaturated carbonyl function) are such electrophiles and are called enones or Michael acceptors. Depending on their reactivity, they can react on their electrophilic β -position with thiol groups in a Michael addition^[13] (Scheme 2), the organic reaction type first described by Arthur Michael.^[14]



Scheme 2: Michael addition of a pharmacologically active α,β -unsaturated carbonyl compound (enone, Michael acceptor) to the thiol group of a cysteine in a protein.

Enones can be divided into different substance classes due to their different structure and/or function.^[12, 15] Some natural products are given as examples in Figure 3.

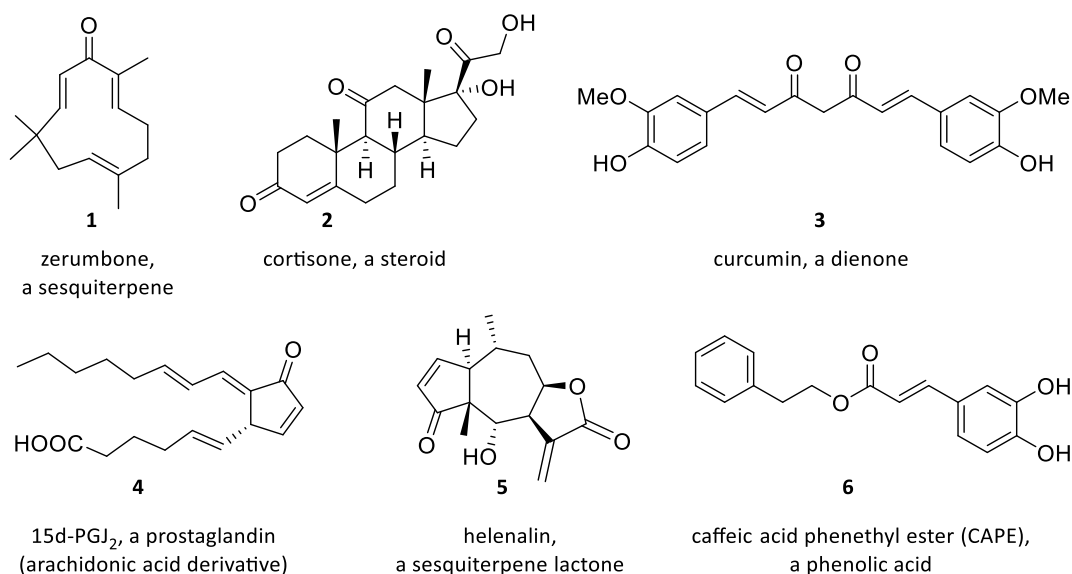


Figure 3: Examples of natural products with α,β -unsaturated carbonyl function.^[12, 15]

In the literature, anti-inflammatory, antimicrobial, neuroprotective and antiproliferative properties based on their Michael acceptor activity are described for some of these compounds.^[13, 15-16] However, depending on their structure, other chemical properties of the substances, radical scavenging properties, isomerization at the double bond or oxidation and reduction can also be the reason for their biological activity.^[13]

The mechanism of the anti-inflammatory effect of electrophiles and enones in particular by reacting with surface thiols of proteins can be explained by two major signaling pathways. On the one hand, they can inhibit the NF- κ B signal transduction pathway at multiple

points. As shown in Figure 4A, enones can react with surface thiols of IKK, I κ B α or NF- κ B itself. This causes protein alkylation, which inactivates them. Thus, the transcription of pro-inflammatory genes is inhibited by direct deactivation or prevention of activation of NF- κ B.^[2] Some natural products such as polyphenols and terpenes are NF- κ B inhibitors,^[17] for example curcumin (**1**, Figure 3) from *Curcuma longa*, CAPE (**6**) from *Apis mellifera* or gallo-catechins from *Camellia sinensis*, just to name a few. On the other hand, enone electrophiles can trigger the synthesis of anti-inflammatory enzymes by activating the Nrf2 pathway (Figure 4B). Nrf2 (nuclear factor-erythroid-2-related factor) is a transcription factor, which is inactive by the binding to a complex of the two inhibitor proteins Keap1 (Kelch-like ECH-associated protein 1) and Cul3 (cullin 3). More precisely, Keap1 and Cul3 binding leads to ubiquitination and degradation of Nrf2. If cysteines of Keap1 are oxidized to disulfides or alkylated by electrophiles, Nrf2 is released and activated.^[18] By binding to its DNA targets, Nrf2 triggers an increased synthesis of anti-inflammatory proteins, including heme oxygenase 1 (HO-1).^[19] Various enones have been described to inactivate Keap1 by Michael addition on surface thiols.^[20]

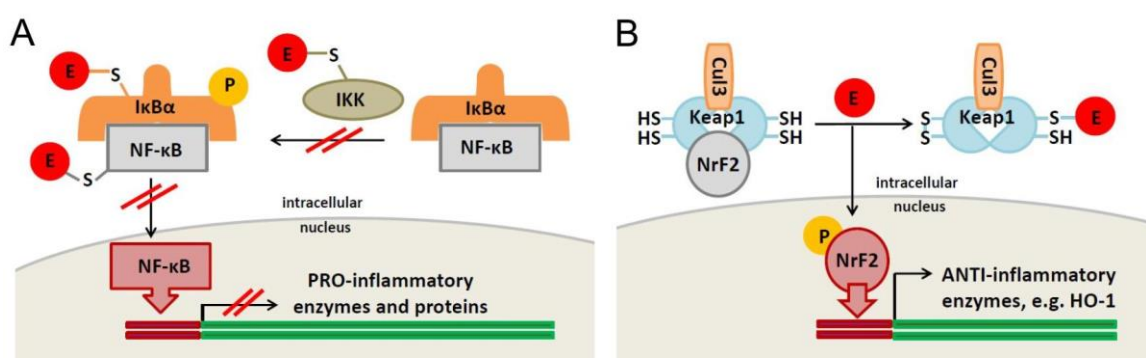
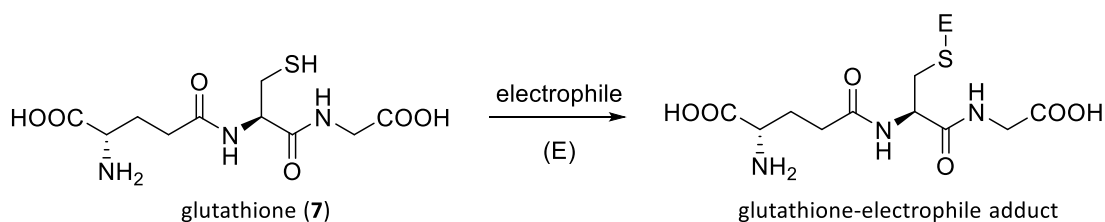


Figure 4: Mechanisms of the anti-inflammatory activity of α,β -unsaturated carbonyl compounds. **A:** Inhibition of the NF- κ B pathway. E: enone, NF- κ B: nuclear factor kappa B, IKK: I κ B kinase, I κ B α : kappa B inhibitor. **B:** Mechanism of the Keap1-Nrf2 signal transduction pathway. E: enone, Keap1: Kelch-like ECH-associated protein 1, Cul3: cullin 3, Nrf2: nuclear factor-erythroid-2-related factor 2, HO-1: heme oxygenase 1.

Thus, all natural substances, but also synthetically altered derivatives and completely synthetically produced substances with α,β -unsaturated carbonyl functions possess the potential to have an anti-inflammatory effect. However, in the search for new drugs from nature or in synthetic drug development, the therapeutic index (or ratio) that describes the relationship between efficiency and toxicity must always be taken into account. Electrophilic active substances in particular are known for causing toxicity besides their pharmacological potency.^[21] This is due to their more or less high reactivity at the electrophilic site, with which they can also bind to non-target biomolecules in a non-specific way. As a countermeasure, cells have developed detoxification systems that can mitigate or eliminate toxic effects of highly reactive substances. Electrophiles in particular can react with the

cellular detoxification agent glutathione (GSH, **7**, Scheme 3), which is intracellularly present in high concentration (1-10 mM^[22]). GSH is a tripeptide with a cysteine thiol functionality that is reactive towards electrophilic carbons of cell toxins.^[23]



Scheme 3: Structure of glutathione (**7**) and its reaction with electrophiles (E).

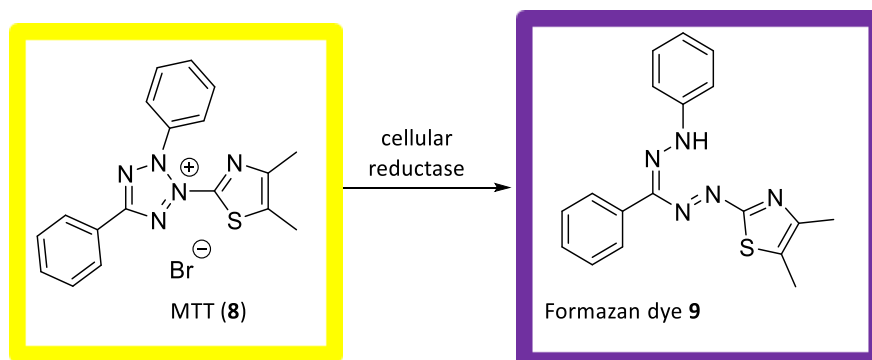
In order to face the problem of the right balance between activity and toxicity, synthetic-organic drug research often uses substance libraries, which are identical in essential structural elements, but whose properties can be modulated by further building blocks and/or substituents of different kinds. Since the intensity of the biological effect also depends on the reactivity of enones at the β -position of their double bond, reactivity and reaction rate play an important role in these investigations. By combining a pharmacologically active core structure with reactivity-varying substituents and building blocks, it is possible to fine-tune the reactivity and therefore also influence biological activity and selectivity. Furthermore, determining the reactivity of new electrophiles can be a tool in the search for new potential pharmacological agents.

A 1.3 In-vitro cell assays to determine the toxicity and anti-inflammatory activity of compounds

Cell viability

The standard procedure performed in in-vitro assays is the following: first, the cell toxicity of substances has to be evaluated in a cell viability assay. Toxicity is characterized by IC values (inhibitory concentration) expressing the percentage of non-surviving cells after incubation with the corresponding concentration of the test compound. Most important are the IC₅₀, which is the general value for the toxicity of the test substance, and the IC₂₀, the so-called toxicity limit. With >80% cell survival rate, the latter concentrations of test compounds are generally considered as non-toxic for the specific cell line and are used in follow-up activity assays. In this work, the so-called MTT cell viability assay^[24] was performed to determine the toxicity of substances. This is a quantitative, colorimetric assay in 96 well plate format, which was performed on the murine macrophages cell line RAW264.7. After the incubation of cells together with the test compounds at physiological conditions, MTT

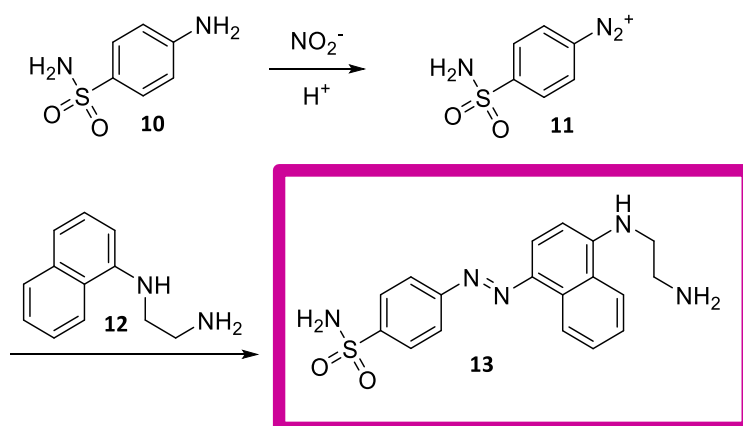
(3-(4,5-dimethylthiazol-2-yl)-2,5-diphenyl-tetrazolium bromide, **8**) is added. Only living cells with active metabolism are able to reduce this yellow tetrazolium salt to the purple formazan dye **9** (Scheme 4). The absorbance of **9** can be measured by UV-Vis spectroscopy at 560 nm and is a direct measure for the percentage of surviving cells.



Scheme 4: Colorimetric reaction of MTT (**8**) to the formazan dye **9** in the MTT cell viability assay.

Anti-inflammatory activity

After non-toxic concentrations are determined, the main activity assay can be performed. In this work, the anti-inflammatory activity of the test substances is determined by their ability to suppress the NO synthesis caused by an iNOS up-regulation as described in chapter A 1.1. Murine RAW264.7 macrophages are used due to their ability to synthesize iNOS. LPS is added to induce inflammation in the cells, which are incubated together with the test compounds. The resulting NO, quickly transformed into NO_2^- (**Scheme 1**), is detected in the cell culture medium by the colorimetric Griess reaction (Scheme 5).



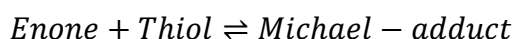
Scheme 5: Colorimetric reaction in the iNOS assay to detect NO via diazotation and coupling to a diazo dye.

Under acidic conditions, sulfanilamide (**10**) reacts with NO_2^- by diazotation to the diazonium cation **11**, then couples to *N*-(1-naphthyl)ethylenediamine (**12**), which forms the pink azo dye **13**. The absorbance measured at 560 nm is inversely proportional to the inhibition of

NO production and is compared to those of cells in absence of the test compound. A high ability to inhibit NO production is thus associated with anti-inflammatory properties.^[25]

A 1.4 General methodological access to kinetic measurements for the determination of the reactivity of compounds

In chemical reactions, the reaction order describes the type and number of individual molecules that react with each other to form a certain number of product molecules. The reaction rate of the bimolecular reaction



depends linearly on the concentration of the two educts enone and thiol, which each contribute to the reaction with first order. Thus, the reaction follows a second order kinetics. Since the data for these mathematical thermae are difficult to access experimentally, kinetics research often uses the simplification of pseudo-first order kinetics. The principle is the presence of one reaction component in excess so that its concentration does not change significantly during reaction. The reaction rate still depends on the concentrations of both reaction partners, but the concentration of the excess component can be neglected mathematically. Experimental data of pseudo-first order reactions can be mathematically treated like those of first order reactions. In experiments, the time-dependent concentration change of the reaction participant in the low concentration is measured by monitoring the change of analytical properties, for example pressure, conductivity or spectroscopic parameters. The parameter used for the characterization of the reactivity, the reaction rate constant k , can be determined from a first order reaction with the rate law equation **(1)**, where v is the reaction rate and k is the reaction rate constant. If **(1)** is resolved, an exponential function **(2)** is obtained with $c(A)$ being the low-concentration starting material and $c(A_0)$ its initial concentration.

$$v = -\frac{dc(A)}{dt} = k * c(A) \quad (1)$$

$$c(A) = c(A_0) * e^{-kt} \quad (2)$$

After the adjusting of the reaction equilibrium, k is obtained from the slope of **(2)** after linearization or by a curve fit of **(2)** with function **(3)** alternatively.

$$A_t = A_0 - e^{-k_{obs}t+c} \quad (3)$$

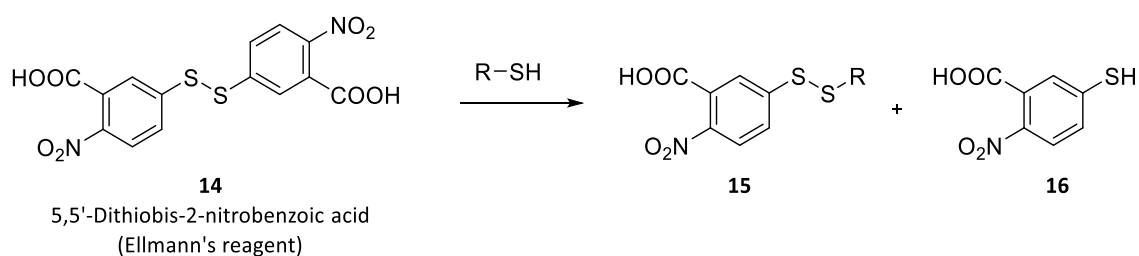
In the Arrhenius equation **(4)**

$$k = A * e^{-E_a/RT} \quad (4)$$

it becomes clear that k depends on the temperature. Therefore, in kinetic experiments, the temperature must always be taken into account and specified. Usually 25 °C is used.

There are numerous reported measurement methods to get access to the reactivity of compounds. A non-quantitative NMR assay was published in 2011 to identify which natural products with enone functionality are Michael acceptors towards cysteamine in DMSO- d_6 by observing the enone signals in the 1H NMR spectrum.^[26] Also, considering that thia-Michael additions require polar solvents, reversibility of those reactions could be investigated with a 1:20 dilution in $CDCl_3$. Another work group used LC-MS and NMR measurements to follow the reaction of various electrophiles, including enamides, towards glutathione **7** (Scheme 3) under pseudo-first order conditions.^[27] Based on the time-dependent data, the kinetic rate constants $k_{pseudo-1}$ were calculated and compared. A similar LC-MS method was developed to investigate the structure-activity-reactivity relationship of new covalent EGFR-2 inhibitors.^[28] These methods are technically relatively complex, more or less expensive and not available in every work group as they require highly developed devices. However, simple and fast methods that use spectroscopic measurements are also available.

For example, the amount of the unreacted thiol of the Michael reaction can be indirectly determined by adding Ellman's reagent (**14**) (5,5'-dithiobis-2-nitrobenzoic acid). Since the late 1950s, this method has been used for the determination of low amounts of thiols in biochemical solutions.^[29] Reagent **14** forms a mixed disulfide **15** with free or unreacted thiols R-SH, respectively, releasing **16** which is present as an anion in buffers with a pH > 7 (Scheme 6). The absorbance of **16** can be read out at 412 nm and is inversely proportional to $c(R-SH)$. For example, this method was used under second order conditions to establish the reactivity-bioactivity relationship for a set of Nrf2 inhibitors^[30] or to compare predicted kinetic data with experimental data of GSH (**7**) to Michael-type acceptors.^[31]



Scheme 6: Principle of the determination of free thiols by the use of Ellmann's reagent.

Even simpler is the direct and permanent monitoring by the absorbance decrease of the test compounds during the reaction. This technique was used for example by Dinkova-

Kostova et al to determine k_2 rate constants under pseudo-first order conditions for the reaction of electrophiles to various simple thiols, including GSH and mercaptoethanol, in a mixture of Tris-HCl buffer pH 7.4 and acetonitrile.^[32]

In this specific project, chalcone derivatives were the compounds of interest. Their reactivity and anti-inflammatory activity were determined and evaluated. A new easy-to-use 96-well UV-Vis assay has been tailored to the new class of compounds by adapting and optimizing the solvent system and measurement conditions.

A 1.5 The Kinetic Thiol Assay for electrophiles and its application in the determination of the reactivity of chalcone derivatives

Chalcones are aromatic compounds with two aromatic units A and B, which are connected via an α,β -unsaturated carbonyl unit and belong to the natural compounds class of flavonoids. Due to their electrophilic nature, they possess anti-inflammatory and anticarcinogenic properties, among others, by alkylation and inhibition of proteins involved in the NF- κ B pathway.^[33] The unsubstituted chalcone diphenyl-prop-2-ene-1-one (**17**, Figure 5) has numerous hydroxy-, alkoxy and glycosyl derivatives, which occur in a great variety of plants, fruits and vegetables as well as spices.^[33] These are also biosynthetic precursors of flavanones and other cyclic flavonoids.^[34] One project already published concerning electrophiles of the enone-type in the working group Amslinger was the synthesis, characterization and reactivity evaluation of chalcones and their fully synthetic derivatives as depicted in Figure 5.^[35] ^[36]

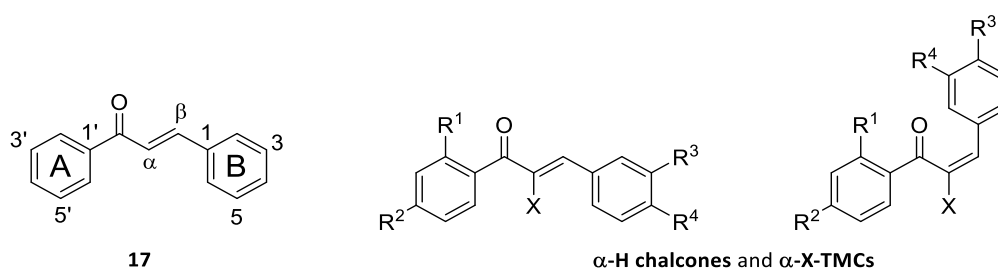


Figure 5: Basic structure chalcone **7** and synthetically varied derivatives studied in the work group of PD Dr. Sabine Amslinger. $\alpha\text{-X-TMCs}$: $R^{1,2,3,4} = \text{OCH}_3$; $X = \text{H, CH}_3, \text{CF}_3, \text{CN, NO}_2, \text{COOH, COOEt, F, Cl, Br, I, Ph, } p\text{-H}_3\text{CO-Ar, } p\text{-NO}_2\text{-Ar}$; $\alpha\text{-H chalcone derivatives}$: $R^{1,2,3,4} = \text{OH, OCH}_3, \text{OiPr}$; $X = \text{H}$. Members of the work group of PD Dr. Sabine Amslinger contributing to this project were: Nafisah Al-Rifai (PhD thesis, 2013) and Hannelore Rucker (PhD thesis, 2014).

Substituents were introduced to the aromatic rings (hydroxy and alkoxy groups, $\alpha\text{-H chalcones}$ ^[35]) and moreover the enone α -position of tetramethoxychalcone was varied with electron-withdrawing and electron-pushing functional groups X ($\alpha\text{-X-tetramethoxychalcones}$, $\alpha\text{-X-TMCs}$) to investigate their influence on the electrophilicity.^[36] In order to

estimate the reactivity of chalcones with regard to their electrophilicity at the β position of their enone system towards thiol nucleophiles, a kinetic assay using UV-Vis detection in 96 well plate format was developed.^[35] In this assay, cysteamine (**18**, Figure 6) is used as model compound, imitating cysteine residues in biomolecules. The reaction with cysteamine interrupts the chalcone chromophore between 300 and 450 nm and the yellow absorbance band disappears in the spectrum. This absorbance decrease is recorded time-dependently at a suitable wavelength whereby the decreasing exponential functions (**2**) are obtained. Figure 6 shows as example the absorbance spectra of α -H-tetramethoxychalcone (α -H-TMC) measured at ten-minute intervals after addition of a 60-fold excess of cysteamine as well as the kinetic absorbance decrease obtained.

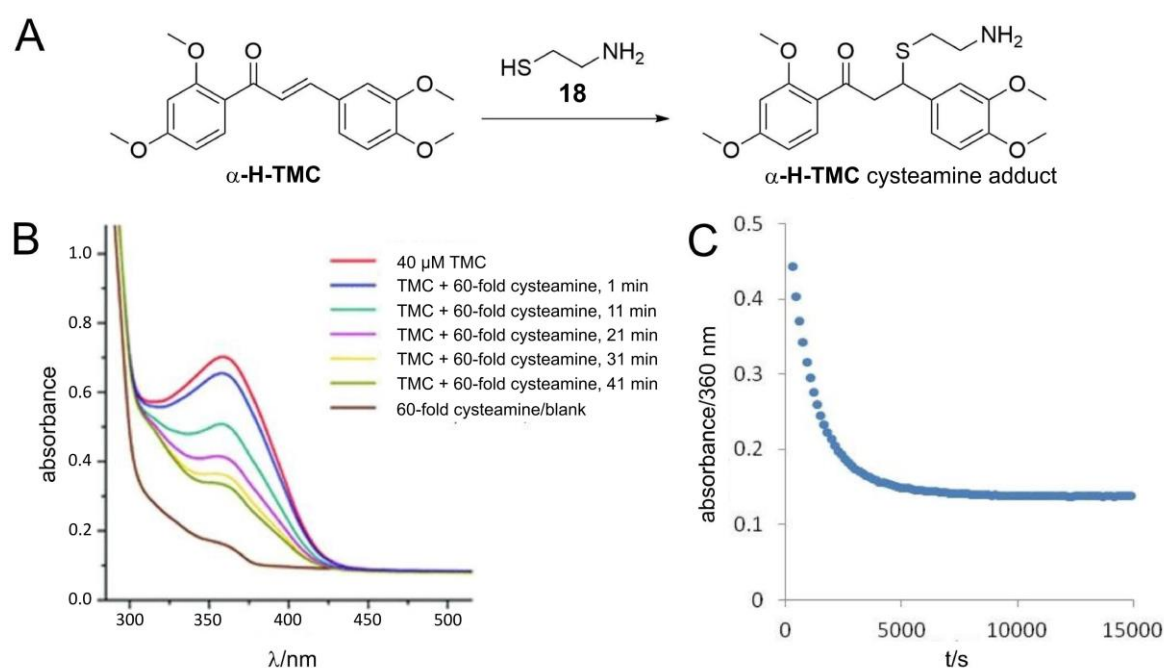


Figure 6: Principle of the kinetic thiol assay for the Michael addition of cysteamine to chalcones using the example of α -H-TMC. **A:** Reaction equation; **B:** Time-dependent UV-Vis spectra with and without cysteamine at 25 °C; **C:** Kinetic progress of the reaction with 60-fold thiol, measurement at 360 nm.^[35]

This reaction follows a second order kinetic with the rate constant k_2 (**5**).

$$-\frac{dc(\text{chalcone})}{dt} = k_2 * c(\text{chalcone}) * c(\text{cysteamine}) \quad (5)$$

Due to the excess of cysteamine, a reaction kinetics of pseudo-first order with k_{obs} as pseudo-first order rate constant can be assumed (**6**), (**7**).

$$\begin{aligned} c(\text{cysteamine}) &\gg c(\text{chalcone}) \\ \rightarrow c(\text{cysteamine}) &= \text{const.} = c(\text{cysteamine})_0 \end{aligned} \quad (6)$$

$$-\frac{dc(\text{chalcone})}{dt} = k_2 * c(\text{cysteamine})$$

$$-\frac{dc(\text{chalcone})}{dt} = k_{obs} * c(\text{chalcone}) \quad (7)$$

The obtained e-functions are mathematically fitted with the program Origin according to a decreasing first order exponential function, thus eliminating the need for linearization. From these mathematical equations (**3**) the k_{obs} values for all thiol concentrations can be read out. It must be considered that Michael additions are reversible, thus equilibrium reactions and therefore the reaction must be monitored until the equilibrium is achieved. The excess cysteamine concentration determines the associated k_{obs} value, the reaction rate for each cysteamine concentration, which describes the net effect of the forward and backward reactions. From the linear ratio of different excess thiol concentrations to their corresponding k_{obs} values k_2 , the desired rate constant of the reaction is obtained (**8**).

$$k_{obs} = k_2 * c(\text{cysteamine})_0 \rightarrow k_2 = \frac{k_{obs}}{c(\text{cysteamine})_0} \quad (8)$$

A mixture of 100 mM Tris-HCl buffer with 2 mM EDTA pH 7.4 (20 %) and ethylene glycol (80 %) was optimized as the reaction medium. The neutral pH in the buffer mimics physiological conditions while ethylene glycol increases the solubility of test substances and slows the reaction rate of very fast-reacting compounds to a level observable by the user. Medium to fast, slow and very slow reacting chalcones were easily measured in 96-well microtiter plates via microplate photometer. Stopped-flow measurements were performed for very fast-reacting chalcones. This assay can be used to examine a large number of test substances to compare their reaction rates under the same conditions. The requirement is an absorption at a wavelength > 300 nm, more precisely a sufficient chromophore, which decreases during the reaction with cysteamine, but also complete solubility at test concentrations of 40-80 μM . Wavelengths < 300 nm are not suitable for measurement due to the self-absorption of the assay material (buffer, 96-well plate, cover foil). In **α -H-chalcones**, k_2 values of 0.103 to 5.08 $\text{M}^{-1}\text{s}^{-1}$ were obtained under these conditions. In addition, relationships between the substituents on both aromatic rings and the reactivity of the corresponding compounds could be detected.^[35]

A structure-reactivity relationship was also found for the **α -X-TMCs** since a high influence of the substituent X on the reaction rate was demonstrated.^[36] It has been shown that the more electron-withdrawing the substituent X is, the faster the reaction with cysteamine takes place. The lowest reactivity is found in **α -COOH-TMC**, which is present as an anion under assay conditions and thus increases the electron density to the detriment of a

nucleophilic attack. The k_2 range for α -X-chalcones comprises a total of more than six orders of magnitude. Furthermore, the determined reactivity of α -X-TMCs was compared to their anti-inflammatory activity concerning HO-1 activation and NO inhibition. Structure-activity relationships were established. Kinetic and biological results are summarized in Table 1.

Reactivity of α -X-TMCs correlates with their HO-1 induction properties. The stronger the reactivity determined by the thiol assay, the stronger the HO-1 induction and thus inflammation inhibition, but the cell toxicity tends to increase simultaneously. The same goes for the NO-inhibition properties that follow the same order with α -CF₃-TMC as most potent inhibitor, as it inhibits 84.6% of NO production at a very small concentration of 0.5 μ M. Two obvious exceptions are the most reactive derivatives, α -CN- and α -NO₂-TMC, in which no or only small anti-inflammatory activity and relatively low cell toxicity was detected. The electrophilic properties of these two substances are strong enough that they are most likely rapidly inactivated by the cellular detoxification agent glutathione (GSH, **7**, Scheme 3).

Table 1: Results of the reactivity of α -X-TMCs determined by the kinetic thiol assay and biological data.

α -X-TMC X =	k_2 [$M^{-1}s^{-1}$]	Toxicity limit [μ M] ^[a]	HO-1 induction	Inhibition of NO production	
				C α -X-TMC [μ M]	inhibition [%]
CN	5750 \pm 130	25	-	1	16.4 \pm 8.7
NO ₂	749 \pm 9.0	25	-	1	1.7 \pm 8.5
CF ₃	17.1 \pm 1.8	0.5	+++	0.5	84.6 \pm 8.9
Br	2.89 \pm 0.08	1	+++	1	67.4 \pm 11.7
Cl	1.65 \pm 0.021	5	+++	1	47.2 \pm 14.6
p-NO ₂ -Ar	0.293 \pm 0.025	25	++	1	1.1 \pm 9.8
I	0.282 \pm 0.015	5	++	1	22.0 \pm 12.4
COOEt	0.281 \pm 0.029	10	-	5	46.0 \pm 9.4
H	0.193 \pm 0.019	10	+	5	60.9 \pm 18.8
F	0.0168 \pm 0.00035	25	-	5	29.6 \pm 20.2
p-OMe-Ar	0.00856 \pm 0.0013	25	-	5	-2.2 \pm 4.3
Me	0.00750 \pm 0.00039	25	-	5	-34.7 \pm 15.2
Ph	0.00669 \pm 0.00029	25	-	5	9.7 \pm 12.9
COOH	0.00371 \pm 0.00006	25	-	5	-0.7 \pm 12.2

The induction of HO-1 expression in RAW 264.7 macrophages was determined by Western Blot. +++ = strong induction; ++ = medium; + = weak induction in comparison to control; - = no induction. Kinetic and biological data were measured and/or analyzed by Nafisah Al-Rifai, Hannelore Rucker, Dita Fritsch and Sabine Am-slinger.^{[35] [36] [37]}

The excellent correlation of these data shows how well a reactivity study can predict the biological activity of a substance class. Figure 7 visualizes this relationship by using the logarithmic k_2 and IC₅₀ values which give a linear correlation. With α -CF₃-TMC, an optimal reactivity/activity window was found for the α -X chalcones. However, as toxicity also increases, the question arises whether optimization within the substance class could still be

achieved. It can also be promising to test potent active substances such as chalcones for further positive cell effects. In continued research, some selected compounds have been investigated in further assays concerning cytoprotectivity with very promising results for *E*- α -*p*-OMe-Ar-TMC.^[38] A clear antiapoptotic effect was found at nontoxic concentrations.

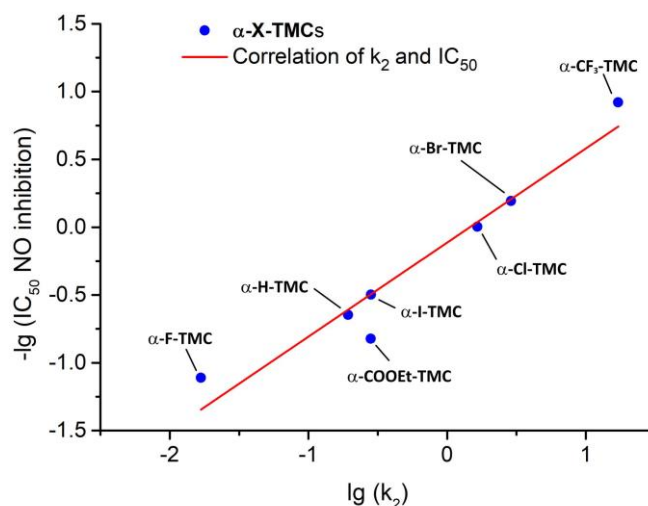


Figure 7: Correlation of the inhibition of NO production with the second-order rate constants ($\lg(k_2)$) of the Michael addition of α -X-TMCs with an anti-inflammatory activity and cysteamine. Line indicates the linear fit.

A 1.6 α -X-Hydroxychalcones (α -X-HCs)

The investigation of chalcones was further developed towards an improvement of their reactivity and biological activity. Nafisah Al-Rifai synthesized 8 substituted, methoxylated chalcones with a 2'-OH group during her PhD thesis, called α -X-hydroxychalcones, α -X-HCs (University of Regensburg, 2014, Figure 8).^[39]

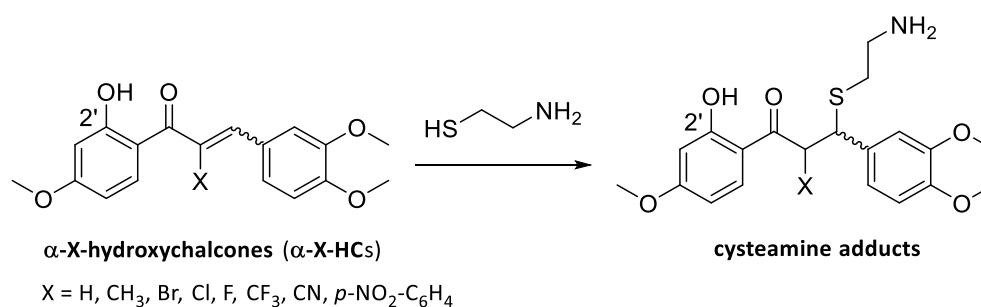


Figure 8: α -X-HCs and their cysteamine addition products. Syntheses and investigations by Nafisah Al-Rifai (Dissertation, 2015, University of Regensburg).^[39]

Due to the free 2'-OH group, an enhancement of electrophilicity in comparison to α -X-TMCs is expected, which might be beneficial also for the biological activity. Table 2 shows the summary of the kinetic and biological investigations so far. Indeed, a two- or threefold

increased reactivity of α -F-HC and α -H-HC respectively in comparison to their TMC analogues was proven.^[35] However, for all α -X-HCs a significant decrease or complete loss of toxicity and biological activity was found when compared to α -X-TMCs.

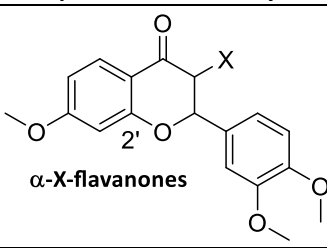
Table 2: Kinetic results and biological activities of α -X-HCs (unpublished results) compared to their corresponding α -X-TMCs.^[36]

α -X compound X =	k_2 [$M^{-1}s^{-1}$]		Cell viability IC ₅₀ [μ M]		Inhibition of NO production IC ₅₀ [μ M]	
	TMC	HC	TMC	HC	TMC	HC
CN	5750 ^[a]	n. d.	> 100	> 100	n. d.	30.8 \pm 1.2
CF ₃	17.1 ^[a]	n. d.	7.91 \pm 0.98	> 100	0.120 ^[c]	n. a.
Br	2.89 ^[a]	n. d.	9.65 \pm 1.04	43.1 \pm 6.8	0.640 ^[c]	n. a.
Cl	1.65 ^[a]	n. d.	13.1 \pm 2.4	57.0 \pm 1.8	0.992 ^[c]	31.8 \pm 7.4
<i>p</i> -NO ₂ -Ar	0.293 ^[a]	n. d.	> 100	> 100	n. d.	99.4 \pm 11.4
H	0.193 ^[b]	0.717 \pm 0.019	23.7 \pm 5.7	37.5 \pm 2.9	4.44 ^[c]	9.84 \pm 3.32
F	0.0168 ^[a]	0.0347 \pm 0.0029	> 100	52.2 \pm 7.2	12.9 ^[c]	15.8 \pm 3.0
Me	0.00750 ^[a]	n. d.	> 100	> 100	n. d.	55.0 \pm 21.3

[a]: Value taken from Al-Rifai et al.^[36]; [b]: value taken from Amslinger et al.^[35]; [c]: value taken from Rucker et al.^[37]; n. a.: not active at non-toxic concentrations; n. d.: not determined.

This effect is explained by the loss of the enone system due to the well-known cyclization to the corresponding flavanones (structure: α -X-flavanones, Table 3).^{[40] [41]} The extent of this reaction depends on various factors, including the α -X-substituent. Table 3 shows UV-Vis and LC-MS investigations of α -X-HCs under kinetic assay conditions. Indeed, flavanone formation was detected for all α -X-HCs containing an electron-withdrawing substituent X. Due to this loss of the electrophilic position, the biomolecular mechanism of action is hindered or even prevented. This applies to the substances only in aqueous medium. All compounds were isolated as chalcones after synthesis and purification.

Table 3: Results of LC-MS studies of α -X-HCs without and with 60-fold cysteamine.

α -X-HC X =	-/+ cyste- amine	Compounds detected by LC-MS		
		α -X-HC		α -X-HC-cysteamine adduct
CN ^[a, b]	-	++	+++	-
	+	-	++	++
CF ₃ ^[a, b]	-	+	++	-
	+	+	++	-
Br ^[a]	-	+	+++	-
	+	tr.	+	-

		Compounds detected by LC-MS		
Cl ^[a]	-	++	+++	-
	+	tr.	+	-
p-NO ₂ -Ar	-	+	+++	-
	+	+	+++	+
H ^[a]	-	> 95%	tr.	-
	+	+	-	+++
F ^[a]	-	> 95%	tr.	-
	+	+++	tr.	++
Me	-	> 95%	tr.	-
	+	> 95%	tr.	tr.

Reactions were carried out in 100 mM Tris-HCl buffer pH 7.4 with 2 mM EDTA/ethylene glycol 20:80 with 40 μ M of α -X-HCs and 1-2 h incubation time prior to measurement. HPLC column temperature: 40 °C. Molecular ratios were estimated by UV-Vis measurement and are assigned as follows: +++: 95-60%; ++: 60-30%; +: 30-5%; tr.: traces. [a]: Additional compounds (fragmentation and elimination products) were detected^[39]; [b]: measured directly after mixing and at 25 °C column temperature.

These results show that more aspects have to be considered when optimizing reactivity and activity, as this strategy only leads to limited success.

A 1.7 Synthesis of oxadiazoline enones (OXEs): a library of new electrophilic substances with an enone unit

The presented concept of a substance library containing a core unit, whose reactivity is influenced by variable substituents in order to optimize the biological activity, was applied in this work group to another, newly designed class of substances. The first results are taken from the doctoral thesis of Anas Rasras^[42] and the Master theses of Rainer Herzog^[43] and Lukas Wirth.^[44]

Molecule design

In the endeavor to create novel fine-tuned electrophiles, which are suitable model compounds for drug development, a new class of compounds was designed and synthesized in the work group of PD Dr. Sabine Amslinger.^[42]

It was chosen to decorate a heterocyclic system with an additional enone unit, which is able to bind covalently to pharmacological targets. Thereby it was important to use a scaffold which allows for a conjugation with the enone unit to modify its reactivity. Thus, nine classes of 3-enone-substituted 2,3-dihydro-1,3,4-oxadiazoles (**oxadiazoline enones, OXEs**) were envisioned. These molecules were composed, according to Figure 9, from three variations in the 2-position, R² - a CH₃, H or CF₃ group - together with three different enone moieties in the 3-position and variations of the aromatic group attached to the 5-position (R¹) of the oxadiazoline skeleton.

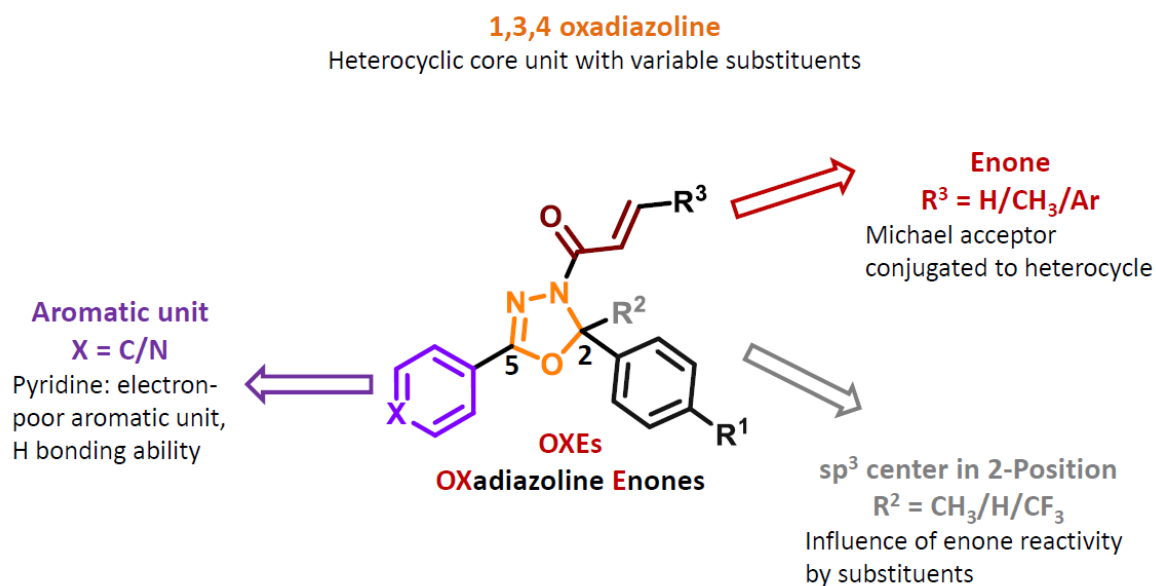


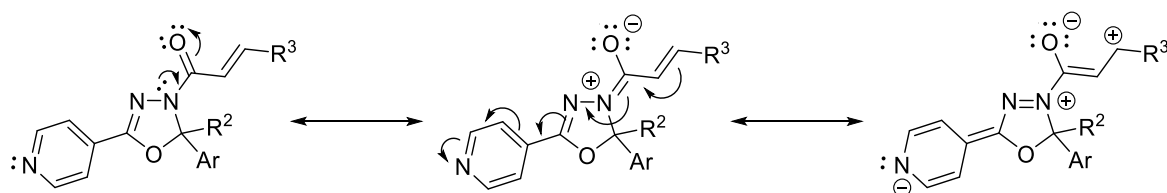
Figure 9: Design and structural features of the compound library of oxadiazoline enones (OXEs).

A combination of the two main structural features enone + R³ and substituent in 2-position (R²) leads to the nine different OXE classes named **OXE1** to **OXE9**, which are summarized in Table 4.^{[43] [44]}

Table 4: Overview and naming of nine OXE classes.

Enone + R ³	Substituent in 2-position / R ²	OXE class
acryl	CH ₃	OXE1
acryl	H	OXE2
acryl	CF ₃	OXE3
crotyl	CH ₃	OXE4
crotyl	H	OXE5
crotyl	CF ₃	OXE6
cinnamoyl	CH ₃	OXE7
cinnamoyl	H	OXE8
cinnamoyl	CF ₃	OXE9

The different substituents decorating the heterocyclic unit should influence the enone reactivity by different effects. The 2-position was chosen to potentially influence the reactivity of the enone unit by a more indirect sp³-coupled variation in the electron density. Substituted phenyls and pyridine are the selected aromatic units in the 5-position. A stronger modulation of electrophilicity was expected when the electron-poor 4-pyridyl-substituent is introduced to the 5-position. Furthermore, pyridine provides a free electron pair to interact with potential pharmacological targets via hydrogen bond. The largest effect was anticipated when the 3-enone functionality itself was modified directly in the β-position to form acrylic, crotonic and cinnamic amides as the electrophilic units. A mesomeric connection between the enone carbonyl and the heterocycle is achieved via the free electron pair of the nitrogen in the heterocyclic 3-position (Scheme 7).



Scheme 7: Mesomeric interaction of the oxadiazoline and enone units in OXEs.

There are few literature-known examples for these kinds of compounds. Prior to the work presented here, a set of six compounds having these structural features were already published,^[45] however without the involvement of the pyridine unit (Figure 10). Since they carry a cinnamoyl unit in the 3-position and are 2-H-substituted, these molecules would be classified as **OXE8s**. They were tested for antibacterial activity on different bacterial cell lines with promising results.

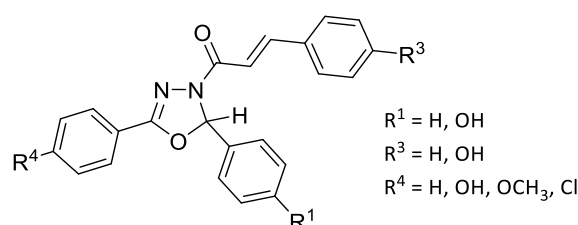
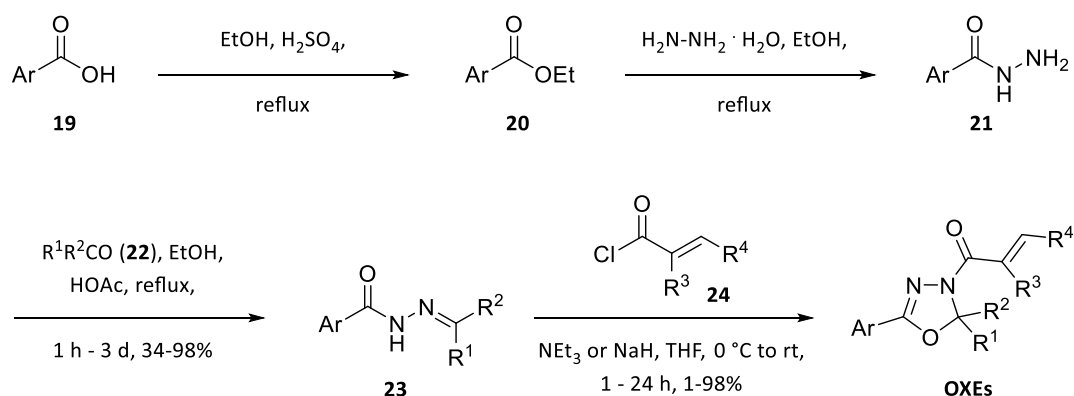


Figure 10: Oxadiazoline derivatives synthesized and tested for antibacterial activity.^[45]

Synthesis of OXEs

The synthesis was done via a classical heterocyclic synthesis forming the 3,4-dihydro-1,3,4-oxadiazole ring in the last step of the sequence containing up to 4 steps (Scheme 8).^[42]

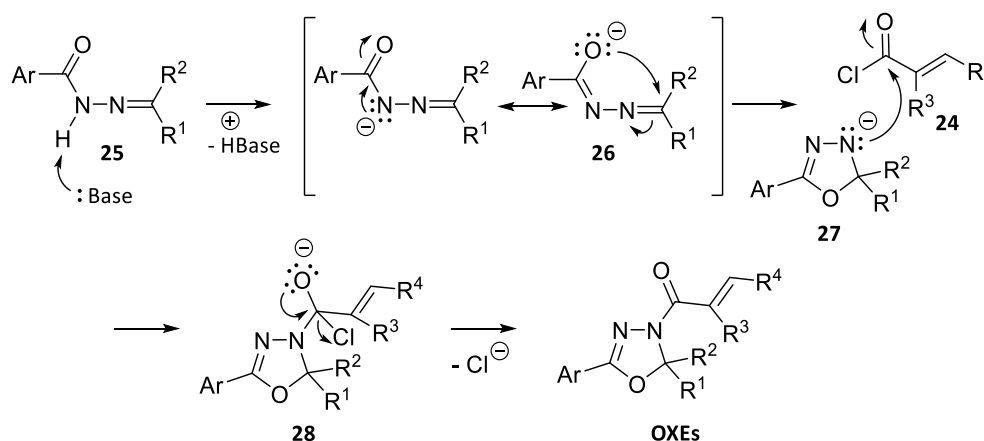


Scheme 8: Synthesis of 2,5-diaryl-3,4-dihydro-1,3,4-oxadiazoles with additional 3-enone unit (OXEs).

Depending on the commercial availability of starting materials, the sequence was either started from carboxylic acids **19** or esters **20** producing with hydrazine mono hydrate known hydrazides **21**,^[46] which were transformed into the mostly known hydrazones **23**.^[47]

using acetophenones or benzaldehydes **22**. In the last step, the heterocyclic ring was formed from hydrazones **23** in the presence of the corresponding acid chlorides **24**.

A mechanism for the oxadiazoline ring formation is proposed in Scheme 9.^[48] Basic conditions lead to the formation of anion **26** which cyclizes to **27** and is subsequently trapped by the electrophile **24**.



Scheme 9: Proposed mechanism for the formation of OXEs^[48].

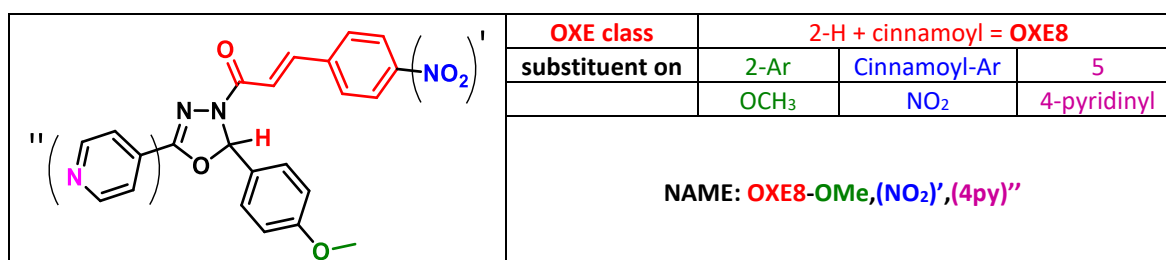
For the nomenclature, first the OXE class is named according to Table 4. Further substituents are reflecting the type of aromatic unit in 5-position as well as *p*-substituents on the different aromatic rings R¹ and R³. Among the aromatic units, only the pyridine residue is termed; phenyl and aryl are not included in the name. The substituents are named in the following order:

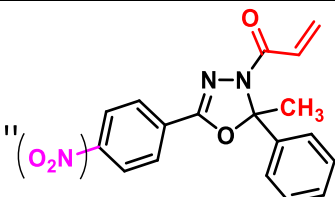
1. Substituents on the aromatic ring in 2-position
2. Substituents on the aromatic ring in β -position of the enone unit (only in the case of cinnamoyl in **OXE7s** and **OXE8s**)
3. Substituents in 5-position (only pyridinyl or a 4-Ar substituent)

and may placed in labelled brackets according to:

1. -
2. ()'
3. ()''

Two examples given in Scheme 10 illustrate these explanations.

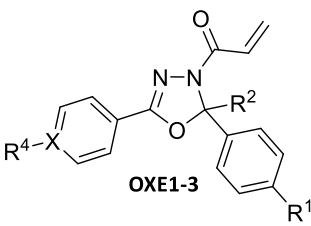
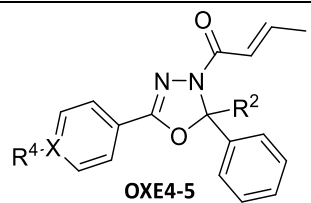


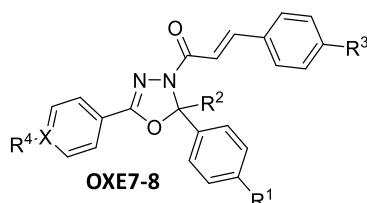
	OXE class	2-CH ₃ + acryl = OXE1		
	substituent on	2-Ar	Cinnamoyl-Ar	5
		-	-	Ar-NO ₂
NAME: OXE1-(NO₂)''				

Scheme 10: Examples for the nomenclature developed for the OXE substance library.

Since it is known that *N*-oxides of pyridines can show special binding properties, three pyridinyl-substituted OXE compounds were turned into their corresponding *N*-oxide derivatives^[44] using the oxidation reagent mCPBA (*m*-chloroperbenzoic acid).^[49] All synthesized OXE compounds are summarized in Table 5 and Figure 11, which reflects seven different classes of OXEs from the nine classes that were envisioned in principle. Attempts to synthesize representatives of **OXE6** and **OXE9** were not successful. Additionally, one control compound was synthesized, **OXE1-(4py)''-H₂**, which represents the dihydro derivatives lacking the enone motif. One α -substituted compound **α -Me-OXE1-(4py)''** was synthesized. More representatives with different structural features were included in the library: the spiro-compound **OXCE-(4py)''** and two compounds with quinolinyl and naphthyl substituents in position 5 (Figure 11).

Table 5: Overview of OXEs of the classes 1-5 and 7-8 synthesized in the Amslinger group.

Classes	NAME	R ¹	R ²	R ³	X	R ⁴	Syn
	OXE1	H	CH ₃	-	C	H	LW
	OXE1-(NO₂)''	H	CH ₃	-	C	NO ₂	RH
	OXE1-(CN)''	H	CH ₃	-	C	CN	RH
	OXE1-(4py)''	H	CH ₃	-	N	-	AR
	OXE1-NO₂, (4py)''	NO ₂	CH ₃	-	N	-	AR
	OXE1-(4py-<i>N</i>-oxide)''	H	CH ₃	-	N ⁺	O ⁻	LW
	OXE1-CF₃, (4py)''	CF ₃	CH ₃	-	N	-	AR
	OXE1-OCF₃, (4py)''	OCF ₃	CH ₃	-	N	-	AR
	OXE1-4py, (4py)''	4-py	CH ₃	-	N	-	Ar
	OXE1-2py, (4py)''	2-py	CH ₃	-	N	-	Ar
	OXE2-(4py)''	H	H	-	N	-	RH
	OXE2-NO₂, (4py)''	H	H	-	N	-	RH
	OXE2-OMe, (4py)''	H	H	-	N	-	RH
OXE3-(4py)''	H	CF ₃	-	N	-	RH	
	OXE4-(4py)''	-	CH ₃	-	N	-	AR
	OXE4-(4py-<i>N</i>-oxide)''	-	CH ₃	-	N	-	LW
	OXE5-(4py)''	-	H	-	N ⁺	O ⁻	LW

Classes	NAME	R ¹	R ²	R ³	X	R ⁴	Syn
	OXE7	H	CH ₃	-	C		AR
	OXE7-(4py)''	H	CH ₃	-	N		AR
	OXE7-OMe,(4py)''	OCH ₃	CH ₃	-	N		AR
	OXE7-(CF₃)',(4py)''	H	CH ₃	CF ₃	N		AR
	OXE7-(OMe)',(4py)''	H	CH ₃	OCH ₃	N		AR
	OXE8-(4py)''	H	H	-	N		AR
	OXE8-(4py-N-oxide)''	H	H	-	N ⁺	O ⁻	LW
	OXE8-NO₂,(4py)''	NO ₂	H	-	N		AR
	OXE8-OMe,(4py)''	OCH ₃	H	-	N		AR
	OXE8-(OMe)₂,(4py)'' ^[a]	2xOCH ₃	H	-	N		RH
	OXE8-OMe,(NO₂)',(4py)''	OCH ₃	H	NO ₂	N		RH
	OXE8-(OMe)',(4py)''	H	H	OCH ₃	N		RH
	OXE8-OMe,(OMe)',(4py)''	OCH ₃	H	OCH ₃	N		RH

Syn = Synthesized by: AR = Anas Rasras, RH = Rainer Herzog, LW = Lukas Wirth; [a]: the 3,4-dimethoxy compound was produced.

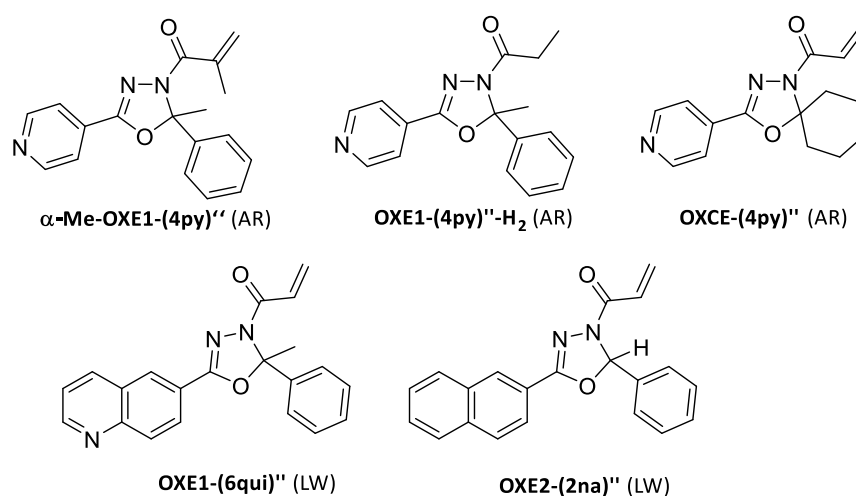


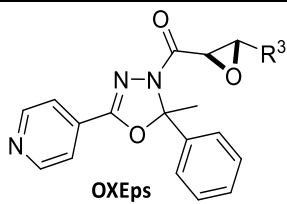
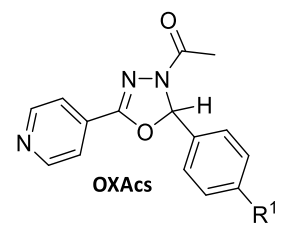
Figure 11: OXEs with further structural features synthesized in the Amslinger work group. Synthesized by: AR = Anas Rasras, RH = Rainer Herzog, LW = Lukas Wirth.

Synthesis of OXE analogues: epoxides and acyl-substituted oxadiazolines

Additionally, the epoxide functionality as alternative electrophilic unit was of interest. This functional group also occurs in natural products that are able to bind covalently to nucleophilic amino acid side chains in active sites of certain enzymes by undergoing epoxide opening.^[12, 50] Some epoxide-containing compounds have been proven to bind to thiol groups of cysteines, e.g. in cysteine proteases, in particular.^[51] Antimicrobial, anti-angiogenic and anti-inflammatory effects are described,^[12, 52] making these compounds important in drug discovery and development for decades. To investigate the effect of a different electrophilic moiety on the OXE compounds, two oxadiazoline representatives with an additional epoxide were synthesized from their **OXE1** and **OXE4** analogues using *n*-BuLi/tBuOOH,^[53] whereby two compounds were produced^[44] (Table 6). As further control compounds, three representatives of **OXAc-(4py)''**'s known from the literature were

synthesized.^[54] **OXAc**s stem from **OXE2-(4py)** and carry an acyl group in 3-position instead of acryl (Table 6).

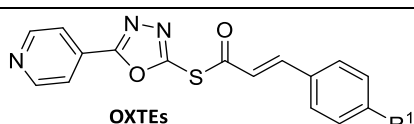
Table 6: Synthesized OXE analogues: **OXEp** and **OXAc** compounds. Syn = synthesized by: AR = Anas Rasras, LW = Lukas Wirth.

Classes	NAME	R ¹	R ³	Syn
 OXEps	OXEp1-(4py)	-	H	LW
	OXEp2-(4py)	-	CH ₃	LW
 OXAcS	OXAc-(4py)	H	-	AR
	OXAc-NO₂-(4py)	NO ₂	-	AR
	OXAc-OMe-(4py)	OCH ₃	-	AR

Synthesis of oxadiazol-thioesters

For a variation of the heterocyclic scaffold, a further structure concept differing from the OXE skeleton was designed. It was constructed from a saturated oxadiazole core unit with the enone moiety linked to the heterocycle in 2-position via a thioether and also pyridinyl in 5-position. Two compounds of this type were synthesized and named **oxadiazol-thioesters OXTE** and **OXTE-OMe** (Table 7).^[42]

Table 7: Oxadiazol compounds synthesized by Anas Rasras. Syn = synthesized by AR = Anas Rasras.

Structure	NAME	R ¹	Syn
 OXTEs	OXTE	H	AR
	OXTE-OMe	CH ₃	AR

A 1.8 Synthesis of further electrophiles in the Amslinger work group

Phenylacrylamide derivatives as reactive units in drug development

Reactive units that differ from the enone functionality are able to react as Michael acceptors with nucleophilic pharmacological targets as well. Before combining those varied reactive units to drug-like fragments, the assessment of a structure-reactivity relationship is useful to find out if the electrophilicity of the unit is tunable by different substituents as described before for **α-X-TMCs**. For that purpose, a library of simplified molecules of the

aromatic acrylamide type and of the phenylethene sulfonamide type were synthesized by Lukas Wirth.^[44] Figure 12 gives an overview of all synthesized compounds.

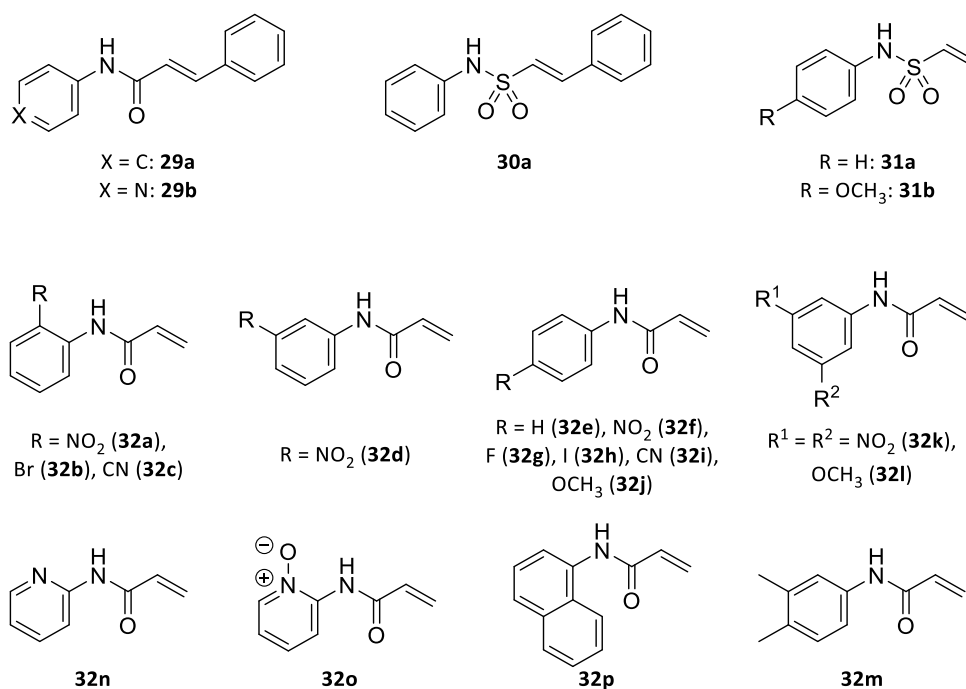


Figure 12: *N*-Phenylacrylamide and phenylethenesulfonamide derivatives synthesized by Lukas Wirth.^[44]

For compounds **29** and **30** only the unsubstituted and the pyridine derivatives were synthesized. With **31a** and **31b** an unsubstituted and a OMe-decorated representative of *N*-phenylethenesulfonamides was obtained. But in the case of *N*-phenylacrylamides **32**, a library of 16 compounds with a great variety of electron-withdrawing and electron-pushing substituents in various positions was produced. Although OXEs can be considered as enamide derivatives as well, the difference between acrylamides and OXEs is that the amide nitrogen is not included in a heterocycle but *N*-aryl substituted.

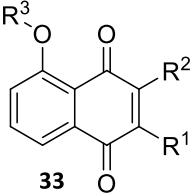
Reactivity assessment methods for electrophiles binding to thiols in a covalent fashion were previously reported also for this so-called fragment-based approach.^[55] [30] The aim is to establish a structure-reactivity relationship so that the reactivity can easily be tuned by simply exchanging substituents. These reactivity fragments can subsequently be combined to one or more small, drug-like fragments to find the optimal toxicity/activity window for a certain biological effect. Since it has often been shown that reactivity and biological activity correlate, electrophilicity can be used as a modification tool in the first place.

Juglone and Juglone derivatives

Another project dealing with the synthesis, kinetic and biological evaluation of small electrophilic molecules was the investigation of the natural product juglone (5-

hydroxynaphthalene-1,4-dione, **33a**), a naphthoquinone found in *Juglans* (walnut) species^[56] in the course of the Master thesis of Sebastian Schlegel.^[57] Table 8 summarizes the substance library of **33a** and 14 of its synthesized derivatives, which are *O*-methylated (R^3) and/or substituted in position 2 or 3 (R^1 and R^2). Compound **33e** could only be obtained as a mixture of two chloro-substituted regioisomers due to separation issues.

Table 8: Structures and names of Juglone **33a** and its derivatives synthesized by Sebastian Schlegel.^[57]

	Nr	R^1	R^2	R^3	name
	a	H	H	H	H
b	H	H	H	CH ₃	<i>O</i> -Methyljuglone
c	H	H	Br	H	3-Bromojuglone
d	H	H	Br	CH ₃	3-Bromo- <i>O</i> -methyljuglone
e	Cl/H	Cl/H	H	H	2- and 3-Chlorojuglone (mixture)
f	H	H	Cl	CH ₃	3-Chloro- <i>O</i> -methyljuglone
g	H	H	F	CH ₃	3-Fluoro- <i>O</i> -methyljuglone
h	H	H	N ₃	H	3-Azidojuglone
i	H	H	N ₃	CH ₃	3-Azido- <i>O</i> -methyljuglone
j	H	H	NH ₂	H	3-Aminojuglone
k	H	H	NH ₂	CH ₃	3-Amino- <i>O</i> -methyljuglone
l	H	H	piperidino	H	3-Piperidinojuglone
m	piperidino	H	H	H	2-Piperidinojuglone
n	H	H	morpholino	H	3-Morpholinojuglone
o	morpholino	H	H	H	2-Morpholinojuglone

Biological activity such as anticancer^[58], anti-inflammatory^[59] and antimicrobial^{[60] [61]} activity of **33a** has been described, which is explained by the redox properties of the quinone system, including the formation of radical species, as well as Michael addition with nucleophiles of various pharmacological targets.^[62] Therefore, not only studies of the biological activity but also the reactivity of juglone and some derivatives are published. For example, the thia-Michael addition of hydrogen sulfide^[63] and GSH^[64] to juglone (**33a**) were kinetically investigated. Furthermore, a study was published on the relationship between the reactivity of the addition-elimination reaction of 3-OR-substituted juglone derivatives and their anticancer activity.^[65]

In the work group of PD Dr. Sabine Amslinger the compounds were tested towards their anti-inflammatory properties in the NO inhibition assay. All compounds with an amine substituent in 2- or 3-position (**33j-o**) and bromo-substituted **33d** provided anti-inflammatory activity in the μ M range. 3-Amino-*O*-methyljuglone **33k** was the most active substance with an IC₅₀ of 1.10 μ M. All other derivatives were inactive at nontoxic concentrations. All IC₅₀ values in the MTT toxicity assay were determined in the range of 4.05 – 63.3 μ M with a medium of 30.0 μ M; no relation between toxicity and anti-inflammatory activity was found.^[57] Biological results determined by Sebastian Schlegel and Sina Malenke are summarized only for compounds with an anti-inflammatory activity in Table 9.

Table 9: Biological data of Juglone derivatives with anti-inflammatory properties. Evaluation of toxicity and NO-inhibition properties in murine macrophages RAW264.7. Cell viability (MTT) assay was performed and evaluated by Sebastian Schlegel. Anti-inflammatory (iNOS) assay was performed by Sina Malenke and evaluated by Sina Malenke and Monika Enzinger.

Compound	Cell viability MTT (IC ₅₀ / μ M) \pm SD	Inhibition of NO production (IC ₅₀ / μ M) \pm SD
3-Aminojuglone 33j	36.7 \pm 8.1	5.95 \pm 2.20
3-Amino-O-methyljuglone 33k	18.8 \pm 6.9	1.10 \pm 0.49
3-Piperidinojuglone 33l	63.3 \pm 19.8	9.48 \pm 0.66
2-Piperidinojuglone 33m	41.8 \pm 7.8	4.18 \pm 0.48
3-Morpholinojuglone 33n	36.4 \pm 3.3	12.3 \pm 8.8
2-Morpholinojuglone 33o	30.9 \pm 5.0	17.0 \pm 7.8
Bromo-O-methyljuglone 33d	22.5 \pm 12.4	5.82 \pm 1.09

A 1.9 Further development of the kinetic thiol assay towards the investigation of colorless electrophiles

Purpose and concept of the new assay

The previous chapters have dealt with enones that have an absorbance in the range of 300-350 nm or higher. But there are some interesting electrophiles which are not suitable for the presented assay due to unsuitable absorbance properties. Figure 13 shows examples for compounds which absorbance bands do not extend as far as < 300 nm and can therefore not be kinetically evaluated by the thiol assay.

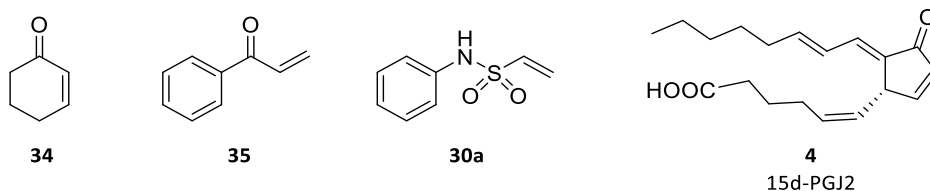


Figure 13: Compounds that cannot be examined by the kinetic thiol assay due to insufficient absorbance properties.

Compounds **34** (cyclohexenone) and **35** (phenylvinylketone or acrylophenone) are structural motifs that occur in biologically active molecules. For example, antimicrobial^[66] and EGF-receptor (epidermal growth factor receptor) inhibition^[67] properties have been found for **35**, which are probably at least partly based on their Michael acceptor activity. Based on the kinetic properties of these two simple test substances, it would also be possible to estimate the reaction rates of substances containing these structural elements. 15d-PGJ2 (**4**, 15-deoxy- Δ 12,14-prostaglandine J2) is the most active representative of cyclopentenone-type prostaglandins which show strong anti-inflammatory activity *in vitro* and *in vivo*. This is based, among other mechanisms, on their Michael acceptor activity provided by the

electrophilic cyclopentenone moiety which alkylates, among other targets, the IKK subunit of the I κ B kinase, leading to an inhibition of NF- κ B as transcription factor for inflammation-triggering proteins.^[68] Therefore, a quantification of the Michael acceptor properties of **4** would be of great interest.

As a result, this work examines strategies and approaches to further develop the present assay in favor of an investigation of completely colorless enones. The concept is to reverse the roles of the two reactants enone and thiol. Since the enone test substances lack the required chromophore, thiol dyes should be produced that change their absorption properties by Michael addition. These thiol dyes function as the probe or probes in the new assay. The concept of new assay in comparison to the existing kinetic thiol assay is shown in Figure 14. To obtain the desired change in the UV spectrum from free thiol to alkylated thiol, it is advantageous of the thiol group to be directly attached to the chromophore to increase the effect of electronic variations. Therefore, the concept initially includes only aromatic thiol dyes but attempts are also made towards alkyl thiols.

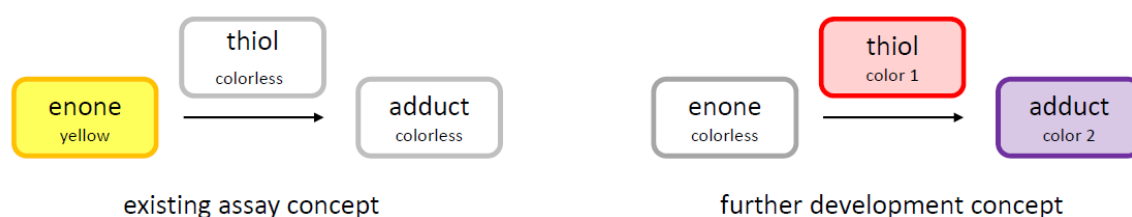


Figure 14: Concepts of the existing kinetic thiol assay for electrophiles and the envisioned new kinetic thiol assay for colorless enones.

Studies in the context of a Master's thesis and a Bachelor's thesis have shown that the principle for an UV-Vis assay works and the desired effect was found in anthraquinone derivatives^[69] (**36**) and *p*-nitrothiophenols^[70] (**37**, both structures see Figure 15). In contrast to the free thiolates of **36**, the absorption band of the alkylated thiols occurred at shorter wavelengths whereas alkyl derivatives of **37** had an absorbance maximum < 300 nm.

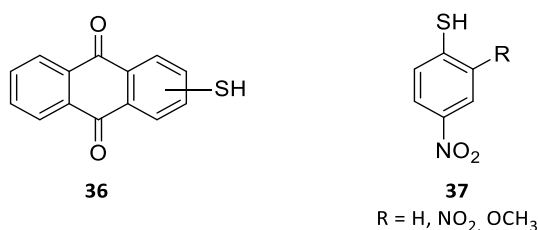


Figure 15: Aromatic thiols investigated as probes in a further development of the kinetic thiol assay.

However, the following problems occurred:

1. Free aromatic thiols were prone to oxidation to disulfides.
2. Aromatic thiols reacted very slowly with electrophiles.
3. Relatively high concentrations must be used for sufficient absorption.

In the course of both works, some improvements have been made to problem 1. Careful degassing, covering with foils and antioxidant additives are promising measures. Oxidation must be prevented because disulfide formation led to absorbance decrease as well, pretending a higher reaction rate. The low reactivity of aromatic thiols compared to cysteamine could also be accepted, although this already represents a large limit for test substances. The biggest hurdle was posed by the high concentrations of both thiol dyes and test compounds. In order to maintain pseudo-first-order reaction conditions, the test compounds must be present in excess in the new assay. Under these conditions, it was impossible to use test substances of all kinds in the high μM and mM range, and optimization attempts with regard to co-solvents were also unsuccessful. It was therefore decided to use fluorescent dyes instead of UV-Vis active thiol dyes. Fluorescence-active substances can be used even at very low concentrations $< 1 \mu\text{M}$. This can also reduce the concentration of electrophiles, but also increase the overall excess, which speeds up reaction times and reduces possible thiol oxidation.

Target compounds as thiol probes

Figure 16 gives an overview of thiol-containing substances with fluorescence properties which can be investigated towards their applicability as thiol probes in the new assay. All three structures **DCY**, **Acetyl-MSTI** and **NBD** are literature-known^{[71] [72] [73]} and were originally used for non-kinetic fluorescence-based investigations, which are explained in more detail below.

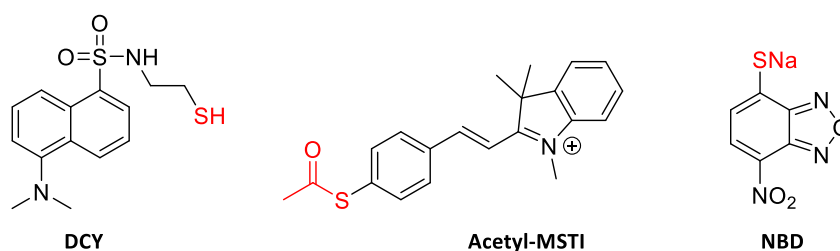


Figure 16: Target structures of fluorescent thiol dyes envisioned in this work.^{[71] [72] [73]}

Avonto's research group focused on the synthesis and characterization of **DCY** (dansyl cysteamine) which was used in a new HTS (high throughput screening) assay (DCYA, dansyl cysteamine assay) to identify potential allergenic chemicals.^[71] The purpose of the new assay is to replace animal experiments, for example in the cosmetics industry, with animal-

free chemoassays. Electrophiles of all kinds are held responsible for skin sensitizing effects and allergies through their non-specific reaction with nucleophilic residues in proteins.^[74] **DCY** was therefore designed as a "fluorescent cysteamine" to quickly detect particularly reactive substances in a 96-well format. As the measurement principle, unreacted **DCY** is isolated by reaction to silica-bound maleimide and subsequent fluorescence spectroscopy of the adduct. The reactivity of the electrophilic test compound is therefore indirect proportional to the measured fluorescence intensity. The assay principle is depicted in Figure 17. **DCY** was chosen to be tested for the applicability as fluorescent thiol probe for the planned further development of the kinetic thiol assay in the course of the work for this thesis.

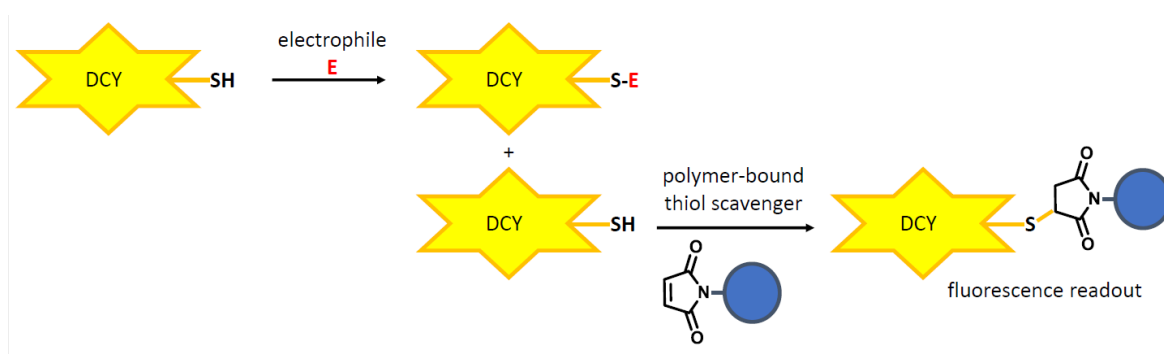
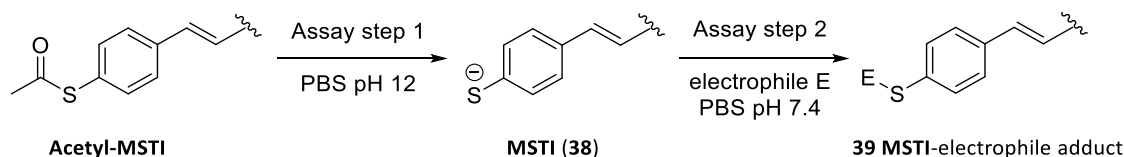


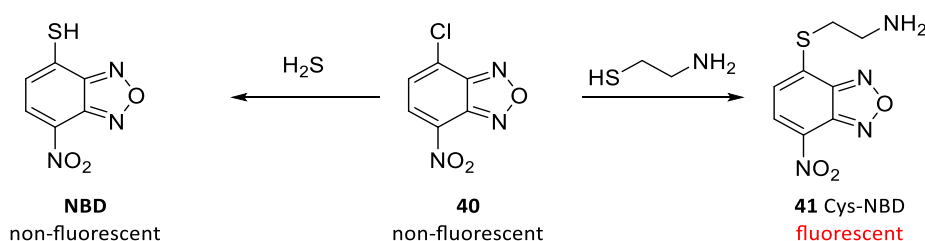
Figure 17: Principle of the **DCY** HTS assay to identify highly reactive electrophiles as potential skin sensitizers developed by Avonto et al.^[71]

McCallum and coworkers followed a similar approach with the synthesis of **Acetyl-MSTI** (**MSTI** = mercaptostyryl-trimethylindolium iodide, Figure 16), and its use in a HTS for the identification of highly reactive electrophilic compounds in the early state of drug development.^[72] With this new assay, these electrophiles are to be detected and excluded from further drug development, since their potential for side effects due to non-specific alkylation of biological targets is very high. Since the free thiol **MSTI** (**38**, Scheme 11) was found to be highly susceptible to oxidation, the alkylated form was used for the assay and **38** was produced *in situ* in a first step. In the second step, the test substances are added and the fluorescence measurement is performed after a short time. The occurrence of **MSTI**-electrophile adducts (**39**) is indicated by a decrease of fluorescence due to alkylation of **MSTI** to a certain level and electrophiles with too high reactivity are sorted out by a hit-or-no-hit principle. It is reported that **Acetyl-MSTI** and **MSTI** (**38**) have different fluorescence emission properties, therefore they would be perfectly suited for the planned further development of the kinetic thiol assay. The principle of the HTS assay is depicted in Scheme 11.



Scheme 11: Principle of the HTS assay to identify highly reactive electrophiles in the early state of drug development by McCallum et al.^[72]

The non-fluorescent **NBD** (7-nitrobenzo[c][1,2,5]-oxadiazol-4-thiolate) was also a candidate of interest for the thiol probe in the planned assay. The basis for this is the work of Montoya et al., which describes differences in the fluorescence properties of free **NBD** and alkylated **NBD** compound **41**; these properties are used for example in fluorescence microscopy.^[73, 75] The ability of non-fluorescent **NBD** to gain fluorescence activity when alkylated is a very promising property for the planned assay (Scheme 12).



Scheme 12: **NBD** and derivatives show different fluorescence properties.

A 1.10 Aim of the present work

The work presented in this chapter focuses on the reactivity study of the synthesized compounds and compound libraries presented using the kinetic chemoassay for enone-type electrophiles towards thiols. Therefore, all substances were first examined for their general applicability for the assay by UV-Vis spectroscopy and LC-MS. Measurement parameters and second order rate constants k_2 were determined and detailed investigations of product formation and stability under assay conditions were performed.

Figure 18 provides an overview of the investigated compounds. In addition to the already existing substances, the library of oxadiazoline enones (OXEs) was extended by further representatives that are relevant for a structure-reactivity analysis. In cooperation with Sina Malenke and Dita Fritsch, all substances were investigated towards their toxicity and anti-inflammatory activity using the two in-vitro cell assays. The murine macrophages cell line RAW264.7 was used due to the ability to express the inflammatory-inducing enzyme iNOS. Structure-activity/reactivity relationships (SAR) were analyzed and derived from the assay results.

In a fragment-based approach, the presented set of *N*-phenylacrylamides was investigated towards its reactivity and the influence of substituents. The natural product juglone (**33a**) and its derivatives (**33b-o**) were also tested towards their suitability for the use in the kinetic thiol assay.

Furthermore, another required member of the group of α -X-HC derivatives, namely α -NO₂-HC, was synthesized and investigated within this work.

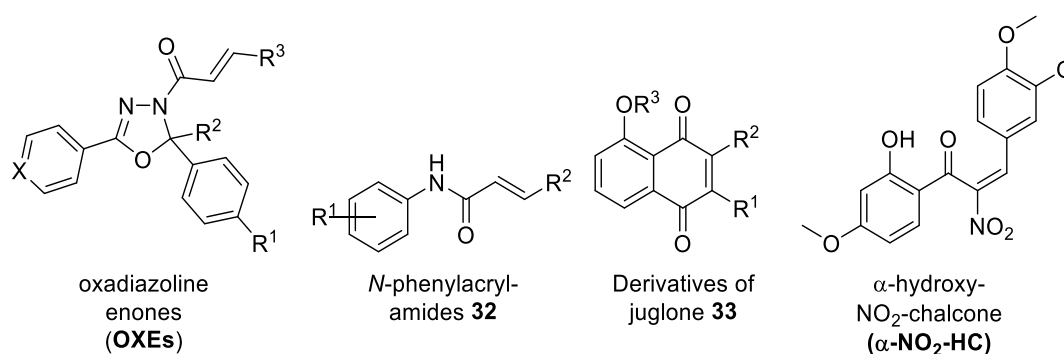


Figure 18: Compounds and compound libraries synthesized and evaluated towards their reactivity and biological activity in this study. Note: Since each project is a cooperation of Amslinger group members, the contribution of each person is listed in the respective chapter.

Investigations towards the further development of the kinetic thiol assay for the use of colorless enones with absorptions < 300 nm as test compounds as described in A 1.9 were performed. In addition to the literature-known thiol compounds **DCY**, **Acetyl-MSTI** and **NBD**, further fully synthetic fluorescent dyes with thiol function were investigated towards their synthesis.

A 2 Results and Discussion I: Synthesis, kinetic and biological evaluation of oxadiazoline enones (OXEs): a library of new anti-inflammatory electrophilic compounds

These results are not published yet (05/2019).

The following persons and work groups participated in this project as follows:

Group members of the work group of PD Dr. Sabine Amslinger participated in this project according to the participation list.

Josef Kiermaier, MS department of the University of Regensburg: MS measurements.

Georgine Stühler, Anette Schramm and Fritz Kastner, NMR department of the University of Regensburg: kinetic NMR measurements.

Dr. Sandra Schlee and Thomas Klein, Department of Biochemistry II, University of Regensburg, work group of Prof. Dr. Sterner: Introduction to and help with Stopped-Flow measurements.

I gratefully acknowledge the help, support and expertise of everyone involved in this project.

Participation list of Amslinger work group members

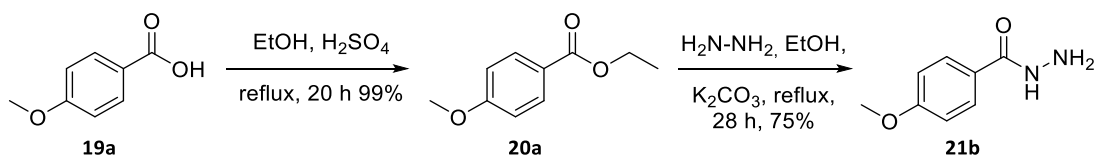
Group member	Work for the project presented in this chapter
Dr. Anas Rasras (PhD thesis)	Syntheses: OXE1-(4py)" ; OXE1-NO ₂ ,(4py)" ; OXE1-CF ₃ ,(4py)" ; OXE1-OCF ₃ ,(4py)" ; OXE1-4py,(4py)" ; OXE1-2py,(4py)" ; α-Me-OXE1-(4py)" ; OXE1-(4py)"-H ₂ ; OXE4-(4py)" ; OXE7; OXE7-(4py)" ; OXE7-OMe,(4py)" ; OXE7-(CF ₃)',(4py)" ; OXE7-(OMe)' ,(4py)" ; OXE8-(4py)" ; OXE8-NO ₂ ,(4py)" ; OXE8-OMe,(4py)" ; OXCE-(4py)" ; OXAc-(4py)" ; OXAc-OMe,(4py)" ; OXAc-NO ₂ ,(4py)" ; OXTE; OXTE-OMe and precursors
Lukas Wirth (Master thesis)	Syntheses: OXE1; OXE1-(6qui)" ; OXE1-(4py-N-oxide)" ; OXE2-(2na)" ; OXE4-(4py-N-oxide)" ; OXE5-(4py)" ; OXE8-(4py-N-oxide)" ; OXEp1-(4py)" ; OXEp2-(4py)" and precursors
Rainer Herzog (Master thesis)	Syntheses: OXE1-(CN)" ; OXE1-(NO ₂)" ; OXE2-(4py)" ; OXE2-NO ₂ ,(4py)" ; OXE2-OMe,(4py)" ; OXE3-(4py)" ; OXE8-(OMe) ₂ ,(4py)" ; OXE8-OMe,(NO ₂)',(4py)" ; OXE8-(OMe)' ,(4py)" ; OXE8-OMe,(OMe)' ,(4py)" and precursors
Monika Enzinger (this work)	Syntheses: OXE1; OXE1-(OMe)" ; OXE1-OMe,(4py)" ; OXE1-(6qui)" ; OXE3-(4py)" ; OXE4-(4py-N-oxide)" ; OXE8-(OMe)' ; OXE8-OMe,(4py)" ; OXE8-(4py)"-H ₂ ; OXE8-(4py-N-oxide)" ; OXEp1-(4py)" and precursors

Group member	Work for the project presented in this chapter
	Biological testing and evaluation: OXE1 ; OXE1-(6qui) ''; OXE3-(4py) ''; OXE8-(OMe) ''; OXE8-(OMe)',(4py) ''; OXE8-(4py) ''-H ₂ ; OXE8-(4py-N-oxide) ''; OXEp1-(4py) ''; OXEp2-(4py) ''; OxAc-(4py) ''; OxAc-OMe,(4py) ''; OxAc-NO₂,(4py) '' and precursors UV-Vis characterization, kinetic measurements, stopped-flow kinetic (with the help of Sandra Schlee and Thomas Klein), LC-MS analysis and LC-MS kinetic measurements (together with Josef Kiermaier): all OXEs and OXE analogues NMR kinetics (together with Anette Schramm): OXE1-(4py) ''
Sina Malenke (PhD thesis)	Biological testing and evaluation: OXE1-(OMe) ''; OXE1-(4py-N-oxide) ''; OXE2-(2na) ''; OXE3-(4py) ''; OXE4-(4py-N-oxide) ''
Dita Fritsch (Technical staff)	Biological testing: all other OXEs and OXE analogues
Sabine Amslinger	Evaluation of biological testing: all other OXEs and OXE analogues

A 2.1 Synthesis

Synthesis of OXEs

In this work new hydrazones and OXEs were synthesized, which contain further required structural elements. In addition, several known substances were synthesized to complete the analytical data. The synthesis was generally carried out according to the established method^[42] (Scheme 8), some procedures were adapted to counteract product instabilities and increase yields. Hydrazone **23c** was synthesized starting from the corresponding acid in three steps (Scheme 13 and Table 10) and four further hydrazones **23** were synthesized from pre-existing hydrazides **21a** and **21c**, summarized in Table 10. With the exception of **23c**, hydrazones **23** were received in moderate to good yields. Due to their low solubility, compounds **23** were usually already crystalline after quenching of the reaction with water and could easily be isolated by filtration, making a further purification step unnecessary. Reasons for lower yields are the formation of side products and/or the appearance of the product in very small and fine crystals, partly dissolved as colloids (turbid aqueous phase), which led to filtration issues.

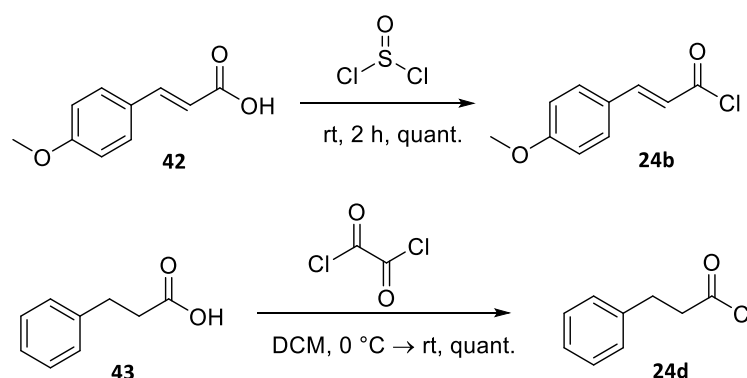


Scheme 13: Synthesis of hydrazide **21b** as a precursor in the synthesis of hydrazone **22c**.

Table 10: Synthesis of hydrazones **23** performed during this work.

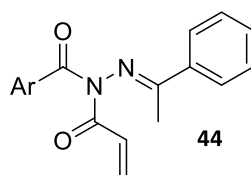
		$\text{R}^1\text{R}^2\text{CO (22a-e),}$ EtOH, HOAc, $\xrightarrow{\text{reflux}}$							
	Ar	R ¹	R ²	Ar	R ¹	R ²	t, yield		
21a	Ph	22a	Ph	CH ₃	23a	4-OMe-C ₆ H ₄	Ph	CH ₃	18 h, 71%
21b	4-OMe-C ₆ H ₄	22b	4-NO ₂ -C ₆ H ₄	CH ₃	23b	4-pyridyl	4-NO ₂ -C ₆ H ₄	CH ₃	24 h, 68%
21c	4-pyridyl	22c	4-OMe-C ₆ H ₄	CH ₃	23c	4-pyridyl	4-OMe-C ₆ H ₄	CH ₃	24 h, 22%
		22d	Ph	H	23d	Ph	Ph	H	26 h, 94%
		22e	Ph	CF ₃	23e	4-pyridyl	Ph	CF ₃	24 h, 41%

Carboxylic acid chloride **24b** needed in the last synthesis step, the OXE heterocycle formation, was easily obtained in quantitative yield by heating of the corresponding carboxylic acid **42** in excess thionyl chloride, which was removed on high vacuum after completion of the reaction. Another method was used to obtain the saturated cinnamic acid chloride **24d**, which was required for the further saturated control substance **OXE8-(4py)''-H₂**. The starting material **43** reacted with oxalyl chloride at room temperature^[76] and **24d** was received in quantitative yield (Scheme 14).

**Scheme 14:** Synthesis of carboxylic acid chlorides **24**.

With the synthesized and pre-existing precursors in hand, OXEs were synthesized by the reaction of hydrazones **23** and aldehydes/ketones **22** under basic conditions. All compounds produced in this work including the literature-known **OXE8-(OMe)''**^[45] are summarized in Table 12. In general, the syntheses gave moderate to good yields, but due to the difference in the steric and electronic properties of the involved educts, a great variety in the type and number of side products was observed during reaction control by thin layer chromatography (TLC). This resulted in low yields of 1-11% for some representatives. Especially OXEs lacking the pyridinyl unit, namely **OXE1**, **OXE1-(OMe)''** and **OXE1-(6qui)''**, were prone for low yields due to a high amount of side products. A recurring problem in these

cases was the ongoing product decomposition during the workup steps. For **OXE1**, decomposition in solution (CDCl_3) within 24 h was monitored by NMR. Improvement of yields were achieved for **OXE1** (9% to 48%) and **OXE1-(6qui)''** (2% to 11%) by shortening of the reaction times with accepting incomplete consumption of the starting material, quick workup and low temperatures on the rotary evaporator water bath. A typical side product for these OXEs was the open-chained *N*-acryl-substituted hydrazone **44** (Figure 19). Here, the reaction of anion **26** with acrylic acid chloride **24a** occurred faster than cyclisation to **27** (Scheme 9).



Ar = Ph, Ar-OCH₃, quinoline

Figure 19: Open-chained side product received in the OXE cyclization reaction.

Side products of the type **44** have the same molecular weight as their corresponding OXEs but the two compounds can be distinguished by the characteristic ¹³C NMR peaks. The heterocyclic C-2 in OXE compounds appear at 90-100 ppm. This peak is not found in **44**, while their spectra show an additional carbonyl peak instead. In the attempted synthesis of **OXE1-(OMe)''** with NaH as base, **44** appeared as the main product and no desired product was formed at all. Using triethylamine (TEA) instead gave no reaction within seven days at room temperature. As a result, the synthesis of **OXE1-(OMe)''** was only successful without the use of a base after stirring both educts **23d** and **24a** in THF at room temperature for 7 days. A yield of 10% was received from a complex mixture after normal phase column chromatography and additional reversed phase HPLC purification.

Particularly **OXE3-(4py)''** gave only a very poor yield since multiple purification steps were necessary to isolate the desired product from a complex mixture. Interestingly, the product was formed within 1 h during the reaction, visible by a very prominent TLC spot, but decomposed rapidly during workup and purification. Due to this finding, an optimization of reaction conditions was inefficient, but also workup variations did not lead to higher yields. Attempted optimizations of the reaction conditions were shorter reaction times (1 h) and lower temperatures (0-5 °C). The workup was also varied. The reaction was quenched with water and the crude product was extracted in EtOAc. Furthermore, the solvent was removed from the reaction mixture without quenching and at the same time a dry-load in silica gel was produced. Finally, filtration experiments of the reaction mixture were performed through layers of kieselgur (Celite®), Al₂O₃, normal and reversed phase silica gel,

as it was suspected that by-products or salts in the reaction mixture or the crude product cause the rapid decay of **OXE3-(4py)**". No measure resulted in a yield of more than 1%.

Table 11: Additional hydrazones **23f-j** produced in this work group used for the synthesis of OXEs.

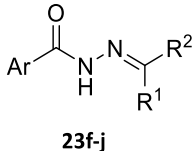
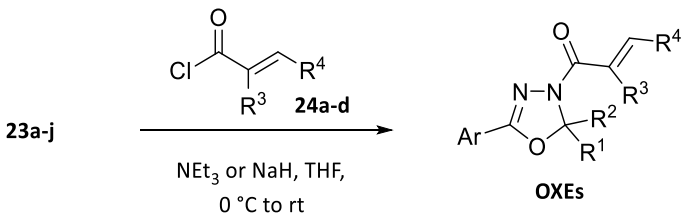
 23f-j		Ar	R¹	R²
	23f	Ph	CH ₃	Ph
	23g	6-quinoliny	CH ₃	Ph
	23h	4-pyridyl	H	4-NO ₂ C ₄ H ₆
	23i	4-pyridyl	H	Ph
	23j	4-pyridyl	H	4-H ₃ CO-C ₄ H ₆

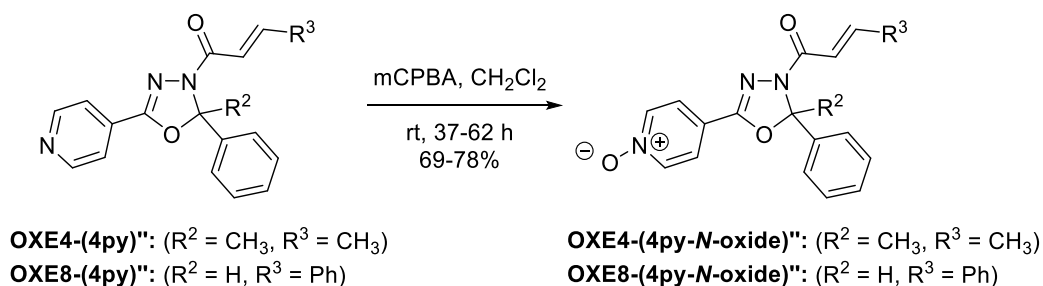
Table 12: Syntheses of OXEs performed during this work.

23a-j									
	R³	R⁴	Ar	R¹	R²	R³	R⁴	t, yield	
24a	H	H	OXE1	Ph	Ph	CH ₃	H	H	4 h, 48%
24b	H	4-OMe-C ₆ H ₄	OXE1-(OMe) " ^[a]	4-OMe-C ₆ H ₄	Ph	CH ₃	H	H	7 d, 10%
24c	H	Ph	OXE1-OMe,(4py) "	4-pyridyl	4-OMe-C ₆ H ₄	CH ₃	H	H	23 h, 29%
24d	H ₂	HPh	OXE1-(6qui) "	6-quinolyl	Ph	CH ₃	H	H	1 h, 11%
			OXE2-NO₂,(4py) "	4-pyridyl	4-NO ₂ -C ₆ H ₄	H	H	H	1.5 h, 45%
			OXE3-(4py) "	4-pyridyl	Ph	CF ₃	H	H	1 h, 1%
			OXE8-(OMe) '	Ph	Ph	H	H	4-OCH ₃ -C ₆ H ₄	20 h, 41%
			OXE8-OMe,(4py) "	4-pyridyl	4-OMe-C ₆ H ₄	H	H	Ph	5 h, 66%
			OXE8-(4py)"-H₂ " ^[b]	4-pyridyl	Ph	CH ₃	H ₂	H, Ph	10 min, 75%

[a] The compound was synthesized by stirring hydrazone **23d** and acyl chloride **24a** in THF without a base; [b] The saturated compound was produced.

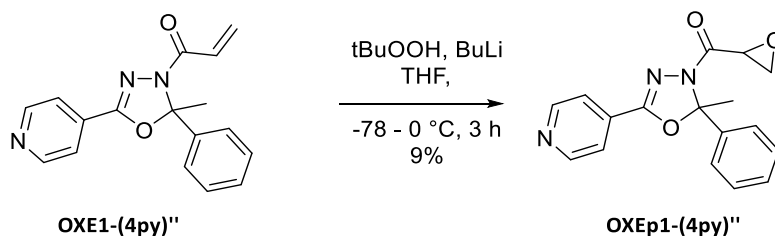
Synthesis of OXE-N-oxides and OXEp1-(4py)"

The synthesis of **OXE4-(4py-N-oxide)**" and **OXE8-(4py-N-oxide)**" from pre-existing precursors was also carried out according to the already established procedure,^[44] giving a slightly improved yield (**Scheme 15**).



Scheme 15: Synthesis of **OXE-(4py-N-oxide)"** compounds.

Less successful was the synthesis of **OXEp1-(4py)"**, which yielded only 9% product despite many trials (Scheme 16). The problem was also here, as with **OXE3-(4py)"**, a continuous degradation during the workup which required several cleaning steps. In addition, the product decomposed during the reaction. There was no improvement in keeping reaction times short and temperatures low.



Scheme 16: Synthesis of **OXEp1-(4py)"**.

With all these substances in hand, the preliminary studies on reactivity were approached. Figure 20 shows a complete overview of all synthesized and subsequently investigated substances from this project.

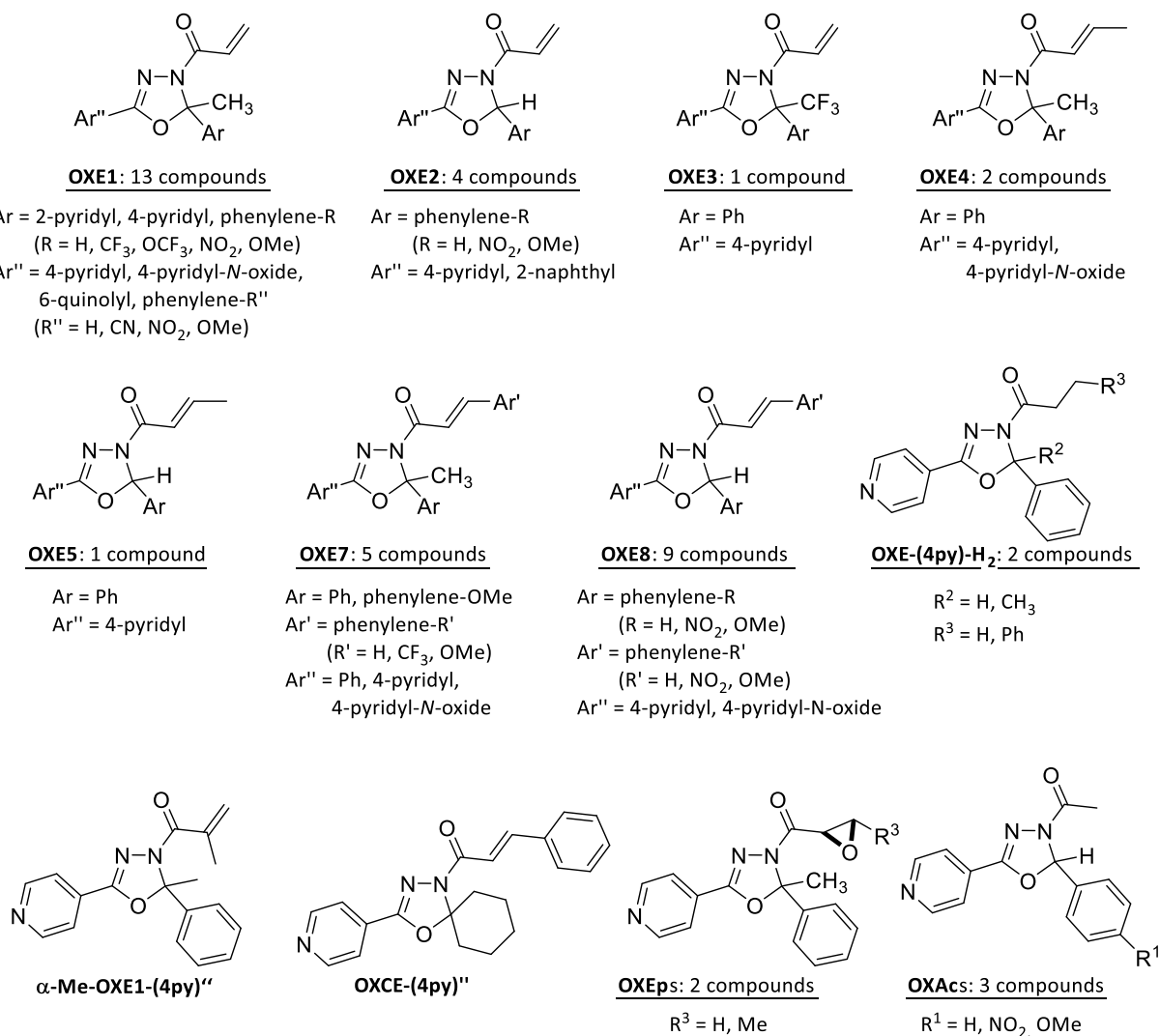


Figure 20: Overview of all OXE, OXCE, OXE_p and OXAc compounds synthesized in the work group of PD Dr. Sabine Amslinger. Synthesized by: Anas Rasras, Rainer Herzog, Lukas Wirth and Monika Enzinger.

A 2.2 UV-Vis spectral properties of OXEs and OXE analogues

Selected OXEs and OXE analogues were investigated using UV-Vis spectroscopy regarding their chromophores. All measurements were performed with 40 μM substance concentration in 100 mM Tris-HCl buffer pH 7.4 with 2 mM EDTA/ethylene glycol 20:80, which is further referred to as kinetic thiol assay solvent system. The substance spectra regarding the influence of the substituent in the 5-position of the oxadiazole ring on the molecule chromophore (Figure 21A) show the expected effects.

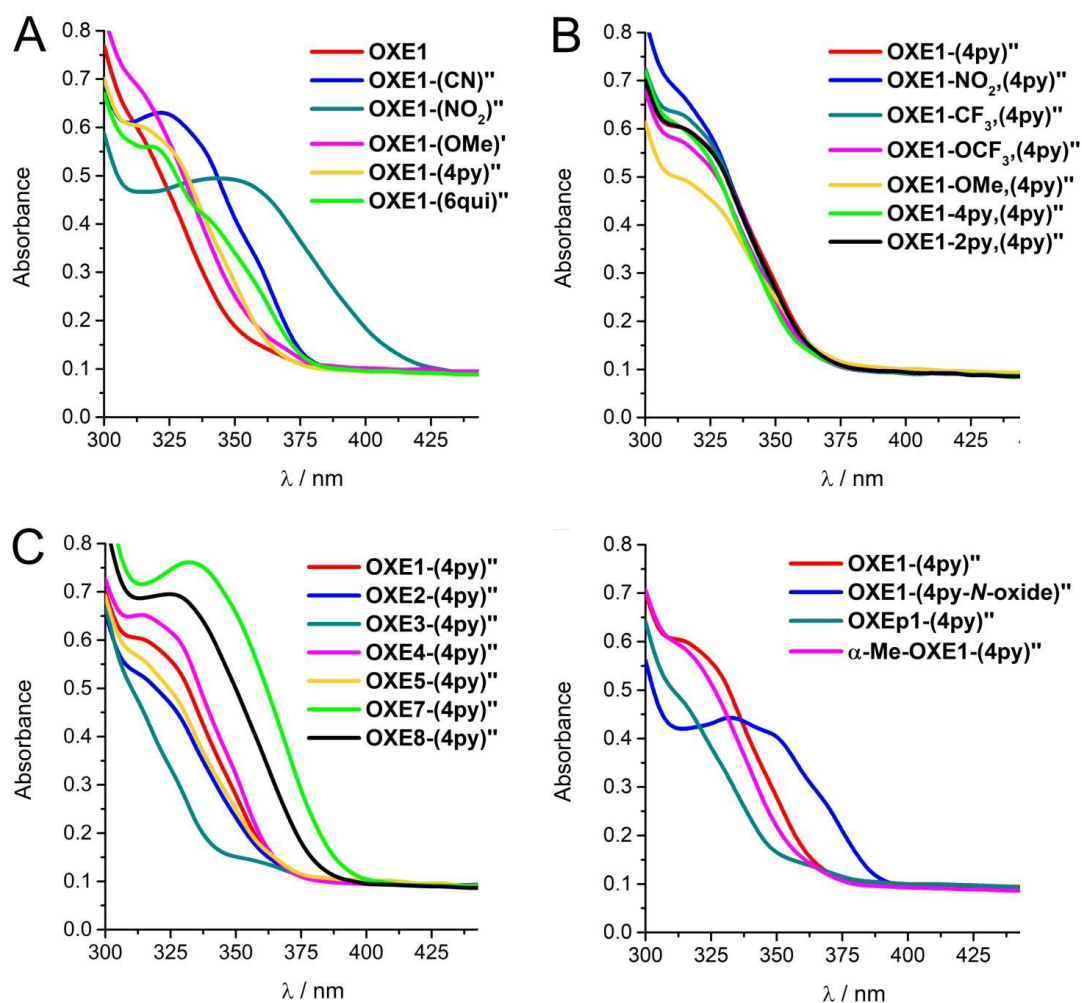


Figure 21: UV-Vis spectra of OXEs. **A:** OXE1s with different substituents in the 5-position of the oxadiazoline ring; **B:** OXE1-(4py)"s with different substituents in the 2-position of the oxadiazoline ring; **C:** OXE-(4py)"s; **D:** Comparison of OXE analogues.

In comparison to the unsubstituted phenyl ring in **OXE1** (Figure 21A, red spectrum), **OXE1**s with a -M substituent show a chromophore enhancement due to an increased conjugated electron system. In Figure 21A, a hyperchromic and bathochromic shift for **OXE1-(CN)"** and a bathochromic shift for **OXE1-(NO₂)"** is visible (blue and cyan, resp.). The electronic rearrangement is shown in Figure 22A for **OXE1-(NO₂)"**. Also, **OXE1-(OMe)"** (pink spectrum) with a +M substituent shows a small chromophore shift towards longer wavelength when compared to unsubstituted **OXE1**, which can also be explained by chromophore enhancement as visualized in Figure 22B.

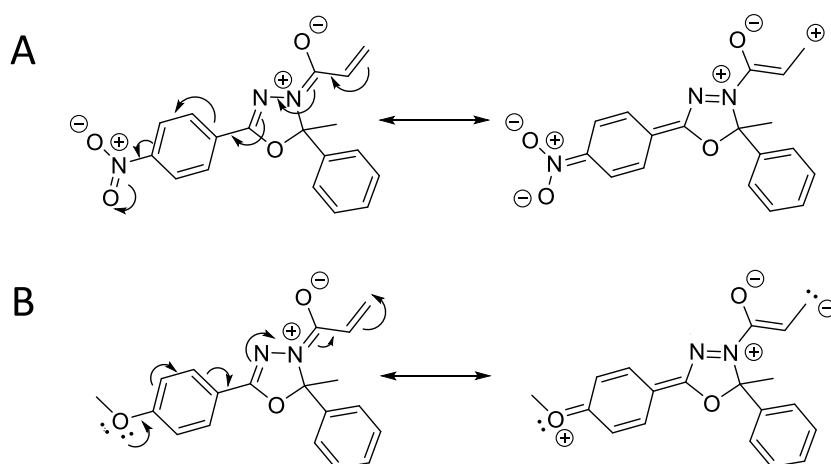


Figure 22: Chromophore enhancement **A:** by -M substituent (**OXE1-(NO₂)**), **B:** by +M substituent (**OXE1-(OMe)**).

The influence of the inductive effect of Ar-X-substituents in position 2 of the oxadiazoline ring is visible in the UV-Vis spectra of **OXE1s** (Figure 21B). Increased UV-Vis intensity in the spectra of **OXE1-(4py)**'s with -I substituents were found, most prominent for **OXE1-CF₃,(4py)**' (Figure 21B, blue spectrum). Only **OXE1-OMe,(4py)**' has a reduced absorbance due to its +I methoxy substituent (yellow).

An overview of the UV-Vis spectra of all synthesized unsubstituted **OXE-(4py)**'s is shown in Figure 21C. In general, phenyl substitution of the enone causes a chromophore enhancement due to an enlargement of the chromophore by the phenyl π -system. Therefore, **OXE8-(4py)**' (black spectrum) and **OXE7-(4py)**' (blue spectrum) have the most prominent chromophores. The influence of the inductive effect on the OXE chromophore is visible by the 2-substituent: A methyl group in position 2 of the oxadiazoline unit (**OXE1**, **OXE4**, **OXE7**) gives a chromophore enhancement in comparison to H in **OXE2**, **OXE5** and **OXE8**. A remarkable decrease in the absorbance intensity is visible in the spectrum of **OXE3-(4py)**' (Figure 21C, cyan spectrum), giving the lowest absorbance intensity of all OXE compounds. These differences are explained by the stabilization of the mesomeric structure (especially the positive charge on nitrogen, see chapter A 1.7, Scheme 7 or Figure 22) by the +I effect of the methyl group. This stabilization is not provided by 2-H and CF₃ in 2-position even destabilizes the system by its -I effect.

When regarding certain **OXE1** analogues, the expected effects are found: *N*-oxidation leading to a bathochromic shift due to chromophore enhancement (Figure 21D, blue) while the chromophore decreases by epoxidation (Figure 21D, cyan).

A 2.3 Kinetic evaluation of OXE and OXE analogues

Pre-investigation of the compounds under assay conditions

All substances were kept in 10 mM DMSO stock solutions at -20 °C and were stable under these conditions for at least one year. Initial UV-Vis screenings of all OXE compounds were used to determine the appropriate parameters for the kinetic measurements. For these investigations, the UV-Vis spectra of the substances were measured in the later used assay concentrations of 40 μ M in kinetic thiol assay solvent system, both as controls and during the reaction with cysteamine. By following the reactions with excess cysteamine concentrations of 20, 100 and 500-fold, it was possible to estimate the appropriate thiol concentration range for each compound and the measurement interval to cover the whole reaction time. Figure 23 shows two examples for these pre-kinetic investigations via UV-Vis. For the reaction of **OXE1** with cysteamine (Figure 23A) an excess of 100-fold thiol is shown and the reaction is finished after 2 h, which is visible because the spectra do not change any more. On the other hand, the reaction of **OXE7-(4py)**^{*} and 500-fold cysteamine is completed within 135 h (more than five days, Figure 23B). These spectra show that **OXE7-(4py)**^{*} is too slow for a full kinetic measurement which should be complete within three days.

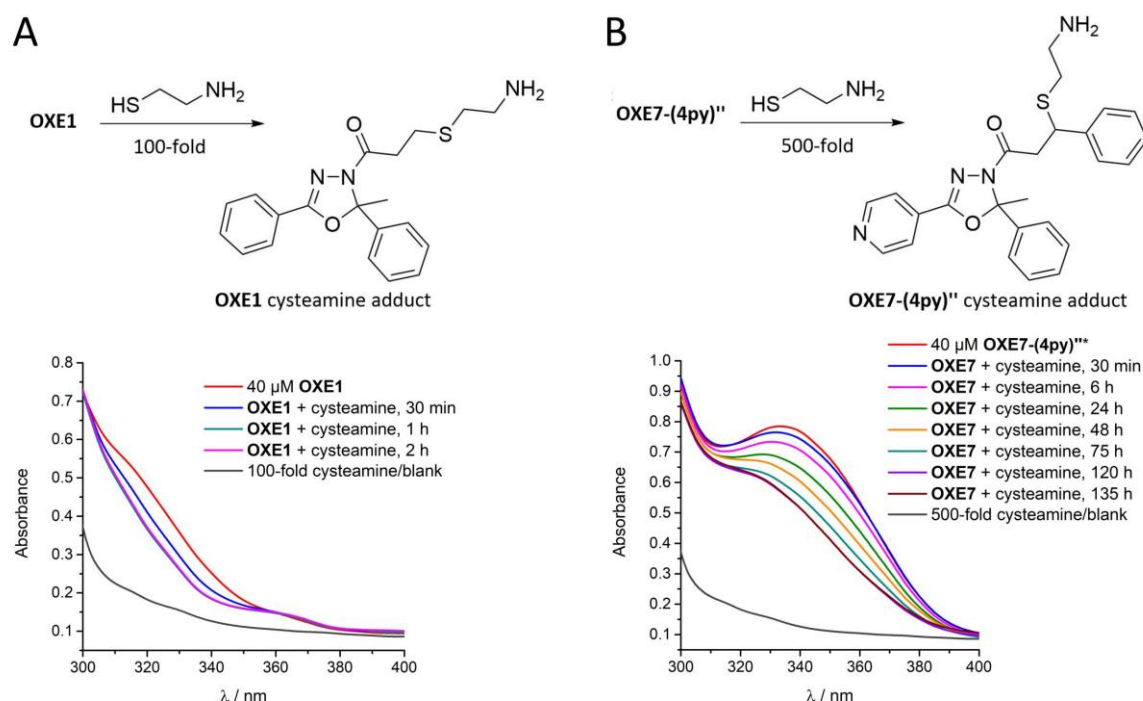


Figure 23: Pre-kinetic UV-Vis investigations: Reaction equations and absorption spectra of 40 μ M OXEs in 100 mM Tris-HCl buffer pH 7.4 with 2 mM EDTA/ethylene glycol 20:80. **A:** **OXE1** + 100-fold cysteamine, **B:** **OXE7-(4py)**^{*} + 500-fold cysteamine, * = **OXE7-(4py)**^{*} is abbreviated **OXE7**.

Additionally, the product formation and potential byproducts were confirmed before the kinetic measurement by LC-MS analysis. With both analysis methods it was furthermore possible to compare both the UV spectra of starting materials and products. Thus, for each substance the best wavelength was determined for the kinetics measurements, i.e. a wavelength at which the absorption bands of educts and products do not overlap. In all **OXE** and **OXE-(4py-N-oxide)** compounds a time-dependent decrease of the absorbance in the range of 300 – 400 nm was observed, which fulfills the requirement for the kinetic UV-Vis measurement. An expected exception was the control compound **OXE1-(4py)**-H₂, which contains no electrophilic enone site for the addition of cysteamine. Furthermore, cysteamine does also not get attached at the heterocycle of **OXE1-(4py)**-H₂. Byproduct formation of this kind was detected in **OXE2s** and **OXE8s** and is discussed later in the stability chapter.

For **OXEps** the product formation was proven by LC-MS but both epoxide-containing compounds were unsuitable for a UV-Vis kinetic measurement, which is discussed in more detail later. However, pre-kinetic UV-Vis and MS studies performed with **OXTEs** show quantitative cleavage of both thioesters and also their cysteamine adducts by the buffer ingredient ethylene glycol (Figure 24). Detectable reaction products are ethylene glycol esters of the cinnamic acids **46** and their cysteamine adducts **47**. Pyridinyloxadiazol-thiol **45** could not be detected under standard LC-MS conditions, therefore further cleavage products of **45** are assumed. Due to this instability, the two compounds **OXTE** and **OXTE-OMe** were excluded from further investigations.

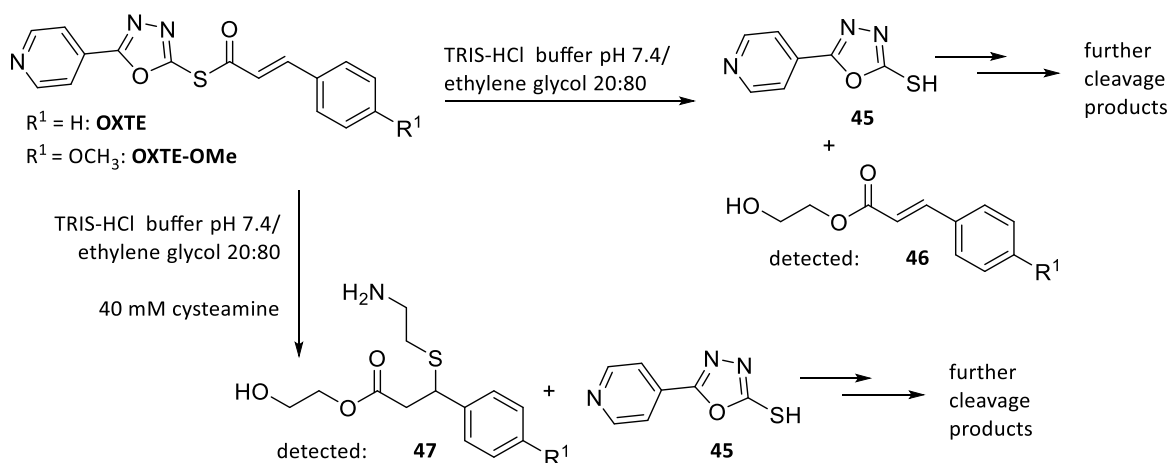


Figure 24: **OXTE** and **OXTE-OMe** and their cleavage products in kinetic thiol assay solvent system.

Chemical reactivities towards thiols were determined by using the electrophilicity assay, which was developed in this work group^[35] and presented in chapter A 1.5, termed as kinetic thiol assay. It is based on the Michael addition of the model thiol cysteamine to the enone moiety of **OXEs** (Figure 25A) and provides the second-order rate constant k_2 . By UV-Vis monitoring of the reaction of **OXEs** with five excess cysteamine concentrations in kinetic

assay buffer, k_{obs} values can be obtained by a decrease of the electrophile chromophore (Figure 25B and C). Plotting of these k_{obs} against their corresponding thiol excess concentrations yields k_2 of the reaction (Figure 25C, insert). When the reaction equilibrium is reached after 30 – 60 min, the chromophore of the **OXE1-(4py)''**-cysteamine adduct has a similar absorbance as the saturated control compound **OXE1-(4py)-H₂**, which is depicted for comparison in Figure 25B.

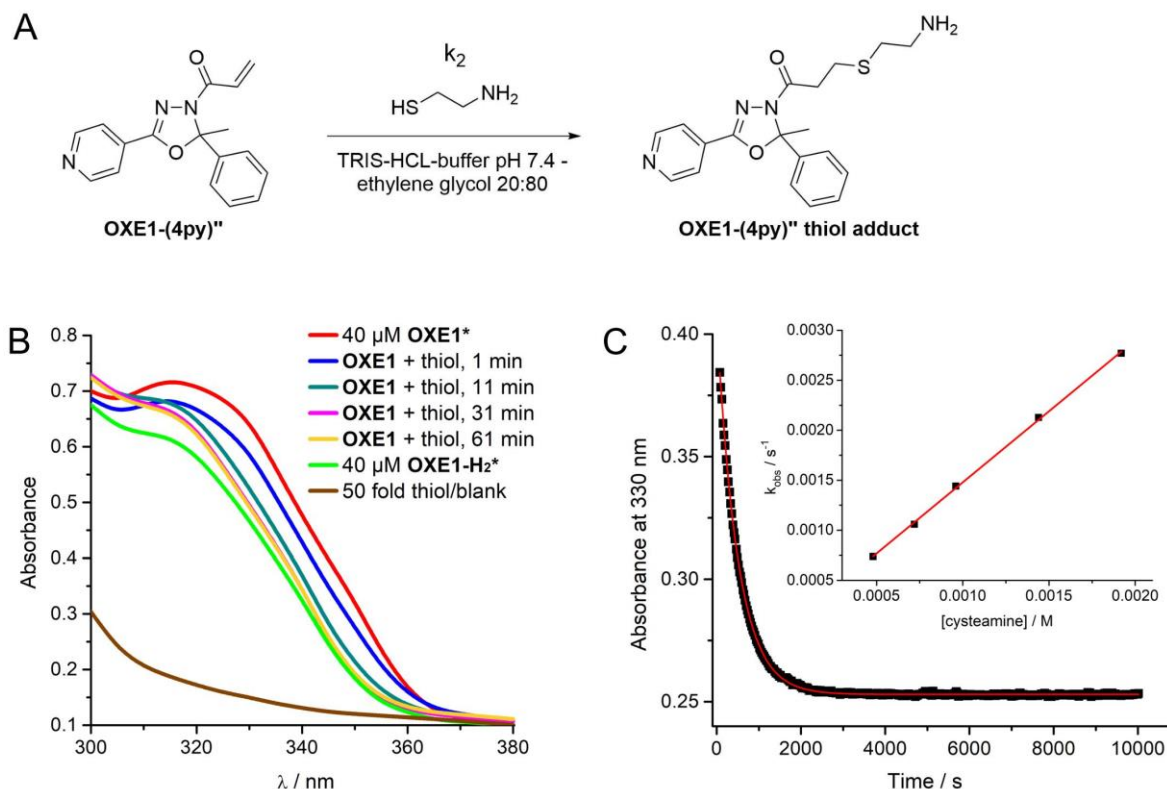


Figure 25: Kinetic studies on the thia-Michael addition of cysteamine (thiol) to **OXE1-(4py)''**. **A:** Reaction equation. **B:** Absorption spectra of 40 μM **OXE1-(4py)''** (**OXE1***) in 100 mM Tris-HCl buffer pH 7.4 with 2 mM EDTA/ethylene glycol 20:80 with and without 50-fold cysteamine. **OXE1-H₂*** refers to **OXE1-(4py)''-H₂**. **C:** Time-dependent absorption of **OXE1-(4py)''** at 330 nm after addition of cysteamine. One representative curve with 36-fold cysteamine is shown to determine k_{obs} by the 1st order decay fit: $y = A_1 \cdot \exp(-x/k_{\text{obs}}) + y_0$. **C insert:** Linear regression to determine k_2 , based on five different thiol concentrations in duplicates.

NMR studies with **OXE1-(4py)''** towards product formation and reversibility

NMR studies were performed as well in order to verify the thiol addition to the enone system of the OXEs. For these experiments, **OXE1-(4py)''** was picked together with a 12-fold excess of cysteamine (Figure 26a) in a solution of 1 mL DMSO-d₆. For optimal results in terms of spectra resolution and signal visibility while avoiding precipitation, **OXE1-(4py)''** was used in an amount of 5 mg (17 μmol , 17 mM).

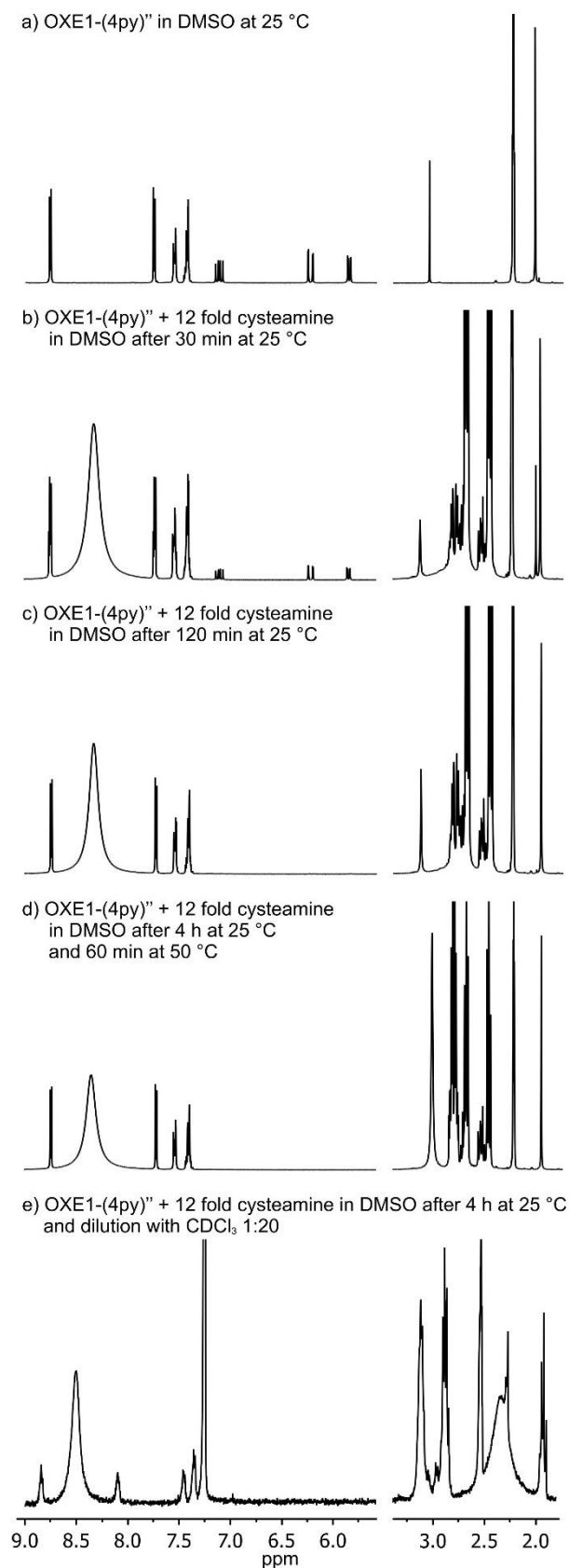


Figure 26: ¹H NMR studies of OXE1-(4py)⁺ with 12-fold cysteamine in DMSO-d₆ under different conditions.

NMR spectra were measured every 30 min over a period of 4 h. The thiol addition is demonstrated by the disappearance of the significant double doublets at 7.13, 6.25, and 5.88 ppm within 4 h, while new signals appear at 3.05 and 2.80 ppm (Figure 26b-c). No shift was detected in all aromatic signals of educt **OXE1-(4py)**'' and product (9 – 7.3 ppm), but a small shift of the methyl group signal from 2.23 to 2.27 ppm is detectable during addition, visible in Figure 26b. Additionally, it was of interest whether reversibility of the Michael addition occurs in this system. Therefore, the NMR sample was heated to 50 °C for 1 h, where reversibility had been found for the compound **α -CN-TMC** under similar conditions.^[36] For **OXE1-(4py)**'', no reversibility was detected (Figure 26d), not even when using a dilution method with CDCl₃^[26] (Figure 26e). All attempts to perform the same experiments with cinnamoyl substituted OXEs led to non-evaluable results due to precipitation and overlapping of the significant signals.

Determination of Michael acceptor activity of OXEs and OXE-N-oxides by kinetic studies

After the pre-kinetic investigations and the determination of all assay parameters, the measurements to determine the second order rate constant k_2 were performed. All parameters are summarized in Table 13 including the overall measuring time for each compound, within which the reaction with excess cysteamine was complete. The results of the kinetic measurements, second-order rate constants k_2 , are also given in Table 13.

Table 13: Parameters and results for the kinetic measurements: Wavelengths, fold cysteamine and time intervals (Δt) used in the kinetic assay for OXEs and resulting k_2 values.

compound	λ [nm]	Fold cysteamine	Δt	t measured ($\Delta t \times 380$)	$k_2 / M^{-1}s^{-1} \pm SD$
OXE1	330	60-108	18 s	1 h 54 min	0.330 \pm 0.017
OXE1-(CN)''	340	12-24	20 s	2 h 7 min	1.20 \pm 0.07
OXE1-(NO ₂)''	355	12-24	20 s	2 h 7 min	1.19 \pm 0.13
OXE1-(OMe)''	330	60-100	25 s	2 h 38 min	0.260 \pm 0.019
OXE1-(4py)''	330	12-48	25 and 30 s	2 h 38 min and 3 h 10 min	1.40 \pm 0.03
OXE1-NO ₂ , (4py)''	330	12-48	20 s	2 h 7 min	2.26 \pm 0.11
OXE1-CF ₃ , (4py)''	330	12-48	20 s	2 h 7 min	1.86 \pm 0.09
OXE1-OCF ₃ , (4py)''	330	12-24	15 s	1 h 35 min	2.10 \pm 0.06
OXE1-OMe, (4py)''	330	12-48	25 s	2 h 38 min	1.18 \pm 0.03
OXE1-4py, (4py)''	330	12-24	15 s	1 h 35 min	2.87 \pm 0.05
OXE1-2py, (4py)''	330	12-24 and 12-48	15 s	1 h 35 min	1.83 \pm 0.19
OXE1-(4py-N-oxide)''	350	12-48 and 20-60	18 s	1 h 54 min	1.51 \pm 0.05
OXE1-(6qui)''	365	50-90	25 s	2 h 38 min	0.534 \pm 0.037
α -Me-OXE1-(4py)'' ^[a]	320-350	500	11 min	3 d (incomplete)	< 0.0001
OXE1-(4py)''-H ₂	320-350	500	11 min	3 d	n. r.
OXE2-(4py)''	330	12-24 and 12-48	15 s	1 h 35 min	3.04 \pm 0.51
OXE2-NO ₂ , (4py)''	330	12-24	15 s	1 h 35 min	4.27 \pm 0.28
OXE2-OMe, (4py)''	330	12-24	19 s	2 h	2.24 \pm 0.14
OXE2-(2na)''	330	12-60 and 30-70	25 and 30 s	2 h 38 min and 3 h 10 min	1.21 \pm 0.11
OXE3-(4py)''	330	100-300	Stopped-Flow	3-5 min	14.3 \pm 3.1

compound	λ [nm]	Fold cysteamine	Δt	t measured ($\Delta t \times 380$)	$k_2 / M^{-1}s^{-1} \pm SD$
OXE4-(4py)''	330	300-500	2 min	12 h 40 min	0.00861 \pm 0.00214
OXE4-(4py-N-oxide)''	370	300-500	4 min	25 h 20 min	0.00764 \pm 0.00088
OXE5-(4py)''	350	300-500	1 and 5 min	6 h 20 min and 31 h 29 min	0.00937 \pm 0.00135
OXE7 ^[a]	320-350	500	11 min	3 d (incomplete)	< 0.0001
OXE7-(4py)'' ^[a]	320-350	500	11 min	3 d (incomplete)	< 0.0001
OXE7-OMe,(4py)'' ^[a]	320-350	500	11 min	3 d (incomplete)	< 0.0001
OXE7-(CF ₃)',(4py)''	340	1000-3000	5 min	31 h 29 min	0.000501 \pm 0.000019
OXE7-(OMe)',(4py)'' ^[a]	320-350	500	11 min	3 d (incomplete)	< 0.0001
OXE8-(OMe)'' ^[a]	320-350	500	11 min	3 d (incomplete)	< 0.0001
OXE8-(4py)''	340	300-500 1000-3000	10 min 5 min	63 h 20 min 31 h 29 min	0.000478 \pm 0.000070
OXE8-NO ₂ , (4py)''	340	300-500 1000-3000	10 min 5 min	63 h 20 min 31 h 29 min	0.000685 \pm 0.000119
OXE8-OMe,(4py)'' ^[b]	340	300-500	133 s	14 h 2 min	< 0.005 ^[b]
OXE8-(OMe) ₂ , (4py)'' ^[b]	350	300-500	135 s	14 h 15 min	< 0.007 ^[b]
OXE8-OMe,(NO ₂)', (4py)'' ^[b]	350	300-500	135 s	14 h 15 min	< 0.01 ^[b]
OXE8-(OMe)', (4py)'' ^[b]	350	300-500	10 min	63 h 20 min	< 0.0009 ^[b]
OXE8-OMe,(OMe)', (4py)'' ^[b]	350	300-500	135 s	14 h 15 min	< 0.005 ^[b]
OXE8-(4py-N-oxide)'' ^[c]	390	300-500 100-300	10 min 9 min	63 h 20 min 57 h	n. e.
OXCE-(4py)'' ^[a]	320-350	500	11 min	3 d (incomplete)	< 0.0001

Reactions were carried out in 100 mM Tris-HCl buffer pH 7.4 with 2 mM EDTA/ethylene glycol 20:80 under pseudo-first order conditions at concentrations of 40 μ M of OXEs together with 12-3000-fold cysteamine. Fold cysteamine: 12-24: 12, 15, 18, 21, 24; 12-48: 12, 18, 24, 36, 48, 12-60: 12, 24, 36, 48, 60; 20-60: 20, 30, 40, 50, 60; 30-70: 30, 40, 50, 60, 70; 60-100: 60, 70, 80, 90, 100; 60-108: 60, 72, 84, 96, 108; 100-300: 100, 150, 200, 250, 300; 300-500: 300, 350, 400, 450, 500; 1000-3000: 1000, 1500, 2000, 2500, 3000; λ [nm]: 320-350 nm: 320, 330, 340, 350 nm was measured over the weekend; [a]: $k_2 < 0.0001 M^{-1}s^{-1}$, reaction is not complete within 3 days and 500-fold cysteamine excess; [b]: cysteamine addition to heterocycle, the represented maximum k_2 values with second addition reaction are given; [c]: k_2 could not be determined, conditions for the two evaluable experiments that gave k_2 values of 0.000933 and 0.00264 $M^{-1}s^{-1}$; n. r. = not reactive, n. e. = not evaluable due to side product formation.

A wavelength of 330 nm was utilized for all **OXE1-X,(4py)''** derivatives, except for the **OXE1-(phenylene-R)''** derivatives, namely **OXE1-(NO₂)''**, **OXE1-(CN)''** and **OXE1-(6qui)''**, where wavelengths of 340 – 365 nm were used for the k_2 determination. All **OXE2**, **OXE3** and **OXE4** compounds were also measured at 330 nm, while **OXE7s** and **OXE8s** were assayed at 340 or 350 nm, according to their chromophore shifted to longer wavelengths. For all 4-pyridyl-N-oxides (**OXE1-(4py-N-oxide)''**, **OXE4-(4py-N-oxide)''**, **OXE8-(4py-N-oxide)''**), the same wavelengths used for their OXE classes were chosen. From the initial screenings the reactivity order of the OXE classes could already be estimated in advance. Additionally, compounds with very low reactivity ($k_2 < 0.0001 M^{-1}s^{-1}$) were detected. Their reaction with cysteamine was not complete within three days and 500-fold excess thiol. For the data analysis it is important to note that the measurements were programmed to collect 380 data points. Table 13 shows that the parameters were varied in some cases, which was done to find the

best combination of excess thiol and Δt . For some slow compounds in particular (**OXE7-(CF₃)',(4py)''**, **OXE8s**) lower thiol concentrations with longer reaction time gave non-evaluable k_{obs} data due to side processes, only partly characterizable via LC-MS (later discussed in "Stability of OXEs in reactivity assay buffer"). Therefore, thiol concentrations of 1000 to 3000-fold excess were also included in the parameters.

In the kinetic measurements k_2 values of $14.3 \text{ M}^{-1}\text{s}^{-1}$ for **OXE3-(4py)''** as the most active electrophile, ranging to the very weak **OXE7** electrophiles with k_2 values below $0.0001 \text{ M}^{-1}\text{s}^{-1}$ were found. In general, for all acrylates (**OXE1s**, **OXE2s**, **OXE3**) a medium strong electrophilicity with values of $14.3 - 1.02 \text{ M}^{-1}\text{s}^{-1}$ was observed. The only exceptions were the more electron-rich compounds **OXE1** and **OXE1-(OMe)''** where the 4-pyridyl substituent in position 5 was replaced by a phenyl or a 4-OMe-phenylene residue, causing k_2 values of 0.338 and $0.260 \text{ M}^{-1}\text{s}^{-1}$. This clearly proves the direct influence of the substitution pattern of the aromatic 5-substituent, since **OXE1-(CN)''** and **OXE1-(NO₂)''** gave k_2 values of 1.20 and $1.19 \text{ M}^{-1}\text{s}^{-1}$, which is in the same range as **OXE1-(4py)''** with $1.40 \text{ M}^{-1}\text{s}^{-1}$. The 6-quinoline residue in **OXE1-(6qui)''** gave a k_2 value of $1.02 \text{ M}^{-1}\text{s}^{-1}$ being significantly lower than for **OXE1-(4py)''**. This proves the effectiveness of 4-pyridyl substituent as an electron-withdrawing substituent when in conjugation. Moreover, after proving that a directly conjugated 5-substituent is very efficient, the question was now whether the substitution pattern at the sp^3 -hybridized 2-position is also influential on the electrophilicity of the enone moiety. Within the **OXE1-R,(4py)''** derivatives, electron-withdrawing residues such as 4-pyridyl with a k_2 value of $2.87 \text{ M}^{-1}\text{s}^{-1}$, 4-NO₂-phenylene ($2.26 \text{ M}^{-1}\text{s}^{-1}$), and 4-OCF₃-phenylene ($2.10 \text{ M}^{-1}\text{s}^{-1}$) gave up to a 2-fold increase of electrophilicity compared to 4-OMe-phenylene ($1.18 \text{ M}^{-1}\text{s}^{-1}$), where a reduction compared to **OXE1-(4py)''** was observed. Thus, the initial concept to have both an sp^2 and sp^3 -coupled handle was achieved. An additional α -substituent on the α,β -unsaturated carbonyl, the enone system, in **α -Me-OXE1-(4py)''** strongly diminished the electrophile activity ($k_2 < 0.0001 \text{ M}^{-1}\text{s}^{-1}$). This is in agreement with results of chalcones (1,3-diphenylprop-2-ene-1-ones), where the **α -Me-TMC** (α -Me-tetramethoxy-chalcone) had a 26-fold lower electrophilicity compared to **α -H-TMC**.^[36] Changing the OXE class from **OXE1** to **OXE2** and **OXE3**, which differ in the non-aromatic substituent at position 3 of the oxadiazoline ring – from Me to H to CF₃ – gave an increase for the k_2 values as exemplified for **OXE2-(4py)''** with $3.04 \text{ M}^{-1}\text{s}^{-1}$ and **OXE3-(4py)''** with $14.3 \text{ M}^{-1}\text{s}^{-1}$. The nature of the neighboring phenylene residue gave further enhancement or reduction of the Michael acceptor activity as seen in the **OXE1** analogues. Switching to **OXE4-(4py)''** and **OXE5-(4py)''** by formally introducing now a crotyl enone unit gave a strong reduction (160-fold) of the electrophilicity, namely k_2 values of 0.00861 and $0.00937 \text{ M}^{-1}\text{s}^{-1}$. This is caused by the electron-donating methyl group on the β -position of the enone unit. Adding a

conjugated aryl ring to the β -position of the enone, which overall represents a cinnamyl residue, gave generally very low electrophilicities for **OXE7s** and **OXE8s**. While k_2 values for **OXE7s** were mostly below $0.0001 \text{ M}^{-1}\text{s}^{-1}$, for **OXE8s** higher reactivities were found. A careful consideration of the LC-MS data of the reactions proved the typical thia-Michael addition for **OXE8-(4py)** and **OXE8-NO₂,(4py)** with k_2 values of 0.000478 and $0.000685 \text{ M}^{-1}\text{s}^{-1}$ while all other more electron-rich **OXE8s** showed a double addition reaction causing false higher k_2 values by further destroying the chromophore. In these cases, the k_2 values given in Table 15 represent only an estimation for the upper limit of k_2 .

For **OXE-(4py-N-oxides)**, similar k_2 values as for their non-*N*-oxide analogues could be detected with $1.51 \text{ M}^{-1}\text{s}^{-1}$ (**OXE1-(4py-N-oxide)**) and $0.00676 \text{ M}^{-1}\text{s}^{-1}$ (**OXE4-(4py-N-oxide)**). A k_2 determination of **OXE8-(4py-N-oxide)** was not possible since the time-dependent absorption curves usually gave no evaluable data due to stability issues and an exothermic side reaction (H_2O condensed on the cover foil, which falsified the absorption). Only two successful experiments yielded k_2 values of 0.000933 and $0.00266 \text{ M}^{-1}\text{s}^{-1}$, which allows to estimate a faster addition of cysteamine to **OXE8-(4py-N-oxide)** than to its non-*N*-oxide analogue.

Kinetic evaluation of OXE_p compounds

During the investigation of the kinetic properties of the epoxide analogues, it turned out that due to the lack of an enone moiety the chromophores of **OXEp1-(4py)** and **OXEp2-(4py)** are unsuitable for the investigation by the kinetic thiol assay. Unlike the reaction of cysteamine with OXEs, which is a thia-Michael addition, the reaction mechanism with both **OXEps** is a nucleophilic substitution reaction, which leads to a ring opening. As the nucleophilic substitution reaction of **OXEp1-(4py)** and cysteamine is a non-regioselective process, both epoxide carbons are attacked by the sulfur nucleophile, leading to two regioisomers which occurred as two diastereomeric pairs each (Figure 28A). Together with the referring enantiomers, the reaction results in a mixture of eight product molecules.

Due to the lack of involved π electrons, no absorption difference between both **OXEps** and their corresponding cysteamine adducts can be detected via UV-Vis spectroscopy. Attempts towards a kinetic measurement of **OXEp1-(4py)** using NMR spectroscopy (Figure 27) was also unsuccessful due to overlapping of relevant analyzable signals 2, 3 even with 12-fold excess of cysteamine (Figure 27b). However, the excess cysteamine cannot be increased very much either since the overlap issue increases dramatically with increasing amount of cysteamine. Therefore, the possibilities of kinetic NMR investigations are limited. The reaction mixture was monitored over 48 h, but after 24 h nearly quantitative cysteamine oxidation in DMSO-d_6 had taken place (Figure 27c). Based on these data, it is not

possible to determine whether **OXEp1-(4py)** reacts with cysteamine at all. Therefore, another method of evaluation had to be found.

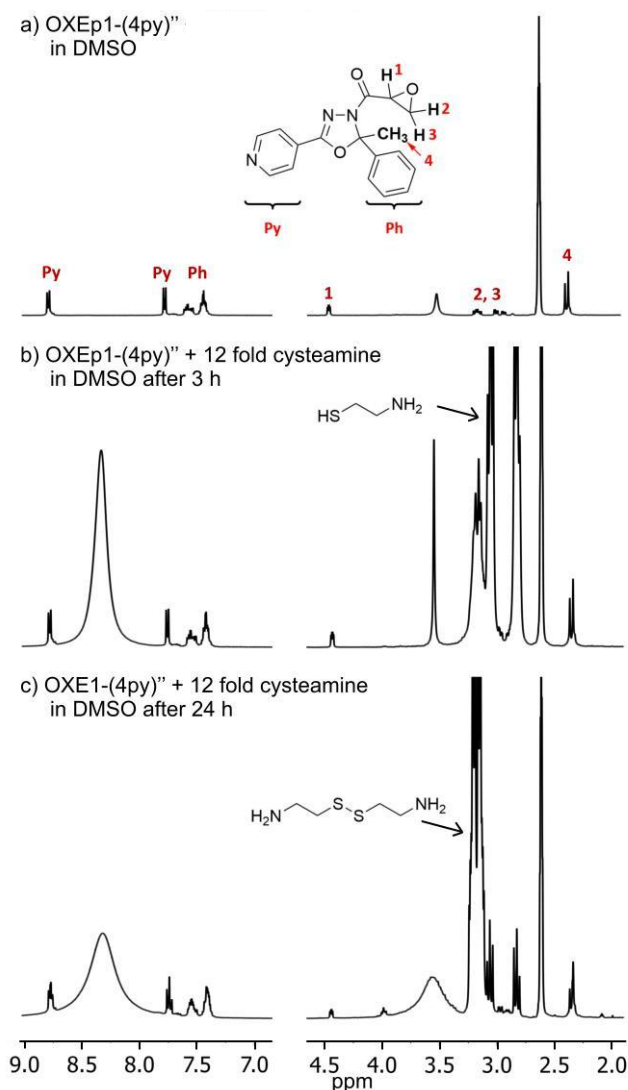


Figure 27: ^1H NMR studies of **OXEp1-(4py)** with 12-fold cysteamine in DMSO- d_6 as attempts for a kinetic measurement.

As a consequence, the reaction was proven by LC-MS and additionally monitored by the time-dependent decrease/increase of the educt/product LC-MS signals (Figure 28B). Encouraged by the first results, it was decided to determine the k_2 for **OXEp1-(4py)** as representative for the two epoxide analogues and for the reaction of epoxide containing compounds with thiols in general. To the best of knowledge, no k_2 for such a reaction has been published so far. **OXE4-(4py)** with a k_2 (determined by the kinetic assay) of $0.00861 \text{ M}^{-1}\text{s}^{-1}$ was selected as comparative compound after approximately estimating the duration of the reaction until equilibrium is reached. Three cysteamine excess concentrations (500-, 600-, 700-fold) were chosen and k_{obs} values were determined in triplicates. Plotting the mean k_{obs} values against their corresponding thiol concentrations yielded the k_2 values. This

method gave k_2 values of $0.00315 \text{ M}^{-1}\text{s}^{-1}$ for **OXEp1-(4py)**" and $0.00381 \text{ M}^{-1}\text{s}^{-1}$ for **OXE4-(4py)**" (Figure 28C). Although the two different detection methods produce different k_2 values for **OXE4-(4py)**", these kinetic constants are of the same order of magnitude and therefore confirm each other. With these data it can be shown that the replacement of the enone functionality by an unsubstituted epoxide leads to the same dramatic decrease of reactivity of **OXE1-(4py)**" as enone methylation in the β -position. Thus, under these conditions, the epoxide unit is a much weaker electrophile than an enone.

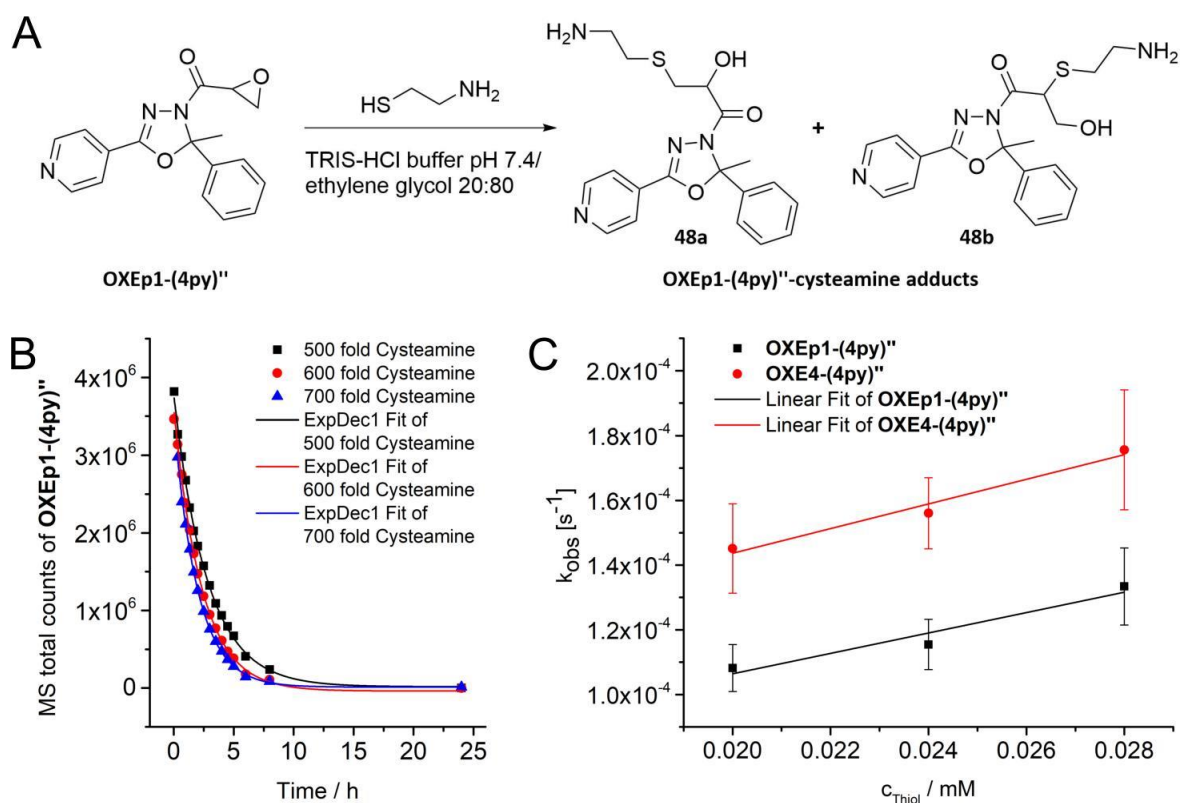
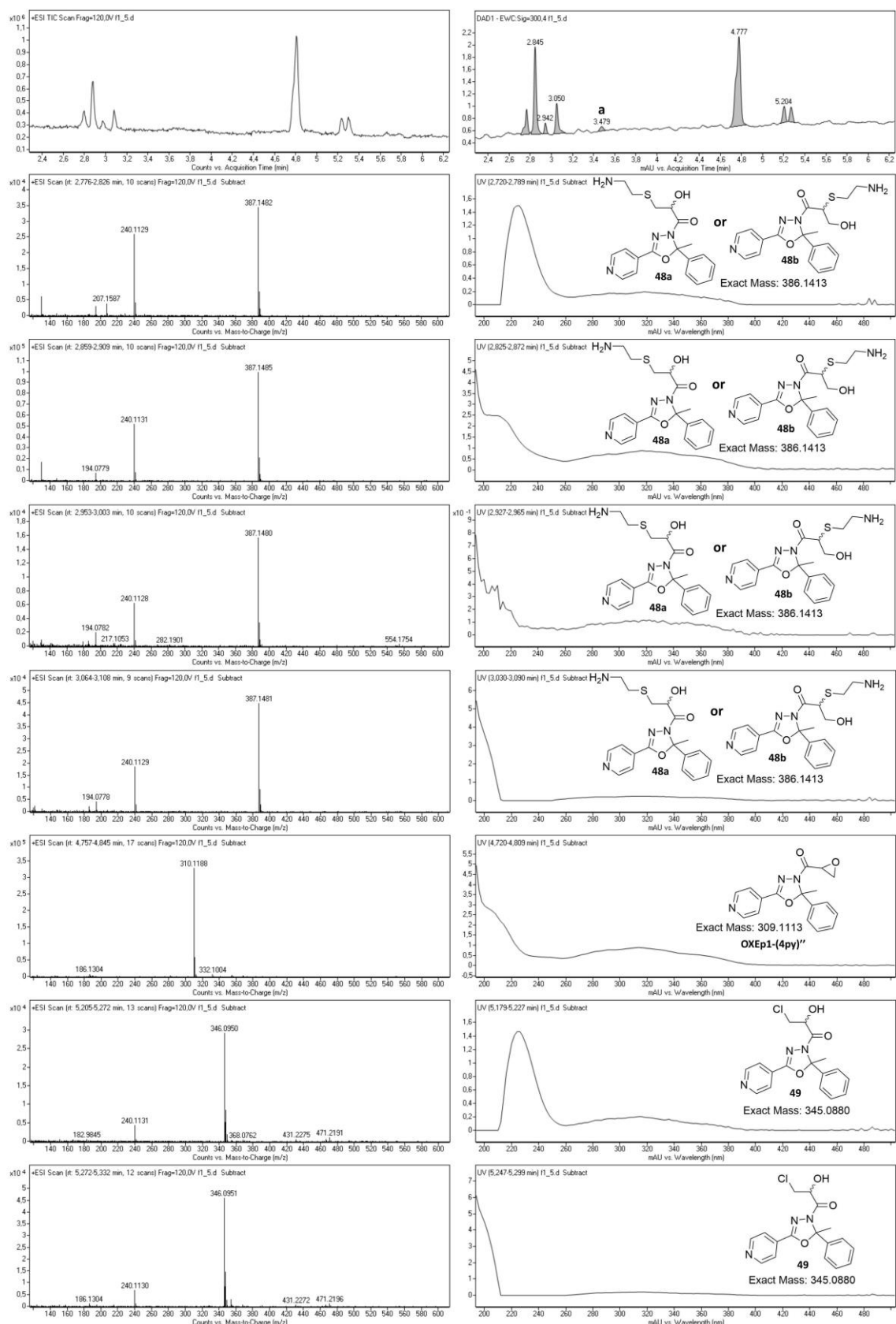


Figure 28: Kinetic studies of the reaction of **OXEp1-(4py)**" with cysteamine. **A:** Reaction equation and structures of the cysteamine adducts. **B:** Decrease of educt during the reactions with excess cysteamine monitored by LC-MS measurement of the total mass signal counts of **OXEp1-(4py)**", one representative experiment for each thiol concentration. **C:** Plotting of k_{obs} values against cysteamine concentrations to determine k_2 based on three different thiol concentrations in triplicates for **OXE4-(4py)**" (red) and **OXEp1-(4py)**" (black). The k_2 values determined from the slope of the linear functions are 0.00381 and $0.00315 \text{ M}^{-1}\text{s}^{-1}$ for **OXE4-(4py)**" and **OXEp1-(4py)**" resp.

Figure 29 shows one representative experiment of **OXEp1-(4py)**" reacting with 500-fold cysteamine in kinetic thiol assay solvent system after 100 min.

Electrophiles of the enone-type and the investigation of their reactivity and biological activity



The product formation showing the two diastereomeric pairs **48a** and **b** (Figure 28A) is proven by the HPLC run. The ring opening products occur in four peaks which represent the two regioisomers and their two diastereomers each, as explained above. Additionally, a small amount of two isomers **49** of the epoxide opening reaction by Cl⁻ (from the Tris-HCl buffer) as a nucleophile was found whose amounts did not change during the time of the reaction. Since the epoxy-CH₂ as the more reactive electrophilic position (for steric reasons) is preferably attacked by nucleophiles, the two isomers detected during the HPLC run can be assigned to structure **49** (Figure 29, again two diastereomers). The other regioisomer of **49** is not formed because Cl⁻ is a much weaker nucleophile than the thiol group.

Stability of OXEs in kinetic thiol assay solvent system

HPLC MS was furthermore used to investigate the stability of OXEs and their cysteamine adducts under assay conditions. OXE species with CH₃ and CF₃ in 2-position of the oxadiazoline ring (**OXE1**, **OXE3**, **OXE4**, **OXE7**) as well as **OXE5-(4py)**'' show no side products in our buffer system. **OXE2** compounds are stable during their short reaction time of < 2 h and show side reactions only after longer incubation time; therefore, their k₂ value is not influenced. Table 14 summarizes the structures and amounts of side reaction products found for **OXE2** and **OXE8** species, which cause a false higher k₂ value in the latter. Especially, the addition of a second cysteamine molecule increases the k₂ by a faster and stronger decrease of the chromophore. This reaction is only found in **OXE8s** with an aromatic methoxy substituent. A mono-adduct with ethylene glycol as alternative nucleophile was found in three compounds after more than 20 h of incubation. Furthermore, hydrolysis can occur on the 5-position of the oxadiazoline ring followed by decomposition to aldehyde and hydrazide fragments (**54**, Table 14 and later, Scheme 17) and was detected in **OXE2-(2na)**'', **OXE8-OMe,(4py)**'' and **OXE8-(4py)-N-oxide)**''. The LC-MS analysis results of **OXE8-(OMe)',(4py)**'' are shown as an example for the detected compounds in Figure 30 for the control and in Figure 31 for the reaction with 500-fold cysteamine.

Table 14: Results of LC-MS studies of **OXE2s**, **OXE8s** and control compounds **OXAc**, **OXE1-(4py)''-H₂** and **OXE8-(4py)''-H₂**. The reaction products with cysteamine and the buffer stability was investigated.

Compound	k_2 [$M^{-1}s^{-1}$] \pm SD	Single cysteamine addition	Double cysteamine addition (52)	Ethylene glycol addition (53)	Hydrolysis (54)
OXE2-(4py)''	3.04 \pm 0.51	+++ (50)	+	+	-
OXE2-NO₂, (4py)''	4.27 \pm 0.28	> 95% (50)	-	-	-
OXE2-OMe, (4py)''	2.24 \pm 0.14	++ (50)	++	-	-
OXE2-(2na)''	1.21 \pm 0.11	++ (50)	-	-	++
OXE8-(OMe)'	< 0.0001	> 95% (50)	-	-	-
OXE8-(4py)''	0.000478 \pm 0.000070	> 95% (50)	-	tr.	-
OXE8-NO₂, (4py)''	0.000685 \pm 0.000119	> 95% (50)	-	-	-
OXE8-OMe, (4py)''	< 0.005	++ (50)	++	-	+
OXE8-(OMe)₂, (4py)''	< 0.007	+++ (50)	++	-	-
OXE8-OMe, (NO₂)', (4py)''	< 0.01	+++ (50)	+	-	-
OXE8-(OMe)', (4py)''	< 0.0009	++ (50)	++	++	+
OXE8-OMe, (OMe)', (4py)''	< 0.005	+++ (50)	+	-	-
OXE8-(4py-N-oxide)''	not evaluable ^[a]	++ (50)	-	-	++
OXAc-(4py)''	-	++ (51)	-	-	-
OXAc-NO₂, (4py)''	-	tr. (51)	-	-	-
OXAc-OMe, (4py)''	-	> 95% (51)	-	-	-
OXE1-(4py)''-H₂	-	-	-	-	-
OXE8-(4py)''-H₂	-	+(51)	-	-	-

Reactions were carried out in 100 mM Tris-HCl pH 7.4 with 2 mM EDTA/ethylene glycol 20:80 with 40 μ M of OXE and OXE analogues and 500-fold excess of cysteamine. The incubation time prior injection was 5-24 h and the HPLC analysis was performed at 40 °C column temperature. Molecular ratios were estimated by UV detection and the relative amounts are assigned as follows: +++ = 95-60%; ++ = 60-30%; + = 30-5%; tr. = traces, < 5%; [a]: due to exothermic side reactions and product mixture, for the results of two successful experiments see Table 13.

Electrophiles of the enone-type and the investigation of their reactivity and biological activity

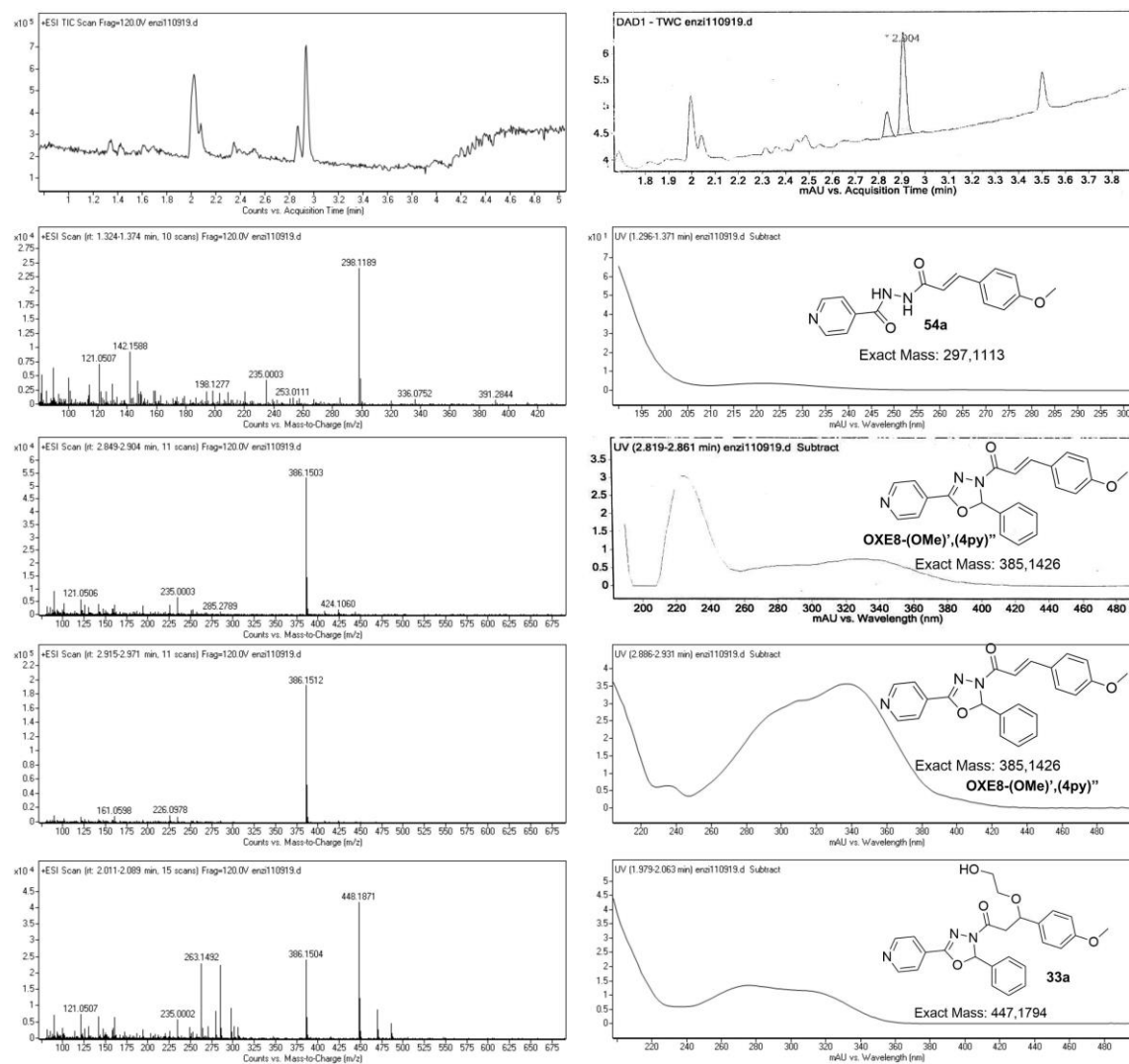


Figure 30: OXE8-(OMe)',(4py)' in kinetic thiol assay solution after 24 h.

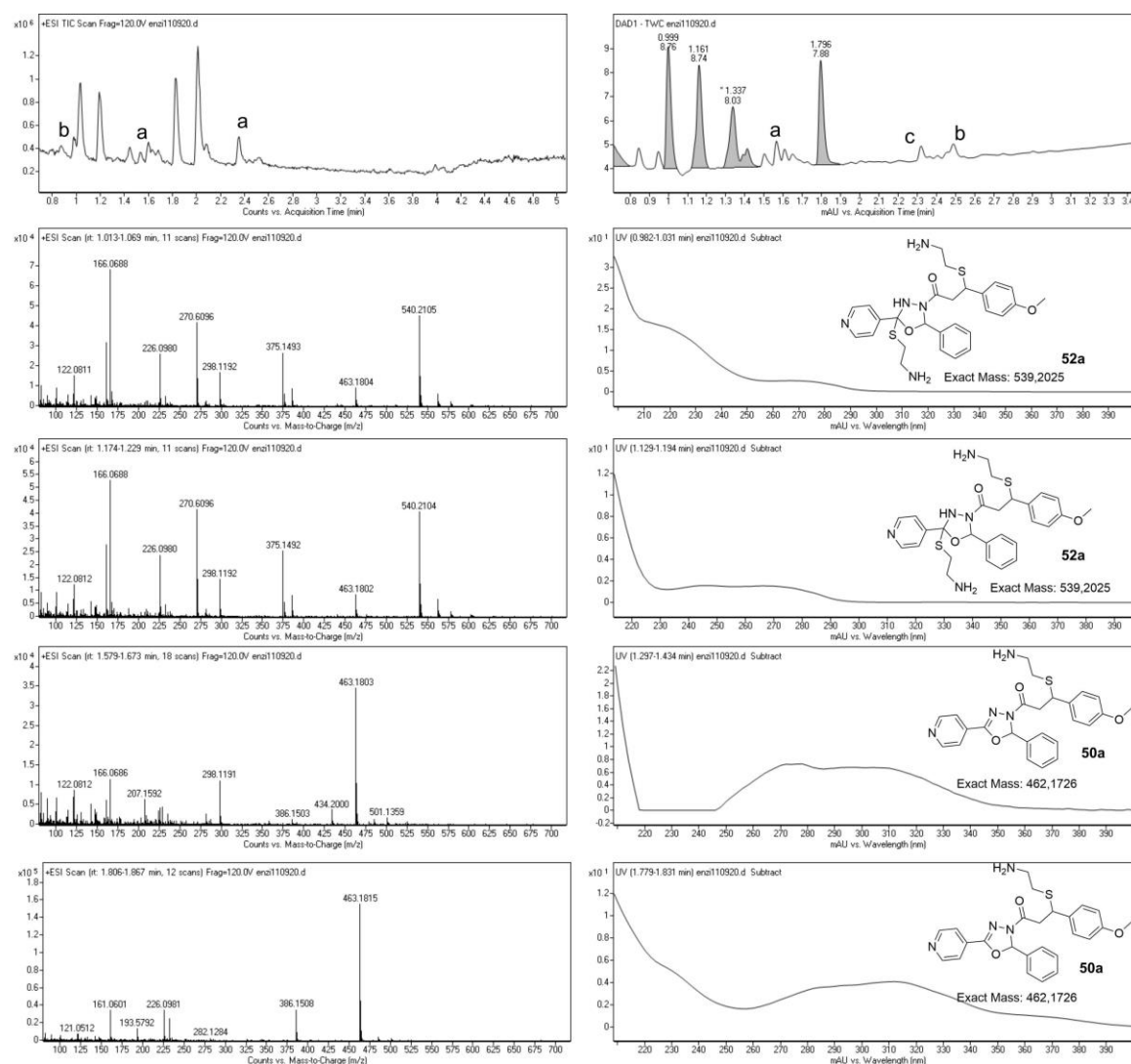


Figure 31: OXE8-(OMe)-(4py) with 500-fold cysteamine after 24 h in kinetic thiol assay solution. a: unknown compounds; b: solvent system fragment, no compound in MS detectable; c: no UV-Vis absorbance > 200 nm.

OXAcs and **OXE8-(4py)-H₂** were used to verify the second cysteamine addition observed in the LC-MS measurements of **OXE2**s and **OXE8**s. They were incubated with 500-fold cysteamine and investigated by LC-MS and UV-Vis spectroscopy as well. In all cases, a decay in the UV-Vis spectra was found, which indicates an addition to the conjugated system. An anticipated addition to the 5-position of the 1,3,4-oxadiazoline ring as the only available electrophilic site was confirmed by MS data, showing the surprisingly stable adducts (Figure 32). Figure 33 shows the detailed results of the UV-Vis measurements. This reaction was fast for **OXAc-OMe-(4py)** (Figure 33C), moderate fast in **OXAc-(4py)** (Figure 33A) and **OXE8-(4py)-H₂** (Figure 33D) and very slow in the NO₂ analogue (Figure 33B). This finding is consistent with the additional products found in **OXE2**s and **OXE8**s. No cysteamine adduct was found in this experiment when performed with another enone-free control compound **OXE1-(4py)-H₂**. These data show that a less electron-rich heterocycle with a 2-H

substituent in **OXE8s** and **OXE2s** allows the second cysteamine addition while the more electron-rich CH₃ group (e.g. in **OXE1s**) prevents this.

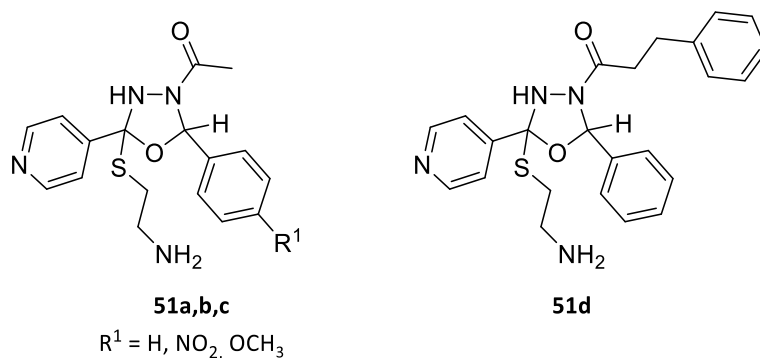


Figure 32: Structures of the products proven by LC-MS of the control compounds **OXAc-(4py)''** (**51a**), **OXAc-NO₂-(4py)''** (**51b**), **OXAc-OMe-(4py)''** (**51c**) and **OXE8-(4py)''-H₂** (**51d**) with 500-fold cysteamine.

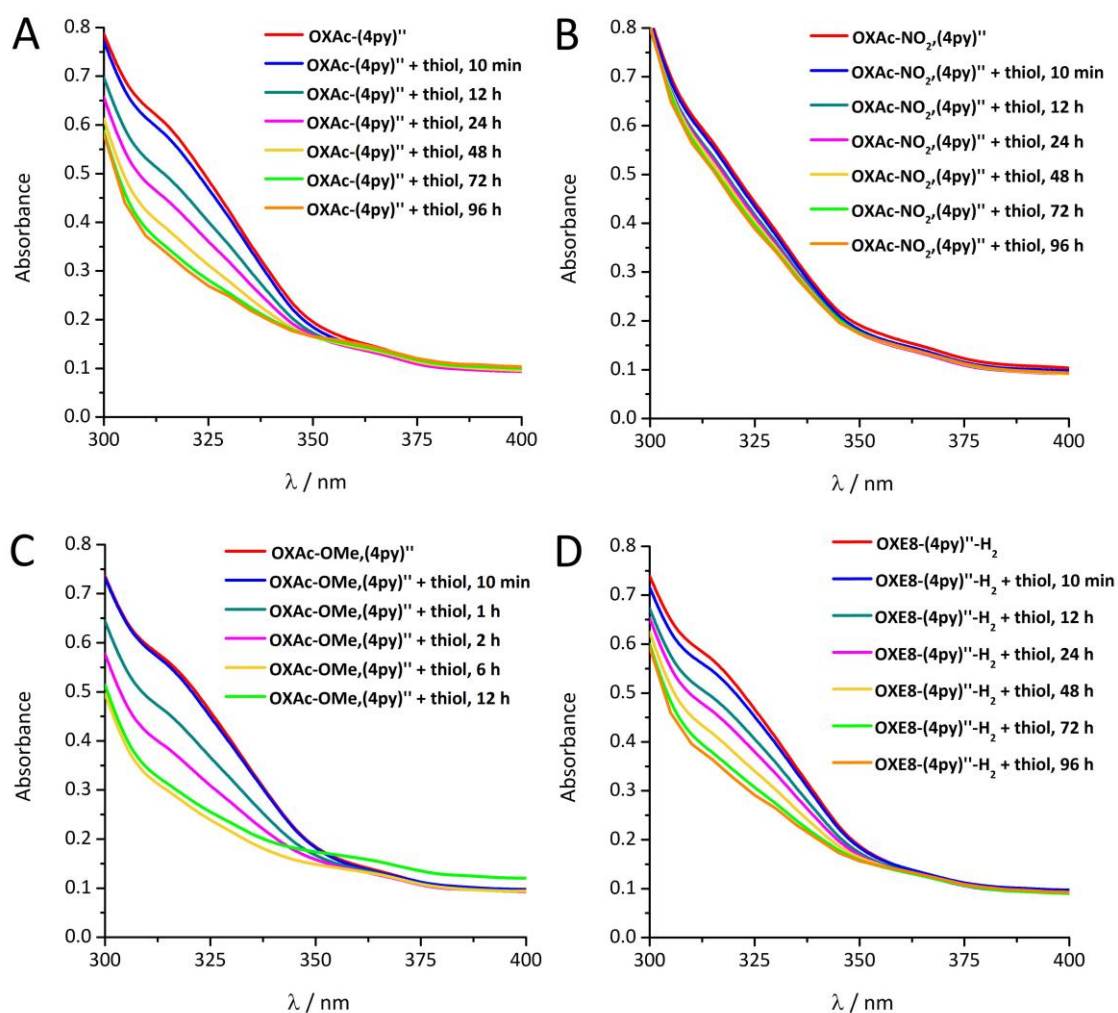
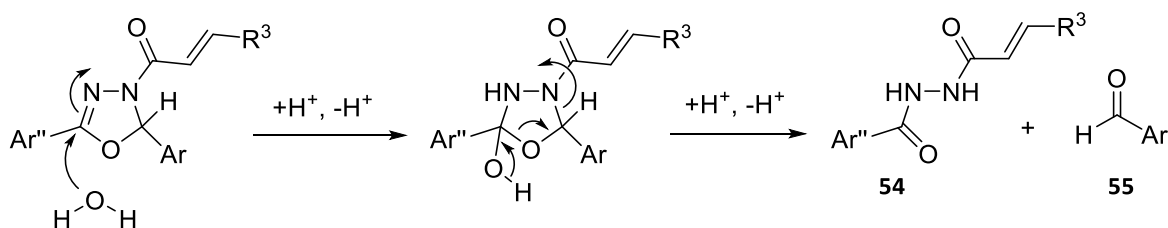


Figure 33: UV-Vis spectra of the time-dependent reactions of the control compounds. **A:** **OXAc-(4py)''**, **B:** **OXAc-NO₂-(4py)''**, **C:** **OXAc-OMe-(4py)''** and **D:** **OXE8-(4py)''-H₂** with cysteamine. Reactions were carried out in kinetic thiol assay solvent system with an electrophile concentration of 40 μM and 20 mM (500-fold excess) cysteamine.

The observed hydrolysis (Table 14) is a cleavage of the heterocycle of the concerned **OXE8s** to the *N*-cinnamoylisonicotinohydrazides **54** and the corresponding aldehydes **55**. This decay occurs for example in **OXE8-(OMe)',(4py)''** in the form of compound **54a** (Figure 30).



Scheme 17: Reaction to form hydrolysis products **54** for **OXE2-(2na)''**, **OXE8-OMe,(4py)''** and **OXE8-(4py-N-oxide)''**. Ar = Ph, C₄H₆OCH₃, Ar'' = pyridyl, py-*N*-oxide, naphthyl, R³ = H, Ph.

For **OXE8-(4py-N-oxide)''**, this effect was very pronounced and led to assay conditions, under which a precise k_2 determination fails as described before. *N*-Cinnamoylisonicotinohydrazide **54a** was additionally synthesized^[43] and investigated towards toxicity and anti-inflammatory activity to exclude any effect caused by this substance.

A 2.4 Biological evaluation of the OXE and OXE analogues substance library

MTT test for the determination of cell viability

In order to find a concentration range in which the tested compounds show no toxicity, the MTT test described in chapter A 1.3 was performed. As explained there, the IC₅₀ value is a measure for that concentration when the cell viability of the murine macrophages RAW264.7 is reduced by 50%. This number can be used to compare the toxicities of compounds. For testing other cellular phenomena, the IC₂₀ value (toxicity limit) is the important factor that indicates the concentration range below which the influence of a reduction of cell viability is neglected in general. The results of both the MTT assay and the later discussed NO-inhibition assay are summarized in Table 15. The toxicity limit is here given as the highest concentration used for the subsequent NO-inhibition assay.

Table 15: Biological data of OXEs and OXE analogues: evaluation of toxicity and NO-inhibition properties in murine macrophages RAW264.7.

Compound	Cell viability MTT (IC ₅₀ / μM) ± SD	Toxicity limit MTT	Inhibition of NO production (IC ₅₀ / μM) ± SD
OXE1	35.8 ± 3.8	10	6.94 ± 0.34
OXE1-(CN)''	32.9 ± 2.8	5	30.6 ± 10.8
OXE1-(NO₂)''	41.8 ± 13.4	10	24.9 ± 20.7
OXE1-(OMe)''	43.1 ± 3.5	25	11.0 ± 0.2
OXE1-(4py)''	38.3 ± 3.9	10	5.34 ± 1.66
OXE1-NO₂,(4py)''	29.5 ± 8.1	6.25	6.31 ± 2.32

Compound	Cell viability MTT (IC ₅₀ / μ M) \pm SD	Toxicity limit MTT	Inhibition of NO production (IC ₅₀ / μ M) \pm SD
OXE1-CF ₃ , (4py)''	24.2 \pm 8.6	6.25	5.15 \pm 3.43
OXE1-OCF ₃ , (4py)''	29.1 \pm 1.6	6.25	3.35 \pm 0.98
OXE1-OMe, (4py)''	46.6 \pm 5.8	30	5.06 \pm 2.57
OXE1-4py, (4py)''	32.0 \pm 1.8	10	5.09 \pm 2.38
OXE1-2py, (4py)''	39.6 \pm 2.6	10	5.60 \pm 3.06
OXE1-(4py-N-oxide)''	46.7 \pm 9.9	15	22.2 \pm 7.0
OXE1-(6qui)''	37.4 \pm 1.8	10	7.16 \pm 1.30
α -Me-OXE1-(4py)''	78.5 \pm 10.6	3.13	n. a.
OXE1-(4py)''-H ₂	> 100 ^[a]	50	n. a.
OXE2-(4py)''	34.2 \pm 0.1	12.5	6.01 \pm 1.39
OXE2-NO ₂ , (4py)''	24.6 \pm 1.6	5	4.22 \pm 1.16
OXE2-OMe, (4py)''	32.3 \pm 5.3	10	6.72 \pm 1.24
OXE2-(2na)''	67.1 \pm 4.6	40	42.6 \pm 31.5
OXE3-(4py)''	40.6 \pm 3.5	20	13.6 \pm 2.2
OXE4-(4py)''	89.6 \pm 31.4	50	61.8 \pm 20.0
OXE4-(4py-N-oxide)''	> 100 ^[a]	> 100	69.4 \pm 26.8
OXE5-(4py)''	29.1 \pm 3.4	10	n. a.
OXE7	84.4 \pm 8.8	40	n. a.
OXE7-(4py)''	47.5 \pm 4.5	6.25	n. a.
OXE7-OMe, (4py)''	17.0 \pm 2.0	5	n. a.
OXE7-(CF ₃)', (4py)''	31.8 \pm 5.4	15	n. a.
OXE7-(OMe)', (4py)''	43.6 \pm 10.5	6.25	n. a.
OXE8-(OMe)'	107 \pm 44	50	> 50 ^[b]
OXE8-(4py)''	18.9 \pm 4.8	0.4	n. a.
OXE8-NO ₂ , (4py)''	14.7 \pm 7.3	1	n. a.
OXE8-OMe, (4py)''	54.1 \pm 4.3	6.25	n. a.
OXE8-(OMe) ₂ , (4py)''	83.7 \pm 31.3	40	n. a.
OXE8-OMe, (NO ₂)', (4py)''	8.40 \pm 2.80	1	n. a.
OXE8-(OMe)', (4py)''	52.8 \pm 7.5	25	n. a.
OXE8-OMe, (OMe)', (4py)''	65.4 \pm 12.4	20	n. a.
OXE8-(4py-N-oxide)''	73.3 \pm 6.2	75	63.1 \pm 17.0
OXE8-(4py)''-H ₂	80.1 \pm 12.1	50	[c]
OXCE-(4py)''	50.5 \pm 10.6	6.25	n. a.
OXEp1-(4py)''	> 100 ^[a]	50	27.7 \pm 1.0
OXEp2-(4py)''	> 100 ^[a]	50	36.8 \pm 3.0
OXAc-(4py)''	> 100 ^[a]	> 100	> 100 ^[b]
OXAc-OMe, (4py)''	> 100 ^[a]	> 100	101 \pm 22
OXAc-NO ₂ , (4py)''	> 100 ^[a]	> 100	> 100 ^[b]
<i>N</i> -cinnamoylisonicotino- hydrazide (54a)	97.8 \pm 23.7	50	n. a.

Biological data were measured and/or evaluated by Dita Fritsch, Sina Malenke, Monika Enzinger and Sabine Amslinger. [a]: no relevant toxicity was observed up to a concentration of 100 μ M; [b]: small anti-inflammatory activity was found up to a concentration of 50 or 100 μ M respectively due to toxicity limits; [c]: small pro-inflammatory effect was detected; n. a. not active at concentrations up to toxicity limit.

OXEs overall show a concentration range for the IC₅₀ values of 8.4 – 89.6 μ M with a mean value of 46.1 μ M. More specifically, for the kinetically most active 13 **OXE1s** most values are 24.2 – 46.7 μ M, where **OXE1-CF₃, (4py)''** is most toxic. A similar IC₅₀ range was found for **OXE2s**, **OXE3-(4py)''** and **OXE5-(4py)''** (24.6 – 40.6 μ M) with the exception of **OXE2-(2na)''** which is less toxic (IC₅₀ of 67.1 μ M). The toxicity of **OXE1-(4py)''** decreases to

78.5 μM by the influence of α -methyl substitution in **α -Me-OXE1-(4py)** and even further to an IC_{50} of $> 100 \mu\text{M}$ by the reduction of the enone double bond in **OXE1-(4py)-H₂**. In contrast, no general toxicity trend was discovered in both phenyl-substituted classes **OXE7s** and **OXE8s**. Very different IC_{50} values were obtained for these compounds, varying from 8.40 μM for **OXE8-OMe,(NO₂),(4py)** as most toxic substance from our library to $> 100 \mu\text{M}$ in **OXE8-(OMe)**.

Regarding the OXE analogues, only a small toxicity ($\text{IC}_{50} > 100 \mu\text{M}$) was found for both **OXEp** compounds, however the toxicity limit (IC_{20}) was 50 μM . In each case of the *N*-oxidized compounds, a lower toxicity was found than in their non-*N*-oxide analogues. This effect is only minor in **OXE1-(4py-N-oxide)** and **OXE4-(4py-N-oxide)** while **OXE8-(4py-N-oxide)** has a four times lower IC_{50} of 73.3 μM than **OXE8-(4py)** (18.9 μM) and is therefore less toxic. **OXAc** compounds, decorated with an acyl unit, were found to be not toxic at all up to a concentration of 100 μM ($\text{IC}_{20} > 100 \mu\text{M}$).

Inhibition of NO production

As explained in chapter A 1, the pro-inflammatory protein iNOS (inducible NO synthase) is an enzyme, whose gene expression is regulated by the transcription factor NF- κ B. Thus, its activity in a cellular setting is a model system for the induction of anti-inflammatory activity in immune cells like macrophages. The cell line RAW264.7 has been extensively used for this purpose and was also applied in prior studies involving the electrophilicity-tuned **α -X-TMCs**. In the case of **α -X-TMCs** the observed inhibition of NO-production was directly linked to the inhibition of NF- κ B activation.^[36] In this work, the in-vitro activity of iNOS in LPS-stimulated murine macrophages RAW264.7 (inhibition of NO production) was used as a measure for anti-inflammatory activity. It is important to note that only concentrations of neglectable toxicity, determined by MTT test, were used for all compounds. All results in the form of IC_{50} values are summarized in Table 15.

In **OXE1s** and **OXE2s**, single-digit IC_{50} values (μM) for NO inhibition of 3.35 – 7.16 μM with a mean of 5.58 μM were found; exceptions are non-pyridinyl-substituted **OXE1-(OMe)**, **OXE1-(CN)**, **OXE1-(NO₂)** and **OXE2-(2na)**. The non-pyridinyl compounds **OXE1-(CN)** and **OXE1-(NO₂)** stand out clearly as they show a five to six times lower IC_{50} value of NO inhibition with 30.6 and 24.9 μM , respectively, while the completely unsubstituted **OXE1** is still in the single-digit range (6.94 μM). **OXE2-(2na)** in comparison with the other **OXE2s** also shows only a small activity with an IC_{50} of 42.6 μM . Steric hindrance and/or electron-withdrawing effect of the additional substituents may result in a weakened binding to pharmacological targets. In other **OXE1s** and **OXE2s** a further influence of functional groups of any kind is not apparent: electron-withdrawing units like in **OXE1-NO₂,(4py)** as well as the

methoxy-containing compound **OXE1-OMe,(4py)** have similar IC_{50} of 6.31 and 5.06 μM , respectively. *N*-Oxidation in **OXE1-(4py-N-oxide)** decreases the IC_{50} to 22.2 μM . But the strongest influence on the anti-inflammatory activity is caused by an alteration of the enone functionality itself: α -CH₃-substituted **α -Me-OXE1-(4py)** and the reduced compound **OXE1-(4py)-H₂** are inactive in concentrations up to 100 μM . Substitution of the β -position of the enone unit with CH₃ or phenyl also has a dramatic effect on the NO inhibition properties of OXEs. Both **OXE4** compounds have an IC_{50} value ten times lower than the average **OXE1s**, while **OXE5-(4py)** and **OXE7s** are inactive. This is also true for most **OXE8s** with the exceptions **OXE8-(OMe)** and **OXE8-(4py-N-oxide)**, where low activity with IC_{50} values > 50 μM was found. For these considerations, however, it must be taken into account that most inactive compounds could not be tested at higher concentrations due to toxicity. Possibly, biological activity could be detected in **OXE8s** and **OXE7s** at concentrations higher than their corresponding toxicity limit. However, this would not be useful, since the anti-inflammatory effect is to be shown in living cells triggered by LPS in their NO synthesis, but otherwise functioning normally. The metabolism of cells damaged or dying by toxins deviates from the normal one and could falsify the assay results.

OXE3-(4py), the most active substance in the kinetic assay, has an IC_{50} value of 13.6 μM and therefore a surprisingly lower activity than **OXE1s** and **OXE2s**. Since it is the only 2-CF₃ compound in this library, it cannot be assumed that this is a general effect with OXEs containing CF₃ in the 2-position such as the hypothetical **OXE6s** and **OXE9s**, CF₃ analogues of **OXE4/5s** and **OXE7/8s**. Trapping of strong electrophiles by the intracellular detoxification agent GSH (**7**) is a possible explanation for lower biological activity, as shown before in **α -X-TMCs**. However, this effect was only found for the very strong electrophiles **α -NO₂-TMC** and **α -CN-TMC** with k_2 values of 749 and 5750 $\text{M}^{-1}\text{s}^{-1}$ resp,^[36] so it is unlikely that this is also true for **OXE3-(4py)** ($k_2 = 14.3 \text{ M}^{-1}\text{s}^{-1}$). Probably, pharmacokinetic and pharmacodynamic properties such as cellular uptake and cytoplasmic stability of **OXE3-(4py)** are impaired by the CF₃ group. Weakened target binding properties due to altered steric and electronical properties in the molecule could be further reasons for such a finding.

A relatively moderate NO inhibition activity was found in the iNOS assay for both epoxide-containing compounds. Steric and electronic effects explain the expected lower anti-inflammatory activity of **OXEp2-(4py)** (36.8 μM) in comparison to **OXEp1-(4py)** (27.7 μM): the additional methyl group in **OXEp2-(4py)** lowers the electrophilicity of the enone and increases steric hindrance. Compared to **OXE1-(4py)** and **OXE4-(4py)**, these epoxide analogues are less active but also less toxic, as discussed above. This may be due to inactivation by other nucleophiles and/or cellular detoxification mechanisms. Small amounts of a chloride adduct were at least proven for **OXEp1-(4py)** by LC-MS (chapter A 2.3, Figure 29).

Nevertheless, these two substances are the second-best class of substances (after **OXE1s**, **OXE2s** and **OXE3-(4py)**) in this library in terms of biological activity.

In summary, for the compound library presented in this study, a free enone or epoxide unit is indispensable for anti-inflammatory activity. This was proven by the completely inactive control compounds **OXE1-(4py)**-H₂ and the three **OXAc**s lacking the electrophilic unit. Furthermore, covalent binding as the key part in the mechanism of action is confirmed. However, the electrophilic unit is also responsible for the cell toxicity that was detected in concentrations of up to 100 μM. Biological activity generally corresponds to the reactivity of the compounds. With the exception of **OXE3/5**, both reactivity and biological activity of OXE classes follows the order **OXE1/2** >> **OXE4** > **OXE8** > **OXE7**. The various substituents within the individual OXE classes were not observed to have an influence on the anti-inflammatory activity. But a reactivity fine-tuning is achieved in **OXE1/2/8** which is explained by ±I/M effects. Another exception of the activity/reactivity correlation is **OXEp1-(4py)**. Interestingly, its biological activity is remarkably high compared to its low reactivity. In comparison to **OXE1-(4py)**, the *k*₂ value of **OXEp1-(4py)** is around 400 times lower, but the IC₅₀ value, which represents biological activity, is only five-fold reduced. However, **OXE4-(4py)**, which is in the same range of electrophilicity as **OXEp1-(4py)**, shows a 12-fold decrease of the IC₅₀ value of biological activity. Together with the promising low toxicity of **OXEps**, one can assume a more specific mode of action due to the different electrophilic moiety.

Based on the data collected, the best window for reactivity/activity in non-toxic concentrations is achieved by an α,β-unsubstituted enone unit in combination with pyridine in 5'-position. These properties were found in **OXE1s** and **OXE2s** with *k*₂ values in the general range of 1.18 – 4.27 μM. For compounds with these structural features and *k*₂, single-digit IC₅₀ values for an anti-inflammatory activity in the iNOS test were found. It can be assumed that further new compounds with these structural characteristics will also show reactivities and biological activities in this range. There are indications that 2-CF₃ substitution on the heterocycle (in further, new compounds of the **OXE3** class) leads to lower anti-inflammatory activity despite higher reactivity. All the discussed influences on structural features of **OXE1-(4py)** as model compound are summarized in Figure 34 for OXEs with an enone functionality and Figure 35 for OXE derivatives with variations on the electrophilic position.

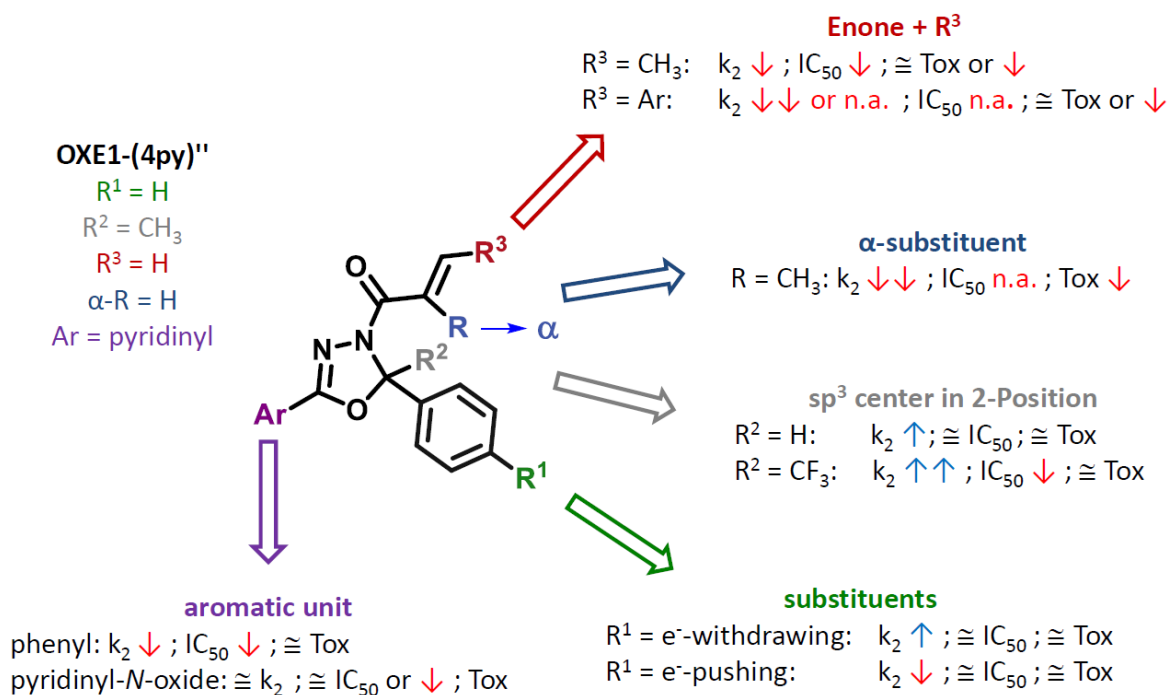


Figure 34: Summary of influences of substituents on **OXE1-(4py)"**. IC_{50} = anti-inflammatory activity, NO-inhibition, Tox = toxicity.

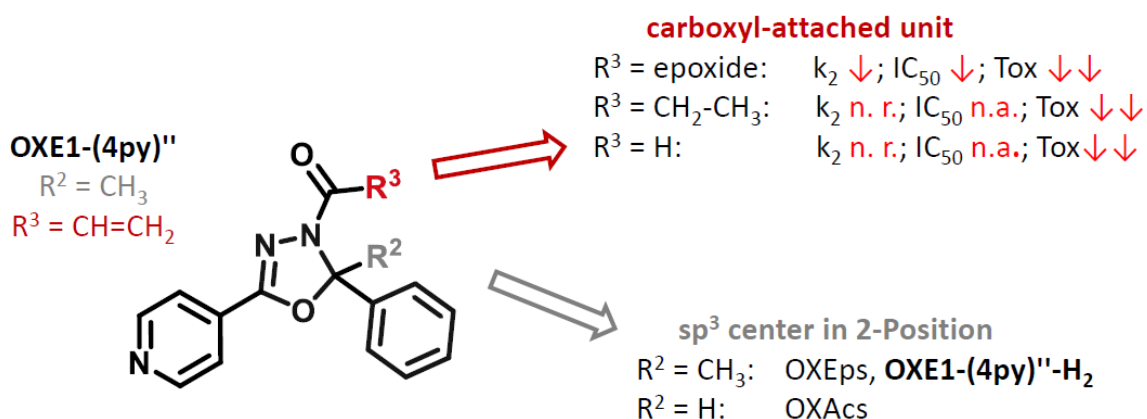


Figure 35: Summary of influences by OXE analogue structural features. IC_{50} = anti-inflammatory activity, NO-inhibition, Tox = toxicity.

Figure 36 shows the relationship between reactivity in terms of the k_2 value and biological activity in terms of the IC_{50} value of some substances that are active in both categories using logarithmic representation. The approximately linear relationship is represented by a straight line. Beside **OXE4s** as lower limit a few outliers can be seen. The "agglomeration area" of the **OXE1s** and **OXE2s** in the graph indicates the current upper limit of the structure activity optimization, which is achieved with the previous substances of the library. It remains the exciting question, in which directions the further development of this field of research must go, in order to exceed these limits.

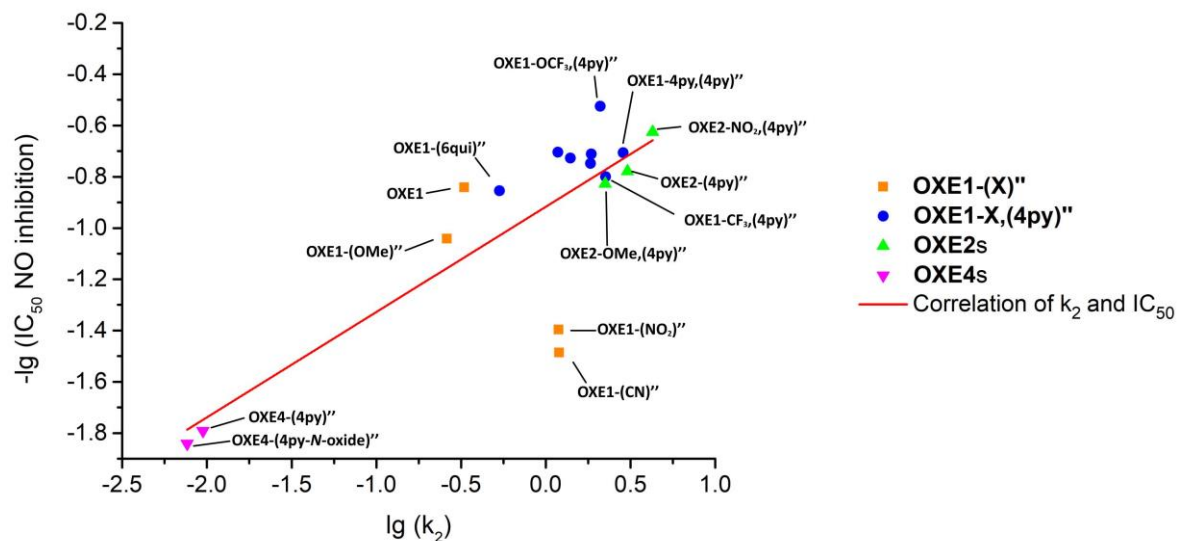


Figure 36: Correlation of the inhibition of the NO production with the second-order rate constants (as $\lg(k_2)$) of the Michael addition of biologically active OXE compounds with cysteamine. Blue circles: **OXE1-X,(4py)**'s, remaining substances in the cluster are **OXE1-(4py)**'', **OXE1-NO₂,(4py)**'', **OXE1-OMe,(4py)**'', and **OXE1-2py,(4py)**''; orange squares: **OXE1-(X)**'s, green triangles: **OXE2s**, pink triangles: **OXE4s**. Line indicates the linear fit.

A 3 Results and Discussion II: Reactivity assessment of further electrophiles by the kinetic thiol assay

A 3.1 Reactivity modification of phenylacrylamide derivatives as reactive units in drug development

These results are not published yet (05/2019).

Participants in this work are: Lukas Wirth: Synthesis of all substances (Master thesis, University of Regensburg, 2016), Monika Enzinger: UV-Vis, kinetics and LC-MS investigations, Sina Malenke and Dita Fritsch: Biological testing.

All compounds of the type **29**, **30**, **31** and **32** (chapter A 1.8) were screened in the UV-Vis thiol assay in a concentration of 80 μM , due to the small chromophore, and with 20, 100 and 500-fold excess cysteamine. In the spectra of the four sulfonamide compounds **30** and **31**, no cysteamine-induced chromophore decreases or any other differences due to a reaction with cysteamine were observed, however a cysteamine adduct was proven for **30a** by LC-MS. Therefore compounds **30** and **31** were excluded from further kinetic investigations because the minimum requirements concerning their chromophores were not fulfilled. More precisely, the lack of a sufficient chromophore > 300 nm leads to no detectable difference between the spectra of products and cysteamine adducts. For compounds **29** and **31**, a time-dependent decrease of the chromophore due to a Michael addition could be detected in their UV-Vis spectra. The cysteamine adduct formation was proven by LC-MS and both educts and products were stable under assay conditions for > 72 h. Compounds **29** only gave a very slow and incomplete reaction within three days ($k_2 < 0.0001 \text{ M}^{-1}\text{s}^{-1}$) with barely visible difference in the educt/product spectra. Figure 37 shows the chromophores of all substances **32** which were recorded during the usual screening prior to the kinetic assay.

Due to their absorbance maxima < 300 nm, most substances were measured at wavelength between 305 and 315 nm except nitrophenylacrylamides **32a** and **32f**, where the NO_2 groups in ortho and para-position lead to a chromophore enhancement as shown for OXEs in chapter A 2.2. Outstanding is the absorbance band with $\lambda_{\text{max}} = 330$ nm for the para- NO_2 substituted compound **32f** (Figure 37A, blue spectrum). All substances were subsequently investigated in the kinetic thiol assay and their reactivity towards cysteamine in the form of k_2 values was determined.

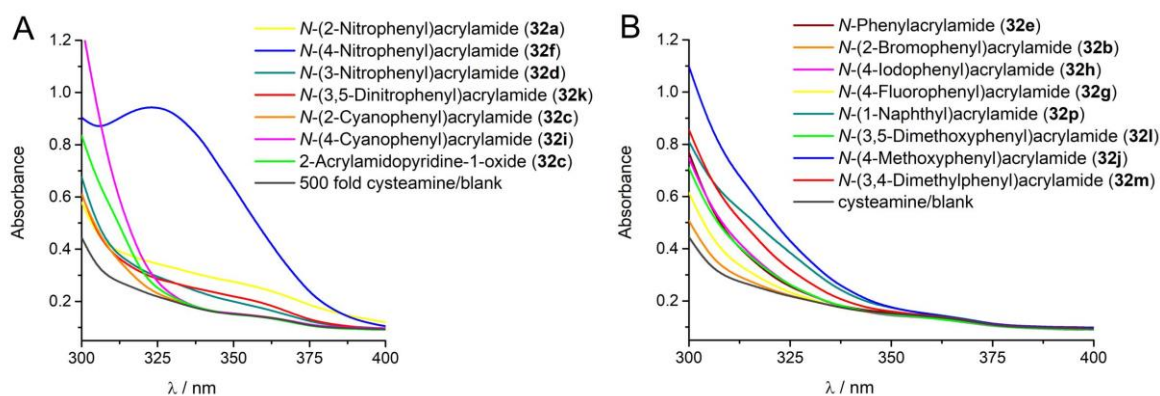


Figure 37: Chromophores of acrylamide derivatives **32** in a concentration of 80 μM in Tris-HCl buffer pH 7.4 with 2 mM EDTA/ethylene glycol 20:80, bearing substituents with **A:** electron-withdrawing properties; **B:** electron-pushing properties and halogen substituents.

The assay conditions and results are summarized in Table 16. k_2 values in the range of 5.20 – 0.00250 $\text{M}^{-1}\text{s}^{-1}$ were obtained for the 16 evaluated compounds **32**. The substances are listed in descending order according to their reaction rates.

Table 16: Parameters for the kinetic measurements and kinetic results of *N*-phenylacrylamide derivatives, listed in descending order according to k_2 values.

Compound	Fold cysteamine	Δt	λ / nm	k_2 / $\text{M}^{-1}\text{s}^{-1} \pm \text{SD}$
(2-Acrylamido)pyridine-1-oxide 32o	12-24	18 s	315	5.20 \pm 0.80
2-(Nitrophenyl)acrylamide 32a	20-100	18 s	350	0.548 \pm 0.027
4-(Nitrophenyl)acrylamide 32f	20-100	25 s	330	0.365 \pm 0.021
3,5-(Dinitrophenyl)acrylamide 32k	60-140	18 s	305	0.310 \pm 0.030
2-(Cyanophenyl)acrylamide 32c	100-300	32 s	310	0.111 \pm 0.012
4-(Cyanophenyl)acrylamide 32i	100-300	32 s	310	0.102 \pm 0.010
(2-Pyridinyl)acrylamide 32n	100-300	43 s	305	0.0925 \pm 0.0072
3-(Nitrophenyl)acrylamide 32d	100-500	43 s	305	0.0493 \pm 0.0094
2-(Bromophenyl)acrylamide 32b	100-500	32 s	310	0.0263 \pm 0.0027
4-(Iodophenyl)acrylamide 32h	100-300	2 min	310	0.0190 \pm 0.0021
(1-Naphthyl)acrylamide 32p	100-300	2 min	310	0.0137 \pm 0.0024
3,5-(Dimethoxyphenyl)acrylamide 32l	100-300	4 min	310	0.0134 \pm 0.0002
4-(Fluorophenyl)acrylamide 32g	100-300	2 min	310	0.00787 \pm 0.00131
<i>N</i> -Phenylacrylamide 32e	300-500	2 min	305	0.00523 \pm 0.00018
4-(Methoxyphenyl)acrylamide 32j	300-500	8 min	310	0.00458 \pm 0.00052
3,4-(Dimethylphenyl)acrylamide 32m	300-500	4 min	310	0.00250 \pm 0.00003
<i>N</i> -(Pyridin-4-yl)-cinammamide 29a	500	11 min	305-330	< 0.0001
<i>N</i> -Phenylcinnamamide 29b	500	11 min	305-330	< 0.0001

Fold cysteamine: 12-24: 12, 15, 18, 21, 24; 20-100: 20, 40, 60, 80, 100; 60-140: 60, 80, 100, 120, 140; 100-300: 100, 150, 200, 250, 300; 100-500: 100, 200, 300, 400, 500; λ [nm] for slow compounds **29**: 305, 310, 320, 330.

The reactivities generally follow a trend caused by the influence of the inductive and mesomeric effects of the aromatic substituents on the enamide unit and are observed in the

following order: pyridine-*N*-oxide > 2/4-NO₂ > CN > halogen > OCH₃ > CH₃. By far the highest k_2 of 5.20 M⁻¹s⁻¹ was found for the only 2-pyridine-*N*-oxide compound **32o**. After **OXE3-(4py)**, this is the second fastest k_2 of all investigated compounds presented in this work. Compared with (2-pyridinyl)acrylamide **32n**, its *N*-oxidation leads to a reactivity enhancement of about 50-fold. This effect can be explained by the strong electron-withdrawing properties of the *N*-oxide which is moreover in close proximity to the reactive unit. NO₂ and CN-substituted compounds have moderate reactivity due to the -I and -M effects of those groups. In both cases the ortho-substituted compounds **32a** and **32c** are slightly more reactive than para-substituted **32f** and **32i**. This is explained by the shorter distance of the ortho substituent to the reactive unit, increasing the influence of the -I effect. An exception is meta-NO₂ substituted phenylacrylamide **32d** with a reactivity ten-fold lower than its ortho or para regioisomers, which is due to the lacking -M effect. However, this is compensated by the presence of two nitro groups in **32k**, whose reactivity is again in the moderate range due to a strong -I effect. The halogen-substituted compounds are next in the order of reactivity with low k_2 values of 0.0263 – 0.00787 M⁻¹s⁻¹, which is due to their -I effect, in comparison to unsubstituted *N*-phenylacrylamide (**32e**). It follows the order Br > I > F which is the same as found in **α -X-TMCs**.^[36] Methoxy- and methyl-substituted phenylacrylamides **32j** and **32m** have the expected lowest reactivity of investigated compounds, which is attributable to +I and +M effects.

A small selection of substances was tested in the two cell assays, toxicity (MTT assay) and anti-inflammatory activity (iNOS assay). Results are summarized in Table 17. For these few examples it was found that reactivity and anti-inflammatory activity correlate in the order of substituents on the acryl group:

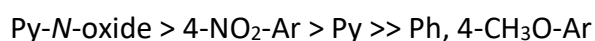


Table 17: Biological data of a selection of *N*-phenylacrylamides and *N*-phenylethanesulfonamide (**30a**). Evaluation of toxicity and NO-inhibition properties in murine macrophages RAW264.7.

Compound	Cell viability MTT (IC ₅₀ / μ M) \pm SD	Inhibition of NO production (IC ₅₀ / μ M) \pm SD
2-Acrylamido)pyridine-1-oxide 32o	36.7 \pm 8.1	5.95 \pm 2.2
4-(Nitrophenyl)acrylamide ^[a] 32f	56.7	2.74
(2-Pyridinyl)acrylamide 32n	> 100	33.6 \pm 10.2
<i>N</i> -Phenylacrylamide ^[a] 32e	> 100	> 100
4-(Methoxyphenyl)acrylamide ^[a] 32j	> 100	> 100
<i>N</i> -Phenylethanesulfonamide ^[a] 30a	47.1	2.49

Biological data were measured and analyzed by Sina Malenke. [a]: These data are taken from the master thesis of Lukas Wirth^[44] and are listed here again for comparison purposes.

Activities in the single-digit μM range were found for the three most reactive substances. A clear correlation between toxicity and activity can be detected.

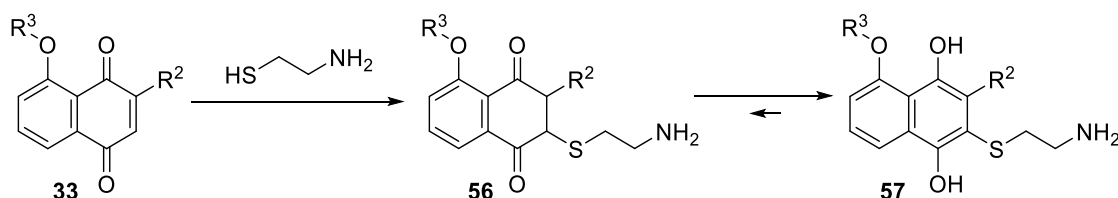
In summary, it can be said that for the presented simplified molecules with different reactive units only representatives bearing the acrylamide unit could be kinetically measured. The spectra show the minimum requirements for the chromophore of test substances to be used in the kinetic thiol assay. The reactivity of the enamide unit can be adjusted by substituents with different electronic properties on the aromatic ring in a range of four orders of magnitude. The order of reactivity follows very exactly the electronic influences of the substituents. Even the expected reactivity differences for *o/m/p* substitution in the case of NO_2 are visible.

A 3.2 Juglone and juglone derivatives and their reactivity towards cysteamine

These results are not published yet (05/2019).

Participants in this work are: Sebastian Schlegel: Synthesis and cell viability (toxicity) assay of all substances (Master thesis, University of Regensburg, 2016), Sina Malenke: Anti-inflammatory (iNOS) assay of all substances, Monika Enzinger: UV-Vis and MS investigations, evaluation of the iNOS assay (together with Sina Malenke).

UV-Vis and LC-MS investigations of juglone derivatives **33** (chapter A 1.8, structures see Table 18, below) were performed in the kinetic thiol assay solvent system to show whether a kinetic evaluation with cysteamine is possible for this substance class. Therefore, the electrophiles were investigated under assay conditions in a concentration of 40 or 80 μM and 500-fold excess cysteamine. In contrast to OXEs or *N*-phenylacrylamides, alkylation of juglone-type electrophiles is expected to lead to an increase in absorption and/or a shift of λ_{max} towards higher wavelengths. This is due to the immediate tautomerization of the products **56** to the more stable aromatic naphthyl system **57** (Scheme 18).



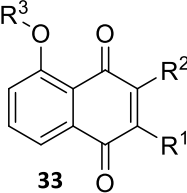
Scheme 18: Michael addition of cysteamine to juglone (**33a**) and its 3-substituted derivatives and the tautomerization to the naphthyl core structure; $\text{R}^2 = \text{H}, \text{OCH}_3, \text{Br}, \text{Cl}, \text{F}, \text{N}_3, \text{NH}_2, \text{piperidino}, \text{morpholino}$; $\text{R}^3 = \text{OH}, \text{OCH}_3$.

In general, the recorded UV-Vis spectra for the different juglone compounds at a concentration of 40 μ M were only partially analyzable due to low absorbance intensities. Therefore, assay concentrations of 80 μ M of juglones **33** and 40 mM cysteamine was used for higher intensity of the compounds absorbances. All UV-Vis spectroscopic data are summarized in Table 18; Figure 38 and Figure 39 show the time-dependent UV-Vis spectra of all 15 compounds of the juglone derivative library without and with 500-fold cysteamine.

In the case of 3-azido-*O*-methyljuglone (**33i**) no distinct educt band in the control sample could be observed, but a broad absorbance band in the range of 330 - 550 nm. Several overlapping absorbance bands in the spectra of the halide-substituted *O*-methyljuglones **33d**, **33f** and **33g** were found. An amine-substituent in 2-position (2-piperidinojuglone **33m**, 2-morpholinojuglone **33o**) led to a broad absorbance band in the region of 420-520 nm each. All other compound control spectra show more or less distinct absorbance bands at 420 and 430 nm and of $A < 0.4$ in general. Exceptions are 3-piperidino- and 3-morpholinojuglone (**33l** and **33n**) with maxima at 480 and 500 nm.

UV-Vis spectra of 3-amino-substituted juglones **33j** and **33k** did not show a change in the presence of cysteamine within 24 h, which indicates no reaction. In all other cases, the absorbance bands in the reaction mixtures increase in intensity compared to those of the controls, as expected for a reaction. A distinct new band, which appeared after the start of the reaction (10 min) could be found in the spectra of non-methylated juglones **33a**, 3-bromojuglone (**33c**), 3-chlorojuglone (**33e**) and 3-azidojuglone (**33h**), all at wavelengths of 360 – 365 nm. For all other compounds a time-dependent decrease of the educt absorbance was observed. However, methylated Juglones, namely *O*-methyljuglone (**33b**), 3-bromo-*O*-methyljuglone (**33d**), 3-chloro-*O*-methyljuglone (**33f**) and 3-azido-*O*-methyljuglone (**33i**) gave several absorbance maxima with cysteamine, which indicates product mixtures. For the basic substituted piperidino- and morpholinojuglones a new product band could be observed at 360 – 370 nm together with an increased absorbance in the range of 450 – 700 nm. An exception is 3-morpholinojuglone (**33n**) where the 370 nm band is missing. The latter results indicate rather a product mixture due to a reaction with the buffer system and/or cysteamine than a clear, single mono-addition reaction, which can be kinetically evaluated by the kinetic thiol assay.

Table 18: Summary of the UV-Vis experiment of 40 μ M of juglone derivatives with/without 500-fold cysteamine in the kinetic thiol assay solvent system.

Compound				Analyzable absorbance bands								
33	R ¹	R ²	R ³	control		reaction						
				λ_{\max} [nm]	A _{max}	λ_{\max} [nm]	A _{max}	t ^[a]				
 33a juglone 33b <i>O</i> -Methyljuglone 33c 3-Bromojuglone 33d 3-Bromo- <i>O</i> -methyljuglone 33e 2- and 3-Chlorojuglone 33f 3-Chloro- <i>O</i> -methyljuglone 33g 3-Fluoro- <i>O</i> -methyljuglone 33h 3-Azidojuglone 33i 3-Azido- <i>O</i> -methyljuglone 33j 3-Aminojuglone 33k 3-Amino- <i>O</i> -methyljuglone 33l 3-Piperidinojuglone 33m 2-Piperidinojuglone 33n 3-Morpholinojuglone 33o 2-Morpholinojuglone				a	H	H	H	425	0.28	365	0.66	1 h
				b	H	H	CH ₃	405	0.27	355 490	0.48 0.17	12 h
c	H	Br	H	430	0.29	360	0.60	3 h				
d	H	Br	CH ₃	350 410	0.28 0.24	350 490	0.50 0.14	2 h				
e	Cl/H	Cl/H	H	425	0.26	365	0.65	2 h				
f	H	Cl	CH ₃	350 410	0.26 0.24	350 490	0.48 0.15	8 h				
g	H	F	CH ₃	350 400	0.28 0.24	350 490	0.45 0.12	3 h				
h	H	N ₃	H	405	0.26	365	0.52	1 h				
i	H	N ₃	CH ₃	none	-	350 490	0.34 0.12	5 h				
j	H	NH ₂	H	425	0.36	425	0.35	5 h				
k	H	NH ₂	CH ₃	400	0.30	400	0.29	8 h				
l	H	piperidino	H	500	0.29	370	0.46	3 h				
m	piperidino	H	H	430 470-500 ^[b]	0.31 0.28	360	0.46	3 h				
n	H	morpholino	H	480	0.34	none	-	18 h				
o	morpholino	H	H	425	0.37	360	0.47	18 h				

[a]: spectra were evaluated when the reaction was finished and/or distinct bands were visible and/or no bands evaluated and no more change in the spectra could be detected; [b]: broad absorbance band.

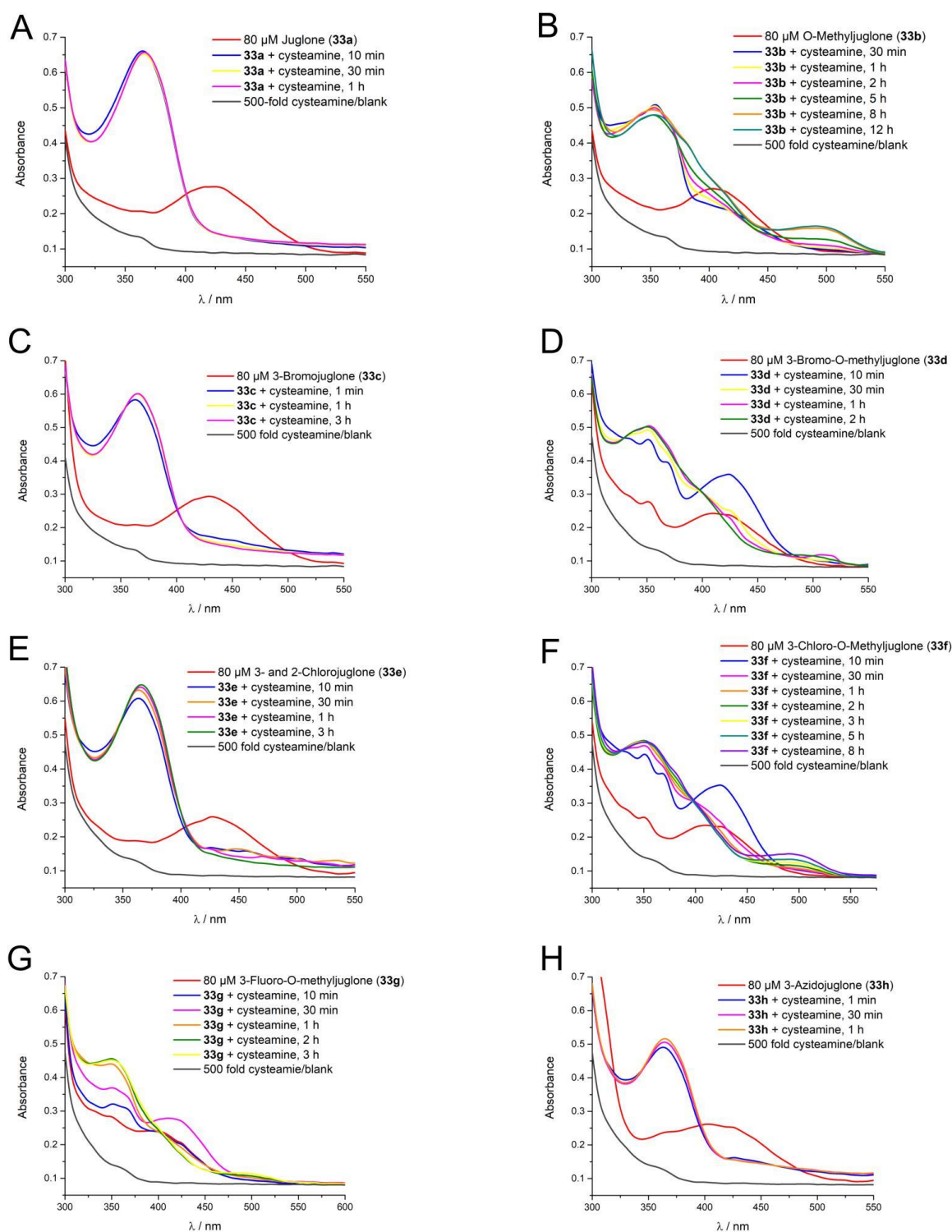


Figure 38: Juglone derivatives (80 μM) in the kinetic thiol assay solvent system without and with 500-fold cysteamine. **A:** juglone (33a); **B:** O-methyljuglone (33b); **C:** 3-bromojuglone (33c); **D:** 3-bromo-O-methyljuglone (33d); **E:** 3- and 2-chlorojuglone (33e); **F:** 3-chloro-O-methyljuglone (33f); **G:** 3-fluoro-O-methyljuglone (33g); **H:** 3-azidojuglone (33h). Note: The reaction was followed over 36 h, here the spectra are shown up to a time, from which no more substantial changes took place.

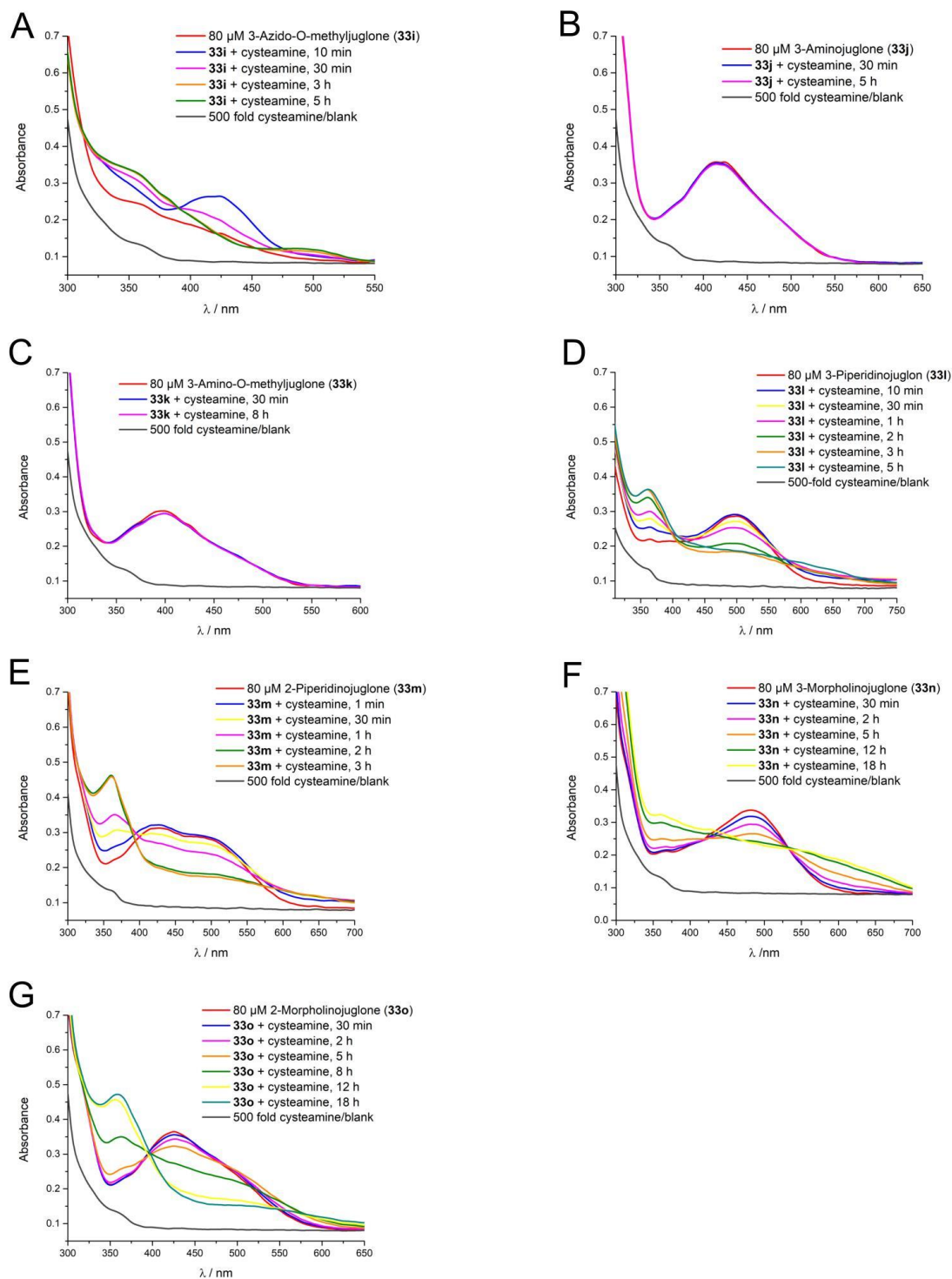


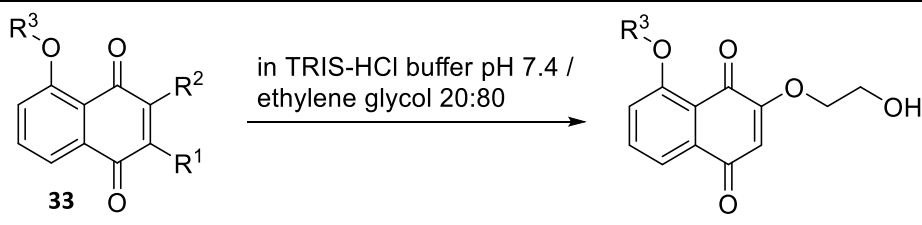
Figure 39: Juglone derivatives in kinetic thiol assay solvent system without and with 500-fold cysteamine. **A:** 3-azido-O-methyljuglone (**33i**); **B:** 3-aminojuglone (**33j**); **C:** 3-azido-O-methyljuglone (**33k**); **D:** 3-piperidinojuglone (**33l**); **E:** 2-piperidinojuglone (**33m**); **F:** 3-morpholinojuglone (**33n**); **G:** 2-morpholinojuglone (**33o**). Note: The reaction was followed over 36 h, here the spectra are shown up to a time, from which no more substantial changes took place.

LC-MS investigations were subsequently performed to provide information about what processes take place. A general experiment was performed with 40 μM compound

concentration and 500-fold excess cysteamine after an incubation time of 3-5 h. The results of the LC-MS experiment are summarized in Table 19 for the control samples and in Table 20 for the reaction mixtures of juglones with 500-fold cysteamine.

Juglone (**33a**), its 14 investigated analogues and the products of the reactions with cysteamine were difficult to detect by MS and UV-Vis upon HPLC separation. In general, the substance signals in the control and reaction samples were very low and partly could only be found in traces. Exceptions were the six amine-substituted compounds **33j-o** where prominent peaks could be found. Probably the buffer/ethylene mixture or the HPLC separation process create conditions for the further conversion of juglones to substance mixtures. Also, low ionization during the usual LC-MS procedures could be a reason. The problem of only very low compound amounts detected by LC-MS occurred also during the analysis of the neat substances in the course of characterization by Sebastian Schlegel. In his work the problem could partly be overcome by changing the method from LC-MS with ESI ionization to GC-MS and EI ionization.^[57]

Table 19: Summary of LC-MS results for control samples of juglone derivatives.

				Mass signals found in control samples		
33	R¹	R²	R³	educt	ethylene glycol substitution	other
a	H	H	H	-	-	no compound detected
b	H	H	CH ₃	✓ (low)	-	-
c	H	Br	H	-	59a	-
d	H	Br	CH ₃	✓ (traces)	59b	-
e	H	Cl	H	-	59a	-
f	H	Cl	CH ₃	-	-	unknown compound
g	H	F	CH ₃	-	-	unknown compound
h	H	N ₃	H	-	59a	-
i	H	N ₃	CH ₃	-	-	no compound detected
j	H	NH ₂	H	✓	-	-
k	H	NH ₂	CH ₃	✓	-	-
l	H	piperidino	H	✓	-	-
m	piperidino	H	H	✓	-	unknown compound
n	H	morpholino	H	✓	-	-
o	morpholino	H	H	✓	-	-

✓ = found

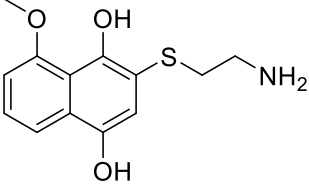
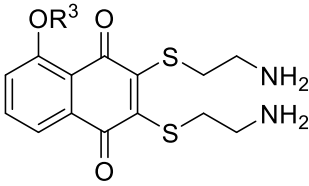
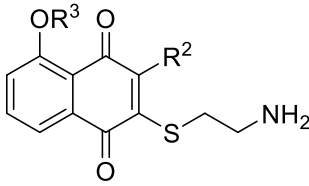
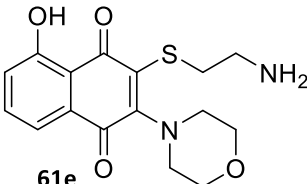
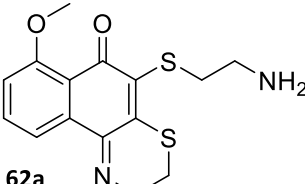
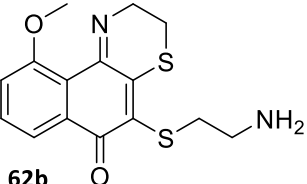
For juglone (**33a**) no substance at all could be found in the control samples despite the experiment was repeated with higher substance concentration and after 10 min – 1 h. Only for the control samples of the amino-substituted juglones **33j-o**, *O*-methyljuglone **33b** and *O*-methyl-bromojuglone **33d** the educts were found (Table 19). All other control samples contained unknown compounds and/or ethylene glycol-substituted juglones **59a** or **59b** (Table 19). These compounds are formed by an addition-elimination mechanism of the nucleophile ethylene glycol to the double bonds of **33** with halogens or N₃ as leaving groups to give structure **59**.

A surprising outcome was also found in the reactions, which resulted partly in mixtures of different grades of complexity (Table 20). *O*-Methyljuglone (**33b**) was the only substance where the anticipated cysteine monoadduct was detected among a mixture of four products in total. All reaction mixtures, except 4, contained products **60a** or **60b** with double added cysteamine due to the high cysteamine excess (Table 20). These products were additionally present in their re-oxidized form. In these cases, as before with the educts, the substituent was eliminated in the 2- or 3-position as leaving group. For some of those double cysteamine-substituted and re-oxidized products, imine formation to a six-membered ring occurred (two isomers **62a** and **b**, Table 20). This reaction is probably favoured by an *O*-methylation, because it only occurs in *O*-methyljuglones **33b**, **33d**, **33f** and **33g**. For all amine-substituted compounds **33j-o**, except **33m** (2-piperidinojuglone), cysteamine monoadducts were initially formed, but were oxidized back to their quinone form each (product mass minus 2H, **61a-e**, Table 20).

Enzymatic re-oxidation by oxygen of electrophiles after Michael addition is a characteristic process in cells.^[61] The oxidized species found in the LC-MS investigations prove that this process takes place for the investigated juglone derivatives without enzymes under these assay conditions over time. This was reported before for other assay systems.^[64]

Some of the reaction samples contained detected mass signals for which no corresponding structures could be proposed, they are listed as unknown compounds in Table 20. The LC-MS data can be viewed in the appendix. Note: Only compounds with distinct and conclusive MS AND UV-Vis data were evaluated. Assay fragments or artifacts and other unknown compounds which appeared only in the LC-run and/or in the UV-Vis detection with no evaluable MS data and/or no UV-Vis absorbance > 200 nm were not considered in the evaluation.

Table 20: Summary of the LC-MS results for reactions of juglone and juglone derivatives with 500-fold cysteamine detected by LC-MS analysis and found oxidized structures in the reaction mixtures.

 <p>57a</p>				 <p>R³ = H: 60a R³ = CH₃: 60b</p>				 <p>R² = NH₂, R³ = H: 61a R² = NH₂, R³ = CH₃: 61b R² = piperidino, R³ = H: 61c R² = morpholino, R³ = H: 61d</p>			
 <p>61e</p>				 <p>62a</p>				 <p>62b</p>			
Educt				Mass signals detected in reaction samples							
33	R ¹	R ²	R ³	Educt	single cysteamine addition	double cysteamine addition	other				
a	H	H	H	-	-	60a	-				
b	H	H	CH ₃	-	57a	60b, 62a and 62b	-				
c	H	Br	H	-	-	60a	unknown				
d	H	Br	CH ₃	-	-	60b, 62a or 62b	-				
e	H	Cl	H	-	-	60a	unknown				
f	H	Cl	CH ₃	-	-	60b, 62a or 62b	-				
g	H	F	CH ₃	-	-	60b, 62a or 62b	unknown				
h	H	N ₃	H	-	-	60a	-				
i	H	N ₃	CH ₃	-	-	60b	-				
j	H	NH ₂	H	✓	61a	-	-				
k	H	NH ₂	CH ₃	✓	61b	-	-				
l	H	pip.	H	✓	61c	60a	-				
m	pip.	H	H	✓	-	60a	-				
n	H	morph.	H	✓	61d	-	unknown				
o	morph.	H	H	✓	61e	-	-				

pip = piperidino, morph = morpholino; ✓ = found; unknown = unknown compound(s) detected, see appendix.

One can summarize that juglone and its derivatives are not easily evaluated in the kinetic thiol assay due to stability issues in the buffer/ethylene glycol system and no distinct single product reaction outcome but rather a complex product mixture. Since for each compound **33** at least two processes always take place, one has to consider that the determined k_2 will be inaccurate, more precisely the value would be an average of the rate constants of all reactions taking place.

With the help of LC-MS analyses, the UV-Vis bands could now be assigned to products and the processes that can be seen in the time-dependent spectra becomes understandable.

Juglon **33a**, 3-azidojuglon **33h** and both halogen-substituted, non-methylated compounds **33c** and **33e** form the group of substances that together with cysteamine form the double-substituted re-oxidized product **60a**, to which the absorption band at 365 nm belongs. A kinetic measurement is very well feasible for this group if it is tolerated that the obtained k_2 value will be a mixture of several processes taking place. It could still be investigated whether only a single addition takes place with less excess cysteamine. However, due to the instability of the substances, which manifests itself within 24 h until un-detectability, it is more recommended to use higher excess concentrations for fast reactions. In order to optimize stability, changing the reaction medium to solvent-free buffers would be a possibility, since ethylene glycol was revealed as the causative component.

In the reaction solutions of all *O*-methylated compounds, as well as in the UV-Vis spectra, substance mixtures were identified as products which also contain the oxidized substances **60**. Since the k_2 value becomes even less accurate due to several products, a kinetic measurement without optimization of the assay conditions (solvent system, excess thiol) is not recommended.

If the further, amine-substituted compounds **33j** and **33k** of the juglon substance library are regarded, one finds a special feature in the two amino compounds, since they have been shown to react to products **61a** and **61b**, but the process is not visible in the UV-Vis. It is most likely that the chromophores of educts and products are very similar so that there is no overall time-dependent change in the course of the reaction. Therefore, kinetic measurement with the kinetic thiol assay is not possible for these two substances either.

Finally, for the last group, the piperidino and morpholino substituted substances **33l** – **33o**, kinetic measurement is possible by UV-Vis measurement but the k_2 value obtained does not reflect a single process but several successive reactions.

In the literature it was shown that the processes of Michael addition and subsequent oxidation can be separated by lowering the reaction temperature to 10 °C. The oxidation takes place sufficiently slowly at this temperature so that a k_2 value of $0.022 \text{ M}^{-1}\text{s}^{-1}$ for the Michael addition of GSH to juglon (**33a**) in HEPES buffer could be determined.^[64] This shows, that optimization of the conditions for a kinetic measurement is possible and also temperature changes can thus be taken into consideration. A detailed kinetic investigation and assay optimization of the juglone substance library could not be performed within this work. In general, a moderate to high reactivity is assumed due to the double electron-withdrawing effect of two carbonyl groups.

Concerning biological activity, the finding that most of all amine-substituted compounds, i.e. more electron-rich electrophiles, have an anti-inflammatory effect, is surprising. This

supports the findings that the biological activity for this compound class in general is not entirely due to its electrophilicity. For the anti-inflammatory activity it seems reasonable, that these properties could be a result of other molecular effects such as radical-scavenging and/or redox properties.

A 3.3 α -Nitro-hydroxychalcone (α -NO₂-HC) as part of the α -X-hydroxy-chalcone (α -X-HC) substance library

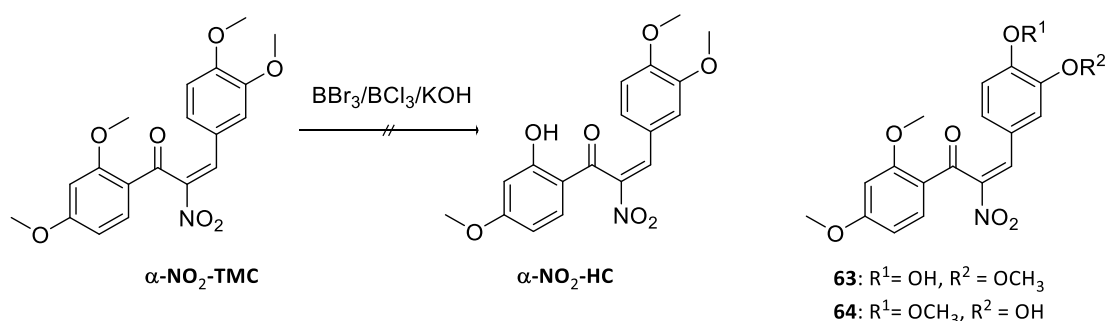
These results are not published yet (05/2019).

Participants in this work are: Nafisah Al-Rifai, Lukas Wirth, Maria Landa and Grigor Gurzadyan: Attempts towards the synthesis of α -NO₂-HC; Monika Enzinger: Synthesis, UV-Vis and MS investigation of NO₂-Flavanone/ α -NO₂-HC; Sina Malenke: Biological testing of NO₂-Flavanone/ α -NO₂-HC.

As NO₂ as further interesting α -substituent was required for this compound library, the synthesis, kinetic and biological investigation of α -NO₂-HC was included in the work of this thesis.

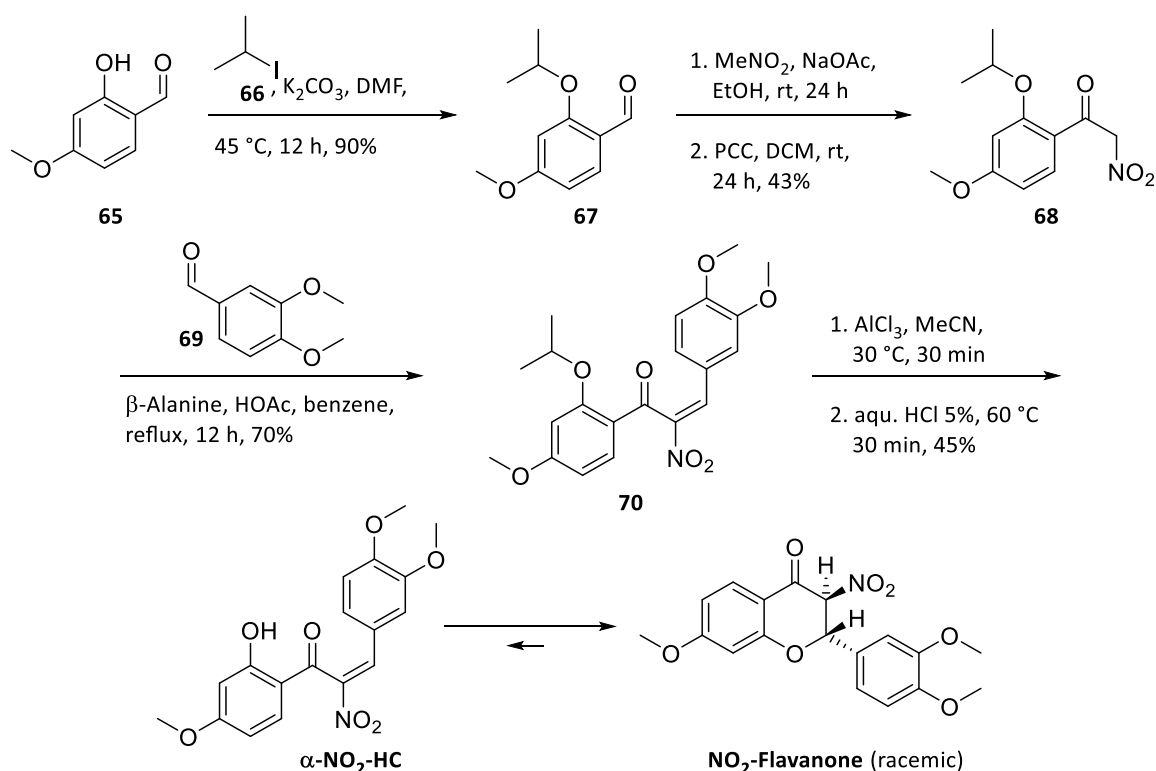
Synthesis

Standard procedures to get the desired structure α -NO₂-HC by demethylation of the 2'-OCH₃ group of the literature-known substance α -NO₂-TMC^[36] had failed before (performed by Lukas Wirth, Maria Landa and Grigor Gurzadyan, unpublished). Several conditions such as BCl₃, BBr₃ and basic cleavage with KOH were screened, but only a mixture of species with free OH groups on ring B was obtained (Structures **63** and **64**, Scheme 19). This was detected by careful evaluation of the MS fragments via LC-MS during the regular pre-kinetic screening under assay conditions.



Scheme 19: Attempt to synthesize α -NO₂-HC by demethylation of α -NO₂-TMC.

Therefore, α -NO₂-HC was provided by the synthesis of the isopropyl-protected precursor **70** and subsequent selective deprotection in 2-position (Scheme 20).



Scheme 20: Synthesis route to obtain $\alpha\text{-NO}_2\text{-HC/NO}_2\text{-flavanone}$.

The first three synthesis steps to obtain the isopropyl-protected $\alpha\text{-NO}_2\text{-hydroxychalcone}$ **70** were performed according to known procedures^{[36] [77]} and moderate to good yields were achieved. For the deprotection two conditions were applied with AlCl_3 in acetonitrile at room temperature^[78] being superior to BCl_3 in DCM at $-78\text{ }^\circ\text{C}$ (45 vs 40% yield). Purification of the crude material was only possible with reversed phase chromatography as the product gave no distinct band on normal silica gel but a yellow area blurred from the baseline to the middle of the TLC plate with various screened solvent mixtures including the addition of TFA. ^1H NMR analysis in CDCl_3 shows the cyclized **$\text{NO}_2\text{-flavanone}$** as main product, recognizable by two prominent doublets at 5.80 and 5.74 ppm with a typical coupling constant ($J = 11.9\text{ Hz}$) and approximately 10% of $\alpha\text{-NO}_2\text{-HC}$. In DMSO-d_6 the equilibrium is completely shifted to the flavanone. It was possible to separate both species by preparative HPLC, but isolation of $\alpha\text{-NO}_2\text{-HC}$ failed due to the quick re-adjustment of the initial 10:1 equilibrium of $\alpha\text{-NO}_2\text{-HC/NO}_2\text{-flavanone}$ in the solvent system water/acetonitrile/ HCOOH (40:60:0.1). It has already been reported that in the case of similar $\text{NO}_2\text{-substituted}$ compounds only the cyclized product was obtained.^[79] For steric reasons, the diastereomer with the nitro and phenyl group *trans*-positioned to each other at positions 2 and 3 is formed as a racemate (2*S*,3*S* or 2*R*,3*R*-configured).

UV-Vis and LC-MS analysis

A 10 mM stock solution in DMSO followed by dilution in kinetic thiol assay solvent system was prepared from the solid **NO₂-flavanone**. The reaction in a concentration of 40 μM with 12, 100 and 500-fold of cysteamine was investigated by UV-Vis spectroscopy over a period of three days. The prominent absorption band with a maximum at 380 nm decreases slowly in the presence of cysteamine. This decay is slow for the 12-fold, faster for 100-fold and complete within 48 h for the 500-fold cysteamine excess.

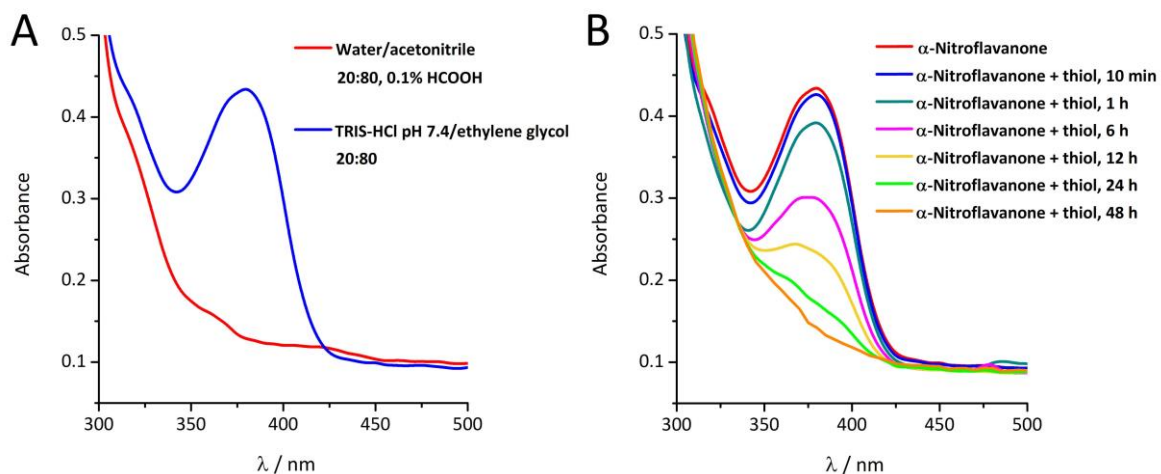
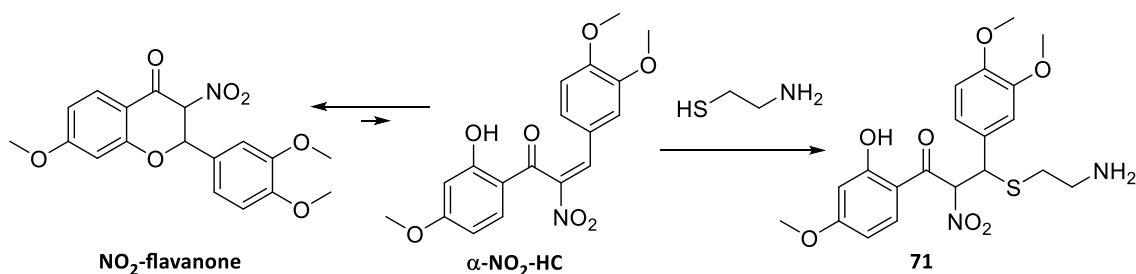


Figure 40: **A:** Comparison of the chromophore of NO₂-flavanone in different solvent systems; blue: 100 mM Tris-HCl buffer pH 7.4 with 2 mM EDTA/ethylene glycol 20:80; red: HPLC solvent mixture Water/Acetonitrile/HCOOH 20:80/0.1%. **B:** Time-dependent UV-Vis spectra of 40 μM NO₂-flavanone and 500-fold (20 mM) cysteamine in thiol assay buffer.

Due to this finding, a reaction of the open-chained **α-NO₂-HC** with cysteamine to adduct **71**, subsequent back equilibration and thus consumption of **NO₂-flavanone** can be assumed (Scheme 21). This would be the expected and well-known thia-Michael addition of thiols to enones such as chalcones.



Scheme 21: Equilibrium of **NO₂-flavanone** and **α-NO₂-HC** with subsequent Michael addition of cysteamine to **71**.

To further investigate the process witnessed by UV-Vis spectroscopy, the reaction of **NO₂-flavanone/α-NO₂-HC** with cysteamine was monitored by LC-MS over a period of 24 h.

Interestingly, the addition product **71** was immediately produced, but only in a very small amount. It is consumed completely during the time between 8 and 24 h. Moreover, the reaction leads to a substance mixture containing educt and product fragments without complete consumption of the starting material. More precisely, **NO₂-flavanone** was still the main compound in the LC run after 24 h. Figure 41 exemplarily shows the results of this experiment after 8 h of reaction time and suggests structures for the substance mixture.

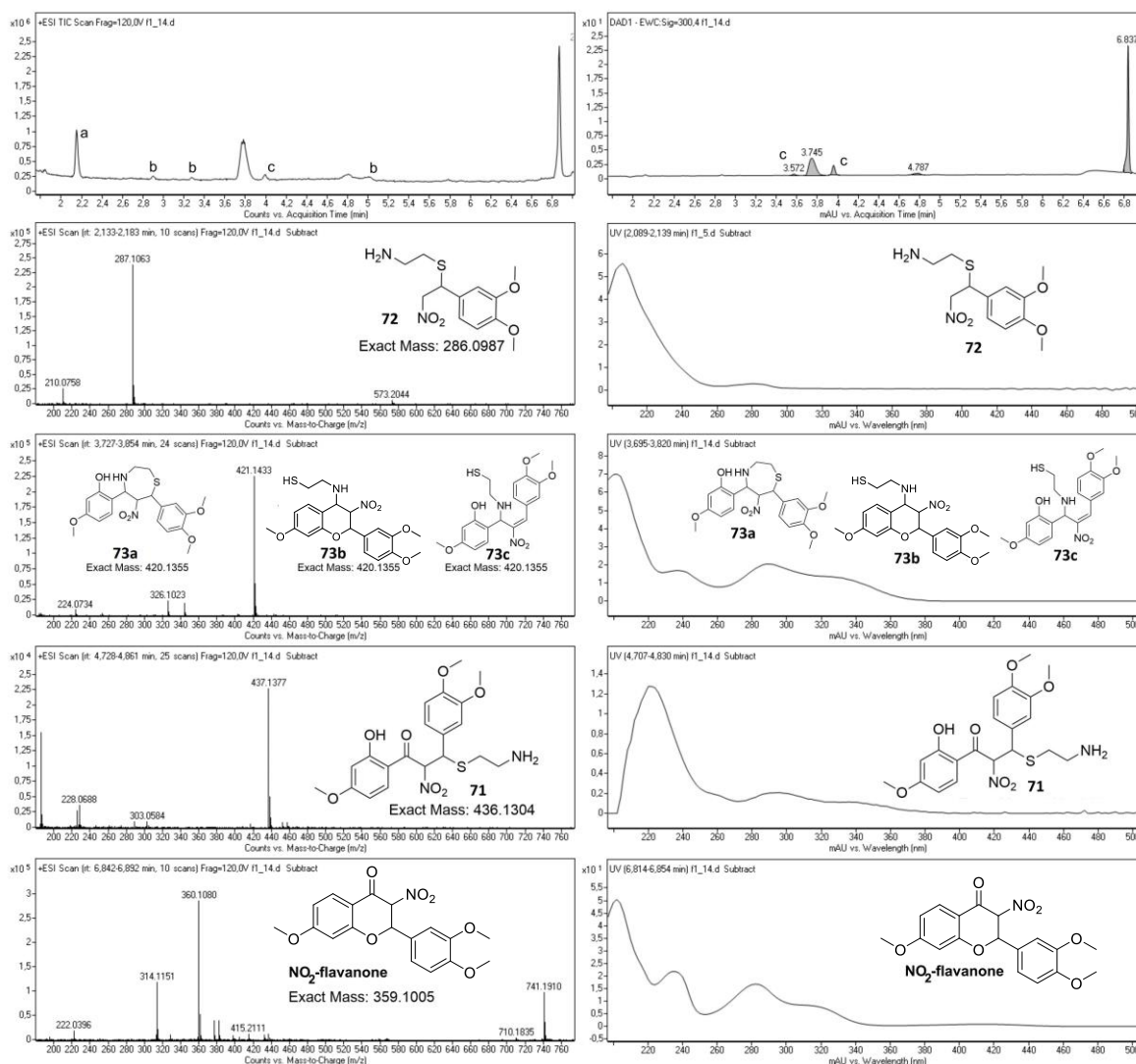


Figure 41: HPLC run of the reaction mixture of **NO₂-flavanone** with cysteamine 500-fold after 8 h, MS and UV-Vis spectra of the fractions and structure suggestions. HPLC-[a]: no UV-Vis detection at 300 nm; [b]: no compounds detected, neither in MS nor in UV-Vis; [c]: UV-Vis-active artifacts with no detectable compounds in MS.

Fragmentation of the cysteamine adduct to **72** was similarly observed in α -X-TMCs and α -X-HCs.^[39] For unknown compound **73**, three structure suggestions are possible. One is produced by a Schiff base formation of the NH₂ moiety of adduct **71** with the carbonyl group and subsequent reduction to **73a** by excess cysteamine which itself is oxidized to its disulfide. This might occur due to the strong electron-withdrawing effect of the nitro group. But

more likely, its -M/-I effect leads to immediate imine formation of **NO₂-flavanone** with cysteamine-NH₂ and subsequent reduction to **73b** as described before. The same process could also occur for the small amounts of **α-NO₂-HC** to **73c**. However, **73b** is the most likely structure, derived from **NO₂-flavanone**. This is also visible in the post-LC UV-Vis spectrum of **NO₂-flavanone** in water/acetonitrile, 0.1% HCOOH (Figure 40A and Figure 41, compounds **73** and **NO₂-flavanone**). Both spectra show a very similar chromophore which excludes **73c**. For **73c**, an absorbance band > 300 nm would be expected.

This poor reactivity is also reflected in the biological activity: neither cell toxicity nor anti-inflammatory properties were found in the in-vitro assays (Table 21).

Table 21: Result of the in-vitro testing of **NO₂-flavanone** with murine RAW264.7 macrophages done by Sina Malenke.

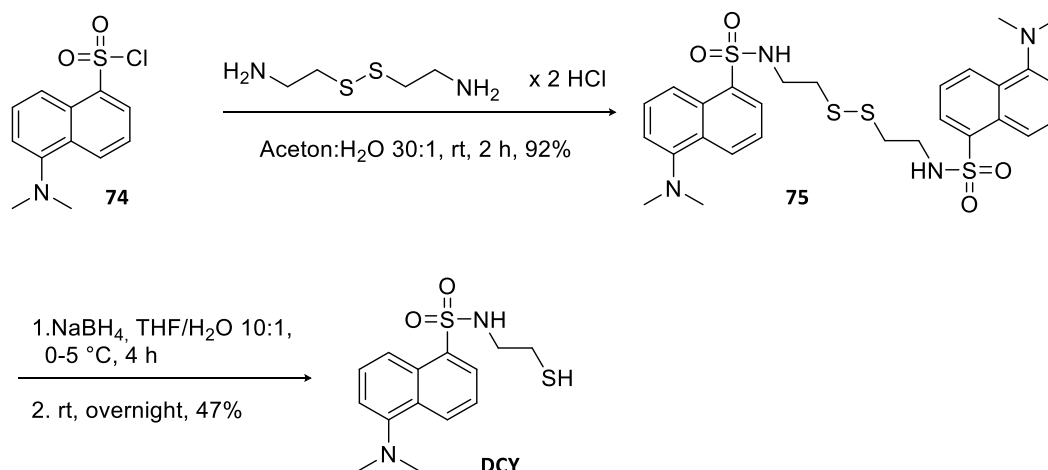
Compound	Cell viability MTT (IC ₅₀ / μM) ± SD	Toxicity limit MTT (IC ₂₀ / μM)	Inhibition of NO production (IC ₅₀ / μM) ± SD
NO₂-flavanone	> 100 μM	> 100 μM	> 100 μM

In summary, it was found that by introducing the NO₂ group, the strong electron withdrawing properties lead to an almost complete conversion of **α-NO₂-HC** into its flavanone form, resulting in the loss of Michael acceptor reactivity and biological activity. The effect is so strong that, in contrast to all other **α-X-HCs**,^[39] the NO₂ compound was not isolated as chalcone but as flavanone.

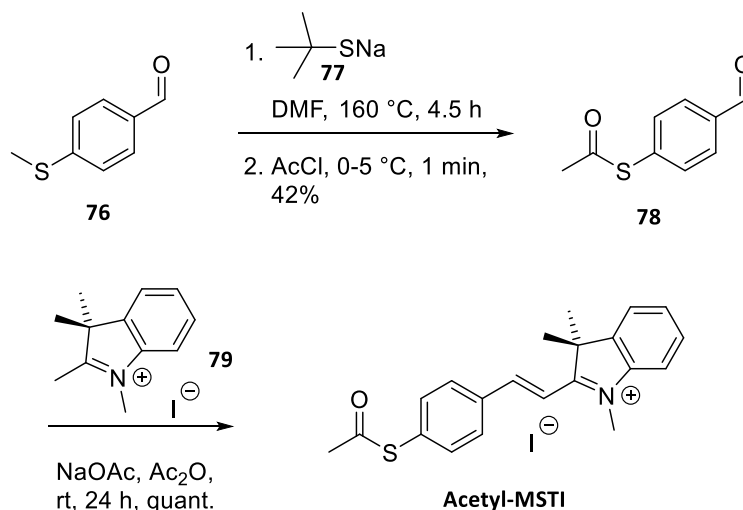
A 4 Results and Discussion III: Investigations for a further development of the kinetic thiol assay towards the use of colorless enones as test substances

A 4.1 Syntheses

For a further development of the kinetic thiol assay towards the kinetic investigation of completely colorless electrophiles (chapter A 1.9), the synthesis of several possible fluorescent thiol probes was approached. All three known compounds **DCY**, **acetyl-MSTI** and **NBD** were synthesized as reported in the literature. **Scheme 22** shows the synthesis path and the yields achieved for **DCY**.^[71] The starting material dansyl chloride (**74**) contains already of the fluorescent molecule part and is equipped with the cysteamine part first by dimerization to **DCY** disulfide **75** which was obtained in a very good yield. The second step was a reduction of the disulfide by NaBH₄ to the desired free thiol compound which was received in 47% yield after column chromatography. One advantage of the substance is its high stability against oxidation.

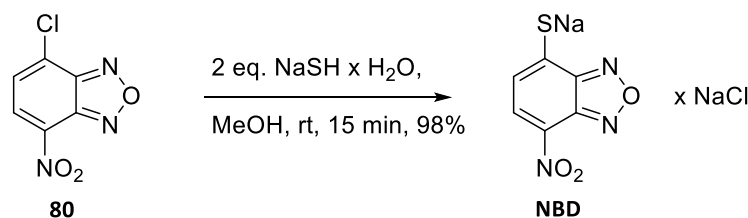
Scheme 22: Synthesis of DCY.^[71]

Acetyl-MSTI was synthesized^[72] according to Scheme 23 by first converting *p*-methylthio-benzaldehyde (**76**) into the non-commercially available acetyl-protected compound **78** which was received in moderate yield. This reaction is a combination of deprotection of the methylated thiol to the free thiolate which is acetylated subsequently. An aldol condensation of **78** and tetramethylindolium iodide (**79**) with NaOAc as base was performed to obtain the target compound **Acetyl-MSTI**. In comparison to the literature^[72] the yield was improved from 55% to quantitative yield by dropwise addition of **78** to the indolium solution over 1 h and a longer reaction time. The obtained orange solid product is stable due to the thiol protection.

Scheme 23: Synthesis of Acetyl-MSTI.^[72]

NBD was obtained by a $\text{S}_{\text{N}}\text{Ar}$ of the chlorobenzofurazan **80** and NaSH in MeOH^[73] in nearly quantitative yield as association with 1 eq. NaCl. This was accepted due to the simplicity of the synthesis, since NaCl does not interfere with all spectroscopic investigations or the

buffer. **80** is converted quantitatively to **NBD** when treated with 2 eq. NaSH. All experiments with less eq. NaSH led to a complex mixture of substances. Likewise, no purification method for the separation of NaCl was successful, it repeatedly led to thiol oxidation and other impurities, which were possibly caused by further nucleophilic substitutions to phenyl-S-phenyl species.



Scheme 24: Synthesis of **NBD**.^[73]

In addition to those known from literature, new fluorescent thiol dyes designed during this work were also originally to be synthesized (Figure 42).

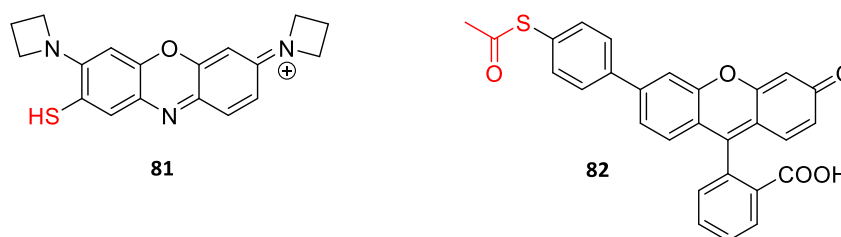
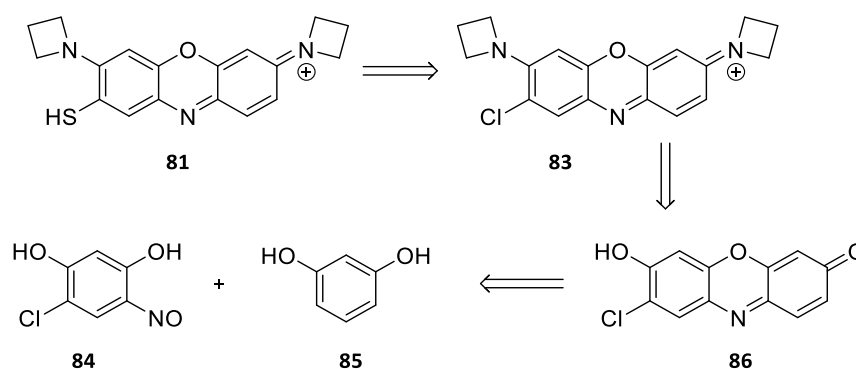


Figure 42: Target structures of new fluorescent thiol dyes approached in this work.

One of these target structures is the azetidine-substituted phenoxazine-thiol **81**, which was inspired by the work of Grimm et al., published in 2015,^[80] in which a large number of new substances for fluorescence microscopy were synthesized and characterized. The group investigated various phenoxazines and found that representatives containing of the double amine-substituted salt structure as in **81** have an improved quantum yield and extinction coefficient, of which azetidine-substituted representatives have the best results. These two properties would help to significantly reduce the concentration of the thiol probe in the assay. Therefore **81** was designed, which carries the required thiol group. Scheme 25 shows the retrosynthesis of **81**. The thiol group can be introduced by nucleophilic substitution of the halogen in **83**, the azetidine groups by a Pd-catalyzed Buchwald-Hartwig coupling. Since substance **86** or similar halogenated phenoxazines are not commercially available, this heterocycle must be synthesized from the two building blocks 4-chloro-6-nitrosoresorcinol (**84**) and resorcinol (**85**).

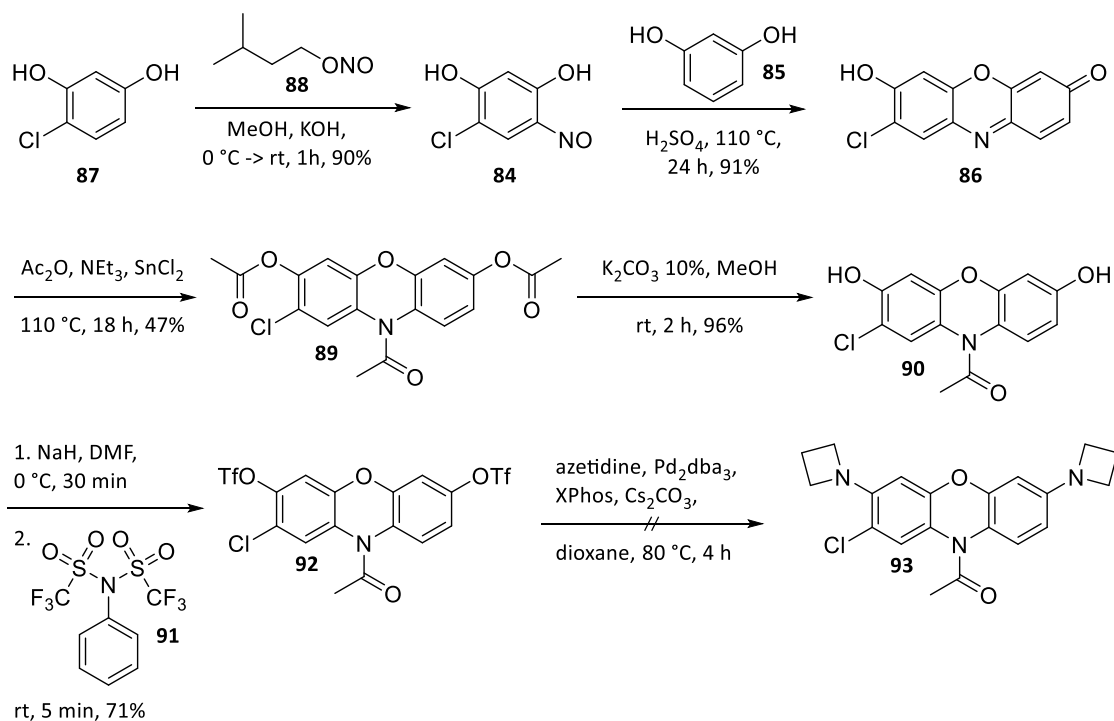


Scheme 25: Retrosynthesis of the desired structure of the thiol-containing phenoxazine dye **81**.

The synthesis of substance **81** could unfortunately not be completed within this work, but most of the precursors were successfully synthesized according to Scheme 26. The known substance 4-chloro-6-nitrosoresorcinol (**84**) could be obtained with a very good yield by electrophilic aromatic substitution with chlororesorcinol (**87**) and isopentyl nitrite (**88**) in methanolic KOH.^[81] Heterocycle **86** was synthesized by heating the two starting materials in concentrated sulfuric acid.^[81] Substance **86** turned out to be a very poorly soluble, dark violet, almost black material, which could not be characterized by NMR but only by MS. In addition, the successful synthesis of triacylated reduced phenoxazine **89** shows the existence of **86**. Since **86** is most soluble in H₂O, NMR experiments were performed to characterize the substance in D₂O, D₂O/NaOD and D₂O/DCl, which was unsuccessful. Substance **89** was obtained by reduction by SnCl₂ followed by acetylation in Ac₂O in moderate yield.^[82] The reason for this was a difficult workup, as the crude product had to be isolated from voluminous insoluble tin salts, which prevented phase separation. One improvement was the workup in a non-polar organic solvent and separating the insoluble residues by filtration. The reduction of the heterocycle is necessary to introduce both azetidinium groups by means of Pd-catalyzed coupling, for which both substitution sites must first carry triflates as leaving groups. For this purpose both hydroxy groups at the phenoxazine phenyl rings were first deprotected,^[82] whereby **90** was obtained in a very good yield. By using a selective method for the deprotection of esters only, the heterocyclic nitrogen remains protected. Also the triflation to ditriflated phenoxazine **92** could be accomplished by the use of trifluoro-*N*-phenyl-*N*-((trifluoromethyl)sulfonyl)methanesulfonamide (**91**) with good yields.^[83] The reaction with triflic acid anhydride as a reagent only produced yields of 1-10% after isolation of product **92** from a complex mixture.

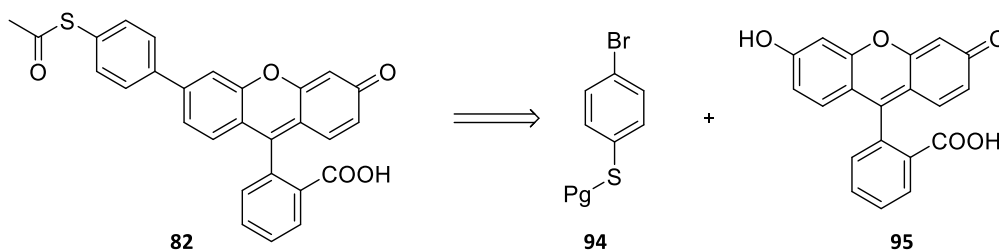
Finally, the palladium-catalyzed Buchwald-Hartwig coupling turned out to be very problematic. Although the reference reports a promising yield of 92% in this reaction if the molecule is not chlorine-substituted,^[80] this could not be observed for substance **93**. A complex mixture of substances was always obtained in the experiments, even if the reaction was carried

out at room temperature or even on ice. After some time, the baseline spot became dominant in TLC control, suggesting oligomerization or polymerization. MS studies showed that the desired product **93** was not present in the mixture. In the context of this doctoral thesis a successful optimization of the reaction was not achieved.



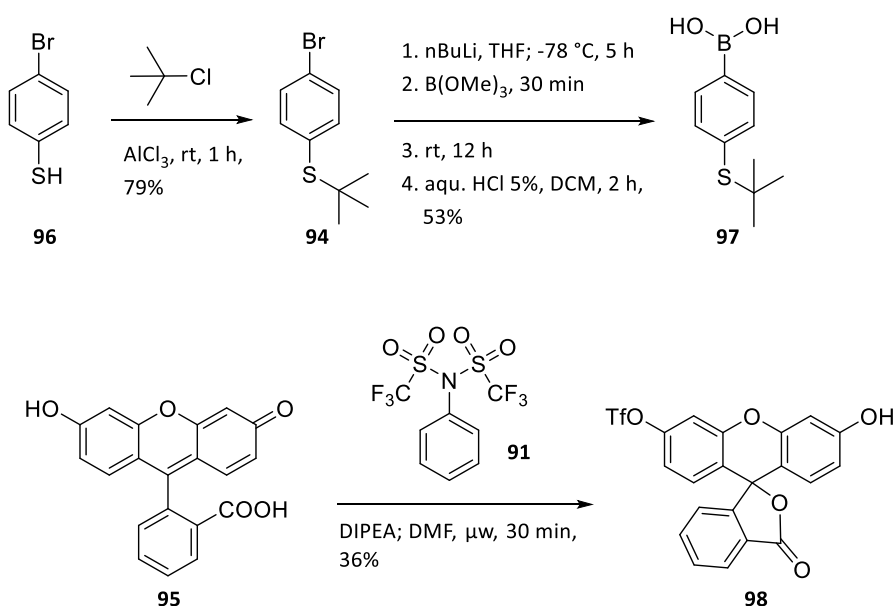
Scheme 26: Attempted synthesis of an azetidine-containing phenoxazine dye.

Another approach for a new substance to be used as a thiol probe in the kinetic thiol assay was the fluorescein derivative **82**. Fluorescein (**95**) was selected as fluorophore because of its excellent and well-known fluorescence properties. Analogous to the assay already presented by McCallum et al for **Acetyl-MSTI**, **72** should also initially be protected with an acetyl residue, which is cleaved in situ to the free thiolate in the first step of the assay. Scheme 27 shows the retrosynthesis: **82** can be produced from fluorescein and a protected *p*-halogen-thiophenol **94** by a palladium-catalyzed coupling.



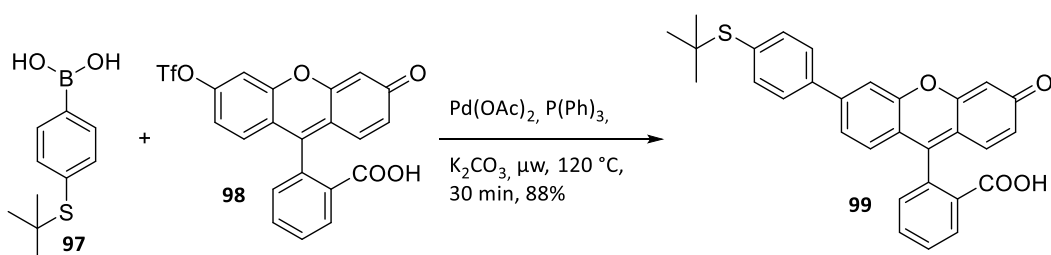
Scheme 27: Retrosynthesis of the thiophenol-substituted fluorescein derivative **72**.

Suzuki coupling was chosen as the method, for which the two literature-known precursors **97** and **98** were synthesized in moderate to good yields (Scheme 28). 4-Bromothiophenol (**96**) was first protected with a *tert*-butyl-group^[84] to **94** and subsequently converted into the phenyl-substituted boronic acid **97** using *n*-BuLi, then B(OMe)₃ and HCl for demethylation.^[85] The monotriflation of fluorescein to form **98** gave only a moderate yield of 40% when stirred in a round-bottom flask for two days,^[86] but was much faster performed using a microwave reactor by accepting a slightly lower yield of 36%.^[87] NMR spectroscopy showed that the lactone structure is present in **98**. Yields could not be improved, since a ditriflated by-product was formed.



Scheme 28: Synthesis of the precursors for a Suzuki coupling reaction.

The Suzuki coupling could be successfully carried out in the microwave reactor and **99** was obtained in good yield.^[88] The final step, the replacement of the *tert*-butyl group by an acetyl protecting group on the thiol to target structure **82**, Figure 16), could not be investigated within the scope of this work.



Scheme 29: Synthesis of *tert*-butyl-protected thiophenol-fluorescein **99**.

A 4.2 Fluorescence investigations of Michael addition reactions

The obtained potential thiol probes **DCY**, **NBD** and **Acetyl-MSTI** were examined towards their spectroscopic properties and their reaction with enone-type electrophiles.

DCY was measured in a concentration of 10 μ M under the usual assay conditions in kinetic thiol assay solvent system. As the excitation wavelength that produces the highest fluorescence at 525 nm, 350 nm was determined and used for all further investigations. Cyclohexenone (**34**), **OXE1-(4py)** and the chalcone **α -Br-TMC** were used as test electrophiles in 20-fold excess in the Michael addition with **DCY**.

Initially, a quick decrease of the fluorescence intensity of **DCY** was found 1 min after the start of the reaction for **OXE1-(4py)** and **α -Br-TMC** (Figure 43 A). No such decrease was found for **34**, although a **DCY**-cyclohexenone Michael adduct was proven by LC-MS. To investigate the possible influence of quenching effects, the non-reactive **DCY** synthesis precursors were additionally investigated as controls. It was shown that mixtures of **DCY** disulfide (**75**) and all three electrophiles show the same decrease in fluorescence intensity as the free thiol **DCY** (Figure 43B). An LC-MS control experiment showed no reaction products of any kind for **DCY** disulfide and **34**, as expected. Figure 43C shows for cyclohexenone **34** that even after 20 min there are no significant changes in the spectra for both **DCY** and its disulfide.

It appears that the relatively high excess of electrophiles has quenching effects on the fluorescence of **DCY**, which is also true for non-reactive fluorescent **DCY** derivative **DCY** disulfide. No indication was found that a detectable reaction occurs. The use of **DCY** for the planned new assay is therefore excluded as the substance is not suitable.

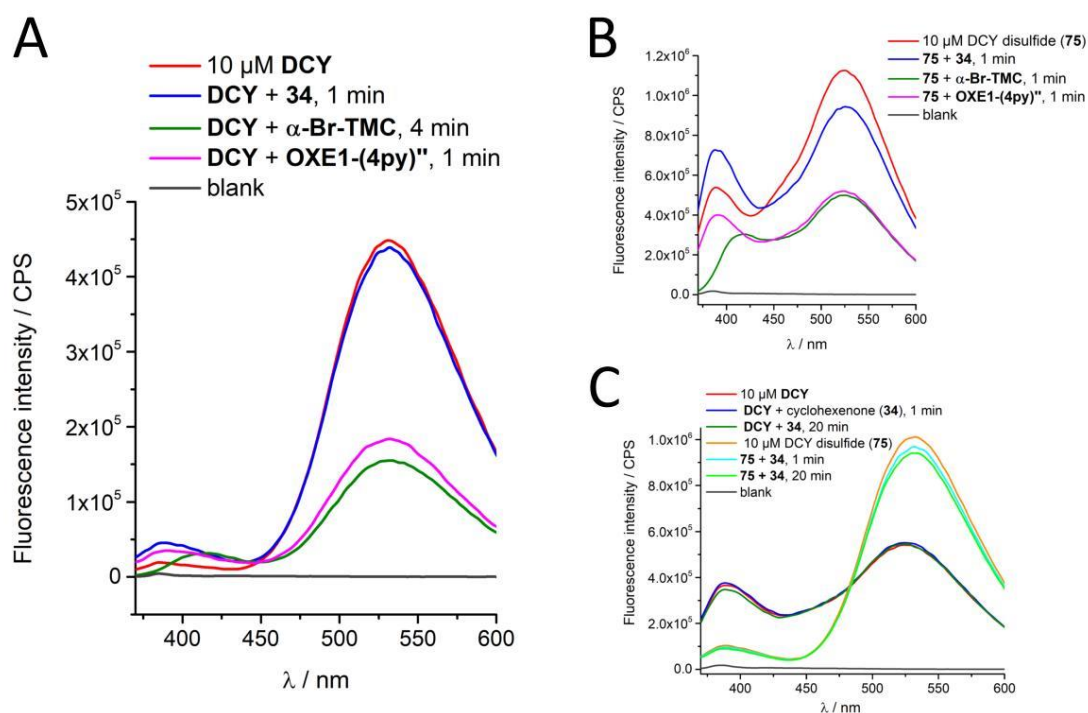


Figure 43: Fluorescence measurements with **DCY** as thiol probe in the reaction with test electrophiles in Tris-HCl buffer pH 7.4 with 2 mM EDTA/ethylene glycol 20:80, $\lambda_{\text{ex}} = 350$ nm. **A:** Fluorescence spectra of the reactions of 10 μM **DCY** and 20-fold excess of three different enone electrophiles: cyclohexenone (**34**), α -Br-TMC and **OXE1-(4py)''** after 1-4 min); **B:** Fluorescence spectra of control compound **DCY disulfide (75)** and 20-fold excess of three different enone electrophiles: cyclohexenone (**34**), α -Br-TMC and **OXE1-(4py)''** after 1-4 min; **C:** Time-dependent fluorescence spectra of **DCY** (dark spectra) and **DCY disulfide (75)**, bright spectra) without and with 20-fold cyclohexenone (**34**).

Furthermore, **Acetyl-MSTI** was tested according to the assay developed by McCallum et al.^[72] **Acetyl-MSTI** was first converted to **MSTI** in PBS pH 12 - MeOH 1:1 and then added to the test electrophile cyclohexenone (**34**) in PBS pH 7.4 (dilution factor PBS pH 12 to PBS pH 7.4: 1:30). The assay concentration of **MSTI** was 30 μM with 12-fold excess of **34**. Non-protected **Acetyl-MSTI** was measured as control compound. Additionally, the very strong electrophile benzoquinone was investigated as it is reported to be a “hit” compound.^[72] Figure 44A shows the probe spectra over time as control while Figure 44B and C shows emission spectra of both investigated reactions. For the *in-situ* deprotected free thiol **MSTI** only a very low fluorescence intensity $< 5 \times 10^{-4}$ CPS (counts per second) was found even with intensity-increasing instrument settings (broadening of the excitation slot, longer detection).

Free thiol **MSTI** and **Acetyl-MSTI** differ significantly in their emission properties. Immediately after starting the reaction of **MSTI** with both electrophilic compounds **34** and benzoquinone, a decrease in fluorescence is observed, leading to a complete decay of the **MSTI** emission band in the reaction with benzoquinone, whereas this only occurred partially for **34**. Subsequent time-dependent measurements of both reaction mixtures showed no

changes (Figure 44B and C). Furthermore, both electrophiles were measured as controls without **MSTI**, whose emission spectra are at the intensity level of the blank and **Acetyl-MSTI**. Unfortunately, the anticipated instability of **MSTI** also becomes apparent (Figure 44A). After 30 min, the emission band of **MSTI** had clearly decreased due to most likely oxidation. Neither optimizations of the conditions with regard to oxidation stability of **MSTI** nor kinetic investigations could be carried out within this work. In order to get meaningful kinetic data, the oxidation sensitivity of **MSTI** must be addressed first. Although, despite the poor emission properties of **MSTI**, the substance would certainly be suitable as a probe in the new assay. Based on these and the previous studies^[72] one can propose that **MSTI** probably reacts very quickly with strong to medium-strong electrophiles. Similar results have also been obtained in studies on the UV-Vis absorbance of **MSTI** with and without test electrophiles under the same conditions (data not shown).

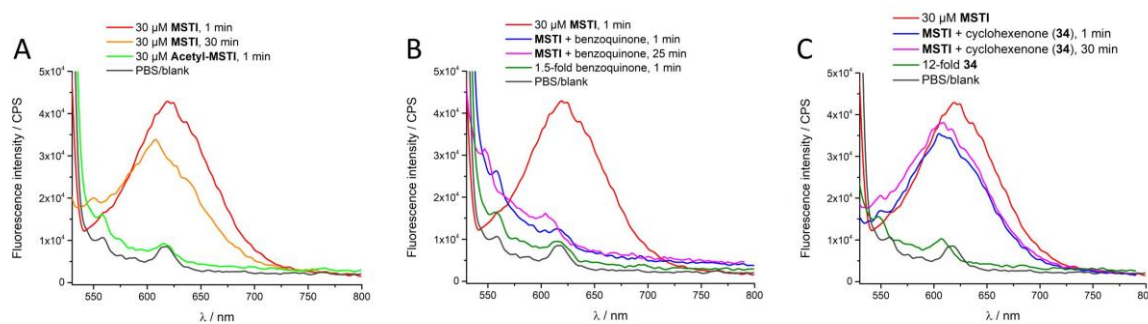


Figure 44: Fluorescence measurements with **MSTI** as thiol probe in the reaction with test electrophiles in PBS buffer pH 7.4, $\lambda_{\text{ex}} = 350$ nm. **A:** 30 μM **MSTI** as control; **B:** 30 μM **MSTI** and 1.5-fold benzoquinone; **C:** 30 μM **MSTI** and cyclohexenone (**34**). Measurements were performed in PBS pH 7.4.

Finally, assessments of **NBD** by fluorescence spectroscopy with various test electrophiles revealed no evidence that a Michael addition was taking place (data not shown). With optimized instrument settings, a small emission could be measured for both **NBD** and test electrophiles alone. In most of the investigated reactions, only a fluorescence addition of both components was detected moreover. A Michael reaction adduct could not be confirmed by LC-MS studies. It was also found that the **NBD** control solution was not stable since emission intensity increased over time. This is probably due to auto- $\text{S}_{\text{N}}\text{Ar}$ reactions to diphenyl sulfide species.

In summary, a suitable thiol probe could not be found in the performed investigations. A Michael addition that could clearly be detected by fluorescence spectroscopy was only measured with **MSTI**, as literature reported before.^[72] Furthermore, the susceptibility of aromatic free thiols to oxidation is a major problem, since false reaction rates would be obtained in kinetic measurements. Two proposals for further thiol probes are shown in Figure 45.^[75] Both are reported in the literature to have different fluorescence properties

depending on whether a free or an alkylated thiol group is present. Since this fact is only mentioned in the literature but not explained in detail, further investigations are needed in the future. Not only the emission properties make these compounds interesting, also a reduced susceptibility to oxidation can be expected, since they are not aromatic but alkyl thiols. During this work syntheses of **100** and **101** were attempted, but due to various issues this work could not be completed. While **100** was detected by LC-MS, but could not be isolated, synthesis attempts of **101** were not successful.

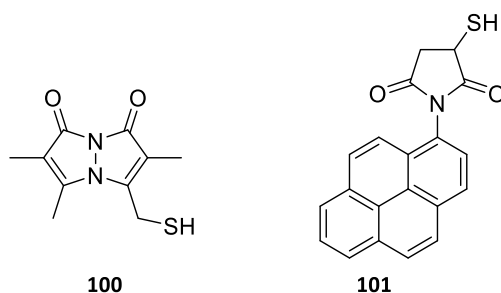


Figure 45: Suggested compounds for further investigations of their suitability as probes in the kinetic assay for colorless electrophiles.^[75]

A 5 Summary of Chapter A

The demanded further representatives of the new compound library of the enone-substituted 1,3,4-oxadiazolines (OXEs) were synthesized. A thia-Michael addition of cysteamine to all compounds bearing the enone unit was proven via LC-MS and UV-Vis spectroscopy, exemplarily also via NMR for **OXE1-(4py)**". Appropriate reactivity assay conditions and the second-order rate constants for all suitable compounds were determined under pseudo-first order conditions. Values between 14.3 and 0.000478 M⁻¹s⁻¹ for k_2 values were measured. Thus, the range of values for this compound library covers five orders of magnitude. A detailed analysis under assay conditions shows by-products for some substances and thus limits for the determination of reactivity. **OXEp1-(4py)**" was unsuitable for UV-Vis kinetic measurement, therefore the reactivity was measured by LC-MS using **OXE4-(4py)**" for comparison and a k_2 value of 0.0032 M⁻¹s⁻¹ was determined for **OXEp1-(4py)**".

Anti-inflammatory properties in the form of an inhibition of NO production by NF- κ B were found in-vitro in acryl- or crotyl-substituted OXE classes and both OXEp compounds. Moreover, the anti-inflammatory activity of the whole compound library correlates with its electrophilic properties and can be controlled and predicted by their structure. An electrophilicity in the form of 0.330 – 4.27 M⁻¹s⁻¹ together with the crucial structure elements free enone group and pyridinyl unit in the 5'-position lead reliably to single-digit IC₅₀ values of NO-inhibition. More compounds need to be synthesized and investigated to see if this

effect can be pushed further, especially the interesting role of CF₃ representatives in the electrophilicity/biological activity ratio needs to be evaluated. This basic work provides a huge variety of structural adjustment features for a further fine-tuning of the desired effects.

A library of small Michael acceptor reactive units was investigated for their reactivity. Reactivity of sulfonic acid derivatives could not be determined due to insufficient absorbance properties of the compound chromophores. For all *N*-phenylacrylamides, the k_2 values were determined and a structure-reactivity relationship was derived.

Spectroscopic properties and reactivity towards cysteamine have been investigated for further electrophiles, juglone derivatives and NO₂-flavanone, using LC-MS and UV-Vis spectroscopy. A small anti-inflammatory activity was established for a few compounds. A k_2 value determination by the kinetic thiol assay is possible for most substances. For reasons of stability and the occurrence of several reactions, however, the assay conditions for kinetic measurements should be optimized first. The demanded NO₂-flavanone was synthesized from simple precursors. Since it is present both isolated and in solution almost quantitatively as flavanone, neither reactivity towards cysteamine nor anti-inflammatory activity could be demonstrated.

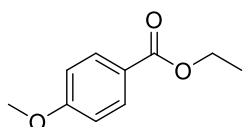
In order to further develop the kinetic thiol assay for the testing of colorless enones with fluorescent dyes as probes, first investigations with literature-known fluorescence-active thiols and thiol precursors were carried out, of which **MSTI** has the best potential. The synthesis and spectroscopic investigation of new aromatic fluorescent thiol dyes could not be completed within this work.

A 6 Experimental

A 6.1 General synthesis information

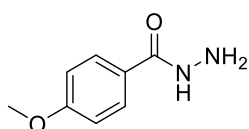
All reagents were purchased from commercial sources and were used without further purification. Solvents were distilled before use. All reactions were carried out under nitrogen gas and the glassware was heated at 110 °C before use when dry conditions were necessary. The reactions were monitored by TLC on silica gel plates 60 F254 by MERCK (Darmstadt, Germany). Spots were detected under UV light ($\lambda = 254$ and 366 nm). Column chromatography was performed on silica gel Geduran Si 60 (0.063-0.200 mm) by MERCK (Darmstadt, Germany), while preparative plates were prepared using silica gel 60 GF254 by MERCK (Darmstadt, Germany). Melting points were determined using BÜCHI melting point B-545 (Flawil, Switzerland) and were uncorrected. ^1H NMR spectra were recorded on a Bruker Avance 300 (Billerica, Massachusetts, USA) (300 MHz) and Bruker Avance 400 (400 MHz) spectrometer. Chemical shifts δ are referenced to CDCl_3 (7.26 ppm), DMSO-d_6 (2.50 ppm) and acetone- d_6 (2.05 ppm). The NMR data were reported in ppm and the abbreviations were mentioned as: s = singlet, brs = broad singlet, d = doublet, t = triplet, q = quartet, sept = septet, m = multiplet, dt = doublet of triplets, dd = doublet of doublets, coupling constants in Hz. ^{13}C NMR spectra were recorded on a Bruker Avance 300 (75 MHz) and Avance 400 (101 MHz) spectrometer and are given in ppm. Chemical shifts δ are referenced to CDCl_3 (77.0 ppm), DMSO-d_6 (39.4 ppm) and acetone- d_6 (29.8 ppm). ^{19}F NMR spectra were recorded on a Bruker Avance 300 (282 MHz) spectrometer. IR spectroscopy was carried out on an Agilent Cary 630 FITR (Agilent, Santa Clara, USA), samples were measured as neat compounds and the wave numbers are reported in cm^{-1} . Mass data were obtained on Agilent Technologies 6540 UHD (Agilent, Santa Clara, USA), Finnigan MAT 95 or Thermo Quest Finnigan TSQ 7000 instruments (Bremen, Germany).

A 6.2 Syntheses of OXEs, OXE analogues and their precursors



Ethyl-4-methoxybenzoate (20a) (synthesized according to a standard procedure). 4-Methoxybenzoic acid (**19a**) (5.00 g, 32.9 mmol, 1.0 eq.) in 250 mL EtOH together with 2 mL H_2SO_4 conc. (1.1 eq.) were refluxed for 20 h and the solvent was removed. The residue was dissolved in EtOAc (300 mL) and the solution washed with sat. aqueous Na_2CO_3 (2 x 200 mL) solution and sat. aqueous NaCl solution (200 mL). After drying over Na_2SO_4 and removal of the solvent, 5.71 g (31.7 mmol, 99%) ethyl-4-methoxybenzoate (**20a**) were received as pale-yellow liquid and used without further purification. ^1H NMR (300 MHz, CDCl_3): $\delta = 8.02$ – 7.98

(m, 2H, CH_{Ar}), 6.94-6.89 (m, 2H, CH_{Ar}), 4.34 (d, *J* = 7.1 Hz, 2H, CH₂CH₃), 3.86 (s, 3H, OCH₃), 1.38 (t, *J* = 7.1 Hz, 3H, CH₂CH₃).

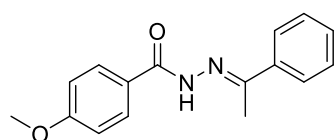


4-Methoxybenzohydrazide (21b).^[89] Ethyl-4-methoxybenzoate (**20a**)

(5.00 g, 27.7 mmol, 1.0 eq.), hydrazine monohydrate (1.67 g, 33.3 mmol, 1.68 mL, 1.2 eq.) and 400 mg (2.89 mmol, 0.1 eq.) K₂CO₃ in 50 mL EtOH were refluxed for 28 h. After completion of the reaction, the hot EtOH solution was separated from solid K₂CO₃ by decantation and the round bottom flask was rinsed out once more with hot EtOH. The solution was cooled to -10 °C and the formed precipitate was filtered off, washed with water (3 x 30 mL) and petroleum ether (3 x 30 mL) to yield 4-methoxybenzohydrazide (**21b**) (3.44 g, 20.7 mmol, 75%), which was used without further purification. ¹H NMR (300 MHz, CDCl₃): δ = 9.68 (s, 1H, NH-NH₂), 7.83–7.77 (m, 2H, CH_{Ar}), 7.00-6.95 (m, 2H, CH_{Ar}), 4.42 (brs, 2H, NH-NH₂), 3.79 (s, 3H, OCH₃).

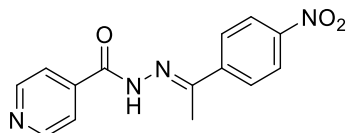
General method for the preparation of hydrazones 23^[90]

Hydrazides **21a-c** (0.500-3.81 g, 3.68-27.8 mmol, 1.0 eq.) and the corresponding aldehydes or ketones **22a-e** (4.01-33.3 mmol, 1.1 eq.) in 10-20 mL EtOH with 0.1-0.2 mL HOAc were refluxed until the reaction was complete. At rt the mixture was poured on 50 mL water and the formed precipitate filtered off, washed with cold water (2 x 50 mL) and petroleum ether (2 x 50 mL) to yield the hydrazones **23a-e**, which were used without further purification. The synthesis of hydrazones **23** with a broad variety of functional groups is widely reported in the literature, for example by van Dijken et al^[90], Thomas et al^[47] and Nigade et al.^[91]

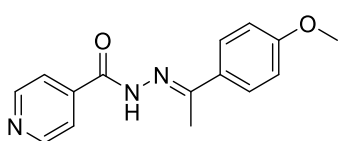


4-Methoxy-N'-(1-phenylethylidene)benzohydrazide (23a). 4-

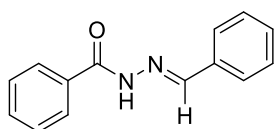
Methoxybenzohydrazide (**21b**) (2.50 g, 15.0 mmol, 1.0 eq.) gave with acetophenone **22a** (1.2 eq.) after 18 h hydrazone **23a** (2.86 g, 10,7 mmol, 71%) as yellow solid. *R_f* = 0.73 (SiO₂, EtOAc); M.p. 174-176 °C (Literature: 171-173.4 °C^[92]); ¹H NMR (400 MHz, DMSO-d₆): δ = 10.70 (s, 1H, NH), 7.90 (d, *J* = 8.6 Hz, 3H, CH_{Ar}), 7.83 (brs, 2H, CH_{Ph}), 7.46–7.41 (m, 3H, CH_{Ph}), 7.04 (d, *J* = 8.7 Hz, 2H, CH_{Ar}), 3.83 (s, 3H, OCH₃), 2.37 (s, 3H, CH₃) ppm; ¹³C NMR (75 MHz, DMSO-d₆): δ = 161.7 (C_{Ar}-OCH₃), 138.1, 130.3, 129.2, 128.3, 126.3, 126.0, 113.4, 55.3 (OCH₃), 14.4 (CH₃) ppm; IR (neat): 3008, 2987, 2840, 1599, 1543, 1212 cm⁻¹; MS (ESI⁺) *m/z* (%): 269 [M+H]⁺ (100); HRMS (ESI⁺) calcd for C₁₆H₁₇N₂O₂ [M+H]⁺ 269.1285, found 269.1288. In the ¹³C-NMR the signals of C=N and C=O do not appear due to low intensity. The NMR data is in accordance with the literature.^[92-93]

**N'-(1-(4-Nitrophenyl)ethylidene)isonicotinohydrazide (23b).**

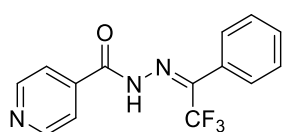
Isonicotinohydrazide (**21c**) (0.522 g, 3.81 mmol, 1.0 eq.) gave with acetophenone **22a** (1.1 eq.) after 24 h hydrazone **23b** (0.734 g, 2.58 mmol, 68%) as a pale yellow solid. $R_f = 0.23$ (SiO₂, EtOAc); ¹H NMR (300 MHz, DMSO-d₆): $\delta = 11.28$ (s, 1H, NH), 8.77-8.76 (m, 2H, CH_{Py}), 8.31-8.29 (m, 2H, CH_{Py}), 8.14-8.11 (m, 2H, CH_{Py}), 7.82-7.81 (m, 2H, CH_{Ar}), 2.44 (s, 3H, CH₃) ppm. The ¹H NMR data is in accordance with those measured before in this work group.^[42] This compound was published and described in the literature with NMR data in DMSO-d₆^[94] and CDCl₃.^[95]

**N'-(1-(4-Methoxyphenyl)ethylidene)isonicotinohydrazide (23c).**

Isonicotinohydrazide (**21c**) (0.500 g, 3.68 mmol, 1.0 eq.) gave with acetophenone **22a** (1.1 eq.) after 25 h hydrazone **23c** (0.241 g, 0.795 mmol, 22%) as white solid. $R_f = 0.28$ (SiO₂, petroleum ether/EtOAc 1:4); ¹H NMR (300 MHz, DMSO-d₆): $\delta = 10.95$ (s, 1H, NH), 8.76 (d, $J = 5.4$ Hz, 2H, CH_{Py}), 7.83 (d, $J = 8.7$ Hz, 2H, CH_{Ar}), 7.79 (d, $J = 5.4$ Hz, 2H, CH_{Py}), 7.00 (d, $J = 8.7$ Hz, 2H, CH_{Ar}), 3.81 (s, 3H, OCH₃), 2.35 (s, 3H, CH₃) ppm; ¹³C NMR (75 MHz, DMSO-d₆): $\delta = 162.1$ (C=O), 160.7 (C-OCH₃), 157.2 (C=N), 150.1 (CH_{Py}), 141.2 (C_{Py}), 130.2 (C_{Ar}), 128.1 (CH_{Ar}), 121.8 (CH_{Py}), 113.8 (CH_{Ar}), 55.3 (OCH₃), 14.7 (CH₃) ppm. The ¹H NMR data is in accordance with those measured before in this work group.^[42] This compound was also published by Shirote et al^[94] (NMR in CDCl₃) and Cordeiro et al^[96] (analytical data not published).

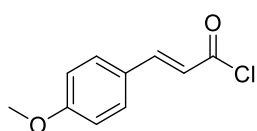
**N'-Benzylidenebenzohydrazide (23d).**

Benzohydrazide (**21a**) (1.00 g, 7.43 mmol, 1.0 eq.) gave with benzaldehyde (**22d**) (1.1 eq.) after 26 d hydrazone **23d** (1.54 g, 6.87 mmol, 94%) as white solid. $R_f = 0.66$ (SiO₂, petroleum ether/EtOAc 1:1); ¹H NMR (400 MHz, DMSO-d₆): $\delta = 11.86$ (s, 1H, NH), 8.48 (s, 1H, N=N=CH), 7.93 (d, $J = 7.4$ Hz, 2H, CH_{Ph}), 7.74 (d, $J = 6.6$ Hz, 2H, CH_{Ph}), 7.59 (d, $J = 7.1$ Hz, 1H, CH_{Ph}), 7.53 (t, $J = 7.4$ Hz, 2H, CH_{Ph}), 7.47-7.42 (m, 3H, CH_{Ph}) ppm; ¹³C NMR (101 MHz, DMSO-d₆): $\delta = 163.6$ (C=O), 148.3 (C=N), 134.8 (C_{Ph}), 133.9 (C_{Ph}), 132.2 (CH_{Ph}), 130.6 (CH_{Ph}), 129.3 (2C, CH_{Ph}/CH_{Ph}), 129.0 (CH_{Ph}), 128.1 (CH_{Ph}), 127.6 (CH_{Ph}) ppm. The NMR data is in accordance with the literature^[97].

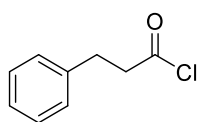
**N'-(2,2,2-Trifluoro-1-phenylethylidene)isonicotinohydrazide (23e).**

Isonicotinohydrazide (**21c**) (3.81 g, 27.8 mmol, 1.0 eq.) gave with 2,2,2-trifluoro-1-phenylethan-1-one **22e** (1.2 eq) after 24 h hydrazone **23e** (3.34 g, 11.4 mmol, 41%) as white solid. $R_f = 0.49$ (SiO₂, EtOAc); M.p. >200 °C (decomposition); ¹H NMR (300 MHz, DMSO-d₆): $\delta = 11.45$ (s, 1H), 8.71 (dd, $J = 4.5, 1.4$ Hz, 2H, CH_{Py}), 7.60-7.58 (m, 5H, CH_{Py}+CH_{Ph}), 7.55-7.48 (m, 2H, CH_{Ph}) ppm; ¹³C NMR (75 MHz,

DMSO- d_6): δ = 164.3 (C=O), 149.9 (CH_{Py}), 140.5 (C_{Py}), 131.1 (CH_{Ph}), 129.4 (CH_{Ph}), 128.4 (CH_{Ph}), 126.8 (C_{Ph}), 122.2 (CH_{Py}), 120.7 (q, J = 275 Hz, CF₃) ppm; ¹⁹F NMR (376 MHz, DMSO- d_6): δ = -65.9 ppm; MS (ESI⁺) m/z (%): 294 [$M+H$]⁺ (100); HRMS (ESI⁺) calcd for C₁₄H₁₁F₃N₃O [$M+H$]⁺ 294.0849, found 294.0860. In the ¹³C-NMR the quartet signal of N-N=C-CF₃ does not appear due to low intensity. The synthesis of **23e** is reported by Bottari et al.^{[98] [99]} without analytical data. This compound is mentioned in further literature.^{[100] [101]}



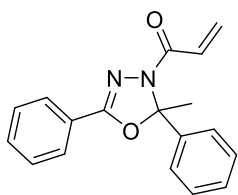
(E)-3-(4-Methoxyphenyl)acryloyl chloride (24b). 4-Methoxycinnamic acid (**42**) (1.00 g, 5.61 mmol, 1 eq) was dissolved in thionyl chloride (5.47 ml, 28.1 mmol, 5 eq). DMF (0.5 mL, 6.50 mmol, 0.2 eq.) was added and the mixture was stirred at room temperature for 2 h until no more gas formation was observed. Excess thionyl chloride was removed on the high vacuum and (E)-3-(4-methoxyphenyl)acryloyl chloride (**24b**) was received as pale brown solid and used without further purification.



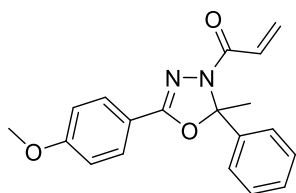
3-phenylpropanoyl chloride (24d). A solution of 4-methoxycinnamic acid (**43**) (1.00 g, 6.66 mmol, 1 eq) in 6 mL DCM was added to a solution of oxalyl chloride (1.27 g, 0.640 ml, 10.0 mmol, 1.5 eq) at 0-5 °C. The mixture was stirred at room temperature for 14 h and DCM was removed. 1.12 g (6.66 mmol) 3-phenylpropanoyl chloride (**24d**) was obtained as pale-yellow liquid in quantitative yield and used without further purification. ¹H NMR (300 MHz, CDCl₃): δ = 7.35-7.19 (m, 5H, CH_{Ph}), 3.24-3.19 (m, 2H, Ph-CH₂-CH₂), 3.02 (t, J = 7.5 Hz, 2H, Ph-CH₂-CH₂). The NMR data is in accordance with the literature.^[76]

General method for the preparation of 2,3-dihydro-1,3,4-oxadiazoles with 3-enone unit (OXEs)

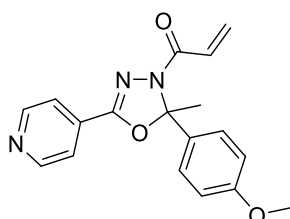
To a suspension of NaH (1.2 eq.) or a solution triethylamine (1.2 eq.) in 1-20 mL absolute THF were added the hydrazones **23a-c** and **23e** (50.0 mg-0.490 g, 0.185 mmol-2.18 mmol, 1.0 eq.) at 0 °C. In the case of hydrazone **23d** the educt was stirred in 15 mL THF without base and cooled to 0 °C. Then a solution of acid chlorides **24a-d** (0.204 mmol-2.40 mmol, 1.1 eq.) in 1-5 mL THF was added dropwise, the mixture warmed to room temperature and stirred until the reaction was complete. After removal of the solvent, the crude products were purified by column chromatography or preparative TLC (SiO₂, petroleum ether/EtOAc, various mixtures: from 10:1 to 1:1) to afford 2,3-dihydro-1,3,4-oxadiazoles with 3-enone unit (OXEs).



1-(2-Methyl-2,5-diphenyl-1,3,4-oxadiazol-3(2H)-yl)prop-2-en-1-one (OXE1). Hydrazone **23f** (0.400 g, 1.68 mmol, 1.0 eq.) gave with NEt_3 (1.2 eq.) and acrylic acid chloride (**24a**) (1.1 eq.) after 4 h **OXE1** (0.237 g, 0.811 mmol, 48%) as colorless oil. $R_f = 0.30$ (SiO_2 , petroleum ether/EtOAc 10:1); $^1\text{H NMR}$ (300 MHz, CDCl_3): $\delta = 7.94\text{--}7.91$ (m, 2H, CH_{Ph}), $7.64\text{--}7.61$ (m, 2H, CH_{Ph}), $7.54\text{--}7.35$ (m, 6H, CH_{Ph}), 7.21 (dd, $J = 17.2, 10.4$ Hz, 1H, $\text{CH}=\text{CH}_2$), 6.44 (dd, $J = 17.2, 1.9$ Hz, 1H, $\text{CH}=\text{CH}_2$), 5.78 (dd, $J = 10.4, 1.9$ Hz, 1H, $\text{CH}=\text{CH}_2$), 2.38 (s, 3H, CH_3) ppm; $^{13}\text{C NMR}$ (75 MHz, CDCl_3): $\delta = 161.2$ (C=O), 154.1 (C=N), 138.9 (C_{Ph}), 131.5 (CH_{Ph}), 129.1 ($\text{CH}=\text{CH}_2$), 128.6 (CH_{Ph}), 128.4 (CH_{Ph}), 128.1 (C_{Ph}), 128.0 ($\text{CH}=\text{CH}_2$), 126.8 (CH_{Ph}), 125.7 (CH_{Ph}), 124.6 (CH_{Ph}), 100.7 (N,O-C- CH_3), 22.8 (CH_3) ppm; IR (neat): $3064, 2989, 2937, 1655, 1424, 1323, 1260, 764$ cm^{-1} ; MS (ESI⁺) m/z (%): 293 [$M+\text{H}$]⁺ (100); HRMS (ESI⁺) calcd for $\text{C}_{18}\text{H}_{17}\text{N}_2\text{O}_2$ [$M+\text{H}$]⁺ 293.1285 , found 293.1296 .

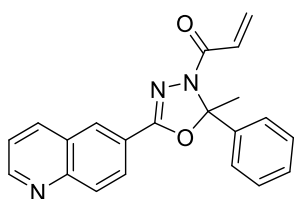


1-(5-(4-Methoxyphenyl)-2methyl-2-phenyl-1,3,4-oxadiazol-3(2H)-yl)prop-2-en-1-one (OXE1-(OMe)'). Hydrazone **23b** (0.300 g, 1.12 mmol, 1.0 eq.) gave with acrylic acid chloride **24a** (1.1 eq.) after 7 d and purification via preparative HPLC 35 mg (0.110 mmol, 10%) **OXE1-(OMe)'** as colorless oil. Preparative HPLC was performed on an Agilent 1260 Infinity (Agilent Technologies, USA). Column: Agilent Flow XDB RP-18, Eurosphere 100 (5 μm , 21.2 x 250 mm); solvents: acetonitrile (degassed, HPLC grade, Merck), H_2O (degassed, Millipore); application: liquid injection in acetonitrile/MeOH 1:1, concentration: 20 mg/mL, injection volume: 1 mL; method: gradient: H_2O /acetonitrile; 60% acetonitrile at $t = 0$ min, 90% acetonitrile at $t = 20$ min, 100% acetonitrile at $t = 22$ min, 60% acetonitrile at $t = 24$ min, flow rate: 20 mL/min. $R_f = 0.45$ (SiO_2 , petroleum ether/EtOAc 3:1), 0.13 (RP18, acetonitrile/ H_2O 3:2); $^1\text{H NMR}$ (300 MHz, CDCl_3): $\delta = 7.86\text{--}7.81$ (m, 2H, CH_{Ar}), $7.61\text{--}7.56$ (m, 2H, CH_{Ph}), $7.42\text{--}7.32$ (m, 3H, CH_{Ph}), 7.16 (dd, $J = 17.2, 10.4$ Hz, 1H, $\text{CH}=\text{CH}_2$), $6.97\text{--}6.92$ (m, 2H, CH_{Ar}), 6.39 (dd, $J = 17.2, 1.9$ Hz, 1H, $\text{CH}=\text{CH}_2$), 5.74 (dd, $J = 10.4, 1.9$ Hz, 1H, $\text{CH}=\text{CH}_2$), 3.86 (s, 3H, OCH_3), 2.34 (s, 3H, CH_3) ppm; $^{13}\text{C NMR}$ (75 MHz, CDCl_3): $\delta = 162.3$ (C=O), 161.1 ($\text{C}_{\text{Ar}}\text{-OCH}_3$), 154.2 (C=N), 139.1 (C_{Ph}), 129.2 ($\text{CH}=\text{CH}_2$), 128.7 (CH_{Ph}), 128.4 (CH_{Ar}), 128.2 (CH_{Ph}), 128.0 ($\text{CH}=\text{CH}_2$), 125.8 (CH_{Ph}), 117.0 (C_{Ar}), 114.1 (CH_{Ar}), 100.5 (N,O-C- CH_3), 55.4 (OCH_3), 22.9 (CH_3) ppm; MS (ESI⁺) m/z (%): 323 [$M+\text{H}$]⁺ (100); HRMS (ESI⁺) calcd for $\text{C}_{19}\text{H}_{18}\text{N}_2\text{O}_3$ [$M+\text{H}$]⁺ 323.1390 , found 323.1391 .



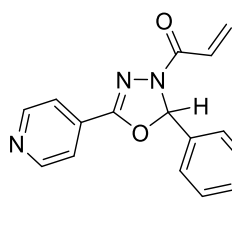
1-(2-(4-Methoxyphenyl)-2-methyl-5-(pyridin-4-yl)-1,3,4-oxadiazol-3(2H)-yl)prop-2-en-1-one (OXE1-OMe,(4py)'). Hydrazone **23c** (0.150 g, 0.557 mmol, 1.0 eq.) gave with triethylamine (1.2 eq.) and acrylic acid chloride (**24a**) (1.1 eq.) after 23 h **OXE1-OMe,(4py)'** (53.0 mg, 0.164 mmol, 29%) as yellow oil. $R_f = 0.30$

(SiO₂, petroleum ether/EtOAc 1:1): 0.49; ¹H NMR (400 MHz, CDCl₃): δ = 8.72 (d, *J* = 5.3 Hz, 2H, CH_{Py}), 7.71 (d, *J* = 5.8 Hz, 2H, CH_{Py}), 7.49–7.45 (m, 2H, CH_{Ar}), 7.13 (dd, *J* = 17.2, 10.4 Hz, 1H, CH=CH₂), 6.91–6.88 (m, 2H, CH_{Ar}), 6.40 (dd, *J* = 17.2, 1.7 Hz, 1H, CH=CH₂), 5.77 (dd, *J* = 10.4, 1.6 Hz, 1H, CH=CH₂), 3.78 (s, 3H, OCH₃), 2.32 (s, 3H, CH₃) ppm; ¹³C NMR (101 MHz, CDCl₃): δ = 161.4 (C=O), 160.3 (C_{Ar}-OCH₃), 152.1 (C=N), 150.3 (CH_{Py}), 132.3 (C_{Py}), 130.5 (C_{Ar}), 128.8 (CH=CH₂), 127.6 (CH=CH₂), 127.2 (CH_{Ar}), 120.3 (CH_{Py}), 113.8 (CH_{Ar}), 101.8 (N,O-C-CH₃), 55.2 (OCH₃), 22.9 (CH₃) ppm; IR (neat): 2937, 2840, 1659, 1513, 1431, 1308, 1249, 1178, 824 cm⁻¹; MS (ESI⁺) *m/z* (%): 324 [M+H]⁺ (100); HRMS (ESI⁺) calcd for C₁₈H₁₈N₃O₃ 324.1343 [M+H]⁺, found 324.1349.

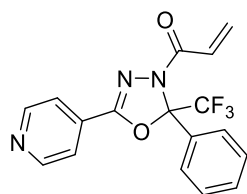


1-(2-Methyl-2-phenyl-5-(quinolin-6-yl)-1,3,4-oxadiazol-3(2H)-yl)prop-2-en-1-one (OXE1-(6qui)''). Hydrazone **23g** (0.200 g, 0.691 mmol, 1.0 eq.) gave with NaH (1.2 eq.) and acrylic acid chloride (**24a**) (1.1 eq.) after 20 h **OXE1-(6qui)''** (26.0 mg, 75.7 μmol, 11%) as white solid. *R_f* = 0.47 (SiO₂, petroleum ether/EtOAc 1:1);

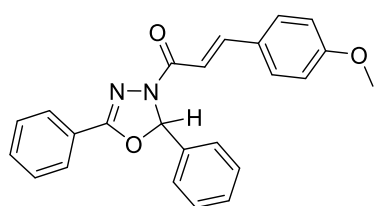
M.p. 117–120 °C; ¹H NMR (300 MHz, CDCl₃): δ = 8.99 (s, 1H, CH_{Qui}), 8.32 (d, *J* = 1.5 Hz, 1H, CH_{Qui}), 8.25 (dd, *J* = 8.9, 1.8 Hz, 1H, CH_{Qui}), 8.22 (d, *J* = 8.3 Hz, 1H, CH_{Qui}), 8.17 (d, *J* = 8.9 Hz, 1H, CH_{Qui}) 7.65–7.59 (m, 2H, CH_{Ph}), 7.48 (dd, *J* = 8.3, 4.2 Hz, 1H, CH_{Qui}), 7.44–7.35 (m, 3H, CH_{Ph}), 7.22 (dd, *J* = 17.2, 10.4 Hz, 1H, CH=CH₂), 6.43 (dd, *J* = 17.2, 1.8 Hz, 1H, CH=CH₂), 5.80 (dd, *J* = 10.4, 1.8 Hz, 1H, CH=CH₂), 2.40 (s, 3H, CH₃) ppm; ¹³C NMR (75 MHz, CDCl₃): δ = 161.4 (C=O), 153.6 (C=N), 151.9 (CH_{Qui}), 149.4 (C_{Qui}), 138.8 (C_{Ph}), 136.6 (CH_{Qui}), 130.2 (CH_{Qui}), 129.4 (CH_{Ph}), 128.5 (2C, CH_{Ph}, CH=CH₂), 127.9 (C_{Qui}), 127.7 (CH_{Qui}), 127.2 (CH_{Qui} or CH=CH₂), 127.0 (CH_{Qui} or CH=CH₂), 125.8 (CH_{Ph}), 122.9 (C_{Qui}), 122.1 (CH_{Qui}), 101.3 (N,O-C-CH₃), 22.9 (CH₃) ppm; ¹H NMR (300 MHz, Acetone-d₆): δ = 9.00 (dd, *J* = 4.2, 1.7 Hz, 1H, CH_{Qui}), 8.49 (dd, *J* = 8.4, 1.3 Hz, 1H, CH_{Qui}), 8.44 (d, *J* = 1.9 Hz, 1H, CH_{Qui}), 8.27 (dd, *J* = 8.9, 1.9 Hz, 1H, CH_{Qui}), 8.15 (d, *J* = 8.9 Hz, 1H, CH_{Qui}) 7.69–7.64 (m, 2H, CH_{Ph}), 7.61 (dd, *J* = 8.3, 4.2 Hz, 1H, CH_{Qui}), 7.48–7.38 (m, 3H, CH_{Ph}), 7.26 (dd, *J* = 17.2, 10.4 Hz, 1H, CH=CH₂), 6.32 (dd, *J* = 17.2, 2.2 Hz, 1H, CH=CH₂), 5.81 (dd, *J* = 10.4, 2.2 Hz, 1H, CH=CH₂), 2.39 (s, 3H, CH₃) ppm; ¹³C NMR (75 MHz, Acetone-d₆): δ = 161.4 (C=O), 154.2 (C=N), 153.0 (CH_{Qui}), 150.3 (C_{Qui}), 140.2 (C_{Ph}), 137.5 (CH_{Qui}), 131.1 (CH_{Qui}), 130.1 (CH_{Ph}), 129.3 (CH_{Ph}), 129.2 (CH=CH₂), 128.8 (C_{Qui}), 128.4 (CH_{Qui} or CH=CH₂), 128.2 (CH_{Qui} or CH=CH₂), 127.4 (CH_{Qui}), 126.8 (CH_{Ph}), 123.5 (C_{Qui}), 123.3 (CH_{Qui}), 102.1 (N,O-C-CH₃), 23.1 (CH₃) ppm; IR (neat): 3060, 2926, 2855, 1655, 1461, 1420, 1327, 1252, 1185, 1059, 977, 883, 839, 764, 693 cm⁻¹; MS (ESI⁺) *m/z* (%): 344 [M+H]⁺ (100); HRMS (ESI⁺) calcd for C₂₁H₁₈N₃O₂ [M+H]⁺ 344.1394, found 344.1404.



1-(2-(4-Nitrophenyl)-5-(pyridin-4-yl)-1,3,4-oxadiazol-3(2H)-yl)prop-2-en-1-one (OXE2-NO₂,(4py))'. Hydrazone **23h** (50.0 mg, 0.185 mmol, 1.0 eq.) gave with NaH (1.2 eq.) and acrylic acid chloride (**24a**) (1.1 eq.) after 2 h **OXE2-NO₂,(4py))'** (27.0 mg, 83.3 μmol, 45%) as beige solid. R_f = 0.17 (SiO₂, petroleum ether/EtOAc, 1:1) M.p. 113-114 °C; ¹H NMR (300 MHz, CDCl₃): δ = 8.78 (d, J = 5.5 Hz, 2H, CH_{Py}), 8.30–8.25 (m, 2H, CH_{Ar}), 7.75–7.67 (m, 4H, CH_{Ar}+CH_{Py}), 7.26 (s, 1H, N,O-C-H), 7.07 (dd, J = 17.2, 10.4 Hz, 1H, CH=CH₂), 6.50 (dd, J = 17.2, 1.6 Hz, 1H, CH=CH₂), 5.89 (dd, J = 10.4, 1.6 Hz, 1H, CH=CH₂) ppm; ¹³C NMR (75 MHz, CDCl₃): δ = 162.6 (C=O), 154.1 (C=N), 150.6 (CH_{Py}), 148.9 (C_{Ar}), 141.8 (C_{Ar}-NO₂), 131.4 (C_{Py}), 130.3 (CH=CH₂), 127.9 (CH_{Ar}), 126.4 (CH=CH₂), 124.1 (CH_{Ar}), 120.4 (CH_{Py}), 91.8 (N,O-C-H) ppm; IR (neat): 2926, 2855, 1659, 1525, 1435, 1331, 1252, 984 cm⁻¹; MS (ESI⁺) m/z (%): 325 [$M+H$]⁺ (100); HRMS (ESI⁺) calcd for C₁₆H₁₃N₄O₄ [$M+H$]⁺ 325.0931, found : 325.0934.

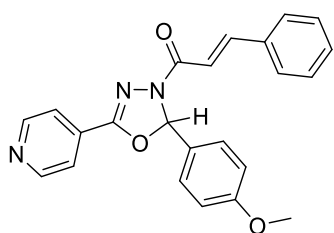


1-(2-Phenyl-5-(pyridin-4-yl)-2-(trifluoromethyl)-1,3,4-oxadiazol-3(2H)-yl)prop-2-en-1-one (OXE3-(4py))'. Hydrazone **23e** (0.377 g, 1.29 mmol, 1.0 eq.) gave with NaH (1.2 eq.) and acrylic acid chloride (**24a**) (1.1 eq.) after 3 h **OXE3-(4py))'** (2.34 mg, 6.74 μmol, 1%) as beige oil. This yield was received after column chromatography (petroleum ether/EtOAc 3:1) and subsequent preparative TLC (petroleum ether/EtOAc 3:1). R_f = 0.45 (SiO₂, petroleum ether/EtOAc 1:1); ¹H NMR (300 MHz, CDCl₃): δ = 8.79 (brs, 2H, CH_{Py}), 7.78 (d, J = 6.0 Hz, 2H, CH_{Py}), 7.68-7.65 (m, 2H, CH_{Ph}), 7.49–7.46 (m, 3H, CH_{Ph}), 7.14 (dd, J = 17.2, 10.4 Hz, 1H, CH=CH₂), 6.50 (dd, J = 17.2, 1.6 Hz, 1H, CH=CH₂), 5.90 (dd, J = 10.4, 1.6 Hz, 1H, CH=CH₂) ppm; ¹³C NMR (101 MHz, CDCl₃) δ = 162.0 (C=O), 151.6 (C=N), 150.3 (CH_{Py}), 131.1 (CH_{Ph}), 131.0 (CH_{Ph}), 130.9 (CH=CH₂), 130.8 (C_{Py}), 128.8 (CH=CH₂), 127.0 (CH_{Ph}), 126.8 (q, J = 1.8 Hz, C_{Ph}), 122.1 (q, J = 290.5 Hz, CF₃), 120.5 (CH_{Py}), 98.8 (q, J = 34.4 Hz, N,O-C-CF₃) ppm; ¹⁹F NMR (376 MHz, CDCl₃): δ = -75.2 ppm; IR (neat): 2926, 2855, 1689, 1640, 1409, 1174, 951 cm⁻¹; MS (ESI⁺) m/z (%): 348 [$M+H$]⁺ (100). The ¹H NMR data is in accordance with previous work in this group.^[43] ¹³C NMR data have not been measured before and were obtained during this work with the compound prepared by Rainer Herzog in this work group.

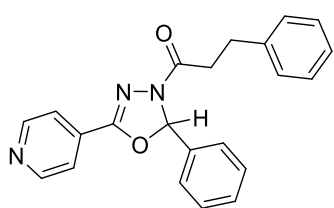


(E)-1-(2,5-Diphenyl-1,3,4-oxadiazol-3(2H)-yl)-3-(4-methoxyphenyl)prop-2-en-1-one (OXE8-(OMe))'.^[45] Hydrazone **23d** (0.490 g, 2.18 mmol, 1.0 eq.) gave with triethylamine (10 eq.) and cinnamic acid chloride **24a** (1.1 eq.) after 20 h **OXE8-(OMe))'** (0.341 g, 0.887 mmol, 41%) as a white solid. R_f = 0.5 (SiO₂, petroleum ether/EtOAc 1:1); M.p. 128-130 °C; ¹H NMR (400 MHz, CDCl₃): δ =

7.98–7.96 (m, 2H, CH_{Ph}), 7.73 (d, *J* = 15.9 Hz, 1H, CH=CH-Ar), 7.59–7.41 (m, 10H, CH_{Ph}+CH_{Ar}), 7.34 (d, *J* = 15.9 Hz, 1H, CH=CH-Ar), 7.23 (s, 1H, N,O-C-H), 6.93 (d, *J* = 8.7 Hz, 2H, CH_{Ar}), 3.84 (s, 3H, OCH₃), ¹³C NMR (101 MHz, CDCl₃): δ = 163.0 (C=O), 161.1 (C_{Ar}-OMe), 155.8 (C=N), 142.6 (CH=CH-Ar), 136.3 (C_{Ph}), 131.6 (C_{Ar}), 129.83 (CH_{Ph}), 129.80 (CH_{Ph}), 128.7 (CH_{Ph}), 128.6 (CH_{Ph}), 127.7 (C_{Ph}), 127.0 (CH_{Ar}), 126.6 (CH_{Ph}), 124.5 (CH_{Ph}), 114.6 (CH=CH-Ar), 114.1 (CH_{Ar}), 92.6 (N,O-C-H), 55.3 (OCH₃); IR (neat): 3012, 2915, 2840, 1648, 1603, 1513, 1431, 1238, 1174 cm⁻¹; MS (ESI⁺) *m/z* (%): 385 [*M*+H]⁺ (100); HRMS (ESI⁺) calcd for C₂₄H₂₁N₂O₃ [*M*+H]⁺ 385.1547, found 385.1553. This compound was published by Arora et al. in 2012 with ¹H NMR data in DMSO-d₆.^[45]

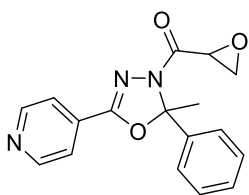


(E)-1-(2-(4-Methoxyphenyl)-5-(pyridin-4-yl)-1,3,4-oxadiazol-3(2H)-yl)-3-phenylprop-2-en-1-one (OXE8-OMe,(4py)). Hydrazone **23j** (41.6 mg, 0.163 mmol, 1.0 eq.) gave with NEt₃ (1.2 eq.) and cinnamic acid chloride **24c** (1.1 eq.) after 5 h **OXE8-OMe,(4py)** (43.5 mg, 0.113 mmol, 69%) as a yellow solid. *R*_f = 0.44 (SiO₂, petroleum ether/EtOAc 1:1); M.p. 156 °C; ¹H NMR (400 MHz, CDCl₃): δ = 8.76 (d, *J* = 5.3 Hz, 2H, CH_{Py}), 7.78 (d, *J* = 6.0 Hz, 2H, CH_{Py}), 7.75 (d, *J* = 16 Hz, 1H, CH=CH-Ph), 7.63–7.61 (m, 2H, CH_{Ph}), 7.45 (d, *J* = 8.7 Hz, 2H, CH_{Ar}), 7.42–7.38 (m, 4H, CH_{Ph} + CH=CH-Ph), 7.20 (s, 1H, N,O-C-H), 6.94 (d, *J* = 8.7 Hz, 2H, CH_{Ar}), 3.81 (s, 3H, OCH₃) ppm; ¹³C NMR (101 MHz, CDCl₃): δ = 162.8 (C=O), 161.0 (C_{Ar}-OCH₃), 153.9 (C=N), 150.4 (CH_{Py}), 143.6 (CH=CH-Ph), 134.8 (C_{Ph}), 132.3 (C_{Py}), 130.2 (C_{Ar}), 128.8 (CH_{Ph}), 128.3 (CH_{Ph}), 128.1 (CH_{Ar}), 127.9 (CH_{Ph}), 120.5 (CH_{Py}), 116.7 (CH=CH-Ph), 114.3 (CH_{Ar}), 93.5 (N,O-C-H), 55.3 (OCH₃) ppm; IR (neat): 3061, 3023, 1651, 1609, 1517, 1434, 1338, 1297, 1253, 1239, 1181 cm⁻¹; MS (ESI⁺) *m/z* (%): 386 [*M*+H]⁺ (100); HRMS (ESI⁺) calcd for C₂₃H₂₀N₃O₃ [*M*+H]⁺ 386.1499, found 386.1501. The NMR data was previously shown in DMSO-d₆ in this work group.^[42]



3-Phenyl-1-(2-phenyl-5-(pyridin-4-yl)-1,3,4-oxadiazol-3(2H)-yl)propan-1-one (OXE8-(4py))-H₂. Hydrazone **23i** (0.100 g, 0.444 mmol, 1.0 eq.) gave with NaH (1.2 eq.) and dihydrocinnamic acid chloride (**24d**) (1.1 eq.) after 1 h **OXE8-(4py))-H₂** (0.119 g, 0.334 mmol, 76%) as beige waxy solid. *R*_f = 0.36 (SiO₂, petroleum ether/EtOAc 1:1); M.p. 105–110 °C; ¹H NMR (300 MHz, CDCl₃): δ = 8.74 (d, *J* = 4.0 Hz, 2H, CH_{Py}), 7.71 (d, *J* = 6.0 Hz, 2H, CH_{Py}), 7.42 (s, 5H, CH_{Ph}), 7.30–7.20 (m, 5H, CH_{Ph}), 7.11 (s, 1H, N,O-C-H), 3.15–2.97 (m, 4H, CH₂-CH₂) ppm; ¹³C NMR (75 MHz, CDCl₃): δ = 169.8 (C=O), 153.7 (C=N), 150.3 (CH_{Py}), 140.7 (C_{Ph}), 135.7 (C_{Ph}), 132.1 (C_{Py}), 130.1 (CH_{Ph}), 128.8 (CH_{Ph}), 128.4 (2C, CH_{Ph}), 126.5 (CH_{Ph}), 126.2 (CH_{Ph}), 120.4 (CH_{Py}), 93.2 (N,O-C-H), 35.4 (CH₂-CH₂-Ph), 30.4 (CH₂-CH₂-Ph) ppm; IR (neat): 3030, 2926, 1707, 1659, 1439, 1342, 1193 cm⁻¹;

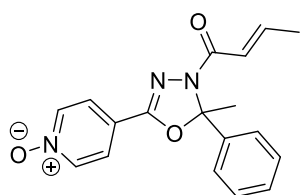
MS (ESI⁺) m/z (%): 358 [$M+H$]⁺ (100); HRMS (ESI⁺) calcd for C₂₂H₂₀N₃O₂ [$M+H$]⁺ 358.1549, found 358.1550.



(2-Methyl-2-phenyl-5-(pyridin-4-yl)-1,3,4-oxadiazol-3(2H)-yl)(oxiran-2-yl)methanone (OXEp1-(4py)''). A solution of *tert*-butylhydroperoxide (5 M in decane, 0.500 mmol, 1.5 eq.) was dissolved in 1 mL dry THF at -78 °C and a solution of butyllithium in hexanes (1.6 M, 586 μ L, 0.366 mmol, 1.1 eq.) was added. The solution was stirred at -78 °C for 5 min, then **OXE1-(4py)''** (0.100 mg, 0.341 mmol, 1.0 eq) in 1 mL dry THF was added. The reaction mixture was allowed to warm to 0 °C, stirred for 4 h, quenched by the addition of solid Na₂SO₃ (30.1 mg, 0.239 mmol, 0.7 eq.) and stirred for another 15 min. The mixture was diluted with 5 mL diethylether and filtered. After concentration of the solution under vacuum, the product was purified by column chromatography (from petroleum ether/DCM/EtOAc 2:1:1 to DCM/EtOAc 1:1) to yield diastereomeric **OXE1-(4py)''** (5.0 mg, 0.016 mmol, 5%) as pale-yellow oil. R_f = 0.41 (SiO₂, DCM/EtOAc 1:1); ¹H NMR (300 MHz, CDCl₃): δ = 8.77 (d, J = 5.9 Hz, 2H, CH_{Py}), 7.77 (d, J = 6.1 Hz, 2H, CH_{Py}), 7.61-7.47 (m, 2H, CH_{Ph}), 7.43-7.36 (m, 3H, CH_{Ph}), 4.31 (dd, J = 6.7, 3.8 Hz, 1H, CH), 3.07-2.94 (m, 2H, CH₂), 2.34 (d, J = 8.2 Hz, 3H, CH₃) ppm; ¹H NMR (300 MHz, DMSO-d₆): δ = 8.78 (dd, J = 4.5, 1.5 Hz, 2H, CH_{Py}), 7.78 (dd, J = 4.5, 1.6 Hz, 2H, CH_{Py}), 7.64-7.51 (m, 2H, CH_{Ph}), 7.50-7.36 (m, 3H, CH_{Ph}), 4.30 (dd, J = 4.3, 2.4 Hz, 1H, CH), 3.03 (ddd, J = 8.7, 6.5, 4.3 Hz, 1H, CH₂), 2.83 (ddd, J = 19.66, 5, 2.4 Hz, 1H, CH₂), 2.26 (d, J = 8.4 Hz, 3H, CH₃); MS (ESI⁺) m/z (%): 310 [$M+H$]⁺ (100). The ¹H NMR data in CDCl₃ is in accordance with the previous work in this group.^[44]

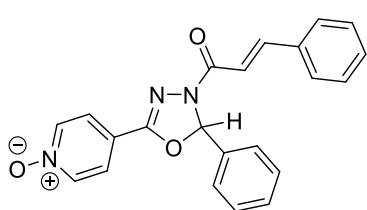
General method for the preparation of 2,3-dihydro-1,3,4-oxadiazoles with *N*-oxide (OXE-(4py-*N*-oxides)'')^[49]

OXE4-(4py)'' or **OXE8-(4py)''** (1.0 eq.) was dissolved in 1.5 mL DCM and a solution of mCPBA (1.7 eq.) in 2 mL DCM was added. The reaction mixture was stirred at rt until completion and quenched with 5 mL aqueous NaOH (0.2 M). The organic phase was separated, washed with water (2 x 20 mL) and dried with MgSO₄. The crude product was purified with column chromatography (from petroleum ether/EtOAc 1:1 to EtOAc/methanol 4:1) to yield *N*-oxidized **OXEs**.



(*E*)-4-(4-(But-2-enoyl)-5-methyl-5-phenyl-4,5-dihydro-1,3,4-oxadiazol-2-yl)pyridine-1-oxide (OXE4-(4py-*N*-oxide)''). **OXE4-(4py)''** (67.0 mg, 0.218 mmol, 1.0 eq.) and mCPBA (67.7 mg, 0.392 mmol, 1.7 eq.) gave after 48 h **OXE4-(4py-*N*-oxide)''** (0.0550 g, 0.170 mmol, 78%) as pale beige solid. R_f = 0.13 (SiO₂, dichloromethane/EtOAc 1:1); M.p. 174-175 °C; ¹H NMR (400 MHz, CDCl₃): δ = 8.20

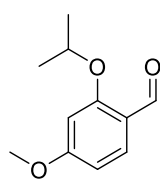
(d, $J = 6.9$ Hz, 2H, CH_{Py}), 7.71 (d, $J = 6.9$ Hz, 2H, CH_{Py}), 7.52-7.49 (m, 2H, CH_{Ph}), 7.41-7.36 (m, 3H, CH_{Ph}), 6.96 (dq, $J = 15.4, 6.7$ Hz, 1H, $\text{CH}=\text{CH}-\text{CH}_3$), 6.79 (dd, $J = 15.4, 1.4$ Hz, 1H, $\text{CH}=\text{CH}-\text{CH}_3$), 2.31 (s, 3H, $\text{N,O}-\text{C}-\text{CH}_3$), 1.92 (dd, $J = 6.7, 1.3$ Hz, 3H, $\text{CH}=\text{CH}-\text{CH}_3$) ppm; ^{13}C NMR (101 MHz, CDCl_3): $\delta = 161.9$ (C=O), 150.6 (C=N), 143.2 ($\text{CH}=\text{CH}-\text{CH}_3$), 139.4 (CH_{Py}), 138.4 (C_{Ph}), 129.4 (CH_{Ph}), 128.5 (CH_{Ph}), 125.6 (CH_{Ph}), 123.4 (CH_{Py}), 121.8 ($\text{CH}=\text{CH}-\text{CH}_3$), 121.7 (C_{Py}), 102.2 ($\text{N,O}-\text{C}-\text{CH}_3$), 23.0 (CH_3), 18.1 ($\text{CH}=\text{CH}-\text{CH}_3$) ppm; MS (ESI⁺) m/z (%): 324 [$M+\text{H}$]⁺ (100). Spectral data are in accordance with the previous work in this group.^[44]



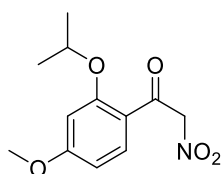
(E)-4-(4-(Cinnamoyl-5-phenyl-4,5-dihydro-1,3,4-oxadiazol-2-yl)pyridine-1-oxide (OXE8-(4py-N-oxide)) (OXE8-(4py)“ (97.5 mg, 0.274 mmol, 1.0 eq.) and mCPBA (85.2 mg, 0.494 mmol, 1.7 eq.) gave after 48 h OXE8-(4py-N-oxide)“ (70.5 mg, 0.190 mmol, 69%) as pale beige solid. $R_f = 0.13$

(SiO_2 , dichloromethane/EtOAc 1:1); M.p. 185-186 °C; ^1H NMR (400 MHz, CDCl_3): $\delta = 8.22$ (d, $J = 7.1$ Hz, 2H, CH_{Py}), 7.77 (d, $J = 7.1$ Hz, 2H, CH_{Py}), 7.74 (d, $J = 16.1$ Hz, 1H, $\text{CH}=\text{CH}-\text{Ph}$), 7.61-7.57 (m, 2H, CH_{Ph}), 7.52-7.48 (m, 2H, CH_{Ph}), 7.44-7.41 (m, 3H, CH_{Ph}), 7.39-7.33 (m, 4H, $\text{CH}_{\text{Ph}} + \text{CH}=\text{CH}-\text{Ph}$), 7.22 (s, 1H, $\text{N,O}-\text{C}-\text{H}$) ppm; ^{13}C NMR (101 MHz, CDCl_3): $\delta = 162.7$ (C=O), 152.7 (C=N), 143.7 ($\text{CH}=\text{CH}-\text{Ph}$), 139.5 (CH_{Py}), 135.5 (C_{Ph}), 134.6 (C_{Ph}), 130.23 (CH_{Ph}), 130.18 (CH_{Ph}), 128.9 (CH_{Ph}), 128.8 (CH_{Ph}), 128.2 (CH_{Ph}), 126.5 (CH_{Ph}), 123.5 (CH_{Py}), 121.1 (C_{Py}), 116.4 ($\text{CH}=\text{CH}-\text{Ph}$), 93.7 ($\text{N,O}-\text{C}-\text{H}$) ppm; MS (ESI⁺) m/z (%): 372 [$M+\text{H}$]⁺ (100). Spectral data are in accordance with the previous work in this group.^[44]

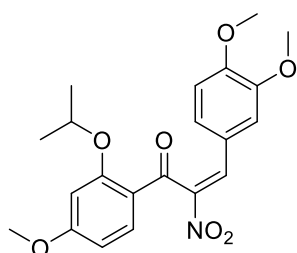
A 6.3 Synthesis of NO_2 -flavanone and precursors



2-Isopropoxy-4-methoxybenzaldehyde (67).^[77] 2-Hydroxy-4-methoxybenzaldehyde (**65**, 1.00 g, 6.60 mmol, 1 eq.) was dissolved in 10 mL dry DMF and 2-iodopropane (**66**, 825 μL , 8.25 mmol, 1.25 eq.) and K_2CO_3 (3.96 g, 28.7 mmol, 4.3 eq.) were added. The resulting yellow suspension was stirred at 45 °C for 12 h, then quenched with 100 mL H_2O . The aqueous phase was extracted with ethyl acetate (3 x 50 mL and the combined organic phase was washed with brine (3 x 100 mL). After drying over MgSO_4 and removing of the solvent, 2-Isopropoxy-4-methoxybenzaldehyde (**67**) was obtained as a pale-yellow liquid (1.15 g, 5.92 mmol, 90%). $R_f = 0.43$ (SiO_2 , petroleum ether/EtOAc 5:1); ^1H NMR (300 MHz, CDCl_3): $\delta = 10.31$ (s, 1H, $\text{O}=\text{C}-\text{H}$), 7.81 (d, $J = 8.7$ Hz, 1H, CH_{Ar}), 6.52 (dd, $J = 8.7, 2.2$ Hz, 1H, CH_{Ar}), 6.44 (d, $J = 2.2$ Hz, 1H, CH_{Ar}), 4.63 (hept, $J = 6.0$ Hz, 1H, $\text{CH}-(\text{CH}_3)_2$), 3.86 (s, 3H, OCH_3), 1.40 (d, $J = 6.1$ Hz, 6H, $\text{CH}-(\text{CH}_3)_2$) ppm; ^{13}C NMR (75 MHz, CDCl_3): $\delta = 188.7$ (C=O), 166.0 ($\text{C}_{\text{Ar}}-\text{OCH}_3$), 162.3 ($\text{C}_{\text{Ar}}-\text{OCH}-(\text{CH}_3)_2$), 130.3 (CH_{Ar}), 119.9 ($\text{C}_{\text{Ar}}-\text{C}=\text{O}$), 105.8 (CH_{Ar}), 99.9 (CH_{Ar}), 71.1 ($\text{OCH}-(\text{CH}_3)_2$), 55.6 (OCH_3), 21.9 ($\text{C}-(\text{CH}_3)_2$) ppm.



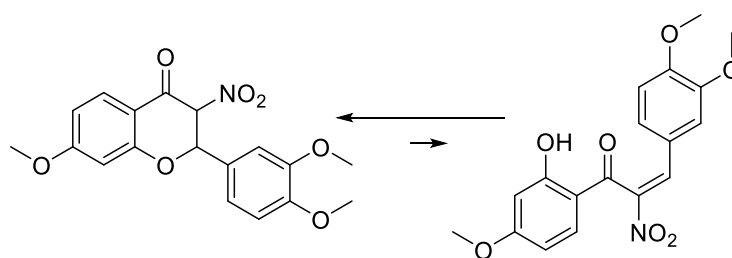
1-(2-Isopropoxy-4-methoxyphenyl)-2-nitroethan-1-one (68).^[36] 2-Isopropoxy-4-methoxybenzaldehyde (**67**, 770 mg, 3.96 mmol, 1 eq.), nitromethane (2.97 mL, 55.5 mmol, 14 eq.) and sodium acetate (4.55 g, 55.5 mmol, 14 eq.) were dissolved in 20 mL ethanol and stirred at room temperature for 24 h. The resulting yellow suspension was diluted with 50 mL H₂O and the aqueous phase was extracted with ethyl acetate (3 x 30 mL). The combined organic phases were washed with brine (3 x 100 mL), dried over MgSO₄ and the solvent was removed. A yellow paste was obtained which was dissolved in dichloromethane. To this solution pyridinium chlorochromate (2.05 g, 9.50 mmol, 2.4 eq.) was added at 0 °C. Without removal of the ice bath the reaction mixture was allowed to warm to room temperature overnight and stirred for 24 h in total. The solvent was evaporated and after column chromatography (petroleum ether/ EtOAc 5:1), 1-(2-isopropoxy-4-methoxyphenyl)-2-nitroethan-1-one (**68**) was obtained as beige solid (428 mg, 1.69 mmol, 43%). *R_f* = 0.44 (SiO₂, petroleum ether/EtOAc 3:1); M.p. 103 °C; ¹H NMR (300 MHz, CDCl₃): δ = 8.03 (d, *J* = 8.9 Hz, 1H, CH_{Ar}), 6.58 (dd, *J* = 8.9, 2.3 Hz, 1H, CH_{Ar}), 6.42 (d, *J* = 2.2 Hz, 1H, CH_{Ar}), 5.74 (s, 2H, O=C-CH₂), 4.71 (hept, *J* = 6.1 Hz, 1H, CH-(CH₃)₂), 3.87 (s, 3H, OCH₃), 1.44 (d, *J* = 6.1 Hz, 6H, CH-(CH₃)₂) ppm; ¹³C NMR (75 MHz, CDCl₃): δ = 184.2 (C=O), 166.3 (C_{Ar}-OCH₃), 159.8 (C_{Ar}-OCH-(CH₃)₂), 133.8 (CH_{Ar}), 117.5 (C_{Ar}-C=O), 106.2 (CH_{Ar}), 99.4 (CH_{Ar}), 85.3 (O=C-CH₂), 71.4 (OCH-(CH₃)₂), 55.7 (OCH₃), 21.9 (C-(CH₃)₂) ppm; IR (neat): 3034, 2982, 2922, 2840, 1651, 1603, 1546, 1208, 1103, 820 cm⁻¹; MS (GC) *m/z* (%): 151.1 (100), 253.1 (5.83) [M]⁺; HRMS (GC) calcd for C₁₂H₁₅NO₅ [M]⁺ 253.0945, found 253.0942.



(E)-3-(3,4-Dimethoxyphenyl)-1-(2-isopropoxy-4-methoxyphenyl)-2-nitroprop-2-en-1-one (70).^[36] 1-(2-Isopropoxy-4-methoxyphenyl)-2-nitroethan-1-one (**68**, 339 mg, 1.34 mmol, 1 eq.) and 3,4-dimethoxybenzaldehyde (**69**, 356 mg, 2.14 mmol, 1.6 eq.) were dissolved in 8 mL benzene and HOAc (215 μL, 3.17 mmol, 2.8 eq.) and β-alanine (11.9 mg, 0.134 mmol, 0.1 eq.) were added. The resulting mixture was refluxed with a Dean-Stark apparatus for 12 h. After completion of the reaction, the benzene phase was washed with H₂O (3 x 50 mL) and the aqueous phase was extracted with dichloromethane (3 x 20 mL). All organic phases were combined and the solvent was evaporated. After column chromatography (petroleum ether/ EtOAc 5:1), **70** was obtained as yellow solid (376 mg, 0.937 mmol, 70%). *R_f* = 0.28 (SiO₂, petroleum ether/EtOAc 3:1); M.p. 120-121 °C; ¹H NMR (300 MHz, CDCl₃): δ = 8.18 (d, *J* = 8.9 Hz, 1H, CH_{Ar}), 7.90 (s, 1H, NO₂-C=CH), 7.06 (dd, *J* = 8.4, 2.1 Hz, 1H, CH_{Ar}), 6.88 (d, *J* = 2.1 Hz, 1H, CH_{Ar}), 6.81 (d, *J* = 8.4 Hz, 1H, CH_{Ar}), 6.60 (dd, *J* = 8.9, 2.3 Hz, 1H, CH_{Ar}), 6.37 (d, *J* = 2.2 Hz, 1H, CH_{Ar}), 4.59 (hept, *J* = 6.1 Hz, 1H, CH-(CH₃)₂), 3.87 (s, 3H, OCH₃), 3.86 (s, 3H, OCH₃), 3.65

(s, 3H, OCH₃), 1.21 (d, *J* = 6.1 Hz, 6H, CH-(CH₃)₂) ppm; ¹³C NMR (75 MHz, CDCl₃): δ = 184.5 (C=O), 166.4 (C_{Ar}-OCH₃), 160.4 (C_{Ar}-OCH-(CH₃)₂), 152.0 (C_{Ar}-OCH₃), 149.1 (C_{Ar}-OCH₃), 148.1 (C-NO₂), 133.6 (CH_{Ar}), 133.1 (O₂N-C=CH), 126.1 (CH_{Ar}), 122.8 (C_{Ar}), 119.2 (C_{Ar}), 112.2 (CH_{Ar}), 111.1 (CH_{Ar}), 106.4 (CH_{Ar}), 99.3 (CH_{Ar}), 71.0 (OCH-(CH₃)₂), 56.0 (OCH₃), 55.7 (OCH₃), 55.6 (OCH₃), 21.9 (C-(CH₃)₂) ppm; IR (neat): 2974, 2844, 1636, 1588, 1506, 1245, 1100 cm⁻¹; MS (ESI⁺) *m/z* (%): 402 (100) [*M*+H]⁺; HRMS (ESI⁺) calcd for C₂₁H₂₄NO₇ [*M*+H]⁺ 402.1547, found 402.1550.

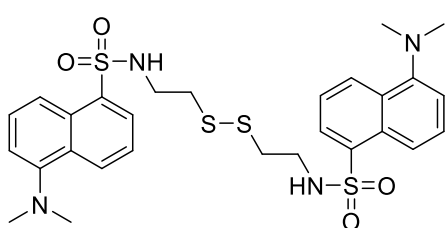
2-(3,4-dimethoxyphenyl)-6-methoxy-3-nitrochroman-4-one (NO₂-flavanone).^[78]



(*E*)-3-(3,4-Dimethoxyphenyl)-1-(2-isopropoxy-4-methoxyphenyl)-2-nitroprop-2-en-1-one (**70**, 109 mg, 0.272 mmol, 1.0 eq.) was dissolved in 4 mL acetonitrile and a solution of AlCl₃ (362 mg, 2.17 mmol, 10 eq.) in 4 mL acetonitrile was added. The mixture was stirred at 30 °C for 30 min, then 0.5 mL of aqueous HCl 5% was added dropwise and stirring was continued at 55 °C for another 45 min. 20 mL DCM was added and the mixture was washed with H₂O (3 x 50 mL). After phase separation, drying over MgSO₄ and evaporation of the solvent, a yellow oil was obtained which was purified by reversed-phase column chromatography (RP-18, acetonitrile/H₂O 2:1). A 1:10 mixture of α-NO₂-HC and NO₂-flavanone (44 mg, 0.122 mmol, 45%) was obtained as yellow solid. *R_f* = 0.63 (reversed-phase SiO₂, acetonitrile/H₂O 6:1); M.p. 128-132 °C; ¹H NMR (300 MHz, CDCl₃, NO₂-flavanone): δ = 7.92 (d, *J* = 8.9 Hz, 1H, CH_{Ar}), 7.05 (dd, *J* = 8.3, 2.1 Hz, 1H, CH_{Ar}), 7.00 (d, *J* = 2.0 Hz, 1H, CH_{Ar}), 6.90 (d, *J* = 8.3 Hz, 1H, CH_{Ar}), 6.72 (dd, *J* = 8.9, 2.4 Hz, 1H, CH_{Ar}), 6.52 (d, *J* = 2.3 Hz, 1H, CH_{Ar}), 5.80 (d, *J* = 11.9 Hz, 1H, O₂N-CH-CH), 5.74 (d, *J* = 11.9 Hz, 1H, O₂N-CH-CH), 3.91 (s, 3H, OCH₃), 3.90 (s, 3H, OCH₃), 3.86 (s, 3H, OCH₃) ppm; ¹H NMR (300 MHz, CDCl₃, α-NO₂-HC): δ = 14.54 (s, 0.1H, OH), 7.77 (d, *J* = 8.8 Hz, 0.1H, CH_{Ar}), 6.96-6.92 (m, 0.1H, CH_{Ar}), 6.83 (dd, *J* = 8.3, 2.1 Hz, 0.1H, CH_{Ar}), 6.76 (s, 0.1H, O₂N-C=CH), 6.65-6.61 (m, 0.2H, CH_{Ar}), 6.36 (d, *J* = 2.3 Hz, 0.1H, CH_{Ar}), 3.84 (s, 0.3H, OCH₃), 3.83 (s, 0.3H, OCH₃), 3.81 (s, 0.3H, OCH₃) ppm (); ¹³C NMR (101 MHz, CDCl₃, NO₂-flavanone): δ = 179.9 (C=O), 167.4 (C_{Ar}-OCH₃), 162.9 (C_{Ar}-O-CH), 152.5 (C_{Ar}-OCH₃), 149.4 (C_{Ar}-OCH₃), 129.8 (CH_{Ar}), 125.9 (C_{Ar}), 120.4 (CH_{Ar}), 112.3 (C_{Ar}), 111.8 (CH_{Ar}), 111.2 (CH_{Ar}), 110.0 (CH_{Ar}), 101.1 (CH_{Ar}), 91.4 (O₂N-CH-CH), 81.3 (O₂N-CH-CH), 56.0 (OCH₃), 55.94 (OCH₃), 55.90, (OCH₃) ppm; ¹H NMR (300 MHz, DMSO-d₆, NO₂-flavanone): δ = 7.82 (d, *J* = 8.8 Hz, 1H, CH_{Ar}), 7.35 (d, *J* = 1.9 Hz, 1H, CH_{Ar}), 7.16 (dd, *J* = 8.3, 2.0 Hz, 1H,

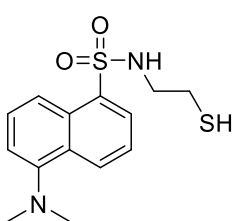
CH_{Ar}), 7.02 (d, *J* = 8.6 Hz, 1H, CH_{Ar}), 6.98 (d, *J* = 12.3 Hz, 1H, O₂N-CH-CH), 6.80 (dd, *J* = 8.8, 2.3 Hz, 1H, CH_{Ar}), 6.74 (d, *J* = 2.3 Hz, 1H, CH_{Ar}), 5.99 (d, *J* = 12.2 Hz, 1H, O₂N-CH-CH), 3.85 (s, 3H, OCH₃), 3.78 (s, 3H, OCH₃), 3.77 (s, 3H, OCH₃) ppm; ¹³C NMR (101 MHz, DMSO-d₆, **NO₂-flavanone**): δ = 181.2 (C=O), 167.0 (C_{Ar}-OCH₃), 162.8 (C_{Ar}-O-CH), 150.0 (C_{Ar}-OCH₃), 148.7 (C_{Ar}-OCH₃), 128.9 (CH_{Ar}), 126.0 (CH_{Ar}), 121.3 (C_{Ar}), 111.8 (CH_{Ar}), 111.5 (C_{Ar}), 111.4 (CH_{Ar}), 111.3 (CH_{Ar}), 101.1 (CH_{Ar}), 90.1 (O₂N-CH-CH), 80.3 (O₂N-CH-CH), 56.2 (OCH₃), 55.6 (OCH₃), 55.4 (OCH₃) ppm; IR (neat): 2974, 2844, 1681, 1610, 1561, 1238, 1018 cm⁻¹; MS (ESI⁺) *m/z* (%): 260 (100) [*M*+H]⁺; HRMS (ESI⁺) calcd for C₁₈H₁₈NO₇ [*M*+H]⁺ 360.1078, found 360.1082.

A 6.4 Synthesis of fluorescent aromatic thiol dyes



***N,N'*-(disulfanediy)bis(ethane-2,1-diyl)bis(5-(dimethylamino)naphthalene-1-sulfonamide) (DCY disulfide, 75).**^[71] (Dimethylamino)naphthalene-1-sulfonyl chloride (Dansyl chloride, **74**, 1.00 g, 3.70 mmol, 2.0 eq.) was dissolved in 42 mL acetone/H₂O 30:1 and

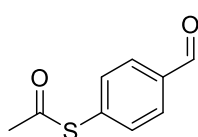
a solution of 2,2'-disulfanediybis(ethan-1-amine) dihydrochloride (cystamine-HCl, 435 mg, 1.90 mmol, 1.0 eq.) in 22 mL aqueous 1 M NaHCO₃ was added dropwise within 15 min. The solution was stirred at room temperature at pH 7-8 for 2 h, poured into 30 mL DCM and after phase separation the aqueous phase was extracted with 30 mL DCM another two times. The combined organic phases were washed with 1 M NaHCO₃ (3 x 200 mL), dried over MgSO₄ and the solvent was removed. Without further purification the product **75** was received as bright yellow solid (1.08 g, 1.75 mmol, 92%). *R_f* = 0.09 (SiO₂, petroleum ether/EtOAc 3:1); ¹H-NMR (300 MHz, CDCl₃): δ = 8.54 (d, *J* = 8.5 Hz, 2H, CH_{Ar}), 8.24-8.22 (m, 4H, CH_{Ar}), 7.55-7.51 (m, 4H, CH_{Ar}), 7.18 (d, *J* = 7.6 Hz, 2H, CH_{Ar}), 5.24 (s, 2H, NH), 3.09 (brs, 4H, CH₂), 2.88 (s, 12H, CH₃), 2.49 (t, *J* = 6.3 Hz, 4H, CH₂) ppm. The NMR data is in accordance with the literature.^[71]



5-(Dimethylamino)-N-(2-mercaptoethyl)naphthalene-1-sulfonamide (DCY).^[71] *N,N'*-(Disulfanediy)bis(ethane-2,1-diyl)bis(5-(dimethylamino)naphthalene-1-sulfonamide) (DCY disulfide **75**, 200 mg, 0.320 mmol, 1.0 eq.) was dissolved in 13 mL degassed THF/H₂O 10:1 at 0-5 °C and NaBH₄ (120 mg, 3.20 mmol, 10 eq.) was added in small portions.

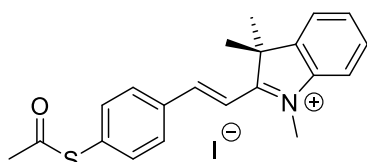
The mixture was stirred on ice for 4 h and overnight at room temperature. THF was removed, the residue was taken up in 50 mL H₂O and the aqueous phase was extracted with 3 x 10 mL diethyl ether. The combined organic phases were washed with brine, dried over MgSO₄ and the solvent was removed. Column chromatography was performed (petroleum ether/EtOAc 3:1) and the product was obtained as bright yellow solid (93.0 mg,

0.300 mmol, 47%). $R_f = 0.38$ (SiO₂, petroleum ether/EtOAc 2:1); ¹H-NMR (300 MHz, CDCl₃): $\delta = 8.55$ (d, $J = 8.5$ Hz, 1H, CH_{Ar}), 8.29-8.24 (m, 2H, CH_{Ar}), 7.56 (ddd, 2H, $J = 16.0, 8.5, 7.5$ Hz, CH_{Ar}), 7.19 (d, $J = 7.5$ Hz, 1H, CH_{Ar}), 5.24 (t, $J = 6.3$ Hz, 1H, NH), 3.08 (q, $J = 6.4$ Hz, 2H, CH₂), 2.89 (s, 6H, CH₃), 2.50 (dt, $J = 8.6, 6.4$ Hz, 2H, CH₂) ppm. The NMR data is in accordance with the literature.^[71]



S-(4-Formylphenyl) ethanethioate (76).^[72] *p*-Methylthiobenzaldehyde (**76**, 0.605 g, 3.97 mmol, 1.0 eq.) was dissolved in 13 mL dry degassed DMF and potassium *tert*-butylthiolate (**77**, 1.02 g, 9.09 mmol, 2.3 eq.)

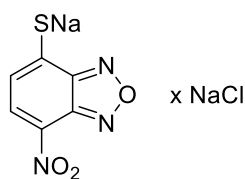
was added. The reaction was stirred at 160 °C for 4.5 h and subsequently cooled to 0-5 °C. Acetyl chloride (793 μ L, 11.1 mmol, 2.8 eq.) was added and the mixture was stirred for 2 h. The reaction was quenched with H₂O, extracted with 3 x 100 mL diethylether and washed with 2 x 200 mL H₂O. The combined organic phases were dried over MgSO₄ and the solvent was evaporated. Column chromatography was performed (petroleum ether/EtOAc 5:1) to yield the product **78** as yellow liquid (300 mg, 1.66 mmol, 42%). $R_f = 0.38$ (SiO₂, petroleum ether/EtOAc 5:1); ¹H-NMR (300 MHz, CDCl₃): $\delta = 10.03$ (s, 1H, Ar-CHO), 8.01-7.82 (m, 1H, CH_{Ar}), 7.70-7.52 (m, 1H, CH_{Ar}), 2.46 (s, 1H, CH₃) ppm; ¹³C-NMR (75 MHz, CDCl₃): $\delta = 192.3$ (C=O), 191.5 (C=O), 136-7 (C_{Ar}), 135.4 (C_{Ar}), 134.5 (CH_{Ar}), 130.0 (CH_{Ar}), 30.9 (CH₃) ppm. The NMR data is in accordance with the literature.^[72]



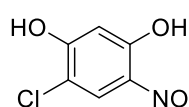
(E)-2-(4-(Acetylthio)styryl)-1,3,3-trimethyl-3H-indol-1-ium iodide (Acetyl-MSTI).^[72] Tetramethylindolium iodide (**79**, 123 mg, 0.410 mmol, 1.0 eq.) and NaOAc (40 mg, 0.50 mmol, 1.2 eq.) were dissolved in 2.5 mL acetic acid an-

hydride and stirred at room temperature for 30 min. S-(4-formylphenyl) ethanethioate (**78**, 74.0 mg, 0.410 mmol, 1.0 eq.) was dissolved in 2.5 mL acetic anhydride, added dropwise to the mixture and the reaction was stirred for 48 h. The solvent was removed via high vacuum. Purification was performed by mixing the crude orange solid and 5 mL diethylether thoroughly via ultrasonic bath in a centrifuge vial. After centrifugation the organic phase was decanted and the washing repeated another two times. Further 3 x 5 mL washing steps were performed with each toluene and petroleum ether. The product was obtained as orange solid (189 mg, 0.407 mmol, 99%). $R_f = 0.38$ (SiO₂, DCM/MeOH 9:1); ¹H-NMR (300 MHz, CDCl₃): $\delta = 8.22$ (d, $J = 16.5$ Hz, 1H, CH=CH=C=N⁺), 8.19 (d, $J = 8.2$ Hz, 2H, CH_{Ar}), 7.82 (d, $J = 16.5$ Hz, 1H, CH=CH=C=N⁺), 7.67-7.52 (m, 6H, CH_{Ar}), 4.45 (s, 3H, O=C-CH₃), 2.45 (s, 3H, N⁺-CH₃), 1.86 (s, 6H, C-(CH₃)₂) ppm; ¹³C-NMR (75 MHz, CDCl₃): $\delta = 192.7$ (C=O), 182.5 (C=N⁺), 152.6 (C_{Ar}), 143.1 (C_{Ar}), 141.4 (C_{Ar}), 134.7 (C_{Ar} *p*-subst.), 134.3 (C_{Ar}), 131.4 (C_{Ar} *p*-subst.), 130.2 (C_{Ar}), 129.7 (C_{Ar}), 122.6 (C_{Ar}), 115.3 (C_{Ar} or CH=C=N⁺), 114.4 (C_{Ar} or CH=C=N⁺),

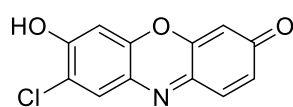
52.8 (C-(CH₃)₂), 37.6 (N⁺-CH₃), 30.6 (O=C-CH₃), 26.6 (C-(CH₃)₂) ppm; MS (ESI⁺) m/z (%): 336 (100) [M-H]⁺. The NMR data is in accordance with the literature.^[72]



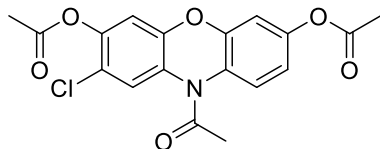
7-Nitrobenzo[c][1,2,5]oxadiazole-4-thiol (NBD).^[73] To 4-Chloro-7-nitrobenzo[c][1,2,5]oxadiazole (**80**, 51.0 mg, 0.256 mmol, 1.0 eq.), dissolved in 2 mL degassed MeOH, a solution of NaSH x 1 H₂O in 2 mL degassed MeOH was added dropwise and the mixture was stirred for 15 min at room temperature. To remove H₂S, the solution was purged with N₂ for 15 min and the solvents were removed under high vacuum. The deep purple solid was further purged with N₂ for 2 h. 69.2 mg (0.249 mmol, 97%) of the product containing 1 eq. NaCl was obtained. R_f = 0.69 (SiO₂, petroleum ether/EtOAc 1:1); ¹H-NMR (300 MHz, MeOD): δ = 8.14 (d, J = 8.7 Hz, 2H, CH_{Ar}), 7.17 (d, J = 8.7 Hz, 2H, CH_{Ar}) ppm. The NMR data is in accordance with the literature.^[73]



4-Chloro-6-nitrosobenzene-1,3-diol (84).^[81] 4-Chlororesorcinol (**87**, 5.09 g, 35.2 mmol, 1.0 eq.) was dissolved in 35 mL of EtOH/H₂O 4:1 containing 2.61 g (46.5 mmol, 1.32 eq.) KOH at 0-5 °C and stirred at this temperature for 10 min. Isopentyl nitrite (**88**, 4.27 g, 36.4 mmol, 1.0 eq.) was added dropwise over 30 min. The mixture was warmed to room temperature and stirred for 1 h. 10 mL 37% aqueous HCl were added dropwise at 0-5 °C and stirred at room temperature for 10 min. The yellow precipitate was filtrated off and washed with 300 mL aqueous HCl solution pH 2, 300 mL H₂O and 200 mL petroleum ether. After drying under high vacuum, the product **84** was obtained as yellow solid (5.24 g, 30.2 mmol, 86%). R_f = 0.53 (SiO₂, petroleum ether/EtOAc 1:4, 0.1% TFA); ¹H-NMR (400 MHz, DMSO-d₆): δ = 13.92 (s, 1H, OH), 11.48 (s, 1H, OH), 7.71 (s, 1H, CH_{Ar}), 5.86 (s, 1H, CH_{Ar}) ppm; ¹³C-NMR (101 MHz, DMSO): δ = 178.7 (C-OH), 162.5 (C-NO), 144.3 (C-OH), 135.6 (CH), 119.4 (C-Cl), 105.6 (CH) ppm; MS (ESI⁻) m/z (%): 172 (100) [M-H]⁻. The NMR data is in accordance with the literature.^[81]

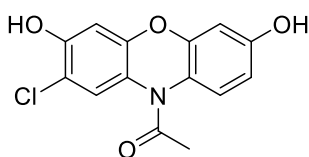


8-Chloro-7-hydroxy-3H-phenoxazin-3-one (86).^[81] Resorcinol (**85**, 1.50 g (13.6 mmol, 1.0 eq.) was dissolved in 12 mL concentrated sulfuric acid at 85 °C. 4-Chloro-6-nitrosobenzene-1,3-diol (**84**, 2.36 g, 13.6 mmol, 1.0 eq.) was added as solid in portions over 30 min and the mixture was stirred at 110 °C for 24 h. After cooling to room temperature, the mixture was poured into 200 mL of ice water. The resulting precipitate was quickly filtered off and washed with 100 mL H₂O. The product was obtained after drying under high vacuum as dark violet solid (3.06 g, 12.4 mmol, 91%) and used without further purification. Due to very low solubility no NMR data was obtained. MS (ESI⁻) m/z (%): 248 (100) [M-H]⁻.



10-Acetyl-2-chloro-10H-phenoxazine-3,7-diyl diacetate (89).^[82] 8-Chloro-7-hydroxy-3H-phenoxazin-3-one (**86**, 100 mg, 0.404 mmol, 1.0 eq.) and SnCl₂ (230 mg, 1.21 mmol, 3 eq.) were dissolved in 1 mL acetic acid anhy-

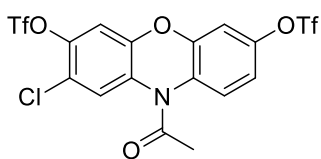
ride (1.08 g, 10.6 mmol) at room temperature and triethylamine (250 μ L, 1.80 mmol, 4.5 eq.) was added. The mixture was stirred at 110 °C for 18 h. After cooling to room temperature acetic acid anhydride was removed by HV. The resulting solid was suspended in 20 mL DCM and mixed thoroughly by stirring and ultrasonic treatment. The mixture was left standing and the solid settled, then the organic phase was decanted. This extraction was repeated twice and the organic phases were combined. DCM was removed by evaporation and the crude product was received as viscous brown oil. Column chromatography was performed (petroleum ether/EtOAc 2:1) and the product was received as beige solid (72.0 mg, 0.192 mmol, 47%). R_f = 0.34 (SiO₂, petroleum ether/EtOAc 2:1); ¹H-NMR (300 MHz, CDCl₃): δ = 7.63 (s, 1H, CH_{Ar}), 7.36 (dd, J = 8.1, 0.9 Hz, 1H, CH_{Ar}), 6.99-6.84 (m, 3H, CH_{Ar}), 2.34 (s, 3H, CH₃), 2.32 (s, 3H, CH₃), 2.30 (s, 3H, CH₃) ppm; ¹³C-NMR (75 MHz, CDCl₃): δ = 169.0 (C=O), 168.9 (C=O), 168.2 (C=O), 150.8 (C_{Ar}-O), 149.4 (C_{Ar}-O), 149.0 (C_{Ar}-O), 145.0 (C_{Ar}-O), 127.5 (C_{Ar}), 126.4 (C_{Ar}), 126.0 (CH_{Ar}), 125.1 (CH_{Ar}), 121.4 (C_{Ar}-Cl), 117.0 (CH_{Ar}), 112.2 (CH_{Ar}), 110.9 (CH_{Ar}), 22.8 (CH₃), 21.0 (CH₃), 20.5 (CH₃) ppm; MS (ESI⁺) m/z (%): 376 (100) [M-H]⁺; HRMS (ESI⁺) calcd for C₁₈H₁₅ClNO₆ [M+H]⁺ 376.0582, found 376.0586.



1-(2-Chloro-3,7-dihydroxy-10H-phenoxazin-10-yl)ethan-1-one (90).^[82] 10-Acetyl-2-chloro-10H-phenoxazine-3,7-diyl diacetate (**89**, 221 mg, 0.588 mmol, 1.0 eq.) and SnCl₂ (230 mg, 1.21 mmol, 3 eq.) were suspended in 3 mL MeOH and 2 mL aqueous KOH

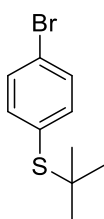
10% was added. The mixture was stirred at room temperature for 2 h, during this time it became a dark violet solution. 20 mL H₂O and 3 M HCl (3 mL) were added and the mixture was stirred for approximately 10 min until it turned to a pale orange suspension. Extraction was performed with EtOAc (3 x 50 mL). The combined organic phases were washed with 1 M HCl (1 x 200 mL) and brine (2 x 200 mL), dried over MgSO₄ and the solvent was removed on the rotary evaporator. After column chromatography (petroleum ether/EtOAc 1:1) the product **90** was received as pale pink foamy solid (157 mg, 0.538 mmol, 92%). R_f = 0.21 (SiO₂, petroleum ether/EtOAc 2:1); ¹H-NMR (300 MHz, acetone-d₆): δ = 9.22 (s, 1H, OH, quickly decreasing due to deuterium exchange), 8.85 (s, 1H, OH, quickly decreasing due to deuterium exchange), 7.55 (s, 1H, CH_{Ar}), 7.30 (d, J = 8.6 Hz, 1H, CH_{Ar}), 6.75 (s, 1H, CH_{Ar}), 6.67-6.55 (m, 2H, CH_{Ar}), 2.24 (s, 1H, CH₃) ppm; ¹³C-NMR (75 MHz, acetone-d₆): δ = 170.1 (C=O), 157.1 (C_{Ar}-O), 152.1 (C_{Ar}-OH), 152.1 (C_{Ar}-OH), 150.9 (C_{Ar}-O), 126.7 (CH_{Ar}), 126.4 (CH_{Ar}), 123.0 (C_{Ar}), 122.0 (C_{Ar}), 114.9 (C_{Ar}-Cl), 111.2 (CH_{Ar}), 105.0 (CH_{Ar}), 104.3 (CH_{Ar}), 22.7

(CH₃) ppm; MS (ESI⁺) m/z (%): 292 (100) [M-H]⁺; HRMS (ESI⁺) calcd for C₁₄H₁₁ClNO₄ [M+H]⁺ 292.0371, found 292.0378.



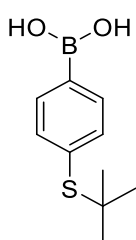
10-Acetyl-2-chloro-10H-phenoxazine-3,7-diyl bis(trifluoromethanesulfonate) (92).^[83] 11-(2-Chloro-3,7-dihydroxy-10H-phenoxazin-10-yl)ethan-1-one (**90**, 272 mg, 0.932 mmol, 1.0 eq.) was dissolved in 15 mL dry DMF and cooled to 0-5 °C.

NaH 60% (82.0 mg, 2.05 mmol, 2.2 eq.) was added and the mixture was stirred on ice and allowed to warm up to room temperature after 30 min. 1,1,1-Trifluoro-*N*-phenyl-*N*-((trifluoromethyl)sulfonyl)methanesulfonamide (**91**, 732 mg, 2.05 mmol, 2.2 eq.) was added and stirred for 5 min. The reaction was poured in to a separation funnel containing 100 mL DCM, washed with H₂O (2 x 150 mL) and brine (1 x 150 mL), dried over MgSO₄ and the solvent was removed. After column chromatography (petroleum ether/EtOAc 3:1) the product was received as yellow solid (317 mg, 0.570 mmol, 61%). R_f = 0.26 (SiO₂, petroleum ether/EtOAc 4:1); ¹H-NMR (300 MHz, CDCl₃): δ = 7.74 (s, 1H, CH_{Ar}), 7.48 (dd, *J* = 3.8 Hz, 1.9 Hz, 1H, CH_{Ar}), 7.17 (s, 1H, CH_{Ar}), 7.15-7.11 (m, 2H, CH_{Ar}), 2.36 (s, 3H, CH₃); ¹³C-NMR (75 MHz, CDCl₃) δ = 168.5 (C=O), 150.7 (C_{Ar}-OTf), 149.0 (C_{Ar}-O), 147.3 (C_{Ar}-O), 143.2 (C_{Ar}-OTf), 129.2 (C_{Ar}), 128.5 (C_{Ar}), 126.9 (CH_{Ar}), 125.9 (CH_{Ar}), 122.3 (C_{Ar}-Cl), 118.5 (q, *J* = 320.8 Hz, CF₃), 118.6 (q, *J* = 320.8 Hz, CF₃), 117.3 (CH_{Ar}), 111.8 (CH_{Ar}), 111.1 (CH_{Ar}), 22.8 (CH₃) ppm; ¹⁹F-NMR (282 MHz, CDCl₃): δ = -73.1, -73.7 ppm. MS (ESI⁺) m/z (%): 556 (100) [M-H]⁺; HRMS (ESI⁺) calcd for C₁₆H₉ClF₆NO₈S₂ [M+H]⁺ 555.9357, found 555.9366.



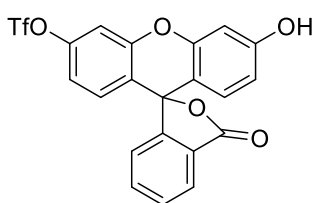
(4-Bromophenyl)(tert-butyl)sulfane (94).^[84] 4-Bromothiophenol (**96**, 1.00 g, 5.29 mmol, 1.0 eq.) was dissolved in 5 mL (45.4 mmol, 8.6 eq.) *tert*-butylchloride and AlCl₃ (35.0 mg, 0.265 mmol, 0.05 eq.) was added in portions at room temperature. The reaction was stirred for 1 h and quenched with 150 mL H₂O. The product was extracted in hexane (3 x 50 mL), the organic phases washed with

water (2 x 150 mL) and the solvent was removed to yield 1.02 g (4.16 mmol, 79%) of a colorless liquid (**94**). R_f = 0.63 (SiO₂, petroleum ether); ¹H-NMR (300 MHz, CDCl₃): δ = 7.47-7.44 (m, 2H, CH_{Ar}), 7.40-7.37 (m, 2H, CH_{Ar}), 1.27 (s, 9H, CH₃) ppm; ¹³C-NMR (75 MHz, DMSO): δ = 138.9 (CH_{Ar}), 131.8 (C-S), 131.6 (CH_{Ar}), 123.4 (C-Br), 46.1 (C-(CH₃)₃), 30.9 (CH₃) ppm. The NMR data is in accordance with the literature.^[84]



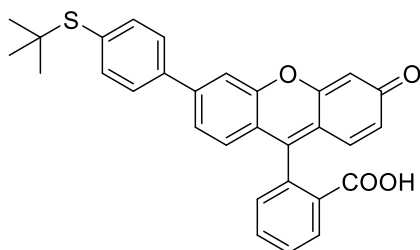
(4-(tert-Butylthio)phenyl)boronic acid (97).^[85] (4-Bromophenyl)(*tert*-butyl)sulfane (**94**, 1.00 g, 4.08 mmol, 1.0 eq.) was dissolved in 5 mL dry THF at -78 °C and a solution of 4.08 mL 1.6 M *n*-BuLi (6.53 mmol, 1.6 eq.) was added. After stirring for 1 h triisopropyl borate (4.86 mL, 21.2 mmol, 5.2 eq.) was added. The reaction was brought to -20 °C and stirred overnight without removing the cooling bath. After 24 h the solvent was removed and the residue was taken up

in 10 mL DCM and 20 mL 5 M aqueous HCl. The mixture was stirred vigorously for 2 h at room temperature. After completion of the reaction, phases were separated and the aqueous phase was extracted with DCM (2 x 15 mL). The combined organic phases were washed with 2 x 20 mL aqueous HCl 1 M, dried over MgSO₄ and the solvent was removed. The crude product was washed with hexane, filtered off and recrystallized in hexane to yield 455 mg (2.17 mmol, 53%) of the product **97** as a white solid. $R_f = 0.73$ (SiO₂, petroleum ether/EtOAc 1:1); ¹H-NMR (300 MHz, CDCl₃): $\delta = 8.20$ -8.17 (m, 2H, CH_{Ar}), 7.69-7.66 (m, 2H, CH_{Ar}), 1.35 (s, 9H, CH₃) ppm; ¹³C-NMR (75 MHz, CDCl₃): $\delta = 138.4$ (C-S), 136.6 (CH_{Ar}), 135.5 (CH_{Ar}), 133.4 (C-B), 46.6 (C-(CH₃)₃), 31.1 (CH₃) ppm; MS (ESI⁺) m/z (%): 211 (100) [M-H]⁺. The NMR data is in accordance with the literature.^[85]



2-(3-Oxo-6-(((trifluoromethyl)sulfonyl)oxy)-3H-xanthen-9-yl)benzoic acid (98**).**^[86] 2-(6-Hydroxy-3-oxo-3H-xanthen-9-yl)benzoic acid (fluorescein **95**, 927 mg, 2.79 mmol, 1.0 eq.) and 1,1,1-trifluoro-*N*-phenyl-*N*-((trifluoromethyl)sulfonyl)methanesulfonamide (**91**, 997 mg, 2.79 mmol, 1.0 eq.) were dissolved in

7 mL dry DMF, DIPEA (1.94 mL, 11.2 mmol, 4.0 eq.) was added and the mixture was stirred at room temperature under exclusion of light for 60 h. A separation funnel was filled with a 1:1 mixture of 200 mL H₂O and EtOAc and the reaction mixture was distributed within. After phase separation the aqueous phase was extracted with EtOAc (2 x 80 mL) and the combined organic phases washed with water (3 x 200 mL), dried over MgSO₄ and the solvent was removed. After column chromatography (petroleum ether/EtOAc 3:1) the product **98** was obtained as bright yellow foamy solid (512 mg, 1.10 mmol, 40%). The same reaction carried out in a microwave reactor (80 °C, 30 min) with 1.07 g (3.22 mmol) starting material in 20 mL DMF gave 36% yield. $R_f = 0.23$ (SiO₂, petroleum ether/EtOAc 3:1); ¹H-NMR (300 MHz, CDCl₃): $\delta = 8.05$ (dd, $J = 6.5, 1.1$ Hz, 1H, CH_{Ar}), 7.74 – 7.63 (m, 2H, CH_{Ar}), 7.24 (d, $J = 2.4$ Hz, 1H, CH_{Ar}), 7.19 – 7.17 (m, 1H, CH_{Ar}), 6.96 (dd, $J = 8.8, 2.4$ Hz, 1H, CH_{Ar}), 6.89 (d, $J = 8.8$ Hz, 1H, CH_{Ar}), 6.77 (d, $J = 2.4$ Hz, 1H, CH_{Ar}), 6.66 (d, $J = 8.7$ Hz, 1H, CH_{Ar}), 6.58 (dd, $J = 8.7, 2.4$ Hz, 1H, CH_{Ar}); ¹H-NMR (300 MHz, DMSO-*d*₆): ¹³C-NMR (75 MHz, DMSO-*d*₆): 168.3 (C=O), 159.8 (C_{Ar}-OH), 152.0 (O=C-O-C-C_{Ar}), 151.3 (C_{Ar}-O), 151.1 (C_{Ar}-O), 149.5 (C_{Ar}-O), 135.9 (CH_{Ar}), 130.4 (2C, CH_{Ar}), 129.1 (CH_{Ar}), 125.5 (C_{Ar}), 124.9 (CH_{Ar}), 124.1 (CH_{Ar}), 119.8 (C_{Ar}), 117.5 (q, $J = 321.0$ Hz, CF₃), 117.1 (CH_{Ar}), 113.4 (CH_{Ar}), 110.6 (CH_{Ar}), 108.7 (C_{Ar}), 102.2 (CH_{Ar}), 81.2 (O=C-O-C) ppm; ¹⁹F-NMR (282 MHz, CDCl₃): $\delta = -73.1$ ppm. The NMR data is in accordance with the literature.^[86]



2-(6-(4-(*tert*-Butylthio)phenyl)-3-oxo-3*H*-xanthen-9-yl)benzoic acid (99). 2-(3-Oxo-6-(((trifluoromethyl)sulfonyl)oxy)-3*H*-xanthen-9-yl)benzoic acid (fluorescein monotriflate, **98**, 200 mg, 0.430 mmol, 1.0 eq.), (4-(*tert*-butylthio)phenyl)boronic acid (**97**, 109 mg, 0.520 mmol, 1.2 eq.), 5.0 mg (0.022 mmol, 0.05 eq.) Pd(OAc)₂ and

P(Ph)₃ (23.0 mg, 0.086 mmol, 0.2 eq.) were degassed using three cycles of N₂/vacuum and dissolved in 5 mL dioxane. K₂CO₃ (89.0 mg, 0.650 mmol, 1.5 eq.) in 500 μL H₂O was added and the reaction mixture heated in a microwave reactor (120 °C, 30 min). The mixture was poured into 200 mL 1 M aqueous HCl and 100 mL EtOAc, the phases separated and the aqueous phase was extracted with EtOAc (2 x 100 mL). The combined organic phases were dried over MgSO₄, the solvent was evaporated and column chromatography was performed (petroleum ether/EtOAc 4:1) to yield the product as orange foamy solid (182 mg, 0.379 mmol, 88%). R_f = 0.23 (SiO₂, petroleum ether/EtOAc 3:1); ¹H-NMR (300 MHz, CDCl₃): δ = 8.05 (dd, *J* = 6.5, 1.1 Hz, 1H, CH_{Ar}), 7.72–7.53 (m, 6H, CH_{Ar}), 7.50 (d, *J* = 1.8 Hz, 1H, CH_{Ar}), 7.26 (dd, *J* = 8.2, 1.8 Hz, 2H, CH_{Ar}), 7.22–7.18 (m, 1H, CH_{Ar}), 6.86 (d, *J* = 8.2 Hz, 1H, CH_{Ar}), 6.81 (d, *J* = 2.3 Hz, 1H, CH_{Ar}), 6.66 (d, *J* = 8.7 Hz, 1H, CH_{Ar}), 6.58 (dd, *J* = 8.7, 2.4 Hz, 1H, CH_{Ar}), 1.32 (s, 9H, CH₃); ¹³C-NMR (101 MHz, CDCl₃) δ = 169.8 (C=O), 158.5 (C=O), 152.5 (C-O), 151.7 (C-O), 143.1 (C_{Ar}), 139.7 (C_{Ar}), 137.9 (2C, CH_{Ar}), 135.2 (C_{Ar}-S), 132.9 (CH_{Ar} or C_{Ar}), 129.9 (CH_{Ar}), 129.4 (CH_{Ar}), 128.5 (CH_{Ar}), 127.3 (C_{Ar}), 127.1 (2C, CH_{Ar}), 126.6 (C_{Ar}), 125.3 (C_{Ar}), 124.1 (CH_{Ar}), 122.5 (CH_{Ar}), 118.1 (CH_{Ar} or C_{Ar}), 115.4 (CH_{Ar}), 112.7 (CH_{Ar}), 111.0 (C_{Ar}), 103.2 (CH_{Ar}), 46.3 (C-CH₃)₂, 31.0 (C-CH₃)₂ ppm; MS (ESI⁺) *m/z* (%): 481 (100) [*M*-H]⁺; HRMS (ESI⁺) calcd for C₃₀H₂₅O₄S [*M*+H]⁺ 481.1468, found 481.1474.

A 6.5 Kinetic evaluation of electrophiles

The kinetic thiol assay for electrophiles was developed in this work group and previously reported.^[35] Pre-kinetic UV-Vis scans and kinetic graphs can be viewed in the appendix.

Kinetic thiol assay solvent system

The solvent system for the kinetic thiol assay contains 100 mM Tris-HCl buffer pH 7.4, 2 mM EDTA/ethylene glycol 20:80 (buffer:solvent). EDTA was added to the buffer as a complexing agent for remaining cations in Millipore water, which are able to catalyze thiol oxidation to disulfides. Ethylene glycol is used as co-solvent and to slow down kinetics. The buffer was adjusted to pH 7.4 using a WTW-inolab pH meter with a SenTix-Mic glass electrode (Weilheim, Germany), mixed 20:80 with ethylene glycol, filtered through a cellulose nitrate

filter (pore size 0.45 μm , Sartorius Stedim, Göttingen, Germany) and degassed via ultrasound for 10 min.

LC-MS studies of the compounds under kinetic thiol assay conditions

LC-MS investigations were performed on an Agilent 1290 Infinity HPLC system coupled to Agilent Technologies 6540 UHD TOF/Q-TOF mass spectrometer (Agilent Technologies, Santa Clara, USA). The assay mixtures in kinetic thiol assay solution were applied to an Agilent Zorbax Eclipse Plus C18, 1.8 μm , 50 x 2.1 mm column in volumes of 0.5 – 1 μL . Chromatography was performed with an eluent system containing of H_2O +0.1% HCOOH /acetonitrile with a gradient of 5-95% acetonitrile over 7-9 min at 40 $^\circ\text{C}$. The detection wavelength range was 200-300 nm. Mass spectra were recorded between m/z 80 and 1400. Data was evaluated using the program MassHunter Workstation (Agilent, Santa Clara, USA). Compounds were identified according to their HR-MS peaks, fragmentation pattern and UV spectra.

Kinetic thiol assay (96-well format) for electrophiles

All test compounds were kept as 10 mM DMSO stock solutions at -20 $^\circ\text{C}$. Suitable parameters were determined prior to the kinetic investigations by UV-Vis monitoring of each compound with 20, 100 and/or 500-fold cysteamine and additional LC-MS measurements. For the assay performance, dilutions of 80 μM for OXEs and 160 μM for phenylacrylamides were prepared in kinetic assay buffer. Dilutions of excess cysteamine were prepared directly in kinetic thiol assay medium freshly for each experiment. All measurements were performed in a Thermo Scientific Multiscan Spectrum UV-Vis microplate spectrophotometer (Thermo Fisher Scientific Inc., Vantaa, Finland). Both separate solutions (thiol and electrophile) were incubated in the instrument for 10 min at 25 $^\circ\text{C}$, measurements were performed at the same temperature. 140 μL of each electrophiles and excess thiol were combined in a deep-well microplate, covered with a foil and shaken thoroughly. 200 μL of each reaction mixture were quickly pipetted into the 96-well measurement plate (ELISA microplates, F-bottom, MICROLON 200, Greiner Bio-one, Frickenhausen, Germany), covered with a PCR foil (Platesealer, Viewseal, transparent, 80 x 140 mm, Greiner Bio-one, Frickenhausen, Germany) and the measurement was started immediately. Each thiol excess concentration was assayed in duplicates, 380 data points were collected with varying time intervals at the appropriate wavelength for each electrophilic compound. The raw data were analyzed by Microsoft Office Excel (Microsoft, Redmond, Washington, USA) with the help of a data sheet programmed by Karl Amslinger. After correction versus the blank the obtained individual kinetic curves were fitted to a first-order exponential decay function with

the program OriginPro 9 (OriginLab Corporation, Northampton, Massachusetts, USA). The value t_1 expresses the k_{obs} value for each curve. K_2 values were obtained from the slope of the linear regression function of k_{obs} values versus their corresponding cysteamine concentrations. All compounds were measured in at least three independent experiments.

Kinetic thiol assay via stopped-flow measurement for OXE3-(4py)''

Measurements were performed on a SX20 stopped-flow instrument (Applied Photophysics, Leatherhead, UK) at 25 °C in kinetic thiol assay solution. Dilutions of 80 μM OXE3-(4py)'' and 100-300-fold cysteamine in kinetic thiol assay solution were prepared freshly before each measurement. Equal volumes of electrophile and cysteamine solutions were mixed in the measurement chamber with instant monitoring of the decrease of absorbance at 330 nm over 30 s – 5 min. Five repetitions were recorded and averaged, the obtained curve was fitted to a first-order exponential decay function with the program Pro-Data SX 2.0 (Applied Photophysics, Leatherhead, UK), yielding the k_{obs} values. This experiment was individually performed for each cysteamine concentration in duplicates. K_2 values were calculated as described before. In total, eight measurements were performed.

Kinetic evaluation of OXEp1-(4py)'' and OXE4-(4py)'' with LC-MS

All measurements were performed in kinetic thiol assay solution. The electrophiles OXEp1-(4py)'' and OXE4-(4py)'' were used in an assay concentration of 40 μM and cysteamine in 500, 600 and 700-fold excess (20, 24 or 28 mM). Each experiment included two reactions in two wells of a 96-well plate: In each well one of the two electrophiles with one cysteamine excess concentration each. For the electrophiles, 80 μM dilutions in kinetic thiol assay solution were prepared from their 10 mM DMSO stock solutions. The cysteamine dilutions of 40, 48 or 56 mM were directly prepared in kinetic thiol assay solution freshly for each experiment. Immediately before the start of the measurement, 150 μL of electrophile and cysteamine dilutions were mixed in a deepwell plate, covered with a foil and shaken thoroughly. 250 μL of the resulting mixtures were pipetted into a 96 well microplate (PS, F-bottom, Greiner Bio-one, Frickenhausen, Germany) and covered with a foil. The reactions were monitored by LC-MS on an Agilent 1290 Infinity HPLC system coupled to Agilent Technologies 6540 UHD TOF/Q-TOF mass spectrometer (Agilent Technologies, Santa Clara, USA). The assay mixtures in kinetic thiol assay solution were applied to an Agilent Zorbax Eclipse Plus C18, 1.8 μm , 50 x 2.1 mm column in volumes of 0.5 – 1 μL . Chromatography was performed with an eluent system containing of $\text{H}_2\text{O}+0.1\%$ HCOOH/acetonitrile with a gradient of 5-95% acetonitrile over 7-9 min at 40 °C. The detection wavelength range was 200-300 nm. Mass spectra were recorded between m/z 80 and 1400. Data was evaluated using

the program MassHunter Workstation (Agilent, Santa Clara, USA). Compounds were identified according to their HR-MS peaks and UV spectra. The instrument was programmed to pick samples from the reaction mixtures 2, 20, 40, 60, 80, 100, 120 min as well as 2.5, 3, 3.5, 4, 4.5, 5, 6, 8 and 24 h after pipetting. For data analysis, the decreasing electrophile HPLC signals (total mass counts) of each measurement were integrated with the software MassHunter (Agilent Technologies, Santa Clara, USA). k_{obs} values were determined by plotting these time-dependent MS signals and fitting the resulting curves to first-order exponential decay functions (software: Origin Pro 9, OriginLab Corporation, Northampton, Massachusetts, USA). k_2 values were calculated by linear regression of the k_{obs} values versus their corresponding thiol concentrations. For the three different thiol excess concentrations, three independent single experiments were performed for each **OXE4-(4py)''** and **OXEp1-(4py)''**. For all experimental k_{obs} graphs and values, see appendix.

A 6.6 In-vitro cell assays

The MTT test for cell viability and the test for the inhibition of NO production (iNOS assay) were performed as reported previously by this work group.^[35-36]

Cell line and culture conditions

Murine macrophages RAW264.7 were used which were cultured in RPMI 1640 medium containing 10% (v/v) heat inactivated fetal calf serum (FCS) and 2 mM glutamine (termed as culture medium) at 37 °C in humidified air containing 5% CO₂.

Cell viability assay (MTT assay)

RAW264.7 cells were seeded in 96-well plates at a density of 5000 per well and cultured in culture medium for 24 h. Test compounds were kept as 100 mM DMSO stock solutions at -20 °C and were diluted freshly for each experiment in culture medium to the following concentrations: 100, 75, 50, 25, 10, 5, 1, 0.1 μM. The cells were incubated at 37 °C with the different concentrations of test compounds for 20 h in culture medium. Controls were cells with culture medium, cells with culture medium and 0.1% DMSO and cell-free wells with only culture medium. The total assay volume was 100 μL and the highest DMSO concentration was 0.1%. MTT solution in a concentration of 4 mg/mL in phosphate buffered saline (PBS) was added in a volume of 10 μL to each well and further incubated for 4 h at 37 °C. The culture medium was removed from the wells and 100 μL of 10% aqueous SDS solution was added and incubated overnight at room temperature. The absorbance was measured at $\lambda = 560$ nm on a Multiscan Spectrum spectrophotometer (Thermo Fisher Scientific Inc.,

Vantaa, Finland) at 25 °C. For each compound concentration, quadruplicates were measured. IC₅₀ values were calculated from three to five individual performed experiments.

Anti-inflammatory assay (NO/iNOS inhibition assay or Griess assay)

RAW264.7 cells were seeded in 96-well plates at a density of 80,000 per well and cultured for 24 h. Test compounds were kept as 100 mM DMSO stock solutions at -20 °C and were diluted freshly for each experiment in two different culture media: one contained 10 ng/mL LPS, the other one without LPS. The cells were incubated with test compounds in four different individual concentrations according to the previously determined toxicity limits for 24 h at 37 °C. The total assay volume was 100 µL and the highest DMSO concentration was 0.1%. Griess reagent was prepared freshly before use by dissolving 50 mg NED (*N*-1-naphthylethylenediamine dihydrochloride), 500 mg sulfanilamide and 175 µL phosphoric acid in 50 mL Millipore water and heating to 60-70 °C for 30-60 min. 50 µL Griess reagent was mixed with 50 µL culture medium at room temperature and air bubbles were removed under a weak nitrogen stream. After 15 min at room temperature, the absorbance was measured at $\lambda = 560$ nm on a Multiscan Spectrum Photometer (Thermo Fisher Scientific Inc., Vantaa, Finland) at 25 °C. To create a calibration curve, NaNO₂ solutions were prepared in concentrations of 0-100 µM and measured in a volume of 100 µL in a 96-well plate. For each compound concentration, quadruplicates were measured. IC₅₀ values were calculated from three to five individual performed experiments. The statistical evaluation of the data using the *t*-test was carried out by Sabine Amslinger.

B Characterization of a new photoactive protein probe for the labeling of BTN3A4

Parts of this chapter are published^[102]:

Andrea Mattarei, Monika Enzinger, Siyi Gu, Mohindar Murugesh Karunakaran, Brigitte Kimmel, Nicole Berner, Erin J. Adams, Thomas Herrmann and Sabine Amslinger: A photo-cross-linkable biotin derivative of the phosphoantigen (*E*)-4-hydroxy-3-methylbut-2-enyl diphosphate (HMBPP) activates V γ 9V δ 2 T cells and binds to the HMBPP site of BTN3A1 *Chem. Eur. J.* **2017**, *23*, 11945 – 11954.

The following persons and work groups participated in this project as follows:

Dr. Andrea Mattarei and PD Dr. Sabine Amslinger, Institute of Organic Chemistry, University of Regensburg: Design and synthesis of the probe BioBP-HMBPP.

Siyi Gu and Prof. Dr. Erin Adams, Department of Biochemistry and Molecular Biology, University of Chicago, USA: Synthesis of BTN3A1 domain B30.2, BTN3A1 B30.2 charge transfer mutant and biotinylated BTN3A1 B30.2.

Mohindar Murugesh Karunakaran, Thomas Herrmann, Institut für Virologie und Immunbiologie, University of Würzburg, and Brigitte Kimmel, Universitätsklinikum Würzburg: Stimulation assays of $\gamma\delta$ T cells by HMBPP and BioBP-HMBPP.

Monika Enzinger, Institute of Organic Chemistry, University of Regensburg: UV-Vis characterization of BioBP-HMBPP and all protein labeling experiments. Laser irradiation was performed by Nicole Berner, work group of Prof. Dr. Dick, Institute of Physical Chemistry, University of Regensburg.

I gratefully acknowledge the help, support and expertise of everyone involved in this project.

B 1 Introduction

B 1.1 The immune modulator role of HMBPP

Phosphoantigens (PAgs) are small organic molecules, which typically contain a diphosphate unit (traditionally known as pyrophosphates, PPs) and are potent activators of human V γ 9V δ 2 T-lymphocytes. V γ 9V δ 2 T cells are an important subpopulation of $\gamma\delta$ T cells and generally involved in the cross talk of the innate and adaptive immune system. The most potent natural phosphoantigen is (*E*)-4-hydroxy-3-methylbut-2-enyl diphosphate (HMBPP,

102, Figure 46) with an EC₅₀ value of T-cell activation in the sub-nanomolar range^{[103] [104] [105] [106]}.

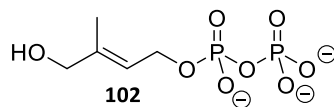


Figure 46: Molecular structure of the phosphoantigen HMBPP (**102**).

HMBPP is an intermediate of the 1-deoxy-D-xylulose 5-phosphate (DOXP) or non-mevalonate pathway of isoprenoid biosynthesis that is common to many eubacteria, plants and apicomplexan parasites and is responsible for the massive V γ 9V δ 2 T cell expansion in some infectious diseases such as malaria.^{[106] [107]} HMBPP is the immediate precursor of isopentenyl diphosphate (IPP) and dimethylallyl diphosphate (DMAPP), which are the key compounds of isoprenoid biosynthesis of all organisms and act as weak phosphoantigens with EC₅₀ values in the micromolar and high nanomolar range, respectively.^[105] Aminobisphosphonates such as zoledronate used for the therapy of tumors or osteoporosis inhibit the IPP-utilizing enzyme farnesyl diphosphate synthase (FPPS) and the resulting increase of IPP levels renders the treated cells into V γ 9V δ 2 T cell activators.^{[108] [109] [110]} Cell surface receptors mandatory for PAg-mediated V γ 9V δ 2 T cell activation are the eponymous V γ 9V δ 2 T cell antigen receptors (V γ 9V δ 2 TCRs) on V γ 9V δ 2 T cells (sometimes called V γ 2V δ 2 TCRs and V γ 2V δ 2 T cells) and butyrophilin 3A1 (BTN3A1) on the phosphoantigen-“presenting” cell.^[111] Two mutually non-exclusive modes of interaction of phosphoantigens with the BTN3A1 protein have been proposed.^[112] One rather debated one proposes binding of the PAg to a shallow binding groove in the extracellular V-domain of BTN3A1.^[113] The binding of the resulting BTN3A1-PAg complex to the V γ 9V δ 2 TCR would then initiate the PAg-specific activation of the V γ 9V δ 2 T cells. The other one emphasizes the importance of PAg binding of the negatively charged diphosphate entity of the PAg to a well-defined positively charged pocket in the PRY/SPRY (B30.2) domain of the intracellular region of BTN3A1. This binding occurs at a micromolar range for HMBPP and at a millimolar range for IPP.^{[114] [115]} ^[116] NMR studies suggest a subsequent conformational change of the membrane proximal parts of the intracellular domain.^[115] This change would precede formation of an active conformation and of cell surface clusters of BTN3A1, as they were observed after treating cells with aminobisphosphonates.^{[111] [117] [118]} The resulting lattice of BTN3A1 or of BTN3A1 in conjunction with other molecules might then serve as binding partner for the V γ 9V δ 2 TCR. The exact nature of such hypothetical additional molecules is unknown, but it is clear that the PAg-induced activation of V γ 9V δ 2 T cells is controlled by gene(s) encoded on human chromosome 6 encoding other components than BTN3A1.^[119]

B 1.2 BioBP-HMBPP as a new photoactive protein probe for the labeling of BTN3A4

To identify potential co-receptors or, in general, proteins involved in HMBPP binding, a multifunctional probe is needed. The probe was designed by connecting the three crucial parts:

HMBPP	high affinity ligand for the V γ 9V δ 2 T cell receptor
benzophenone	can be activated photochemically to make a covalent C-C bond with the α -carbon of amino acids of the bound protein
biotin	allows for detection or purification of attached proteins by streptavidin or avidin-based systems

These three fragments were combined by two linking units, which were connected by three ether functionalities and an amide bond to create a high degree of hydrolytic stability for the probe **BioBP-HMBPP** (BiotinBenzoPhenone-HMBPP, **103**, Figure 47). This design is based on prior work using the benzophenone unit as the photo-crosslinkable core unit^[120] together with isoprenoid diphosphates including HMBPP.^{[121] [122] [123] [124]} A biotinylated photoaffinity ligand very similar to this probe was recently presented.^[125] The main difference is a direct connection of HMBPP to the benzophenone unit by an ester linkage, whereas linker-2 and two ether bonds were used for **103**.

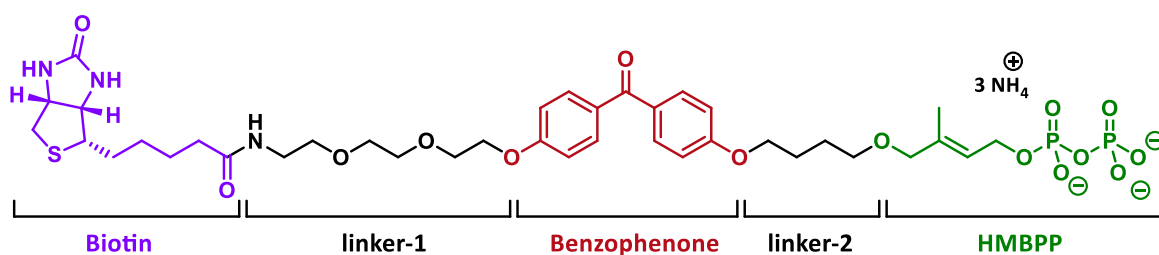
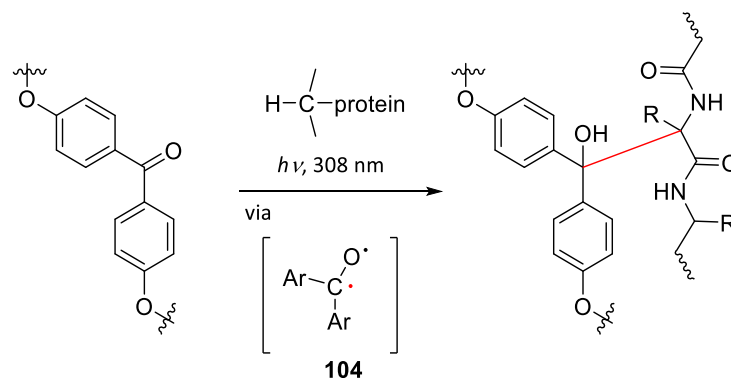


Figure 47: Structure of BioBP-HMBPP (**103**), a biotinylated photo-crosslinkable derivative of the PAg (*E*)-4-hydroxy-3-methylbut-2-enyl diphosphate (HMBPP, **102**).

BioBP-HMBPP (**103**) was designed and synthesized in this work group by Sabine Amslinger and Andrea Mattarei. In a nine-step synthesis **103** was obtained with an overall yield of 16%. For the complete synthesis route, reagents and conditions, yields and analytical data, see Mattarei et al. *Chem. Eur. J.* **2017**, *23*, 11945 – 11954.^[102]

The whole photochemical labeling strategy is based on forming radicals in **103**, which react with proteins. More specifically, exciting the benzophenone chromophore of **103**

transforms the carbonyl C=O double bond into biradical **104** (Scheme 30). When in close proximity to proteins, **104** can abstract H-atoms from α -carbons of the protein backbone and initiate a covalent attachment of the α -carbon of amino acids to the former carbonyl carbon of the benzophenone moiety.



Scheme 30: Photochemically-induced covalent attachment of benzophenone-based probes to proteins.^[123]

Once covalently bound, the protein can be separated from the solution via SDS-PAGE, blotted on a membrane and, if successfully labeled, detected by the streptavidin-horseradish peroxidase (HRPO) system.

B 1.3 Aim of this work

Since probe **103** was only synthesized but not investigated towards its purpose, general and specific protein labeling studies of **103** were performed within this work. UV-Vis spectroscopy was used to determine the chromophore of **103** and follow the processes during irradiation. Four proteins were examined: BSA and papain were used for the general labeling of BioBP-HMBPP towards proteins and furthermore the B30.2 domain of BTN3A1 and a charge reversal mutant of this protein were tested. It was tested *in vitro* whether **103**, despite its increased molecular size, is still a T cell activator through the HMBPP unit (performed by the work group of Prof. Herrmann, University of Würzburg). To prove the specific binding of probe **103** to the HMBPP binding pocket of the B30.2 domain of BTN3A1, competition experiments were performed with the natural ligand HMBPP. Conditions for laser irradiation, probe concentrations and sample volumes were tested and optimized. The labeling efficiency of BioBP-HMBPP was determined using monobiotinylated BTN3A1 B30.2.

B 2 Results and Discussion

B 2.1 Photochemical and UV-Vis evaluation, handling of proteins and probe solutions

UV-Vis characterization of probe **103** without and with BSA

To prove the applicability of **103** as a photo-crosslinkable probe, its spectroscopic and labeling properties were investigated. UV-Vis spectra of **103** at different concentrations in phosphate-buffered saline (PBS) pH 7.4 revealed an absorbance maximum of 302 nm caused by the benzophenone unit (Figure 48A). Thus, a 308 nm excimer laser as the light source was chosen for the photochemical labeling experiments. Laser irradiation allows for defined reaction conditions, in which the radiation is transferred very efficiently into the sample. Moreover, an irradiation of volumes as low as 90 μ L was achieved using 1 mm quartz cuvettes. To establish its general properties, **103** was irradiated with an increasing number of 10 ns laser pulses (pulse energy 215–250 mJ, frequency 1 Hz; Figure 48C). Within 10 pulses, the absorbance of BioBP-HMBPP (**103**) decreases by 50%. This decay of the benzophenone chromophore reveals the formation of biradical **104**, which is quenched by H-atom abstraction from water of the reaction medium PBS.

Having proven its general photochemical activation, **103** was tested towards its pan reaction with proteins. Bovine serum albumin (BSA) was used as a model protein to test for general unspecific protein labeling. Concentrations of 20 μ M BSA and 30 μ M (1.5-fold excess) BioBP-HMBPP **103** were chosen. First, UV-Vis spectra of **103** in PBS pH 7.4 with BSA were measured without irradiation. After incubation of BioBP-HMBPP (**103**) with BSA in buffer for 30 min on ice and in the dark, the radiation was performed. A control sample of 20 μ M BSA alone was also irradiated simultaneously. BSA alone proved to be stable when an increasing number of laser pulses for at least 50 pulses was applied (Figure 48B). Further prolongation of irradiation (300 or more pulses) gave a significant increase in absorption within the whole region scanned. This indicates radiation- or heat-related protein decomposition. When **103** was irradiated (1–600 pulses) in presence of 20 μ M BSA, a very similar decrease of the absorption as in Figure 48B within the first 10 pulses was observed indicating an equally efficient radical reaction (Figure 48D). Whether this effect is due to a reaction with water or the protein backbone cannot be determined based on this data.

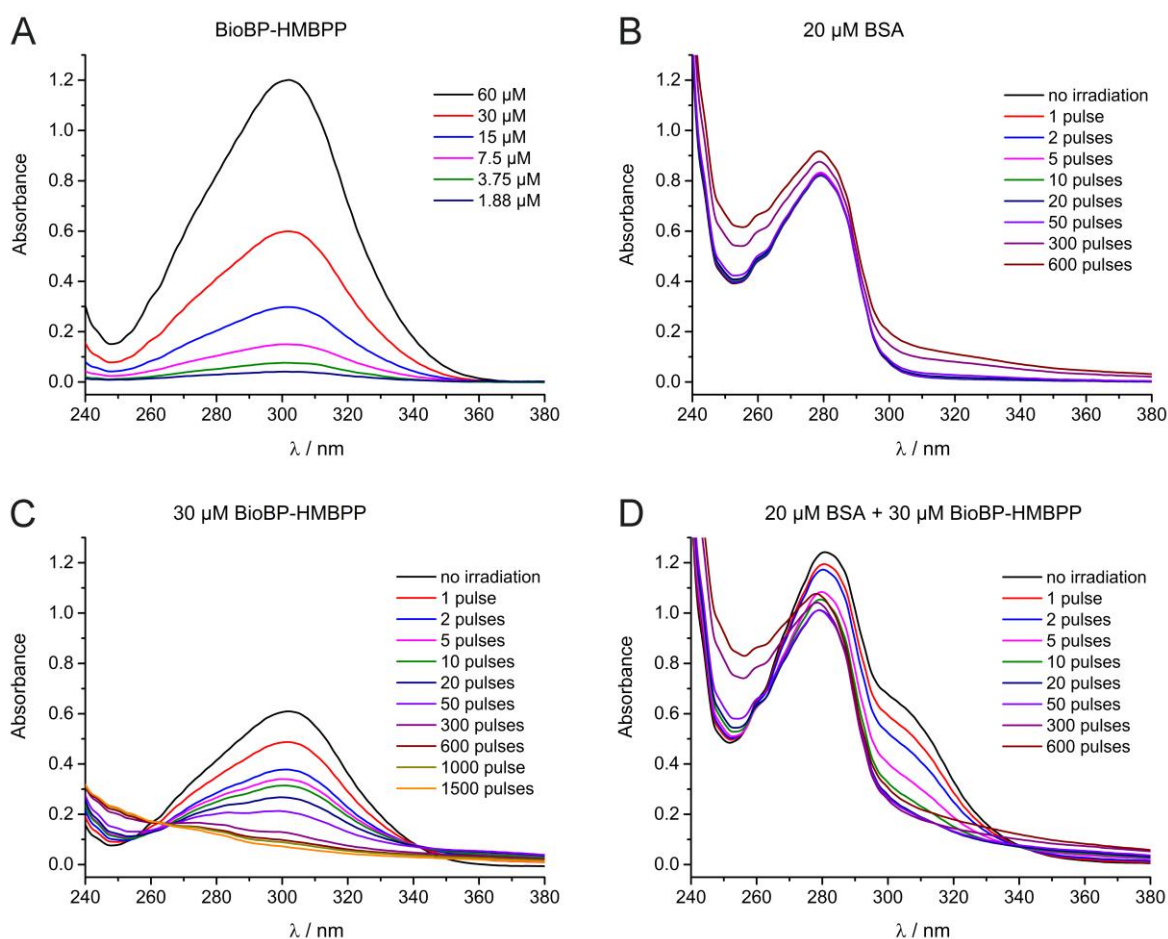


Figure 48: UV-Vis spectra in PBS buffer pH 7.4 of **A:** the probe BioBP-HMBPP (**103**) at different concentrations without irradiation; **B-D:** Samples were irradiated with the indicated number of laser pulses at 308 nm: **B:** 20 μ M BSA; **C:** 30 μ M BioBP-HMBPP (**103**) and **D:** 20 μ M BSA together with 30 μ M BioBP-HMBPP (**103**).

Detection of BioBP-HMBPP-labeled BSA and handling of probe **103**

SDS-PAGE protein separation and subsequent Western blotting were used to prove that the absorbance decrease found by UV-Vis spectroscopy is due to a covalent protein labeling of BSA by **103**. Labeling by **103** is visualized using a streptavidin-coupled HRPO (horseradish peroxidase) chemiluminescence detection system, which relies on binding to the biotin fragment in **103** after transferring the proteins on a PVDF membrane. With this method the successful labeling of BSA by BioBP could be proven by the detection of a strong protein band (Figure 49). BSA as a transporter protein is able to bind various molecules in order to transport them in blood plasma. Due to this general ability, probe **103** can come close enough to BSA to covalently bind to the protein when activated by laser energy according to Scheme 30.

It is important to note that probe **103** turned out to be unstable in DMSO stock solutions at room temperature and daylight for extended time periods. Therefore, aliquots of the 100 mM stock solution were kept at -20 $^{\circ}$ C and were freshly diluted when used.

Furthermore, inadvertent labeling of actually unirradiated control samples was frequently experienced during the first experiments. An example is shown in Figure 49, lanes 1 and 4 (unirradiated). It was assumed that this phenomenon occurs when samples are incubated for longer than 20 min in daylight and/or artificial light. Initially, sample preparation was therefore performed in the darkened laboratory to avoid the effect, but later it was found that the source of the unwanted labeling were certain types of overhead light bulbs in several laboratories. Tests have shown that only a few minutes under the influence of this light are sufficient to induce labeling. In addition, however, the exposure to monochromatic light during the recording of UV-Vis spectra was not high enough in energy to produce labeling, not even during prolonged exposure in a kinetic experiment, which was also tested as an alternative to laser irradiation. Keeping non-irradiated controls with proteins and **103** constantly in the dark and on ice secured that no artificial labeling without laser irradiation was found.

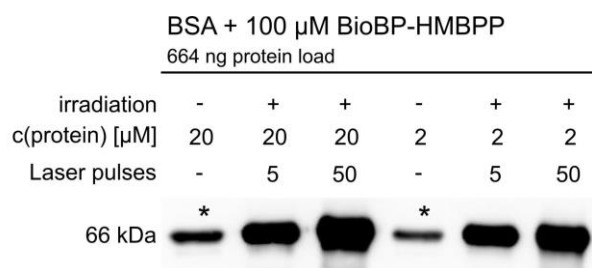


Figure 49: Labeling of BSA by the probe BioBP-HMBPP (**103**) under different conditions. Protein concentration during irradiation in this representative experiment was 20 or 2 μ M together with 100 μ M BioBP-HMBPP with increasing laser pulses. * = Inadvertent, artificial labeling of non-laser-irradiated samples by laboratory overhead lights is visible.

To prove furthermore, that the gradual decrease of absorbance by increasing numbers of laser pulses correlates with an irradiation-dependent protein labeling of BSA, the protein samples of the UV-Vis experiment (Figure 48D) were also isolated and visualized. Additionally, the protein load was stained with Ponceau S for the control of equal protein amounts in each sample. Notably, one laser pulse is enough to induce significant protein labeling by **103** (Figure 50, lane 2). Upon prolonged irradiation, the extent of BSA labeling increased dramatically. Between 50 and 300 laser pulses BSA is partially destroyed; the protein degradation can be seen in lane 9 and 10 (300 and 600 laser pulses) of the Ponceau S control. It was decided to use 10 pulses for further experiments, because significant labeling was observed with this small number of pulses. And, moreover, protein destruction or concentration changes upon heat exposure can be avoided. This was especially important for later investigated BTN3A1 B30.2 which was used in small volumes of 90 μ L.

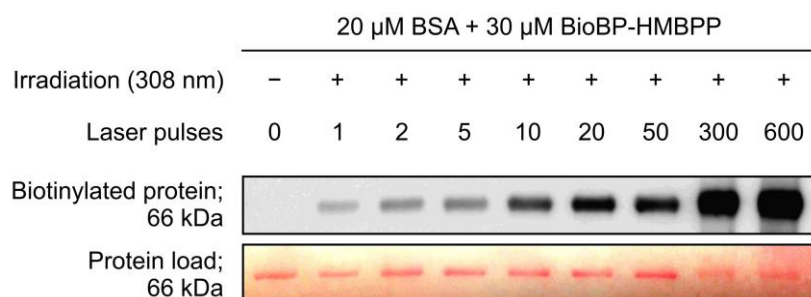


Figure 50: Irradiation of 20 μ M BSA in presence of 30 μ M BioBP-HMBPP (**103**) in PBS pH 7.4 with an increasing number of laser pulses at 308 nm. Biotinylated protein bands are visualized using a streptavidin-coupled HRPO (horseradish peroxidase) chemiluminescence detection system. The protein load is visualized with Ponceau S staining. The Western blot shown is representative of 3 independent experiments.

Labeling of papain

To have a second control, the enzyme papain was also checked for general protein labeling during the first irradiation experiments. A labeling of papain was successfully detected as shown in Figure 51, but to a much smaller extent than BSA (Figure 49). Papain in Figure 51 is only barely visible even with 2.3 μ g protein load on the gel for SDS-PAGE separation. Due to this finding BSA was later chosen as comparison protein for further labeling experiments. This finding can be explained by the fact that papain as an enzyme is very selective for only certain compounds, whereas BSA as a transport protein in the blood is specialized in binding and transporting many different types of substances, and therefore also has a higher affinity for probe **103**. It might also be possible that papain, as a cysteine protease with broad activity range, is able to cleave the amide bond between biotin and linker-1 in probe **103**. Labeling may have taken place, but is no longer detectable due to the lack of biotin.

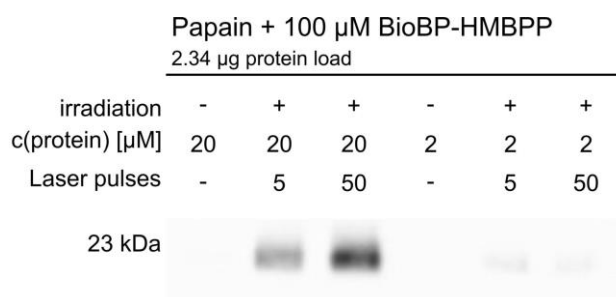


Figure 51: Labeling of papain by BioBP-HMBPP (**103**) under different conditions. Protein concentration during irradiation was 20 or 2 μ M together with 100 μ M BioBP-HMBPP and an increasing number of laser pulses.

B 2.2 Stimulation of $\gamma\delta$ T cells by BioBP-HMBPP (**103**)

Considering that its general applicability for protein labeling was proven, the question was now whether the HMBPP derivative **103** is still a V γ 9V δ 2 T cell activator. Therefore, the activation of V γ 9V δ 2 T cells in a titration experiment in comparison to HMBPP (**102**) was tested. Human PBMCs (peripheral blood mononuclear cells) were cultured with different

concentrations of BioBP-HMBPP (**103**) and HMBPP (**102**). Cultures were then analyzed for the activation of $V\delta 2^+$ T cells by measuring the expression of CD69 after 24 h. In addition, the PBMCs were analyzed for the expansion of the $V\delta 2^+$ population by determining the amount of $V\delta 2^+$ T cells after 7 days. Despite the fact that the HMBPP derivative **103** has a very large extension compared to HMBPP (**102**), probe **103** is still capable of activating $V\gamma 9V\delta 2$ T cells and causing their proliferation (Figure 52). Not unexpectedly, because it is known that the free 4-hydroxy group is also very important^[105], it is less active by a factor of about 3000 compared to HMBPP (**102**).

The EC_{50} of three different donors for CD69 up-regulation after 24 h of culture with BioBP-HMBPP **103** and HMBPP **102**, resp., are summarized in Table 22, resulting in an EC_{50} shift of $2050 \pm SD 1530$. Looking at the proliferation response after 7 days in presence of IL-2 for HMBPP vs. BioBP-HMBPP, an EC_{50} shift of $3360 \pm SD 650$ was found (Table 22).

Table 22: Individual IC_{50} values of the three different PBMC donors for CD69 up-regulation and proliferation response with natural immune modulator HMBPP **102** and label BioBP-HMBPP **103**.

CD69 up-regulation after 24 h		
Donor	EC_{50} HMBPP [M]	EC_{50} BioBP-HMBPP [M]
1	1.88×10^{-9}	3.14×10^{-6}
2	4.98×10^{-10}	1.86×10^{-7}
3	1.69×10^{-9}	1.27×10^{-6}

Proliferation response after 7 d in the presence of IL-2		
Donor	EC_{50} HMBPP [M]	EC_{50} BioBP-HMBPP [M]
1	1.76×10^{-9}	7.06×10^{-6}
2	1.09×10^{-9}	2.95×10^{-7}
3	3.13×10^{-10}	1.05×10^{-6}

The EC_{50} values obtained for each stimulation of one single donor were for BioBP-HMBPP 4.45×10^{-6} , 6.64×10^{-6} , 3.50×10^{-6} M and for HMBPP 4.25×10^{-9} , 3.88×10^{-9} , 2.34×10^{-9} M, respectively, resulting in an EC_{50} shift of $1420 \pm SD 340$.

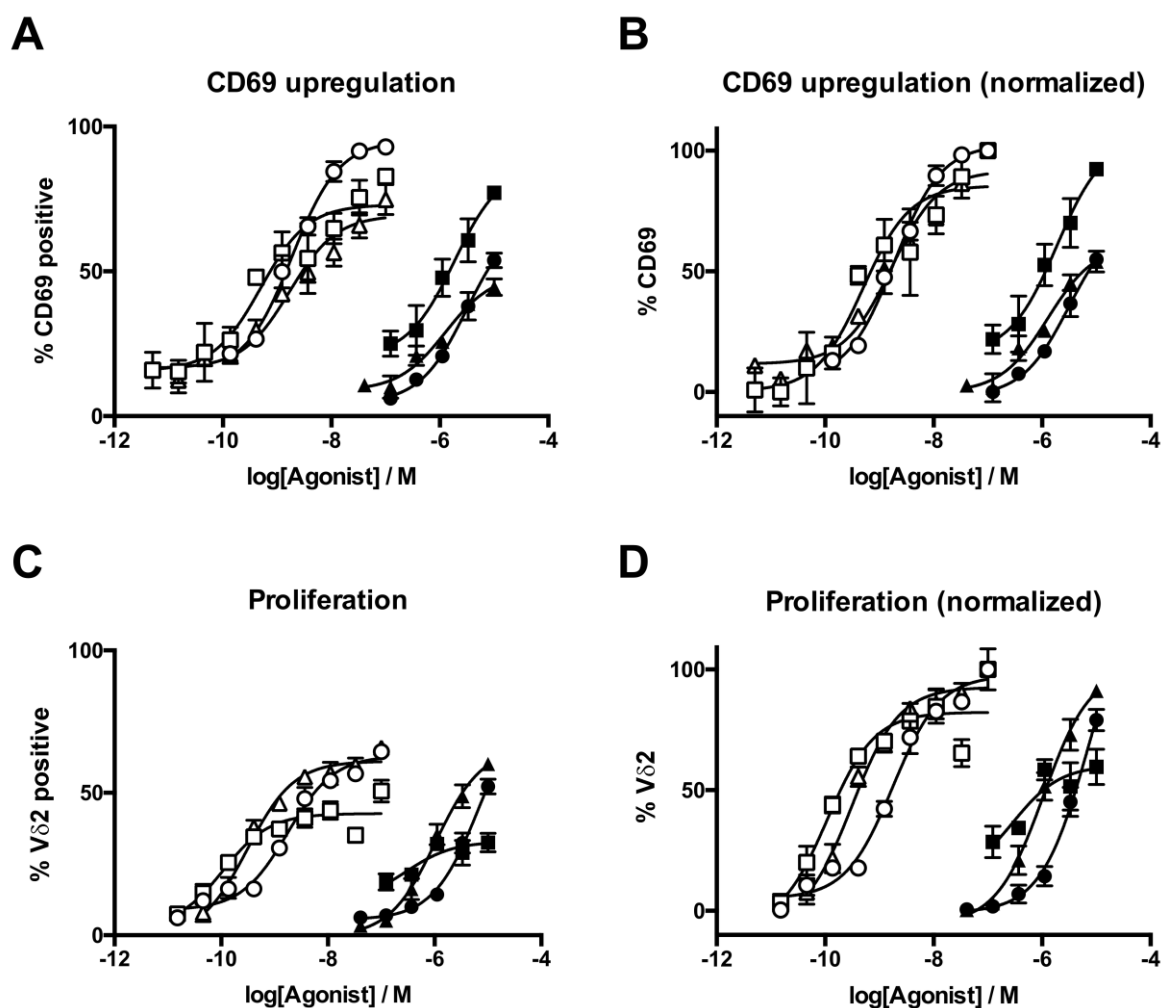


Figure 52: A and B: % CD69 upregulation. **A:** % CD69 expression of V δ 2 T cells after stimulation with BioBP-HMBPP (**59**) or HMBPP (**102**) for 24 h. Values depict data from three donors stimulated with indicated concentrations of HMBPP (open symbols) or BioBP-HMBPP (full symbols) stained for CD69 and V δ 2 expression. Errors are SD of triplicate values from the respective donors. Curves indicate non-linear regression of depicted values. **B:** Data from A) normalized for highest and lowest value (no stimulus) for each condition. Curves indicate non-linear regression of depicted values. **C and D:** proliferation. **C:** % of V δ 2 T cells after 7 d stimulation with BioBP-HMBPP or HMBPP. Values depict data from three donors stimulated with indicated concentrations of HMBPP (open symbols) or BioBP-HMBPP (full symbols) stained for CD3 and V δ 2 expression as described in materials and methods. Errors are SD of triplicate values. Curves indicate non-linear regression of depicted values. **D:** Data from C: normalized for highest and lowest value (no stimulus) for each condition. Curves indicate non-linear regression of depicted values. The experimental procedure can be viewed in the literature.^[102]

This data clearly indicates that despite the attachment of the large biotin-benzophenone moiety to the 4-hydroxyl group of HMBPP, the intact C₅-diphosphate fragment is still capable of activating V γ 9V δ 2 T cells. However, its reduced activity may not only be the consequence of the ether linked extension of the molecule. It might just stem from different pharmacokinetic properties such as a reduced uptake into the cells. This data is in agreement to prior observations in which ester and ether-linked benzophenone HMBPP derivatives were compared^[124]. Here, Morita et al. report a 40–70-fold reduction in the activity of the ether-linked benzophenone HMBPP derivatives compared to the corresponding

esters. Figure 53 shows two examples of structures compared in those experiments. Benzophenone in compound **105** is linked to HMBPP via an ether and in **106** via an ester bond. The esters showed indeed very similar activities as the parent compound HMBPP **102**. The same was found in the work group of PD Dr. Sabine Amslinger when using independently prepared material of the ester linked benzophenone-HMBPP compound (*E*)-4-((4-benzoylbenzoyl)oxy)-3-methylbut-2-en-1-yl diphosphate **106** (Figure 53, named BP-HMBPP in the Amslinger work group, previously named *p*-BZ-C-C₅-OPP ester by Morita et al.^[124]). More specifically, for the investigations performed in the Amslinger work group even a slightly higher stimulation for BP-HMBPP **106** than for HMBPP itself was obtained (data not shown).

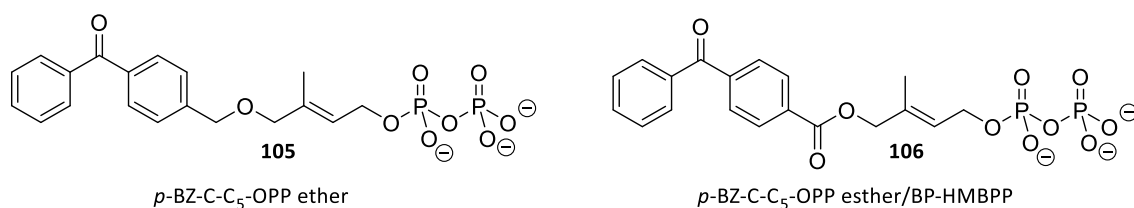


Figure 53: Structures of HMBPP combined with benzophenone by ether (**105**) and ester (**106**) linkage.^[124]

This effect could be based on a potentially higher cellular uptake of the more lipophilic BP-HMBPP **106** combined with a release of active HMBPP (**102**) by ester hydrolysis within the cell. This effect could also explain why ester derivatives are more potent in general than the ether-linked compounds, which display high hydrolytic stability. Although one cannot completely rule out some ether hydrolysis over time, for photoaffinity probes, ether or at least amide bonds are preferable because phosphoantigen-specific labeling depends on an intact probe containing the recognition motif.

B 2.3 Labeling of the B30.2 domain of the protein BTN3A1 by BioBP-HMBPP (**103**) in the absence and presence of HMBPP (**102**)

To prove whether BioBP-HMBPP (**103**) actually binds to the HMBPP binding site, the B30.2 domain of the BTN3A1 protein was used.^[114] Because BioBP-HMBPP (**103**) is about 3000 times less active in stimulating V γ 9V δ 2 T cells, one can imagine that its binding affinity to the B30.2 domain is reduced compared to HMBPP. To test whether this is true and/or both diphosphates **102** and **103** compete for the same binding site, a titration experiment was set up.

Labeling of BTN3A1 B30.2 and concentration studies

BTN3A1 B30.2 was received as 312 and 340 μ M stock solution in HEPES buffer, which were either stored at 4 °C or in aliquots at -20 °C as repeated freezing/thawing in -20 °C led to

dimerization. The protein was first tested for general labeling by BioBP-HMBPP, which was successful (Figure 54A). For good visibility during detection, a sufficient amount of BTN3A1-B30.2 has to be submitted to gel electrophoresis and Western Blot. A protein amount of 1 μg per lane was therefore determined for the further investigations after irradiation. Concentration experiments show strong labeling at a concentration of 60 μM and 100 μM BioBP-HMBPP but only weak and very weak labeling when irradiated solutions contained 6/1.2 μM BTN3A1 and 1.7-fold BioBP-HMBPP. Since the 1.2 μM sample would have required a too-high sample volume for the gel loading, protein precipitation experiments with EtOH to obtain sufficient amounts of protein for loading were performed. As the Ponceau S control (Figure 54A, lane 5 and 6) shows, this method was not successful. To have an optimized visualization, it was decided to use only sufficiently high protein concentrations where precipitation is not necessary for further irradiation experiments. Therefore, further experiments were carried out initially with 60 μM protein. An HMBPP titration experiment was set up using 60 μM BTN3A1 together with 100 μM BioBP-HMBPP (1.7 eq.) in PBS (Figure 54B). 0, 50 and 100 μM HMBPP was added to three aliquots of this solution each. After 30 min incubation on ice and laser irradiation (ten pulses), the labeling was detected as shown and Ponceau S staining is additionally illustrated as control, showing the protein load for both irradiated samples and unirradiated controls. The detection shows a labeling gradient from the HMBPP-free sample, which shows strong protein labeling, to those samples with $\frac{1}{2}$ -molar and equimolar HMBPP concentration in comparison to probe **103**, where labeling significantly decreases. This indicates a displacement of label **103** from the binding pocket of BTN3A1 by the natural, 3000 times more affine ligand HMBPP.

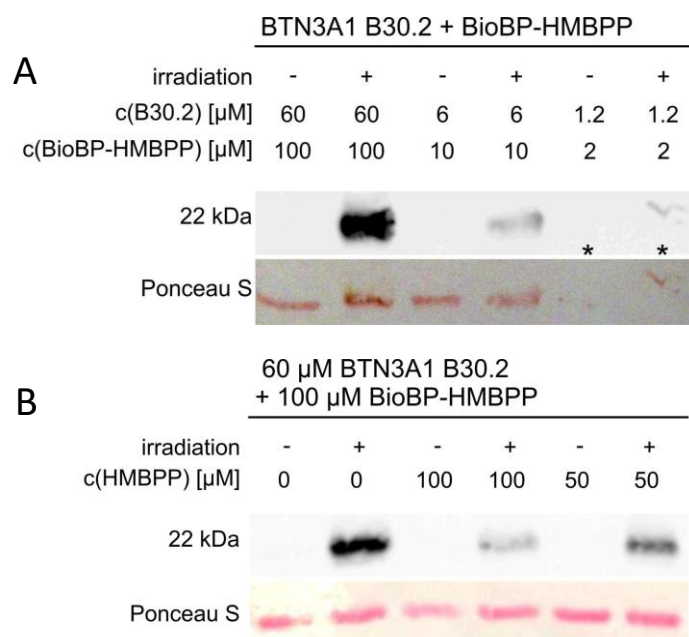


Figure 54: A: Labeling experiments with different concentrations of BTN3A1 and BioBP-HMBPP (1.7-fold label excess each). Protein load: 1 μ g per lane, * = protein was precipitated by EtOH prior to SDS-PAGE. **B:** Labeling of BTN3A1 by BioBP-HMBPP decreases in the presence of 0.5 and 1 eq. HMBPP.

Therefore, further experiments with this protein concentration were initially carried out. But, since these results were not reproducible with a concentration combination of BTN3A1/BioBP-HMBPP 60/100 μ M in all cases, experiments with lower concentrations were carried out for optimization. This should prevent potential protein agglomeration which can lead to irradiation inaccuracy. Figure 55 shows an example for such an experiment. Irradiation was performed on samples with 30, 15 and 5 μ M BTN3A1 and 1.5 eq. BioBP-HMBPP each. To study the effect of HMBPP presence on these sample mixtures, 0, 2 and 10 eq. HMBPP (compared to label BioBP-HMBPP) were added to three aliquots of each sample. A displacement of the probe from the binding site leading to a reduced labeling of BTN3A1 is seen for the 30 and 15 μ M sample, and also in the 5 μ M sample, but to a smaller extent. Based on these experiments 20 μ M protein concentration was used for further studies.

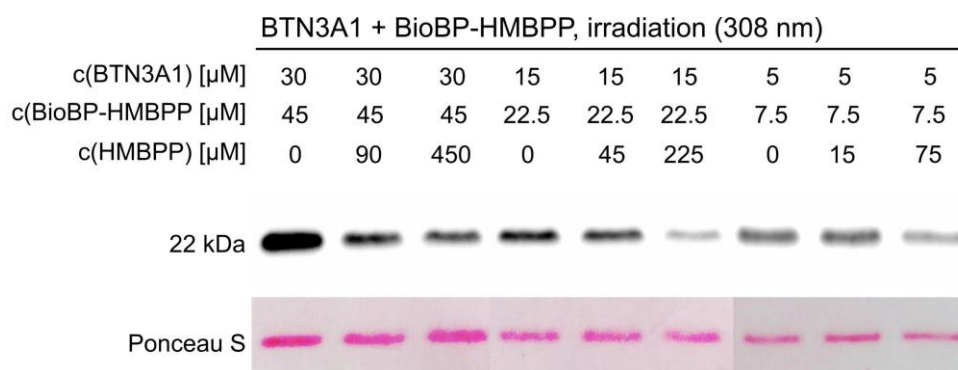


Figure 55: Labeling of BTN3A1 B30.2 by BioBP-HMBPP **103** in the presence and absence of 0, 2 and 20 eq. of HMBPP in comparison to probe **103**. Different concentrations of protein BTN3A1 B30.2 and probe **103** are tested.

Binding of BioBP-HMBPP to the HMBPP binding site of BTN3A1 is displaced by HMBPP, comparison experiments with BSA

Thus, the following concentrations were selected as conditions for this titration experiment: 20 μ M protein solutions of the BTN3A1 B30.2 domain and BSA as control for unspecific binding together with a 30 μ M solution (1.5 equivalents compared to proteins) of BioBP-HMBPP (**103**), as well as different concentrations of the natural phosphoantigen HMBPP (0, 0.50, 1.0, 2.0, 10 equiv. compared to BioBP-HMBPP) (Figure 56 and Figure 57). As can be seen from the protein bands in Figure 56 and Figure 57, upon irradiation, increasing amounts of HMBPP (**102**) strongly decreased the labeling of the B30.2 domain of BTN3A1 in a concentration-dependent manner, whereas for BSA, no such disruption of labeling was observed. Particularly, there was no significant difference between BSA alone and different amounts of HMBPP. Notably, the competition effect by HMBPP is not complete even when HMBPP is present in a 10-times higher concentration than BioBP-HMBPP or even higher (up to 50 equiv., **Figure 56**, lane 7, 1500 μ M HMBPP).

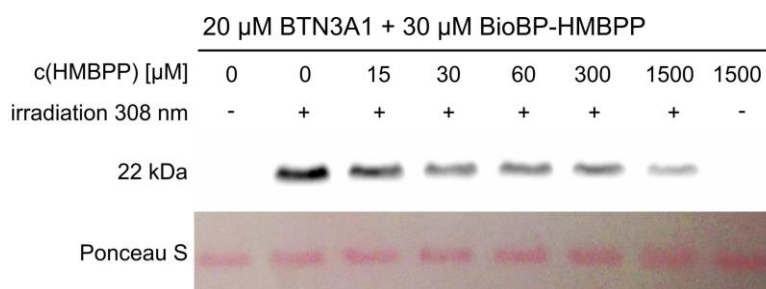


Figure 56: Irradiation experiment with 20 μ M BTN3A1 B30.2 and 30 μ M BioBP-HMBPP **103** in competition with HMBPP in increasing concentrations: 0, $\frac{1}{2}$, 1, 2, 10 and 50-fold excess.

This is an indication that BioBP-HMBPP (**103**) has either some residual binding to the binding pocket in presence of HMBPP or, more likely, binds also in part non-specifically to BTN3A1 as it does to BSA. This demonstration of partial competition of labeling by the

original ligand (HMBPP) makes probe **103** a promising candidate tool to identify HMBPP-binding molecules. A previously presented similar probe by Morita et al. also containing a biotin-linked benzophenone unit attached to HMBPP was not successful in specifically labeling BTN3A1 compared to BTN3A2 and chicken ovalbumin^[125]. Nevertheless, this probe was a very active V γ 9V δ 2 T cell stimulator and most likely is more active than **103**. This stronger bioactivity may be a consequence of attaching the HMBPP unit with an ester linkage and a subsequent release of HMBPP. Moreover, their finding of a non-specific protein labeling is in agreement with our data that proves general protein labeling by such probes. It would also be interesting to learn to which extent it might be inhibited by competition with the physiological ligand HMBPP.

Figures of the detection of all experiments with BTN3A1 and BSA used for the calculations depicted in Figure 57 together with additional experiments performed with 60 μ M BTN3A1/BSA and 100 μ M probe **103** can be viewed in the appendix.

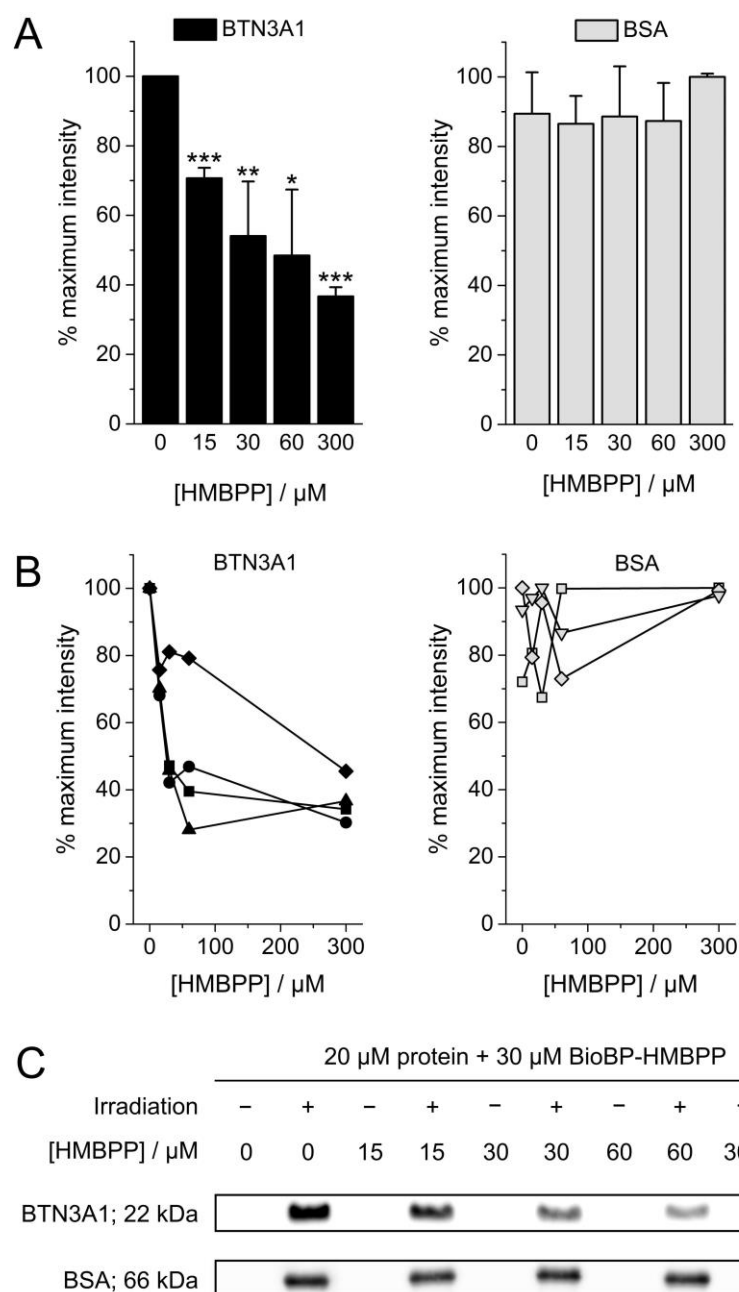


Figure 57: Irradiation at 308 nm of 20 μM of proteins BTN3A1 B30.2 domain (BTN3A1) and BSA in presence of 30 μM BioBP-HMBPP (**103**) together with increasing concentrations of HMBPP (**102**) (0–300 μM). Densitometric evaluation of Western blot graphs from 3–4 independent experiments: **A:** Means with standard deviations; levels of significance: * = $p \leq 0.05$, ** = $p \leq 0.01$, *** = $p \leq 0.001$. **B:** Single experiments: left (black symbols) BTN3A1, right (grey symbols): BSA. **C:** Representative Western blots of biotinylated protein bands.

B 2.4 Labeling of a BTN3A1-B30.2 charge transfer mutant

A charge reversal mutant of the B30.2 domain of BTN3A1 was also available for labeling experiments.^[114] In contrast to the wild type, the mutant of BTN3A1 possesses amino acids with negative instead of positive charged amino acid residues which bind the diphosphate motif of HMBPP or PAgS resp. exactly at the HMBPP binding site of its amino acid sequence. This of course has dramatic effects on the function of the protein, since HMBPP is no longer

able to bind to this site. It also appeared that the stability of this mutant was considerably diminished. During the experiments with the mutant, cleavage into smaller and eventually undetectable fragments occurred with prolonged storage. Neither storage at 4 °C nor in aliquots at -20 °C had any positive effect on its stability.

Like BSA, the mutant was also used to investigate any non-specific labeling by probe **103** and to test the influence of increasing HMBPP concentrations on labeling. Figure 58 shows an experiment where labeling of the BTN3A1 mutant is visible with 60 μM protein concentration and a concentration of 100 μM of probe **103**. In this example, the above-mentioned instability is visible by the appearance of a further protein band with lower molecular weight in both Ponceau S staining and detection of biotinylated proteins. Experiments with both 60/100 μM and 20/30 μM mutant/probe were performed. An influence of HMBPP on the labeling is visible, but not in a concentration-dependent manner. Samples without HMBPP show strongest labeling with the most prominent protein band whereas in the presence of HMBPP labeling decreases (see Figure 58 and appendix). However, the detected protein bands in the HMBPP-containing samples have different intensities which, in contrast to the BTN3A1 wild type, do not correlate with increasing HMBPP concentrations. In all tests with the mutant, the intensities appear rather randomly distributed. It can therefore be stated that the binding of HMBPP to BTN3A1 has deteriorated due to the reversal of the charge in the HMBPP binding pocket. Since otherwise no further changes were made to the mutant in contrast to the wild type, HMBPP can still potentially interact in a non-ionic way with BTN3A1. Therefore, the reduction of labeling by HMBPP is less visible.

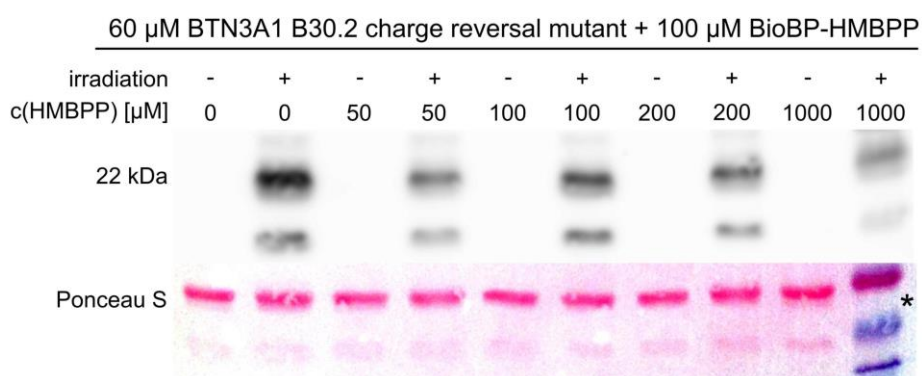


Figure 58: HMBPP titration experiment performed with the charge reversal mutant of BTN3A1 B30.2, showing stability issues, visible by the protein fraction of 20 kDa. * = Sample contains protein ladder marker proteins.

B 2.5 Determination of labeling efficiency by BioBP-HMBPP

To get an idea of the efficiency of the labeling by probe **103**, equal amounts of a monobiotinylated BTN3A1 B30.2 domain with the wild type B30.2 domain that was incubated with BioBP-HMBPP (**103**) and irradiated at 308 nm as usual were compared (Figure 59). Using

the typical conditions of 1.5 equivalents (30 μM) of **103** compared to BTN3A1, a strong protein band in the Western blot was found. The observed band is in between the signals of 10 and 100 ng of the monobiotinylated BTN3A1 protein. Evaluating the intensities of the blot by densitometry, it can be estimated that about 7% of BTN3A1 is typically labeled in these experiments. On the contrary, when using 0.5 equivalents of probe **103**, which is a third of the standard concentration, a significantly lower amount of labeling of around 2% was detected.

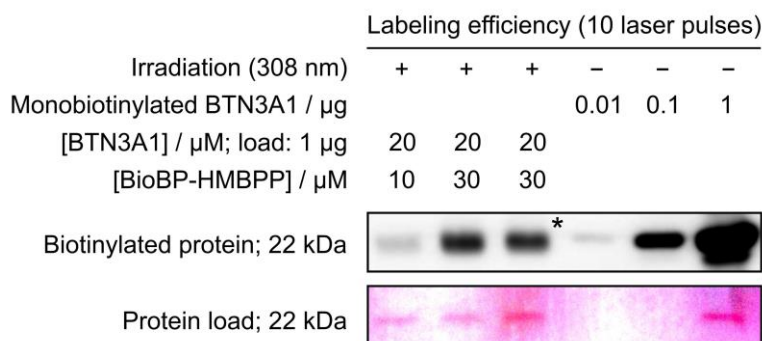


Figure 59: Determination of labeling efficiency. 1 μg irradiated protein samples of 20 μM of the BTN3A1 B30.2 domain with 10 or 30 μM BioBP-HMBPP (**103**) were compared with different amounts of a monobiotinylated BTN3A1 B30.2 domain. * = two samples from independent experiments were loaded.

B 3 Summary of Chapter B

The general labeling ability of the new, photoactivable probe BioBP-HMBPP (**103**) was proven for all four investigated proteins BSA; papain, BTN3A1 B30.2 wild type and charge transfer mutant at concentrations of 2-60 μM protein. Laser irradiation at 308 nm was successfully used for this purpose and proved to be a very effective tool. When the phospho-antigen binding domain of BTN3A1 30.2 was challenged by adding HMBPP (**102**) together with BioBP-HMBPP (**103**), a clear concentration-dependent decay of labeling was observed proving the higher affinity of HMBPP compared to BioBP-HMBPP. This finding is in agreement with the fact that **103** is a V γ 9V δ 2 T cell activator, albeit less active by about 3000 times than natural ligand **102**. However, labeling of the B30.2 domain of BTN3A1 was at least partially non-specific as labeling was detected even with 50-fold excess of HMBPP. The labeling of BSA as a random model protein was not impaired in the presence of additional HMBPP. These results demonstrate the specific binding of BioBP-HMBPP to the C₅-diphosphate binding unit, which occurs in the BTN3A1 30.2 domain. Probe **103** is a useful tool to discover further unknown proteins involved in V γ 9V δ 2 T cell activation.

B 4 Experimental

B 4.1 General information

HMBPP (**102**) was synthesized by Sabine Amslinger according to a previously published procedure.^[104] BSA (Cohn fraction V, pH 5) was purchased from Biomol (Hamburg, Germany) and papain, extracted from *Carica papaya*, from Sigma Aldrich (Buchs, Switzerland). Descriptions of the following procedures are available in the publication:^[102] The probe BioBP-HMBPP was synthesized by Sabine Amslinger and Andrea Mattarei, University of Regensburg.^[102] Stimulation assays were performed by Mohindar Muruges Karunkaran, Brigitte Kimmel and Thomas Herrmann, University of Würzburg.

Stock solutions of the following proteins were prepared by Siyi Gu and Erin J. Adams, Department of Biochemistry and Molecular Biology, University of Chicago, USA, according to known procedures: BTN3A1 domain 30.2 (312 and 340 μM); ^[114] BTN3A1 domain 30.2 charge reversal mutant (77.3 and 135 μM);^[114] biotinylated BTN3A1 domain B30.2 (46.8 μM).^[102]

B 4.2 Photochemical labeling of proteins with BioBP-HMBPP and Western Blot analysis of biotinylated proteins

Sample preparation and irradiation

Stock solutions of BSA (200 μM) and HMBPP (10 mM) were prepared directly in PBS buffer pH 7.4, while a 100 mM BioBP-HMBPP solution in DMSO was further diluted to 1 mM BioBP-HMBPP with PBS buffer pH 7.4 in a second step. Samples of 2 mL for the UV-Vis experiments with BSA and 100 μL in all other cases were prepared containing proteins (either BSA, papain, BTN3A1 domain B30.2 or BTN3A1 reversal charge mutant) in the given final concentrations together with 1.5-1.7 eq. BioBP-HMBPP and increasing HMBPP concentrations, where necessary. All samples were incubated on ice for 30 min in the dark prior to irradiation. Controls (10 μL of each sample) were not irradiated. Pipetting of small volume samples into the narrow cuvettes was performed with Pipettor tips M μ ltiflex® tips (Carl Roth GmbH, Karlsruhe, Germany). Irradiation was performed at room temperature in slit quartz cuvettes (volume 500 μL , slit diameter 2 mm) with the excimer laser Puls-Master PM-840 (LightMachinery, Ottawa, Canada) at a wavelength of 308 nm. For each irradiation 10 or the indicated number of pulses were used. The pulse duration was 10 ns, the pulse energy 215–250 mJ with a frequency of 1 Hz.

SDS-PAGE and Western Blot

The irradiated samples as well as the non-irradiated controls were diluted (PBS buffer pH 7.4 (10 mM Na₂HPO₄, 1.8 mM KH₂PO₄, 137 mM NaCl, 2.7 mM KCl) pH 7.4/loading buffer (60 mM Tris-HCl, 5% sodium dodecyl sulfate, 30% glycerol, 10% saccharose, 3% β-mercaptoethanol, 0.5% bromophenol blue) 1:1) to 10 μL volume that contained 1 μg or the indicated amount of protein, heated at 95 °C for 5 min and separated by 15% SDS-polyacrylamide gel electrophoresis. Then, proteins were blotted on a PVDF membrane (0.45 mm, Millipore, Billerica, MA, USA) with a subsequent blotting control step (Ponceau S staining with 0.1% (w/v) Ponceau S (3-hydroxy-4-(2-sulfo-4-[4-sulfophenylazo]phenylazo)-2,7-naphthalenedisulfonic acid sodium salt) in 5% aqueous acetic acid). For the Ponceau S staining the membranes were shaken in Ponceau S solution for 5 min and the red color was subsequently washed off the membranes with water. After this washing step only the protein bands remained colored red and were photographically documented. The membranes were then blocked with freshly prepared 5% low fat milk suspension in TBS-T (Tris-buffered saline, 20 mM Tris, 140 mM NaCl with 0.1% Tween = washing buffer, 1 h, room temperature or 4 °C, overnight) and incubated with streptavidin-horseradish peroxidase (HRPO, Leinco Technologies Inc., Fenton, Missouri, USA) in washing buffer (0.2 mg/mL streptavidin-HRPO, 30 min, room temperature). After washing (4 x 15 min with washing buffer) the blotted proteins were detected using a chemiluminescence substrate kit (Super Signal West Dura Extended Duration Substrate; Thermo Fisher Scientific, Rockford, Illinois, USA) and the biotinylated proteins were visualized with a luminescent image analyzer (LAS 3000, Fujifilm, Düsseldorf, Germany). Densitometric quantification was performed using the ImageJ for Windows Version: 1.45 software (Softonic International S.A., Barcelona, Spain) and densities were captured from non-saturated images. Comparison between groups was made using a two-sided paired Student's t test. A p value <0.05 was considered statistically significant. Calculations were performed using Microsoft Office Excel 2010.

C Literature

1. Christman, J. W.; Blackwell, T. S.; Juurlink, B. H. J. *Brain Pathol.*, **2000**, *10*, 153-162.
2. Pande, V.; Sousa, S. F.; Ramos, M. J. *Current Medicinal Chemistry*, **2009**, *16*, 4261-4273.
3. Marletta, M. A. *Cell*, **1994**, *78*, 927-930.
4. Korhonen, R.; Lahti, A.; Kankaanranta, H.; Moilanen, E. *Curr. Drug Targets Inflamm. Allergy*, **2005**, *4*, 471-479.
5. Moncada, S.; Palmer, R. M.; Higgs, E. A. *Pharmacol. Rev.*, **1991**, *43*, 109-142.
6. Stamler, J. S.; Lamas, S.; Fang, F. C. *Cell*, **2001**, *106*, 675-683.
7. Szabó, C.; Zingarelli, B.; O'Connor, M.; Salzman, A. L. *Proc. Natl. Acad. Sci. USA*, **1996**, *93*, 1753-1758.
8. Hogg, N.; Kalyanaraman, B. *Free Radic. Res.*, **1998**, *28*, 593-600.
9. Davis, K. L.; Martin, E.; Turko, I. V.; Murad, F. *Annu. Rev. Pharmacol. Toxicol.*, **2001**, *41*, 203-236.
10. Vallance, P.; Leiper, J. *Nat. Rev. Drug Discov.*, **2002**, *1*, 939-950.
11. Tak, P. P.; Firestein, G. S. *J. Clin. Invest.*, **2001**, *107*, 7-11.
12. Gersch, M.; Kreuzer, J.; Sieber, S. A. *Nat. Prod. Rep.*, **2012**, *29*, 659-682.
13. Amslinger, S. *ChemMedChem*, **2010**, *5*, 351-356.
14. Tokoroyama, T. *Eur. J. Org. Chem.*, **2010**, *2010*, 2009-2016.
15. Zhao, L.; Lee, J. Y.; Hwang, D. H. *Nutr. Rev.*, **2011**, *69*, 310-320.
16. (a) Abdul, A. B.; Abdelwahab, S. I.; Al-Zubairi, A. S.; Elhassan, M. M.; Murali, S. M. *Int. J. Pharmacol.* **2008**, *4*, 301-304; (b) Satoh, T.; Lipton, S. A. *Trends Neurosci.*, **2007**, *30*, 37-45.
17. Nam, N.-H. *Mini Rev. Med. Chem.*, **2006**, *6*, 945-951.
18. Buelna-Chontal, M.; Zazueta, C. *Cell. Signal.*, **2013**, *25*, 2548-2557.
19. Kobayashi, M.; Yamamoto, M. *Antioxid. Redox Sign.*, **2005**, *7*, 385-394.
20. Holland, R.; Fishbein, J. C. *Antioxid. Redox Sign.*, **2010**, *13*, 1749-1761.
21. Kalgutkar, A. S.; Dalvie, D. K. *Expert Opin Drug Dis*, **2012**, *7*, 561-581.
22. Forman, H. J.; Zhang, H.; Rinna, A. *Mol. Aspects Med.*, **2009**, *30*, 1-12.
23. Rücker, H. Characterisation of the Anti-inflammatory Activity of Enones Based on their Heme Oxygenase-1 and Inducible NO Synthase Activity. Doktorarbeit, Universität Regensburg 2014.
24. Vega, E.; Pugsley, M. *Proc. West. Pharmacol. Soc.*, **2011**, *54*, 10-4.
25. Tsikas, D. *J. Chromatogr. B*, **2007**, *851*, 51-70.
26. Avonto, C.; Taglialatela-Scafati, O.; Pollastro, F.; Minassi, A.; Di Marzo, V.; De Petrocellis, L.; Appendino, G. *Angew. Chem. Int. Edit.*, **2011**, *50*, 467-471.

27. Flanagan, M. E.; Abramite, J. A.; Anderson, D. P.; Aulabaugh, A.; Dahal, U. P.; Gilbert, A. M.; Li, C.; Montgomery, J.; Oppenheimer, S. R.; Ryder, T.; Schuff, B. P.; Uccello, D. P.; Walker, G. S.; Wu, Y.; Brown, M. F.; Chen, J. M.; Hayward, M. M.; Noe, M. C.; Obach, R. S.; Philippe, L.; Shanmugasundaram, V.; Shapiro, M. J.; Starr, J.; Stroh, J.; Che, Y. *J. Med. Chem.*, **2014**, *57*, 10072-10079.
28. Ward, R. A.; Anderton, M. J.; Ashton, S.; Bethel, P. A.; Box, M.; Butterworth, S.; Colclough, N.; Chorley, C. G.; Chuaqui, C.; Cross, D. A. E.; Dakin, L. A.; Debreczeni, J. É.; Eberlein, C.; Finlay, M. R. V.; Hill, G. B.; Grist, M.; Klinowska, T. C. M.; Lane, C.; Martin, S.; Orme, J. P.; Smith, P.; Wang, F.; Waring, M. J. *J. Med. Chem.*, **2013**, *56*, 7025-7048.
29. Ellman, G. L. *Arch. Biochem. Biophys.*, **1958**, *74*, 443-450.
30. Naven, R. T.; Kantesaria, S.; Nadanaciva, S.; Schroeter, T.; Leach, K. L. *Toxicol. Res. UK*, **2013**, *2*, 235-244.
31. Schwöbel, J. A. H.; Wondrousch, D.; Koleva, Y. K.; Madden, J. C.; Cronin, M. T. D.; Schüürmann, G. *Chem. Res. Toxicol.*, **2010**, *23*, 1576-1585.
32. Dinkova-Kostova, A. T.; Massiah, M. A.; Bozak, R. E.; Hicks, R. J.; Talalay, P. *Proc. Natl. Acad. Sci. USA*, **2001**, *98*, 3404-3409.
33. Yadav, V. R.; Prasad, S.; Sung, B.; Aggarwal, B. B. *Int. Immunopharmacol.*, **2011**, *11*, 295-309.
34. Haensel, R.; Sticher, O., *Pharmakognosie, Phytopharmazie*. 8. ed.; Springer Medizin Verlag: Heidelberg, 2007.
35. Amslinger, S.; Al-Rifai, N.; Winter, K.; Wörmann, K.; Scholz, R.; Baumeister, P.; Wild, M. *Org. Biomol. Chem.*, **2013**, *11*, 549-554.
36. Al-Rifai, N.; Rücker, H.; Amslinger, S. *Chem. Eur. J.*, **2013**, *19*, 15384-15395.
37. Rücker, H.; Al-Rifai, N.; Rasclé, A.; Gottfried, E.; Brodziak-Jarosz, L.; Gerhauser, C.; Dick, T. P.; Amslinger, S. *Org. Biomol. Chem.*, **2015**, *13*, 3040-3047.
38. Kaufmann, K. B.; Al-Rifai, N.; Ulbrich, F.; Schallner, N.; Rücker, H.; Enzinger, M.; Petkes, H.; Pitzl, S.; Goebel, U.; Amslinger, S. *PLOS ONE*, **2015**, *10*, e0142932.
39. Al-Rifai, N. The alpha-Substitution of Chalcones as a Tool to Modulate the Reactivity and Biological Activity. PhD thesis, University of Regensburg, 2014.
40. Shimokoriyama, M. *J. Am. Chem. Soc.*, **1957**, *79*, 4199-4202.
41. Furlong, J. J. P.; Nudelman, N. S. *J. Chem. Soc., Perkin Trans. 2*, **1985**, 633-639.
42. Rasras, A. Synthesis of biologically active enones: 2,3-dihydro-1,3,4-oxadiazoles, alpha-X-cyclopentenones and attempts towards limnophilaspiroketone and zerumbone. PhD thesis, University of Regensburg, 2015.
43. Herzog, R. Synthese, chemische Reaktivitäten bezüglich Cysteamin und Hemmung der NO-Produktion von 2,3-Dihydro-1,3,4-oxadiazolen mit zusätzlicher Enoneinheit. Master thesis, University of Regensburg, 2015.
44. Wirth, L. Synthese von Oxadiazolin- und Anilinderivaten mit unterschiedlichen Reaktiveinheiten, sowie deren chemische und biologische Evaluierung. Master thesis, University of Regensburg, 2016.

45. Arora, P.; Mittal, A.; Kaur, G.; Chauhan, A. *Int. J. Pharm. Sci. Res.*, **2012**, *4*, 419-424.
46. Chidananda, N.; Poojary, B.; Sumangala, V.; Suchetha Kumari, N.; Unnikrishnan *Med. Chem. Res.*, **2014**, *23*, 3979-3997.
47. Thomas, A.; Paradkar, O.; K. Nanda, R.; Tupe, P.; Sharma, P.; Badhe, R.; Kothapalli, L.; Banerjee, A.; Hamane, S.; Deshpande, A. *Green Chem. Lett. Rev.*, **2010**, *3*, 293-300.
48. Zhou, Y.; Wang, B.; Di, F.; Xiong, L.; Yang, N.; Li, Y.; Li, Y.; Li, Z. *Bioorg. Med. Chem. Lett.*, **2014**, *24*, 2295-2299.
49. Kokatla, H. P.; Thomson, P. F.; Bae, S.; Doddi, V. R.; Lakshman, M. K. *J. Org. Chem.*, **2011**, *76*, 7842-8.
50. Drahl, C.; Cravatt, B. F.; Sorensen, E. J. *Angew. Chem. Int. Ed.*, **2005**, *44*, 5788-809.
51. (a) Skarzynski, T.; Mistry, A.; Wonacott, A.; Hutchinson, S. E.; Kelly, V. A.; Duncan, K. *Structure*, **1996**, *4*, 1465-1474; (b) Matsumoto, K.; Mizoue, K.; Kitamura, K.; Tse, W.-C.; Huber, C. P.; Ishida, T. *Peptide Science*, **1999**, *51*, 99-107.
52. Meng, L.; Mohan, R.; Kwok, B. H. B.; Elofsson, M.; Sin, N.; Crews, C. M. *Proc. Natl. Acad. Sci. USA*, **1999**, *96*, 10403-10408.
53. Meth-Cohn, O.; Moore, C.; Taljaard, H. C. *J. Chem. Soc., Perkin Trans. 1*, **1988**, 2663-2674.
54. Maccioni, E.; Alcaro, S.; Cirilli, R.; Vigo, S.; Cardia, M. C.; Sanna, M. L.; Meleddu, R.; Yanez, M.; Costa, G.; Casu, L.; Matyus, P.; Distinto, S. *J. Med. Chem.*, **2011**, *54*, 6394-8.
55. Kathman, S. G.; Xu, Z.; Statsyuk, A. V. *J. Med. Chem.*, **2014**, *57*, 4969-4974.
56. Thakur, A. *J. Med. Plants Res.*, **2010**, *5*, 5324-5330.
57. Schlegel, S. Synthese und Reaktivität von Juglon-Derivaten. Master thesis, University of Regensburg, 2016.
58. Wang, S.-H.; Lo, C.-Y.; Gwo, Z.-H.; Lin, H.-J.; Chen, L.-G.; Kuo, C.-D.; Wu, J.-Y. *Molecules*, **2015**, *20*, 11994-12015.
59. Jeong, H. G.; Pokharel, Y. R.; Lim, S. C.; Hwang, Y. P.; Han, E. H.; Yoon, J.-H.; Ahn, S.-G.; Lee, K. Y.; Kang, K. W. *J. Immunol.*, **2009**, *183*, 6689-6697.
60. Mohammed Rahmoun, N.; Boucherit-Atmani, Z.; Benabdallah, M.; Boucherit, K.; Villemin, D.; Choukchou-Braham, N. *Am. J. Med. Biol. Res.*, **2013**, *1*, 16-22.
61. Inbaraj, J. J.; Chignell, C. F. *Chem. Res. Toxicol.*, **2004**, *17*, 55-62.
62. Klotz, L.-O.; Hou, X.; Jacob, C. *Molecules*, **2014**, *19*, 14902-14918.
63. Perlinger, J. A.; Kalluri, V. M.; Venkatapathy, R.; Angst, W. *Environ. Sci. Technol.*, **2002**, *36*, 2663-2669.
64. Hennig, L.; Christner, C.; Kipping, M.; Schelbert, B.; Rücknagel, K. P.; Grabley, S.; Küllertz, G.; Fischer, G. *Biochemistry*, **1998**, *37*, 5953-5960.
65. Manickam, M.; Boggu, P. R.; Cho, J.; Nam, Y. J.; Lee, S. J.; Jung, S.-H. *Bioorg. Med. Chem. Lett.*, **2018**, *28*, 2023-2028.
66. Kim, J. H.; Park, E.-S.; Shim, J. H.; Kim, M.-N.; Moon, W.-S.; Chung, K.-H.; Yoon, J.-S. *J. Agric. Food Chem.*, **2004**, *52*, 7480-7483.

67. Brownell, H. L.; Lydon, N. B.; Schaefer, E.; Roberts, T. M.; Raptis, L. *DNA Cell Biol.*, **1998**, *17*, 265-274.
68. Rossi, A.; Kapahi, P.; Natoli, G.; Takahashi, T.; Chen, Y.; Karin, M.; Santoro, M. G. *Nature*, **2000**, *403*, 103-108.
69. Enzinger, M. Synthese und Charakterisierung von Thioanthrachinonen als Sonden zur kinetischen Evaluierung farbloser Enone. Master Thesis, University of Regensburg, 2014.
70. Moor, N. Synthese von Nitrothiophenolderivaten als Sonden in einem kinetischen Assay. Bachelor Thesis, University of Regensburg, 2015.
71. Avonto, C.; Chittiboyina, A. G.; Rua, D.; Khan, I. A. *Toxicol. Appl. Pharmacol.*, **2015**, *289*, 177-184.
72. McCallum, M. M.; Nandhikonda, P.; Temmer, J. J.; Eyermann, C.; Simeonov, A.; Jadhav, A.; Yasgar, A.; Maloney, D.; Arnold, A. *J. Biomol. Screen.*, **2013**, *18*, 705-713.
73. Montoya, L. A.; Pearce, T. F.; Hansen, R. J.; Zakharov, L. N.; Pluth, M. D. *J. Org. Chem.*, **2013**, *78*, 6550-6557.
74. Aptula, A. O.; Patlewicz, G.; Roberts, D. W. *Chem. Res. Toxicol.*, **2005**, *18*, 1420-1426.
75. Montoya, L. A.; Pluth, M. D. *Anal. Chem.*, **2014**, *86*, 6032-6039.
76. Murray, J. I.; Spivey, A. C. *Adv. Synth. Catal.*, **2015**, *357*, 3825-3830.
77. Van Veldhuizen, J. J.; Gillingham, D. G.; Garber, S. B.; Kataoka, O.; Hoveyda, A. H. *J. Am. Chem. Soc.*, **2003**, *125*, 12502-12508.
78. Horie, T.; Shibata, K.; Yamashita, K.; Kawamura, Y.; Tsukayama, M. *Chem. Pharm. Bull.*, **1997**, *45*, 446-451.
79. Paparao, C.; Rao, K. V.; Sundaramurthy, V. *Synthesis*, **1981**, 236-237.
80. Grimm, J. B.; English, B. P.; Chen, J.; Slaughter, J. P.; Zhang, Z.; Revyakin, A.; Patel, R.; Macklin, J. J.; Normanno, D.; Singer, R. H.; Lionnet, T.; Lavis, L. D. *Nat. Methods*, **2015**, *12*, 244-250.
81. Loas, A.; Radford, R. J.; Lippard, S. J. *Inorg. Chem.*, **2014**, *53*, 6491-6493.
82. Du, C.; Zheng, C.; Diwu, Z. Fluorescent detection method of hepatitis B surface antigen and antibody. CN101334407, 31.12.2008.
83. Ippoliti, J. T.; Olson, K. E. Alcohol oxidase-based enzyme-linked immunosorbent assay using latent fluorophore or chromophore. US20080286812, 20.11.2008.
84. Pinault, T.; Chérioux, F.; Therrien, B.; Süß-Fink, G. *Heteroat. Chem*, **2004**, *15*, 121-126.
85. Zeng, X.; Wang, C.; Batsanov, A. S.; Bryce, M. R.; Gigon, J.; Urasinska-Wojcik, B.; Ashwell, G. J. *J. Org. Chem.*, **2010**, *75*, 130-136.
86. Dickinson, B. C.; Huynh, C.; Chang, C. J. *J. Am. Chem. Soc.*, **2010**, *132*, 5906-5915.
87. Unciti-Broceta, A.; Rahimi Yusop, M.; Richardson, P. R.; Walton, J. G. A.; Bradley, M. *Tetrahedron Lett.*, **2009**, *50*, 3713-3715.
88. Yusop, R. M.; Unciti-Broceta, A.; Bradley, M. *Bioorg. Med. Chem. Lett.*, **2012**, *22*, 5780-5783.

89. Karabanovich, G.; Zemanova, J.; Smutny, T.; Szekely, R.; Sarkan, M.; Centarova, I.; Vocat, A.; Pavkova, I.; Conka, P.; Nemecek, J.; Stolarikova, J.; Vejsova, M.; Vavrova, K.; Klimesova, V.; Hrabalek, A.; Pavek, P.; Cole, S. T.; Mikusova, K.; Roh, J. *J. Med. Chem.*, **2016**, *59*, 2362-80.
90. van Dijken, D. J.; Kovaříček, P.; Ihrig, S. P.; Hecht, S. *J. Am. Chem. Soc.*, **2015**, *137*, 14982-14991.
91. Nigade, G.; Chavan, P.; Deodhar, M. *Med. Chem. Res.*, **2010**, *21*, 27-37.
92. Zimin, D. P.; Dar'in, D. V.; Rassadin, V. A.; Kukushkin, V. Y. *Org. Lett.*, **2018**, *20*, 4880-4884.
93. Wang, Z.; Zhu, F.; Li, Y.; Wu, X.-F. *ChemCatChem*, **2017**, *9*, 94-98.
94. Shirote, P. J.; Bhatia, M. S. *Arab. J. Chem.*, **2011**, *4*, 413-418.
95. Judge, V.; Narasimhan, B.; Ahuja, M.; Sriram, D.; Yogeeswari, P.; De Clercq, E.; Pannecouque, C.; Balzarini, J. *Med. Chem. Res.*, **2012**, *21*, 1935-1952.
96. Cordeiro Rde, A.; de Melo, C. V.; Marques, F. J.; Serpa, R.; Evangelista, A. J.; Caetano, E. P.; Mafezoli, J.; de Oliveira Mda, C.; da Silva, M. R.; Bandeira Tde, J.; Moreira, J. L.; Brillhante, R. S.; Rocha, M. F.; Sidrim, J. J. *Microb. Pathog.*, **2016**, *98*, 1-5.
97. Andrade, M. M.; Barros, M. T. *J. Comb. Chem.*, **2010**, *12*, 245-247.
98. Bottari, B.; Maccari, R.; Monforte, F.; Ottanà, R.; Rotondo, E.; Vigorita, M. G. *Bioorg. Med. Chem. Lett.*, **2000**, *10*, 657-660.
99. Bottari, B.; Maccari, R.; Monforte, F.; Ottanà, R.; Rotondo, E.; Vigorita, M. G. *Bioorg. Med. Chem. Lett.*, **2001**, *11*, 301-3.
100. Sah, R.; Sinha, A. *J. Chemtracks*, **2015**, *17*, 283-288.
101. Vigorita, M. G.; Ottanà, R.; Maccari, R.; Monforte, F.; Bisignano, G.; Pizzimenti, A. *C. Boll. Chim. Farm.*, **1998**, *137*, 267-276.
102. Mattarei, A.; Enzinger, M.; Gu, S.; Karunakaran, M. M.; Kimmel, B.; Berner, N.; Adams, E. J.; Herrmann, T.; Amslinger, S. *Chem. Eur. J.*, **2017**, *23*, 11945-11954.
103. Hintz, M.; Reichenberg, A.; Altincicek, B.; Bahr, U.; Gschwind, R. M.; Kollas, A.-K.; Beck, E.; Wiesner, J.; Eberl, M.; Jomaa, H. *FEBS Lett.*, **2001**, *509*, 317-322.
104. Amslinger, S.; Kis, K.; Hecht, S.; Adam, P.; Rohdich, F.; Arigoni, D.; Bacher, A.; Eisenreich, W. *J. Org. Chem.*, **2002**, *67*, 4590-4594.
105. Amslinger, S.; Hecht, S.; Rohdich, F.; Eisenreich, W.; Adam, P.; Bacher, A.; Bauer, S. *Immunobiology*, **2007**, *212*, 47-55.
106. Morita, C. T.; Jin, C.; Sarikonda, G.; Wang, H. *Immunol. Rev.*, **2007**, *215*, 59-76.
107. Eberl, M.; Hintz, M.; Reichenberg, A.; Kollas, A.-K.; Wiesner, J.; Jomaa, H. *FEBS Lett.*, **2003**, *544*, 4-10.
108. Kunzmann, V.; Bauer, E.; Feurle, J.; Tony, F. W.; Hans-Peter; Wilhelm, M. *Blood*, **2000**, *96*, 384-392.
109. Gober, H.-J.; Kistowska, M.; Angman, L.; Jenö, P.; Mori, L.; De Libero, G. *J. Exp. Med.*, **2003**, *197*, 163-168.

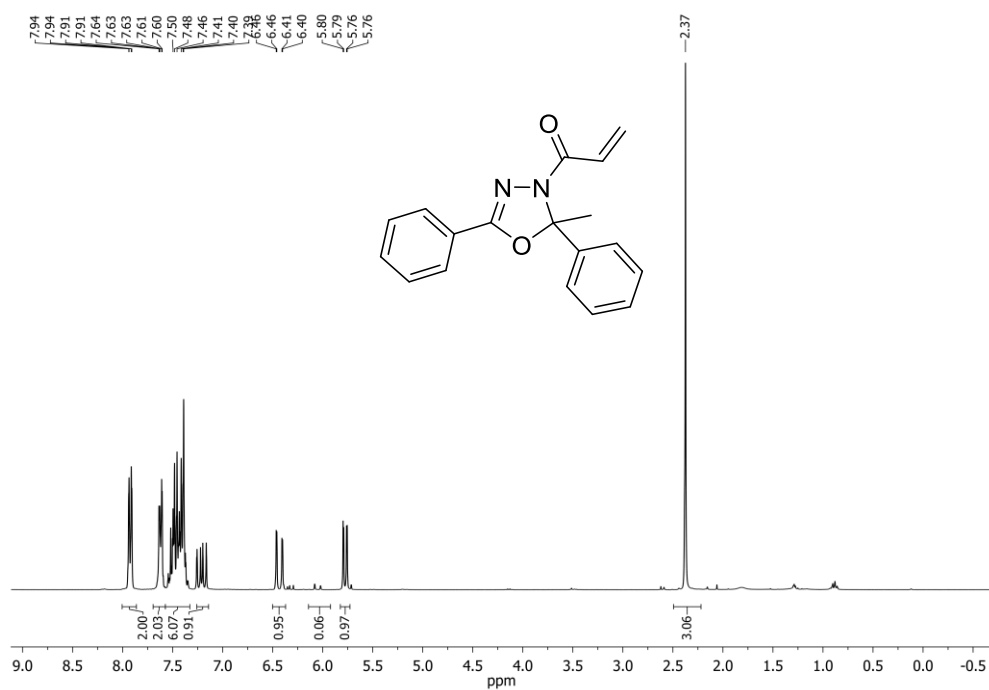
110. Li, J.; Herold, M. J.; Kimmel, B.; Müller, I.; Rincon-Orozco, B.; Kunzmann, V.; Herrmann, T. *J. Immunol.*, **2009**, *182*, 8118-8124.
111. Harly, C.; Guillaume, Y.; Nedellec, S.; Peigné, C.-M.; Mönkkönen, H.; Mönkkönen, J.; Li, J.; Kuball, J.; Adams, E. J.; Netzer, S.; Déchanet-Merville, J.; Léger, A.; Herrmann, T.; Breathnach, R.; Olive, D.; Bonneville, M.; Scotet, E. *Blood*, **2012**, *120*, 2269-2279.
112. Karunakaran, M. M.; Herrmann, T. *Front. Immunol.*, **2014**, *5*, 648-648.
113. Vavassori, S.; Kumar, A.; Wan, G. S.; Ramanjaneyulu, G. S.; Cavallari, M.; El Daker, S.; Beddoe, T.; Theodossis, A.; Williams, N. K.; Gostick, E.; Price, D. A.; Soudamini, D. U.; Voon, K. K.; Olivo, M.; Rossjohn, J.; Mori, L.; De Libero, G. *Nat. Immunol.*, **2013**, *14*, 908-916.
114. Sandstrom, A.; Peigné, C.-M.; Léger, A.; Crooks, James E.; Konczak, F.; Gesnel, M.-C.; Breathnach, R.; Bonneville, M.; Scotet, E.; Adams, Erin J. *Immunity*, **2014**, *40*, 490-500.
115. Hsiao, C.-Hung C.; Lin, X.; Barney, Rocky J.; Shippy, Rebekah R.; Li, J.; Vinogradova, O.; Wiemer, David F.; Wiemer, Andrew J. *Chem. Biol.*, **2014**, *21*, 945-954.
116. Rhodes, D. A.; Chen, H.-C.; Price, A. J.; Keeble, A. H.; Davey, M. S.; James, L. C.; Eberl, M.; Trowsdale, J. *J. Immunol.*, **2015**, *194*, 2390-2398.
117. Palakodeti, A.; Sandstrom, A.; Sundaresan, L.; Harly, C.; Nedellec, S.; Olive, D.; Scotet, E.; Bonneville, M.; Adams, E. J. *J. Biol. Chem.*, **2012**, *287*, 32780-32790.
118. Sebestyén, Z.; Scheper, W.; Vyborova, A.; Gu, S.; Rychnavska, Z.; Schiffler, M.; Clevén, A.; Chéneau, C.; van Noorden, M.; Peigné, C.-M.; Olive, D.; Lebbink, Robert J.; Oostvogels, R.; Mutis, T.; Schuurhuis, G. J.; Adams, Erin J.; Scotet, E.; Kuball, J. *Cell Reports*, **2016**, *15*, 1973-1985.
119. Riaño, F.; Karunakaran, M. M.; Starick, L.; Li, J.; Scholz, C. J.; Kunzmann, V.; Olive, D.; Amslinger, S.; Herrmann, T. *Eur. J. Immunol.*, **2014**, *44*, 2571-2576.
120. Dormán, G.; Prestwich, G. D. *Trends Biotechnol.*, **2000**, *18*, 64-77.
121. Marecak, D. M.; Horiuchi, Y.; Arai, H.; Shimonaga, M.; Maki, Y.; Koyama, T.; Ogura, K.; Prestwich, G. D. *Bioorg. Med. Chem. Lett.*, **1997**, *7*, 1973-1978.
122. Turek, T. C.; Gaon, I.; Distefano, M. D.; Strickland, C. L. *J. Org. Chem.*, **2001**, *66*, 3253-3264.
123. Völkert, M.; Uwai, K.; Tebbe, A.; Popkirova, B.; Wagner, M.; Kuhlmann, J.; Waldmann, H. *J. Am. Chem. Soc.*, **2003**, *125*, 12749-12758.
124. Sarikonda, G.; Wang, H.; Puan, K.-J.; Liu, X.-h.; Lee, H. K.; Song, Y.; Distefano, M. D.; Oldfield, E.; Prestwich, G. D.; Morita, C. T. *J. Immunol.*, **2008**, *181*, 7738-7750.
125. Wang, H.; Henry, O.; Distefano, M. D.; Wang, Y.-C.; Räikkönen, J.; Mönkkönen, J.; Tanaka, Y.; Morita, C. T. *J. Immunol.*, **2013**, *191*, 1029-1042.

D Appendix

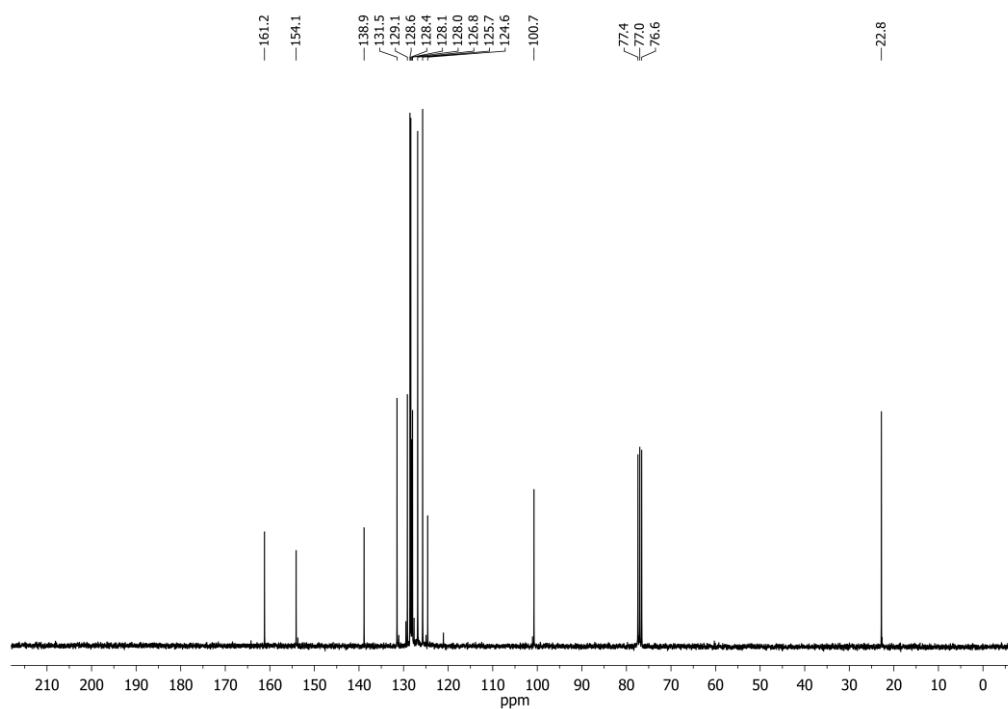
D 1 NMR spectra of synthesized compounds

1-(2-Methyl-2,5-diphenyl-1,3,4-oxadiazol-3(2H)-yl)prop-2-en-1-one (**OXE1**) in CDCl₃

¹H NMR:

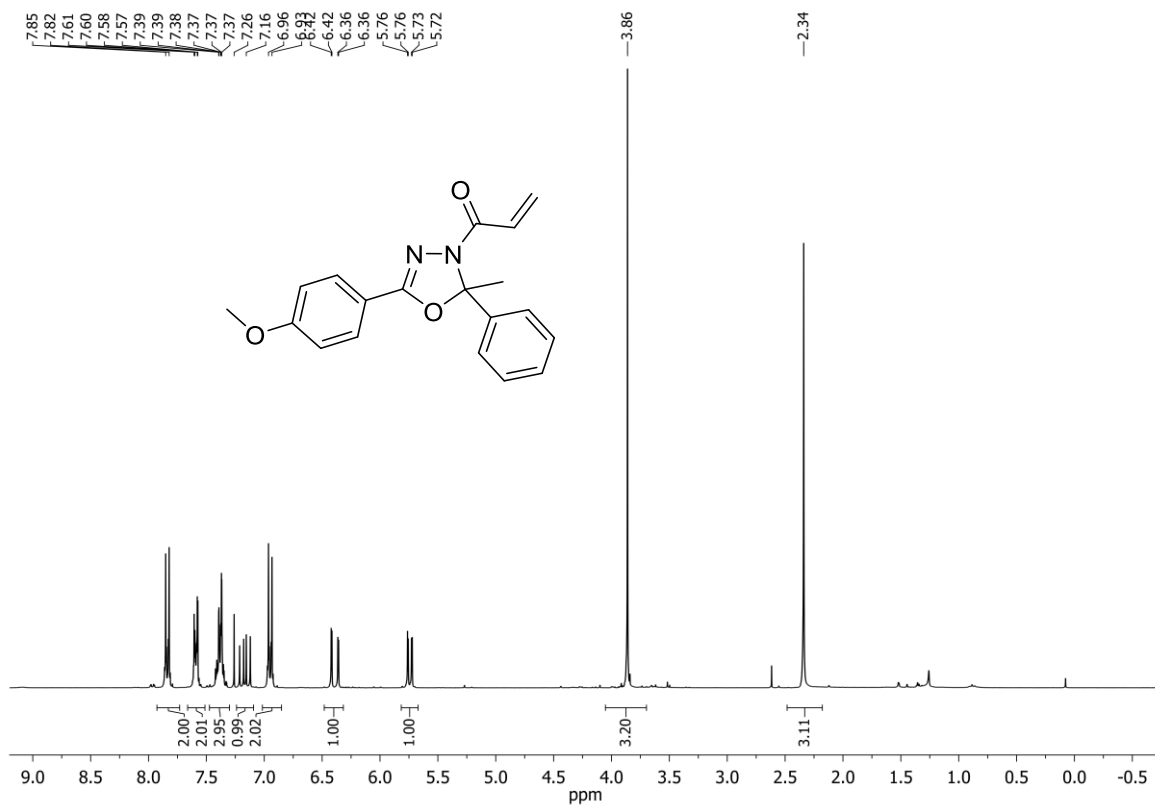


¹³C NMR:

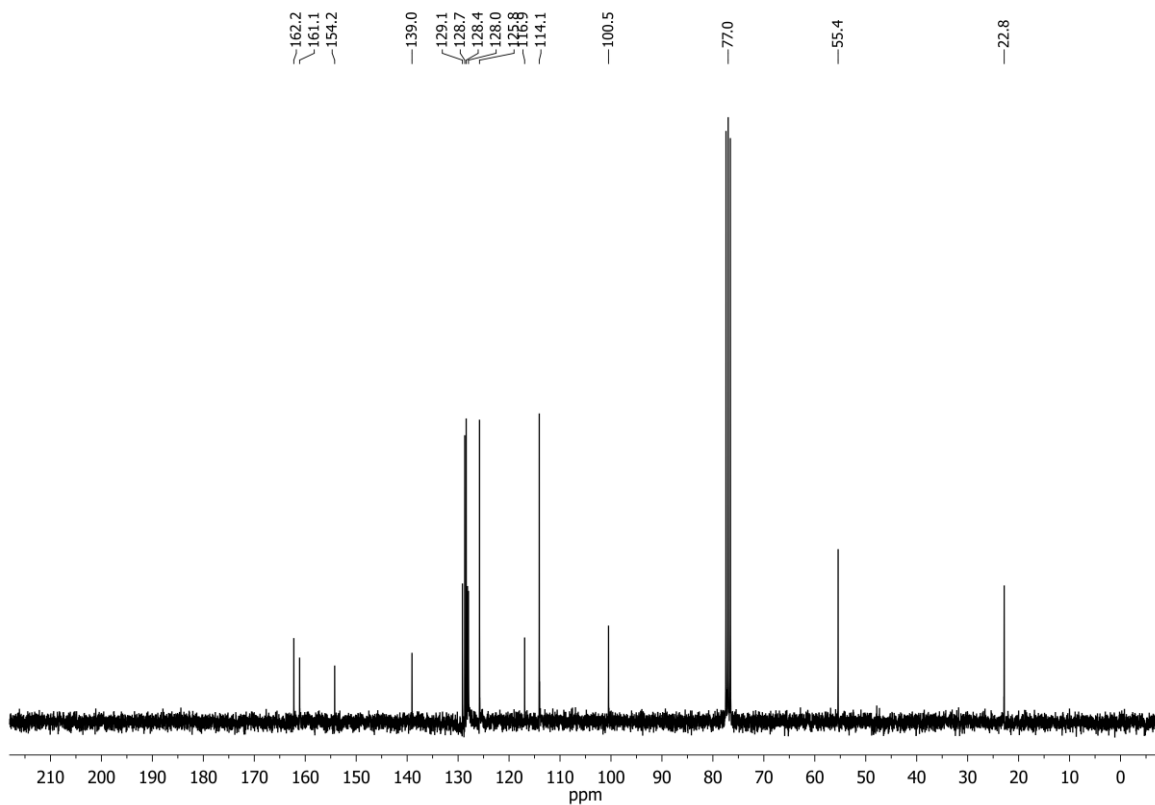


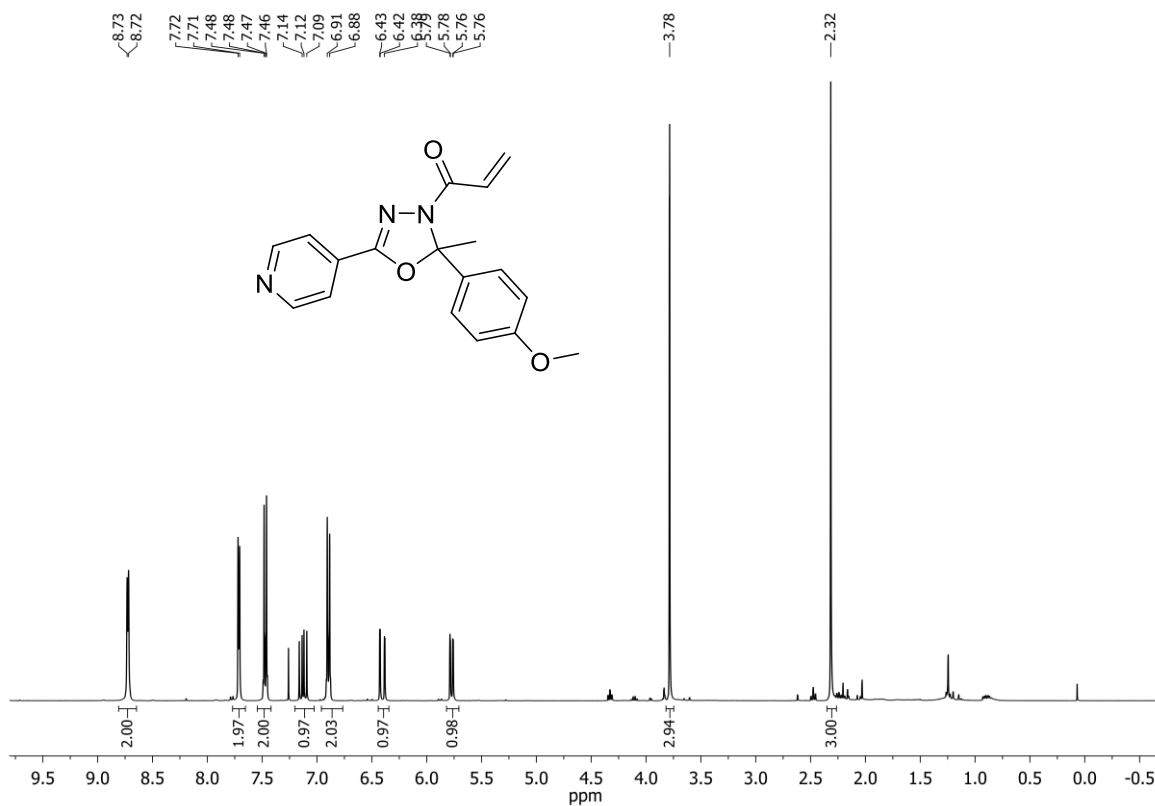
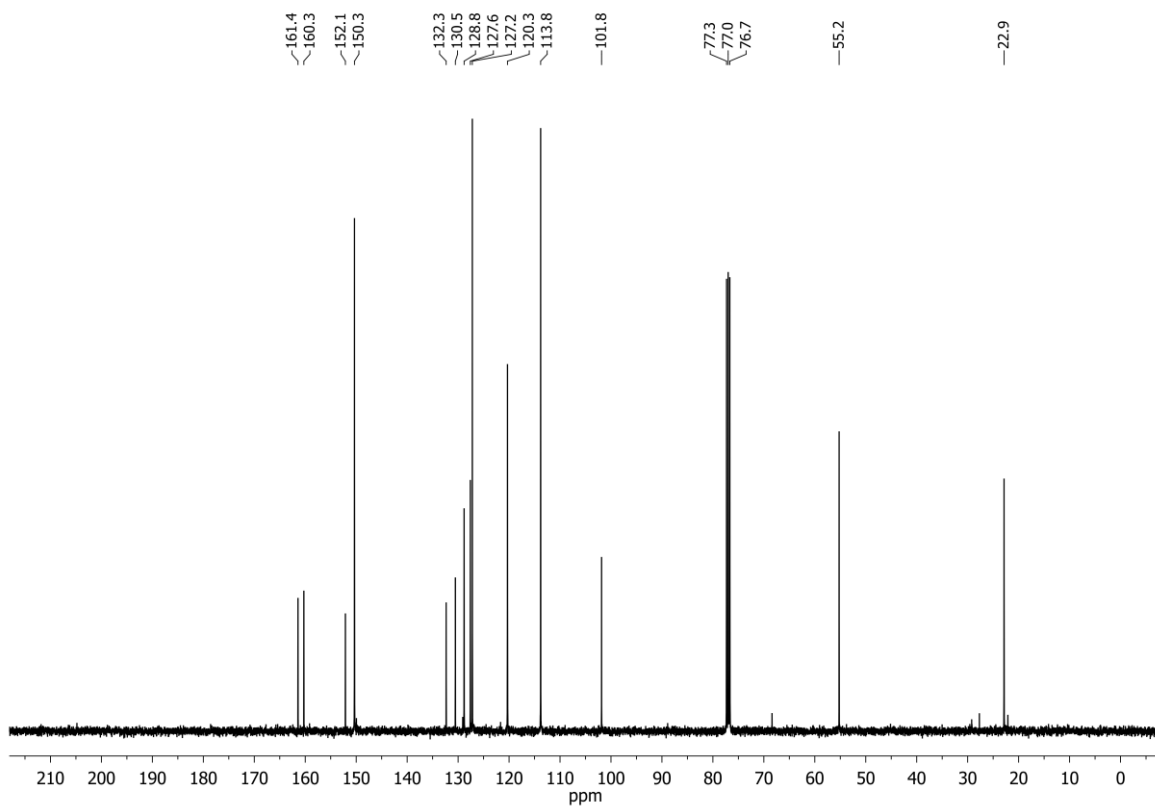
1-(5-(4-Methoxyphenyl)-2-methyl-2-phenyl-1,3,4-oxadiazol-3(2H)-yl)prop-2-en-1-one
(OXE1-(OMe)') in CDCl₃

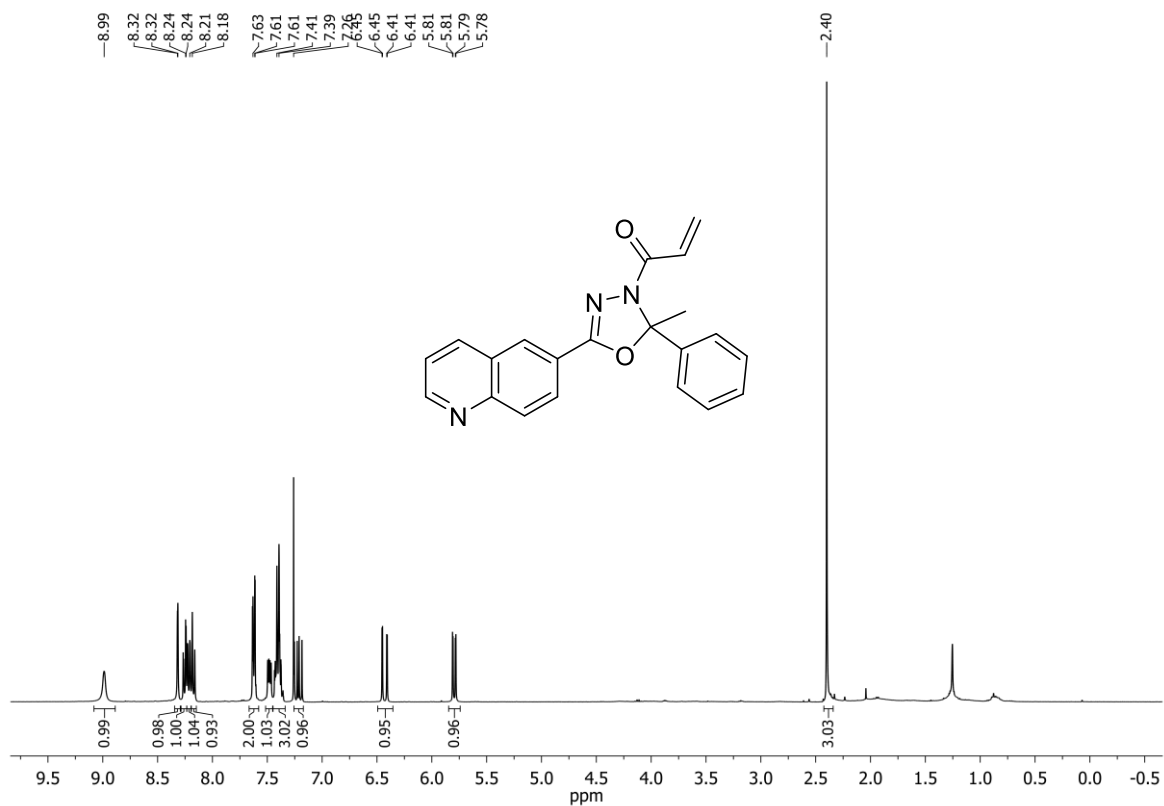
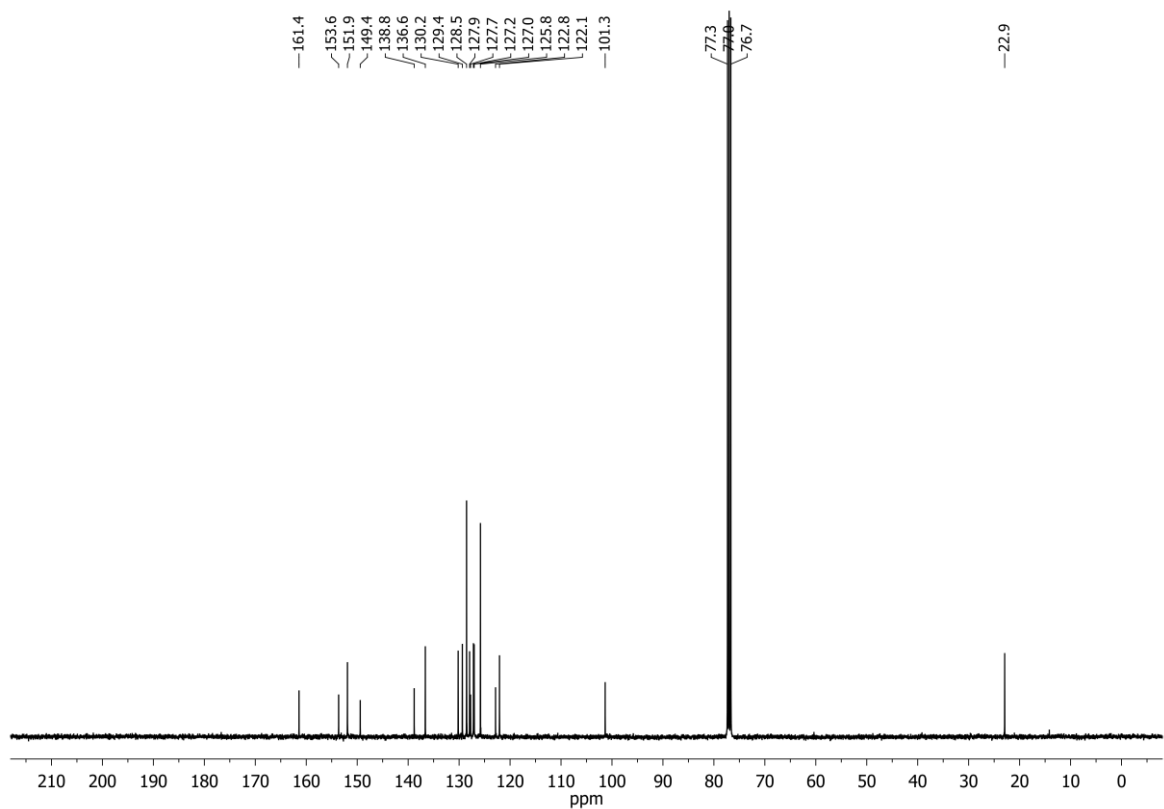
¹H NMR:

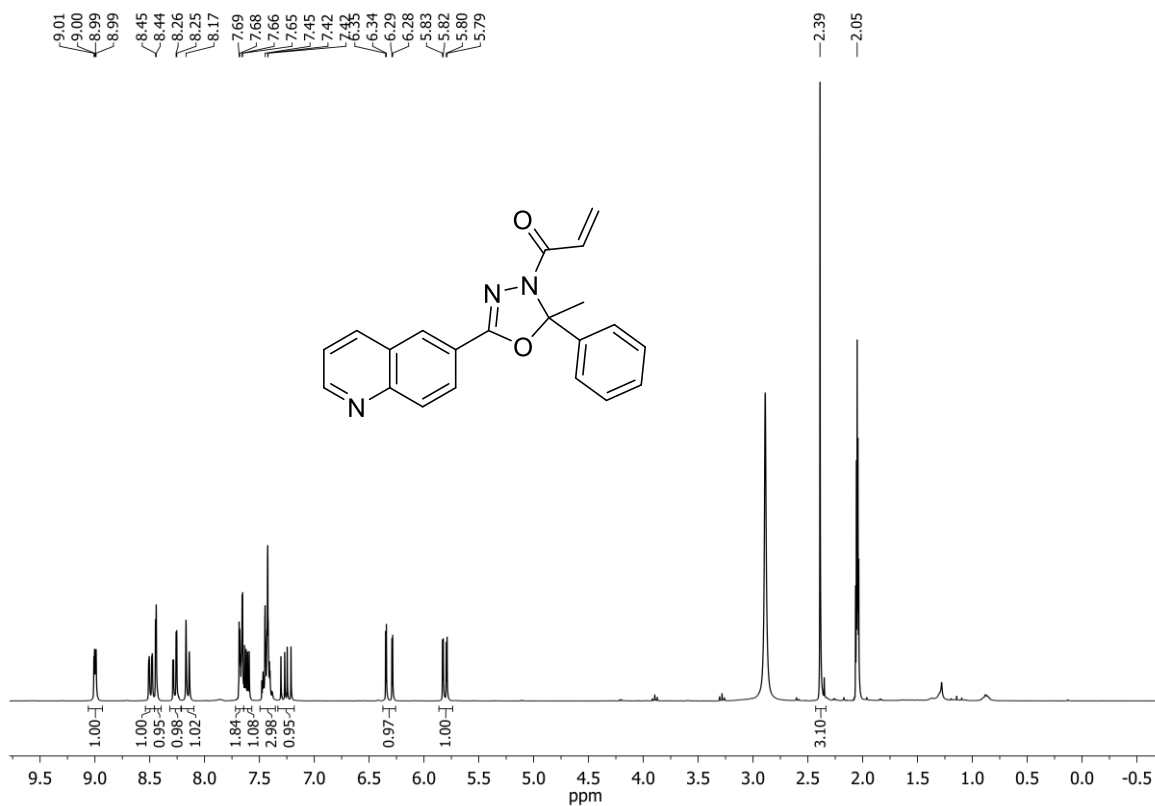
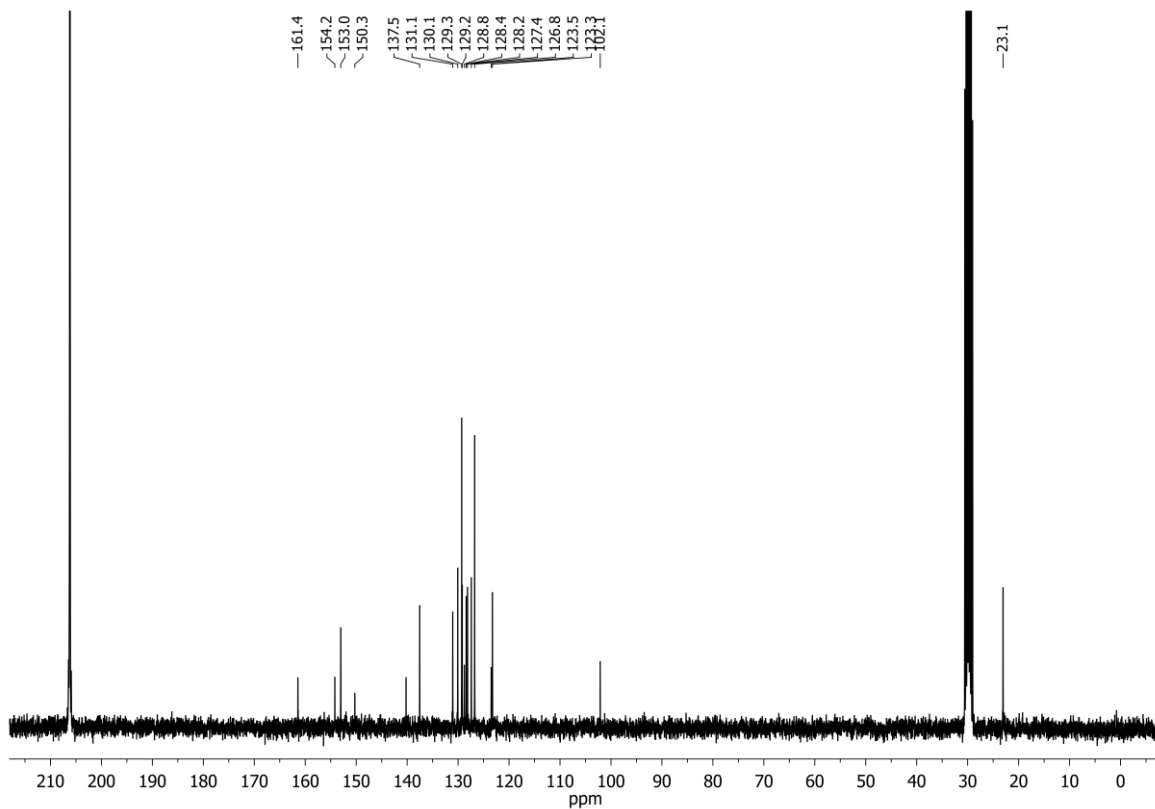


¹³C NMR:



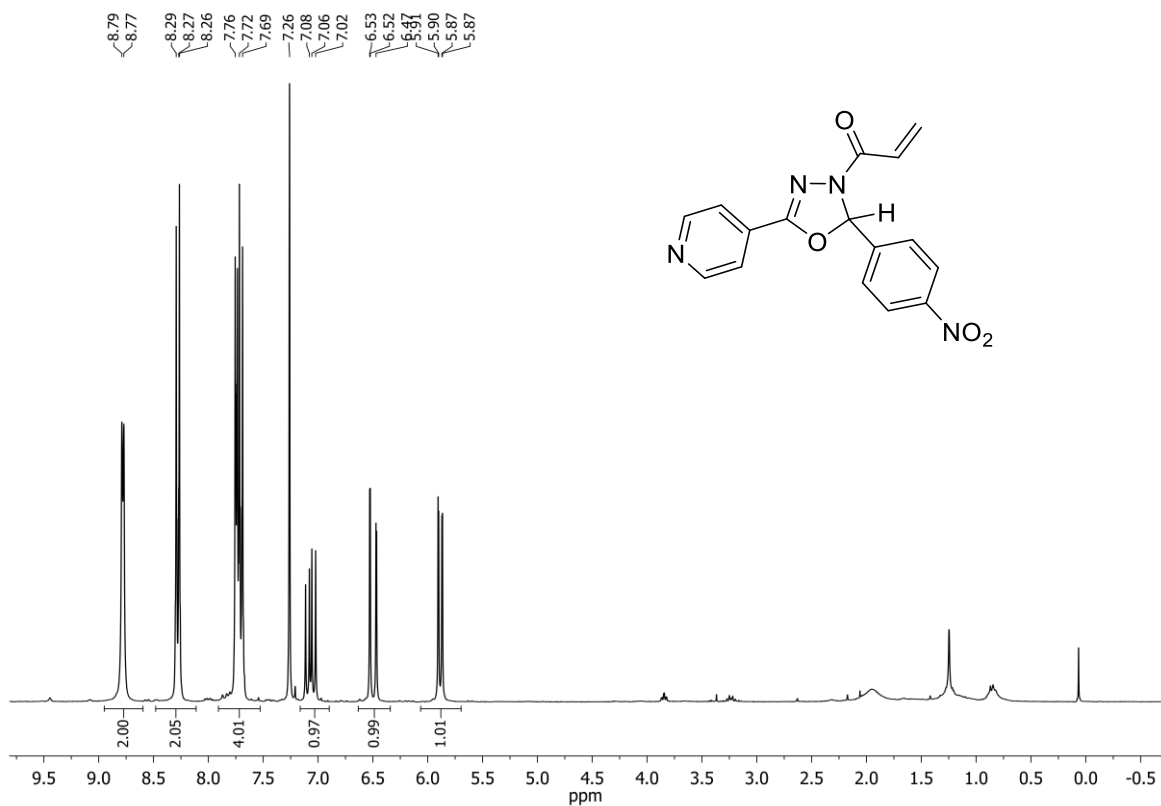
1-(2-(4-methoxyphenyl)-2-methyl-5-(pyridin-4-yl)-1,3,4-oxadiazol-3(2H)-yl)prop-2-en-1-one (OXE1-OMe,(4py)) in CDCl₃¹H NMR:¹³C NMR:

1-(2-Methyl-2-phenyl-5-(quinolin-6-yl)-1,3,4-oxadiazol-3(2H)-yl)prop-2-en-1-one
(OXE1-(6qui)) in CDCl₃¹H-NMR:¹³C NMR:

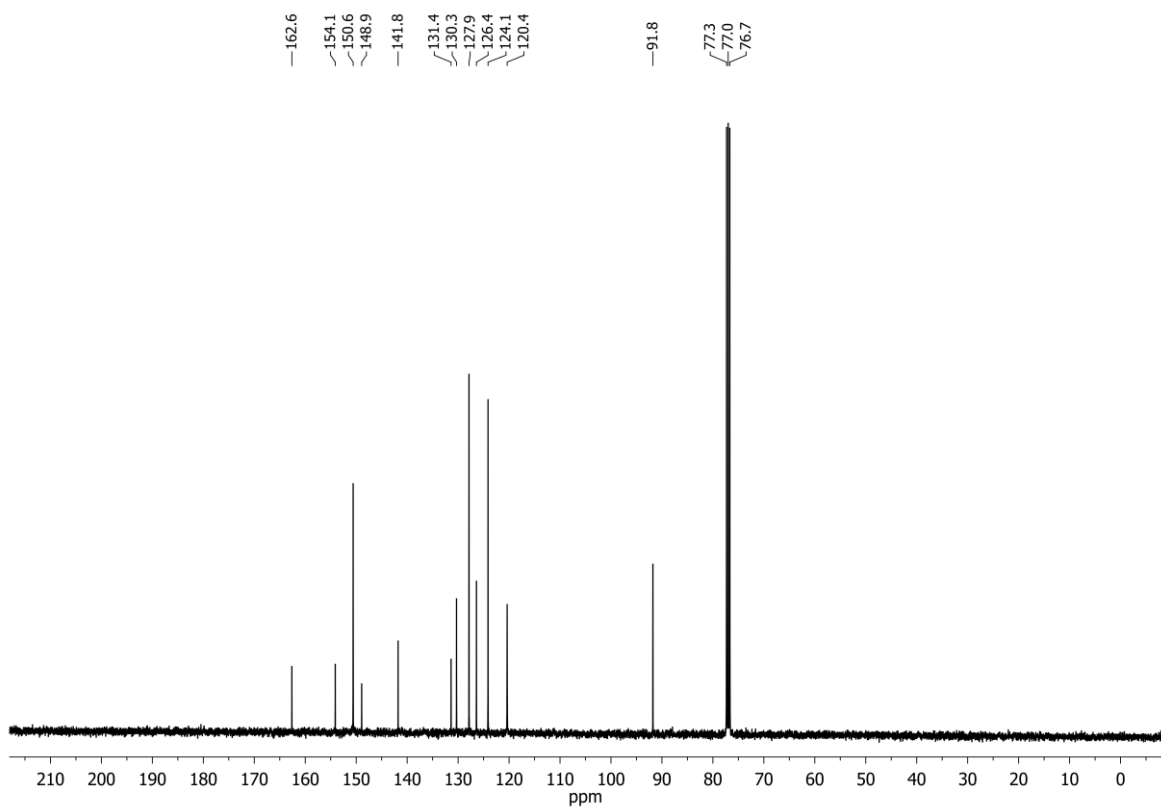
1-(2-Methyl-2-phenyl-5-(quinolin-6-yl)-1,3,4-oxadiazol-3(2H)-yl)prop-2-en-1-one (OXE1-(6qui)) in acetone-d₆¹H-NMR:¹³C NMR:

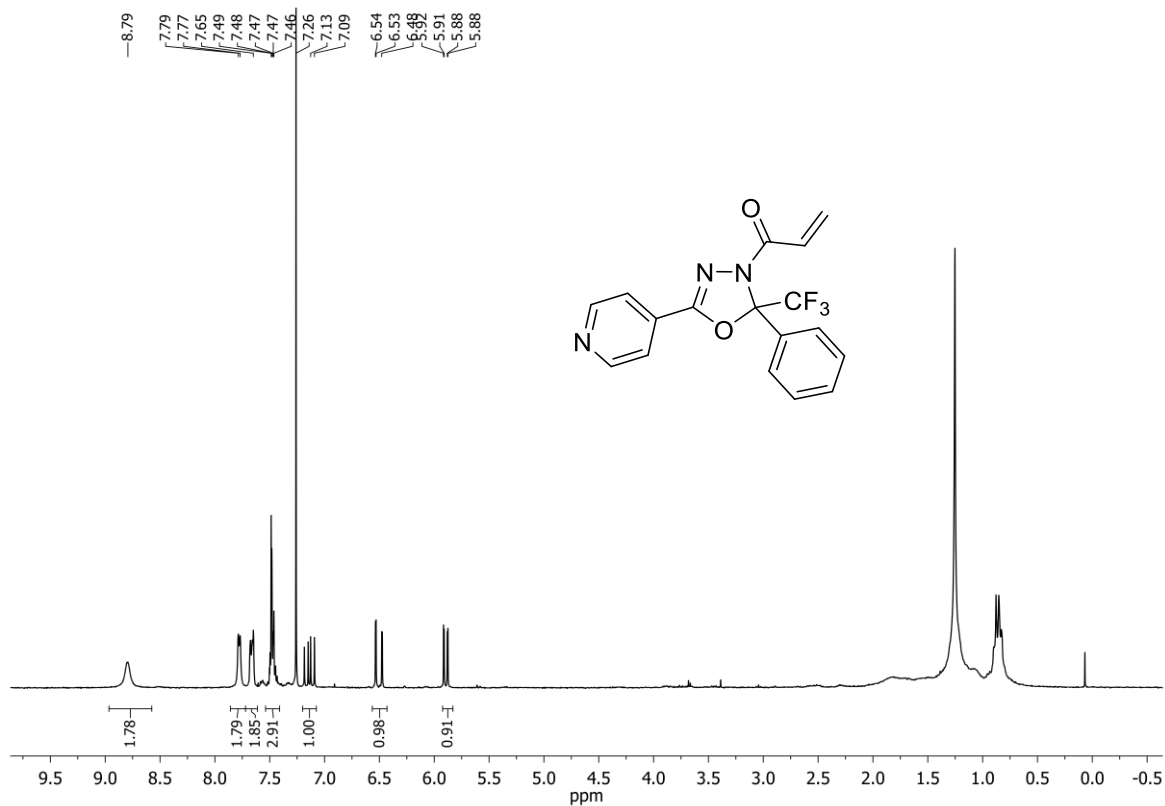
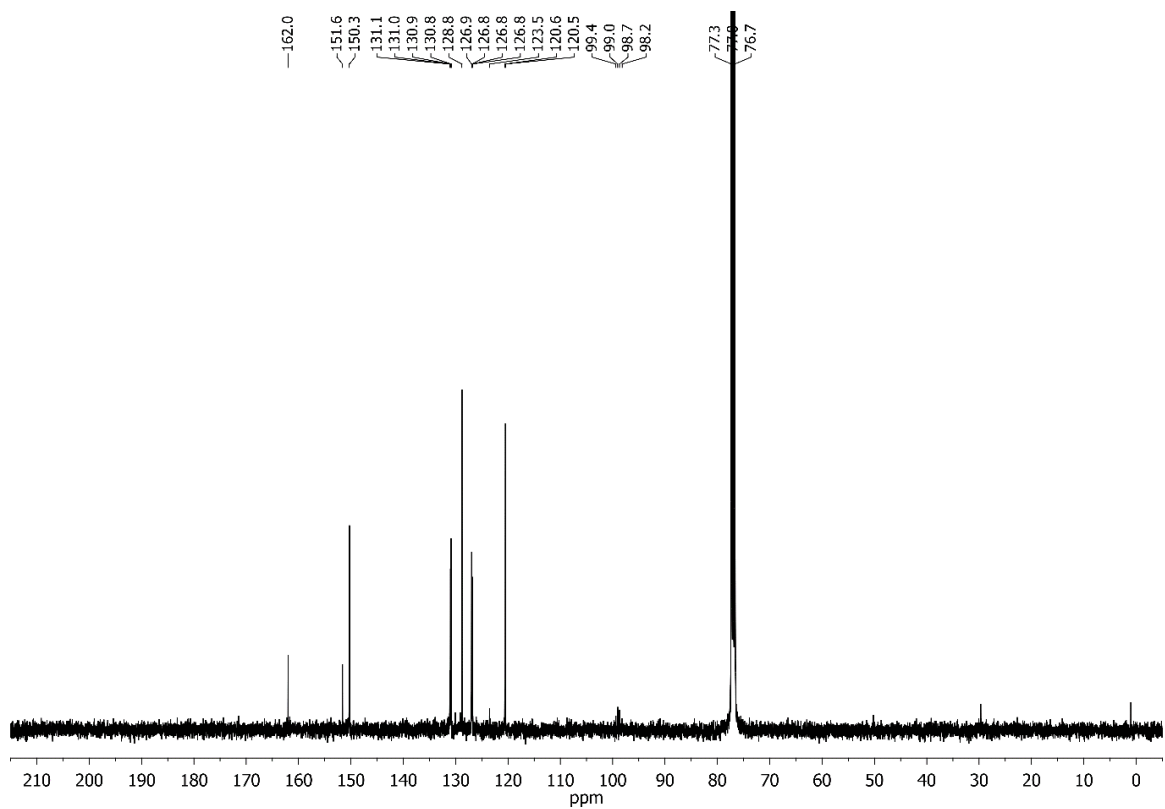
1-(2-(4-Nitrophenyl)-5-(pyridin-4-yl)-1,3,4-oxadiazol-3(2H)-yl)prop-2-en-1-one
(OXE2-NO₂,(4py)') in CDCl₃

¹H-NMR:

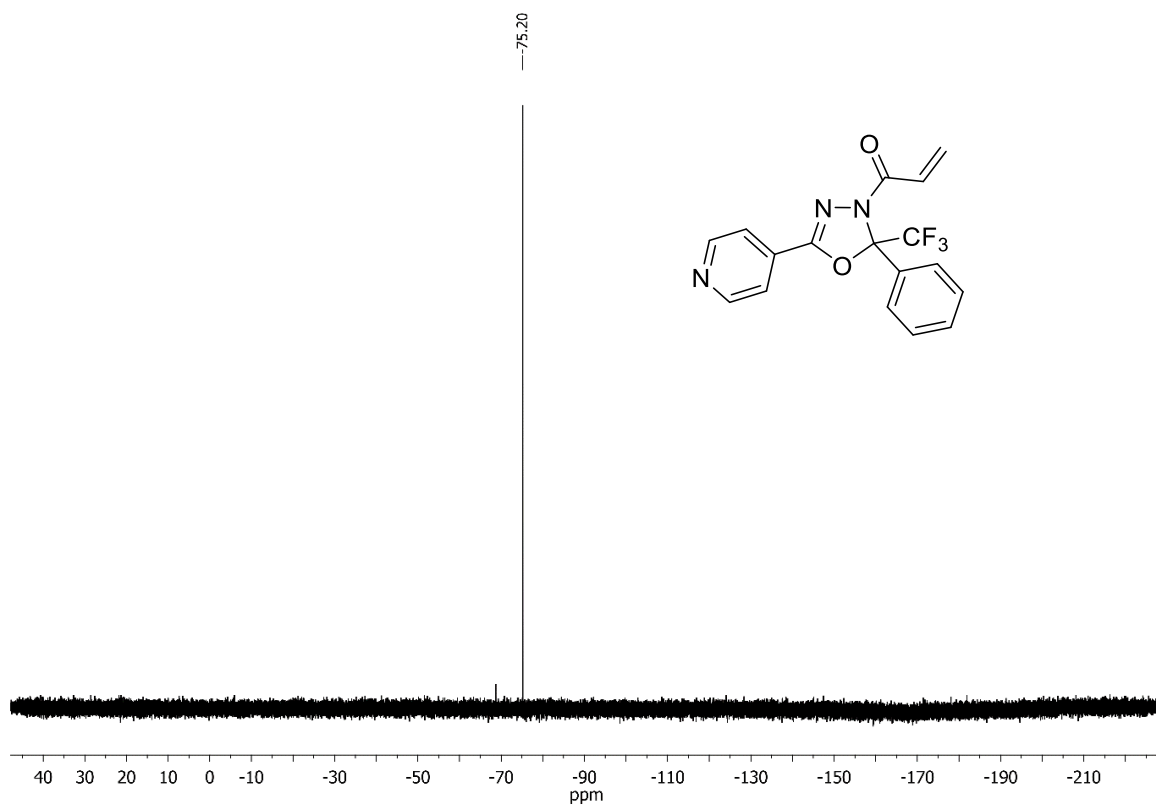


¹³C NMR:



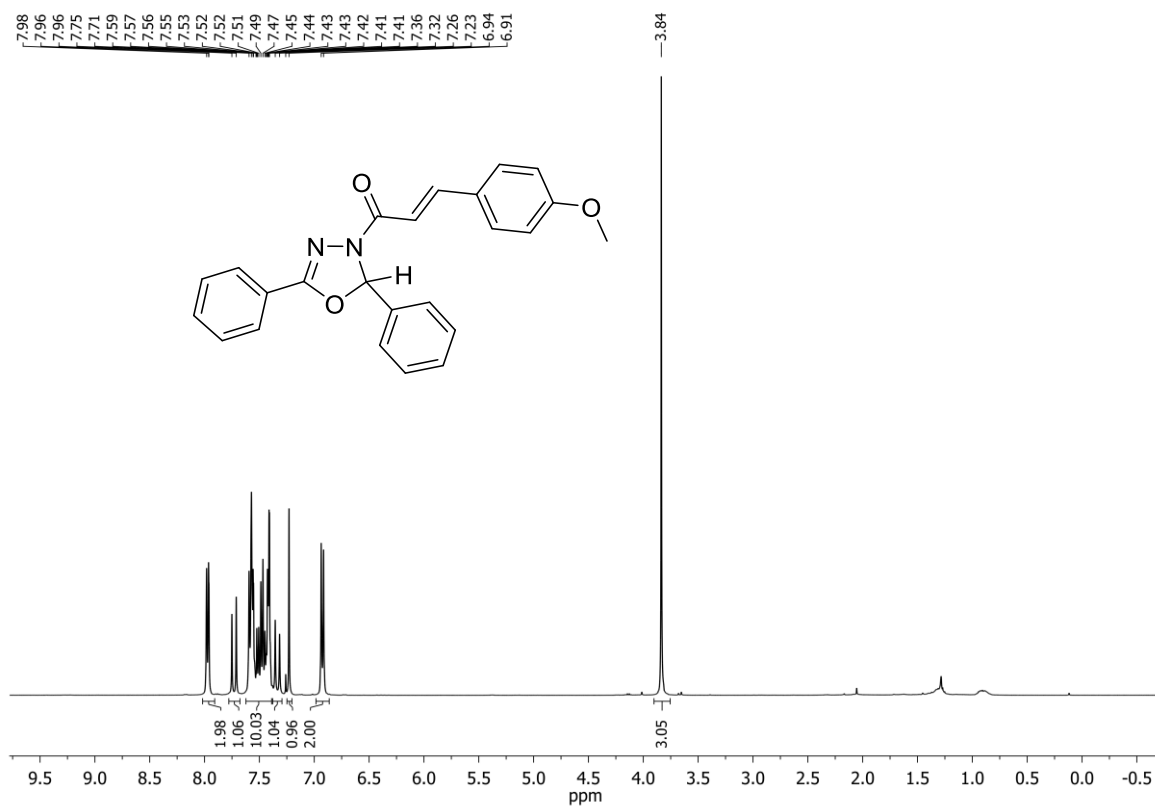
1-(2-Phenyl-5-(pyridin-4-yl)-2-(trifluoromethyl)-1,3,4-oxadiazol-3(2H)-yl)prop-2-en-1-one
(OXE3-(4py)) in CDCl₃¹H-NMR:¹³C NMR:

^{19}F NMR:

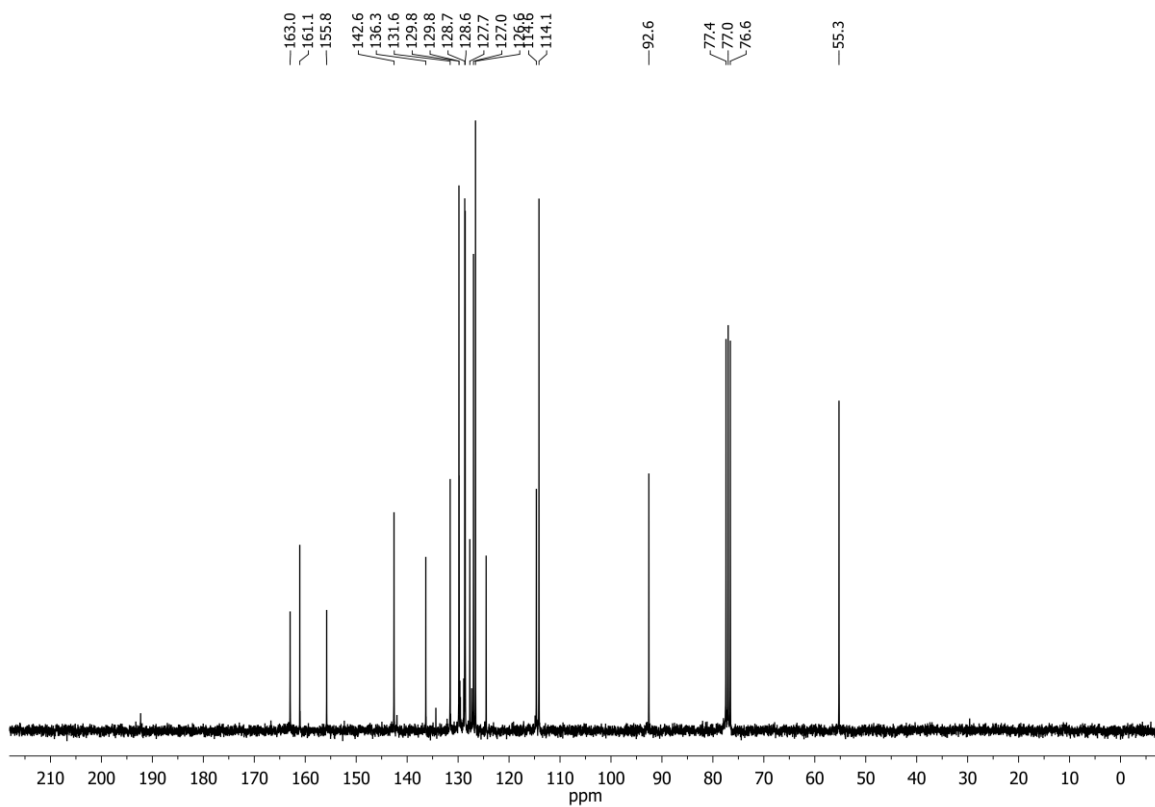


(*E*)-1-(2,5-Diphenyl-1,3,4-oxadiazol-3(2*H*)-yl)-3-(4-methoxyphenyl)prop-2-en-1-one
(OXE8-(OMe)') in CDCl₃

¹H-NMR:

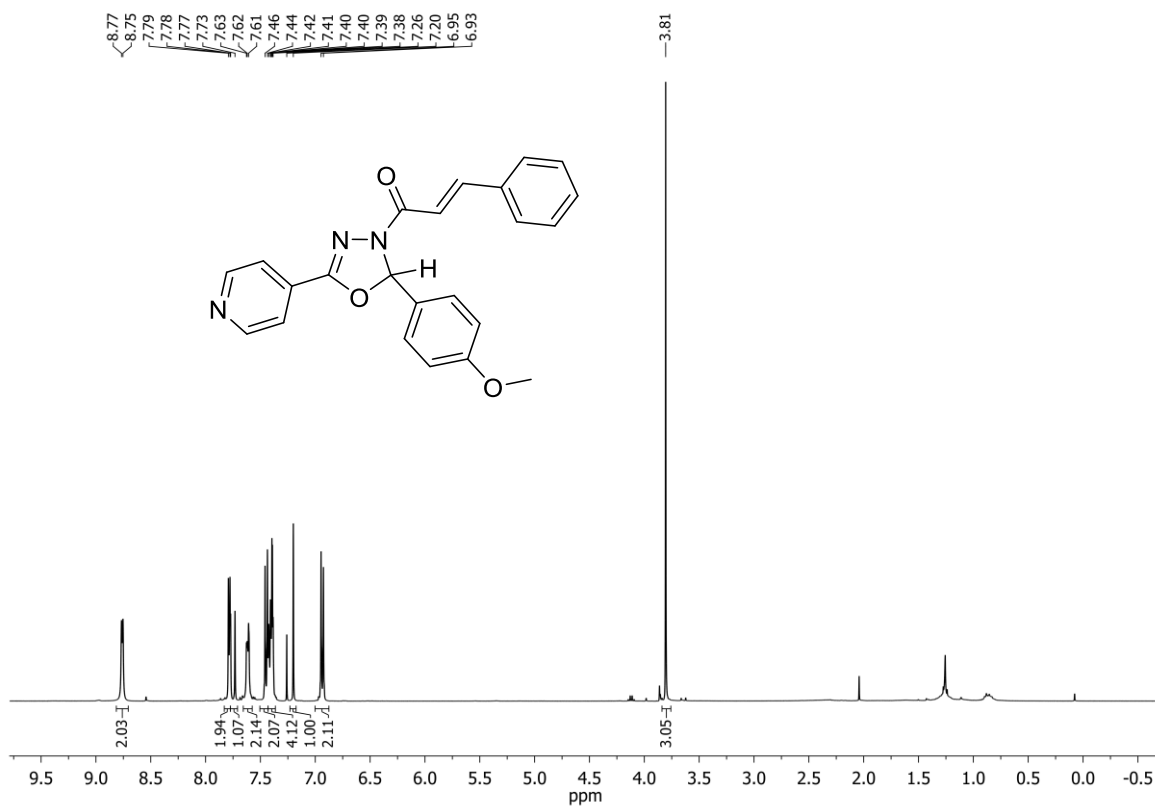


¹³C NMR:

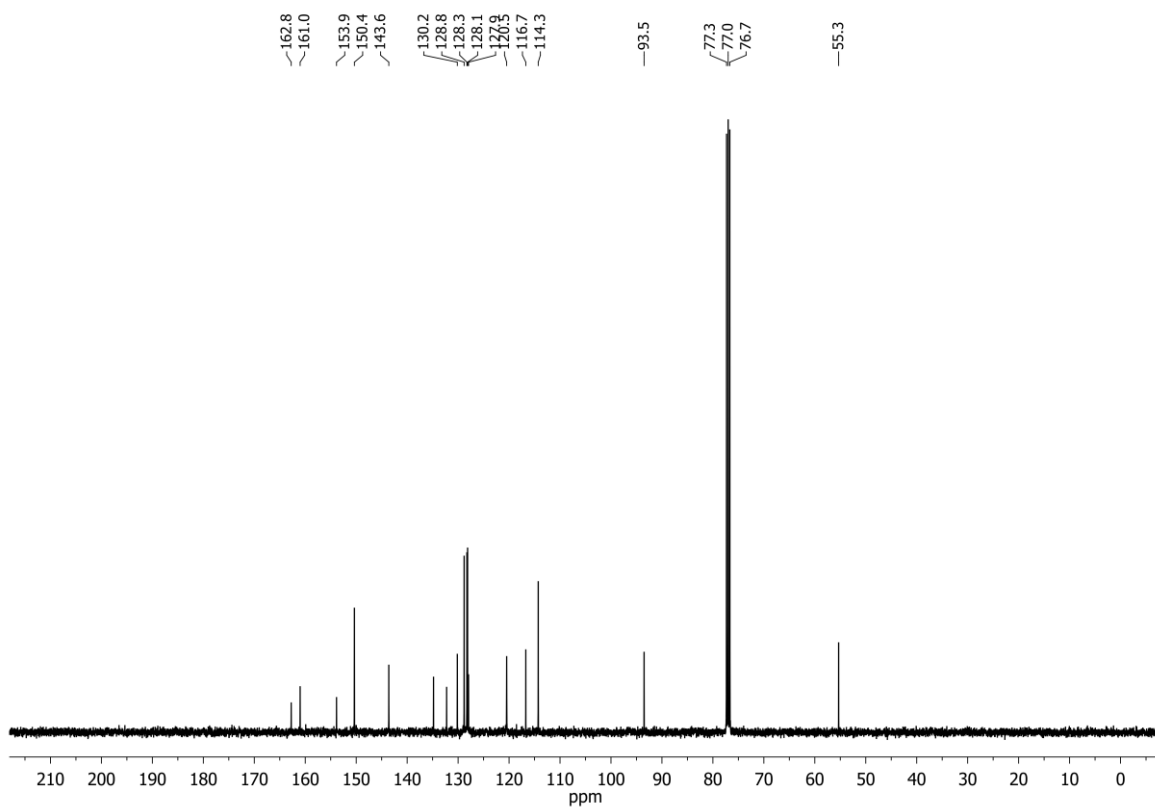


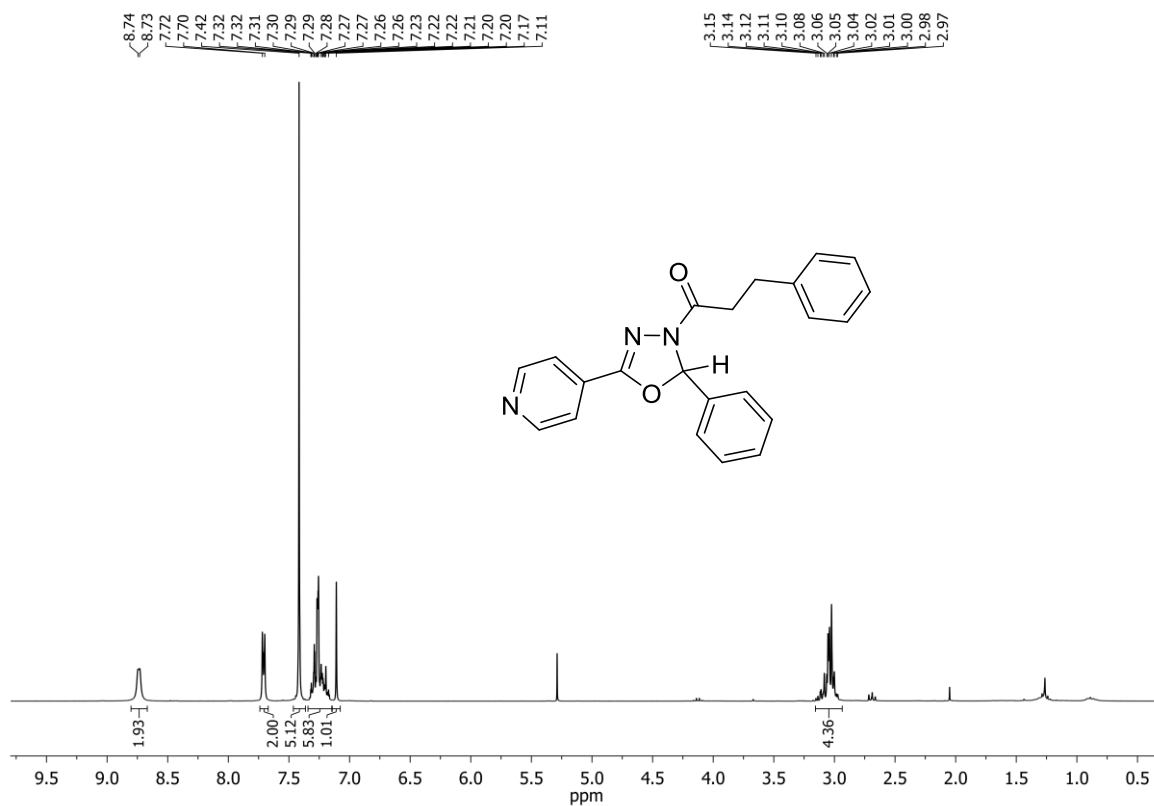
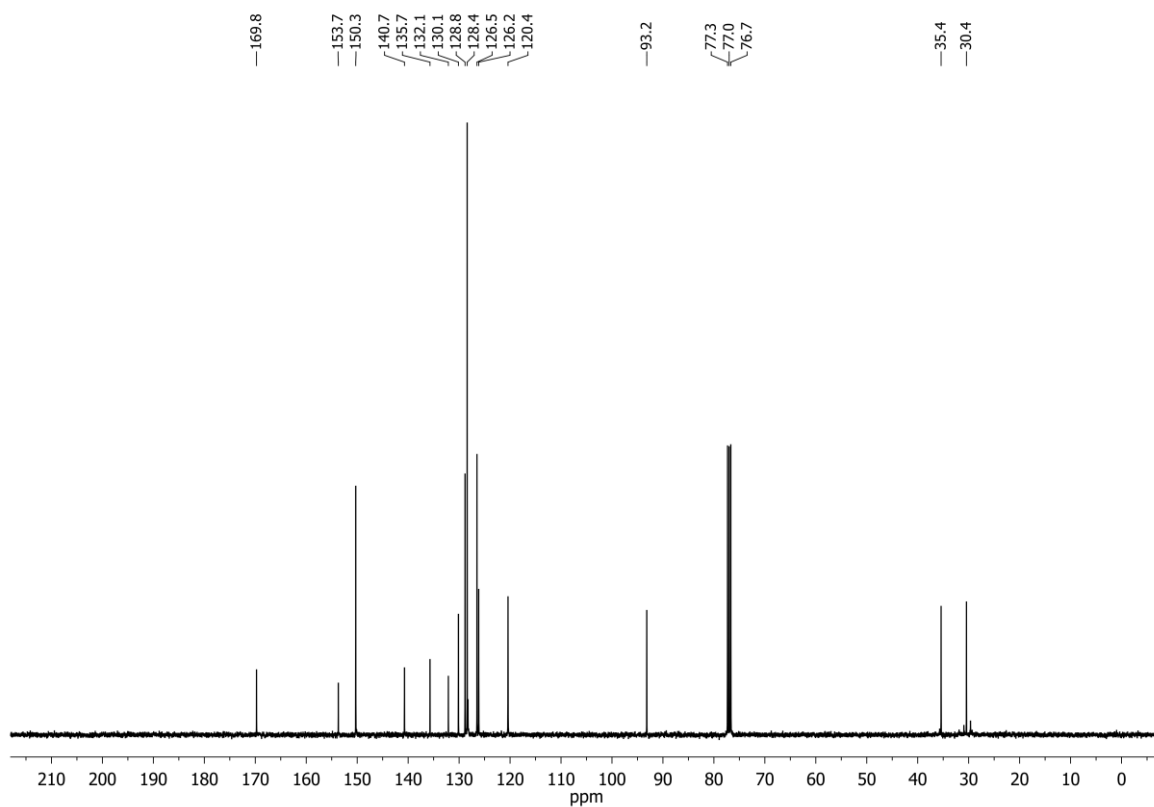
(*E*)-1-(2-(4-Methoxyphenyl)-5-(pyridin-4-yl)-1,3,4-oxadiazol-3(2*H*)-yl)-3-phenylprop-2-en-1-one (OXE8-OMe,(4py)) in CDCl₃

¹H-NMR:



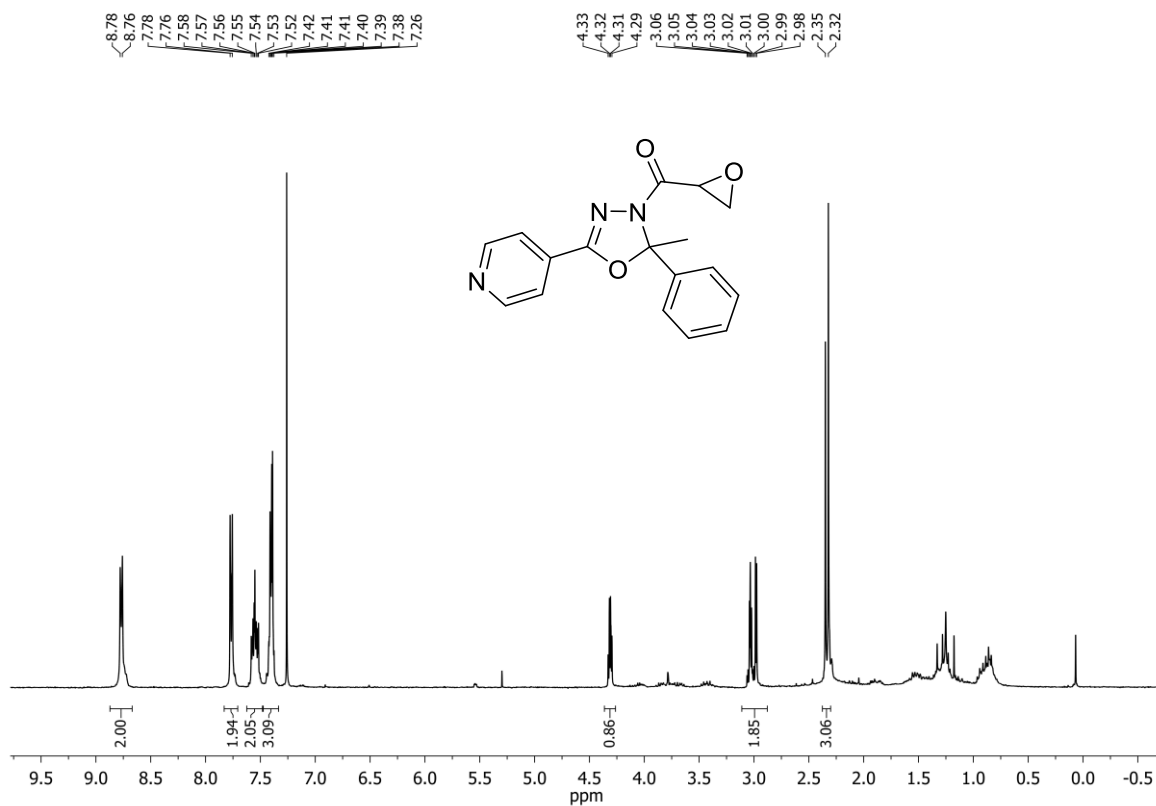
¹³C NMR:



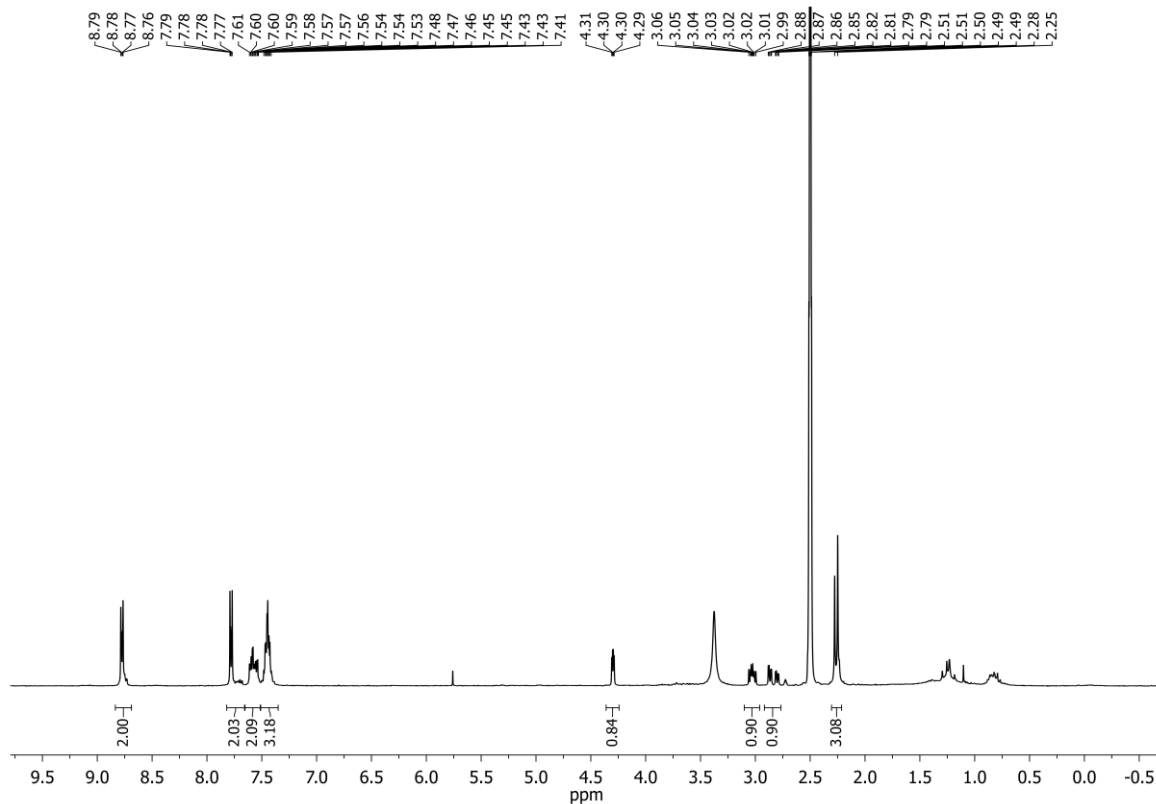
3-Phenyl-1-(2-phenyl-5-(pyridine-4-yl)-1,3,4-oxadiazol-3(2H)-yl)propan-1-one
(OXE8-(4py))'-H₂) in CDCl₃¹H-NMR:¹³C NMR:

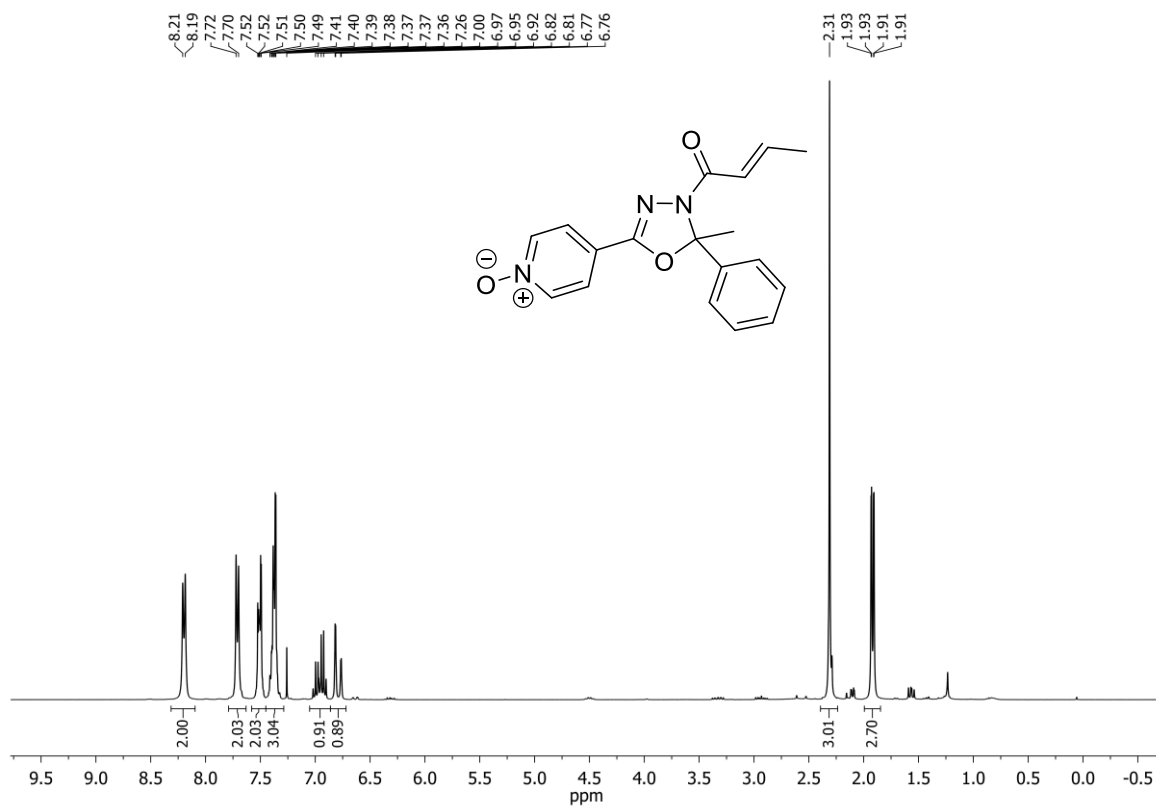
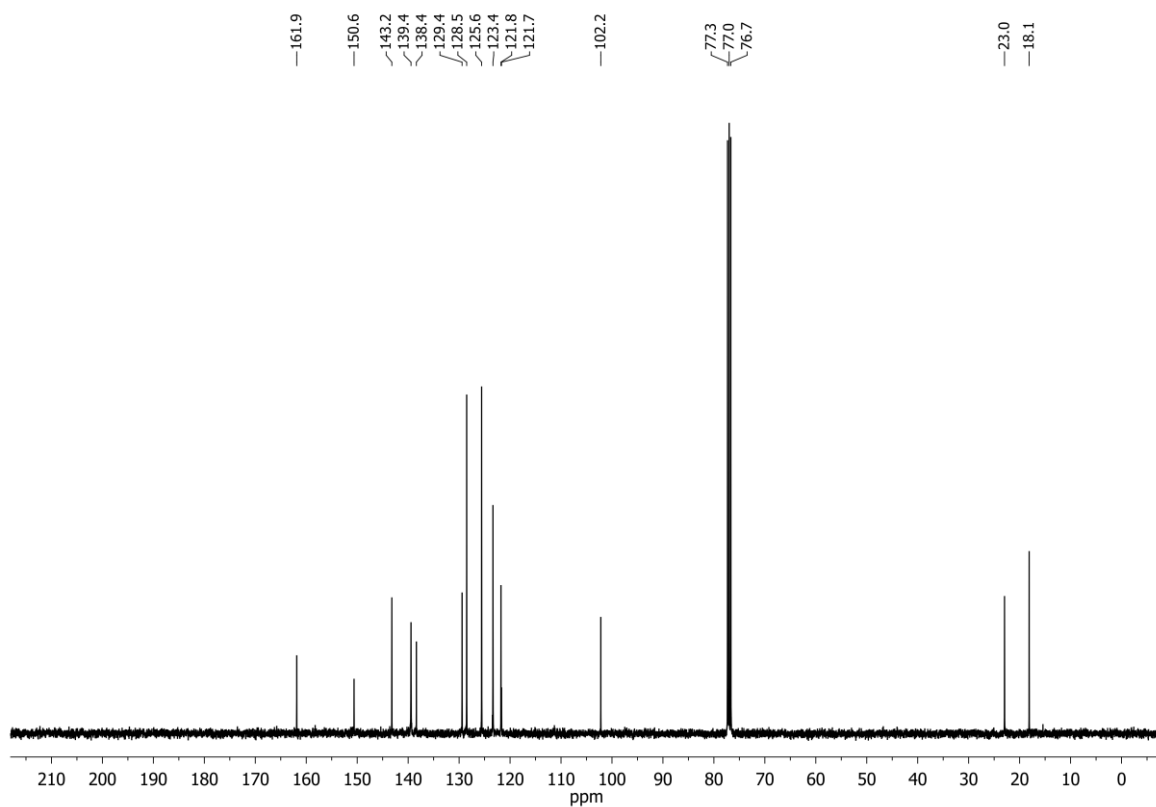
(2-Methyl-2-phenyl-5-(pyridin-4-yl)-1,3,4-oxadiazol-3(2H)-yl)(oxiran-2-yl)methanone
(OXEp1-(4py))

$^1\text{H-NMR}$ in CDCl_3 :



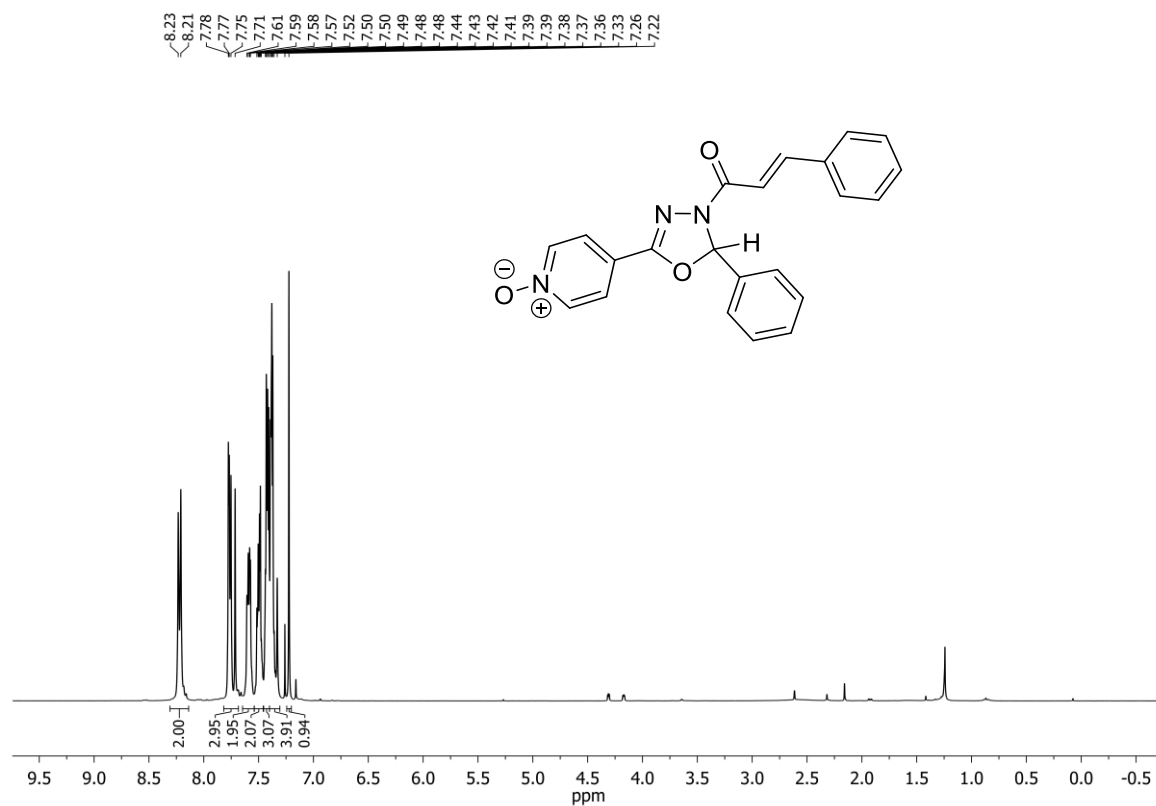
$^1\text{H-NMR}$ in DMSO-d_6 :



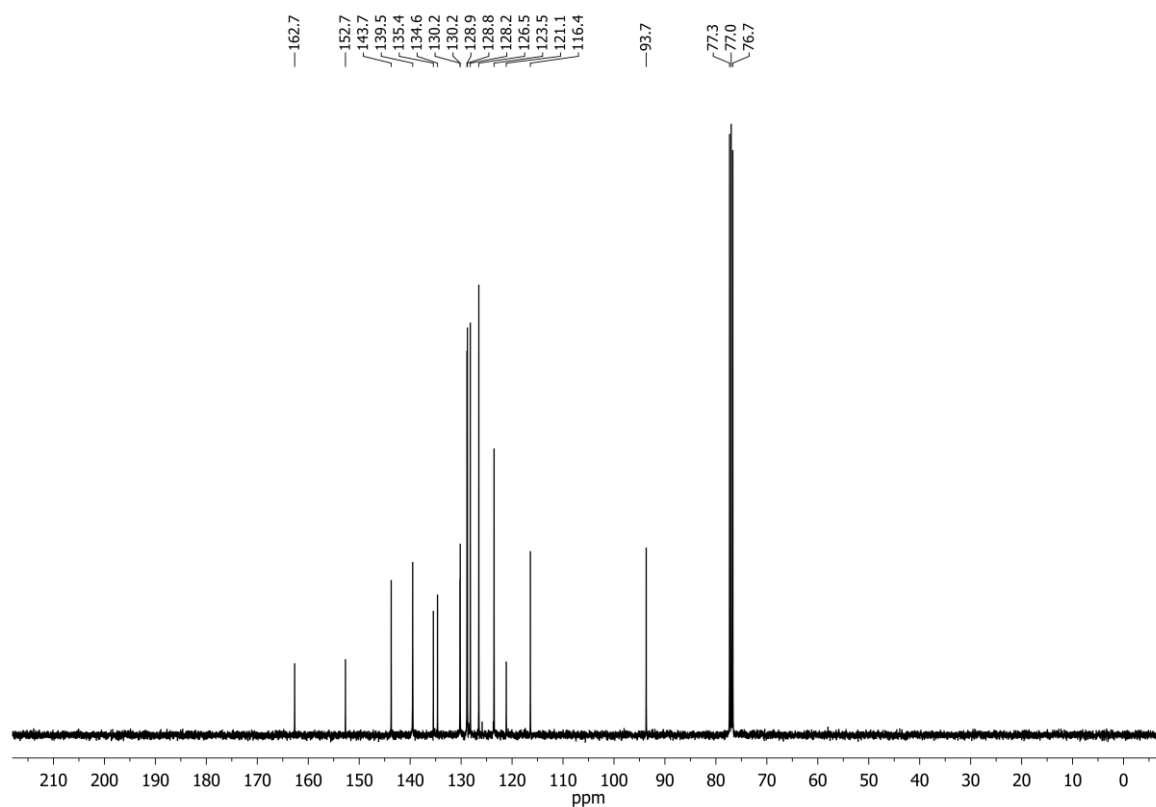
4-(4-(But-2-enoyl)-5-methyl-5-phenyl-4,5-dihydro-1,3,4-oxadiazol-2-yl)pyridine-1-oxide
(OXE4-(4py-N-oxide)) in CDCl₃¹H-NMR:¹³C NMR:

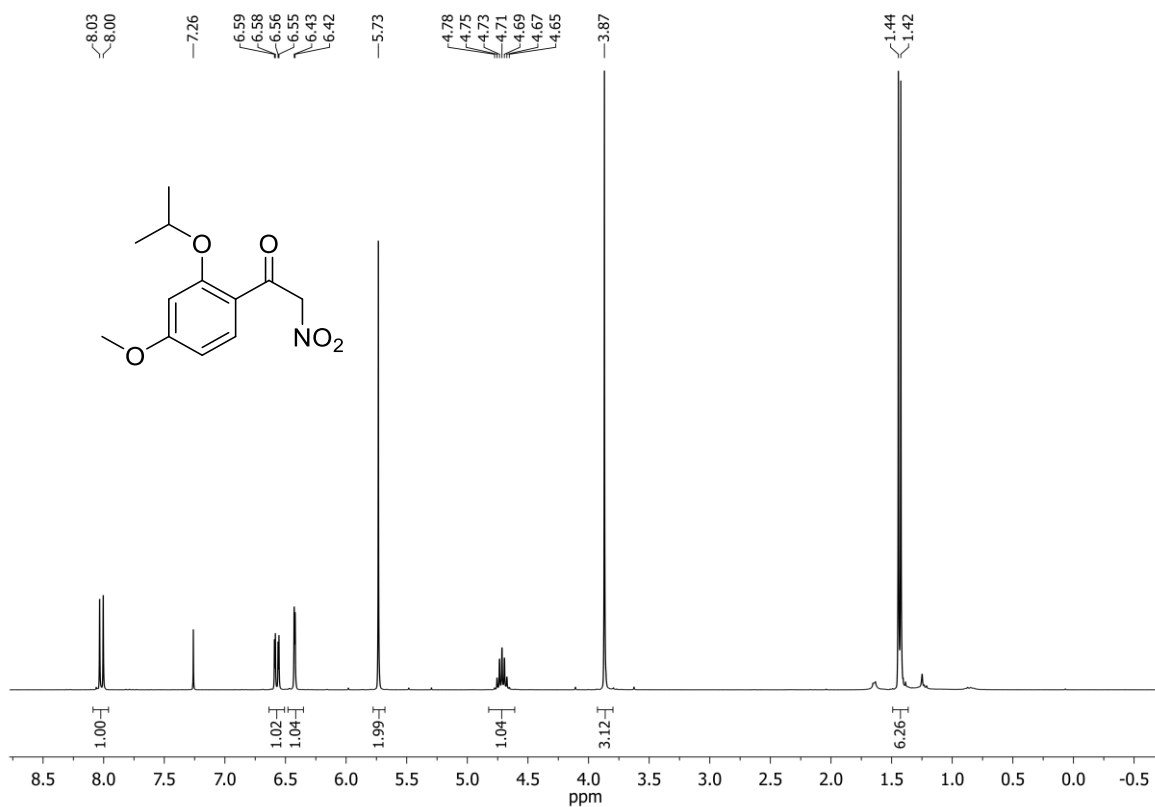
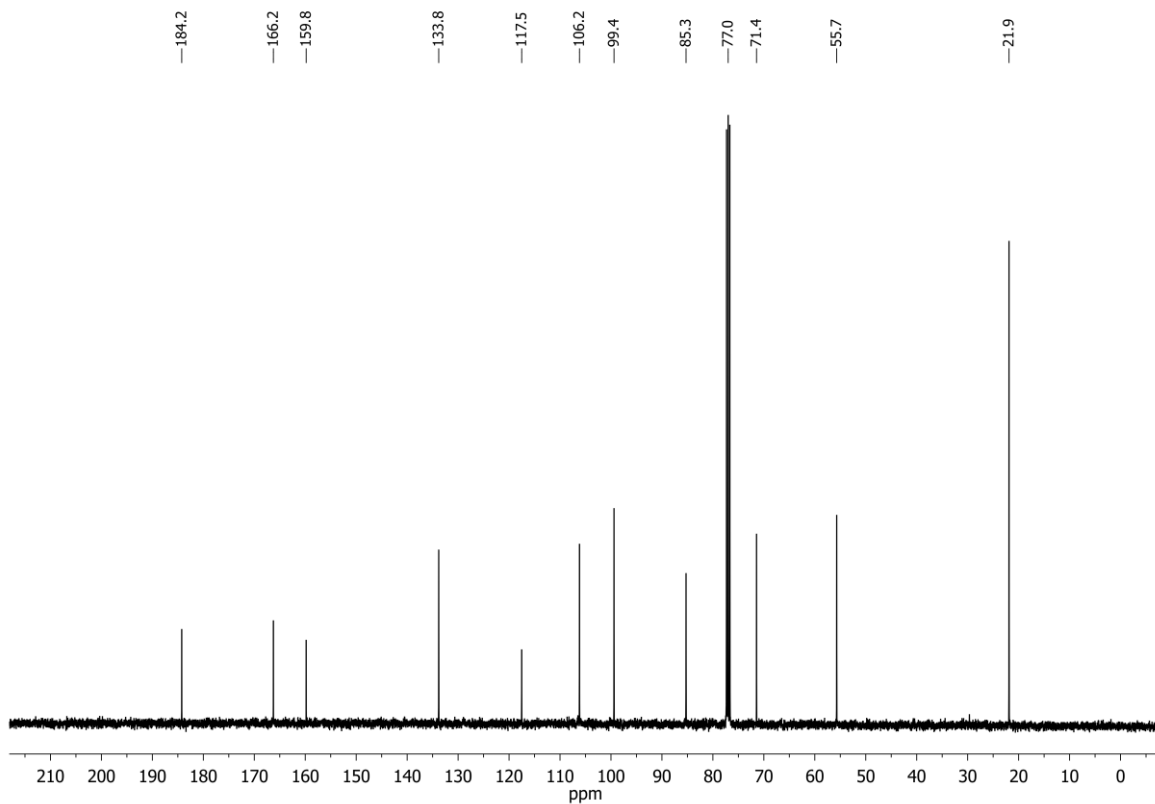
(*E*)-4-(4-(Cinnamoyl-5-phenyl-4,5-dihydro-1,3,4-oxadiazol-2-yl)pyridine-1-oxide
(OXE8-(4py-*N*-oxide)) in CDCl₃

¹H-NMR:



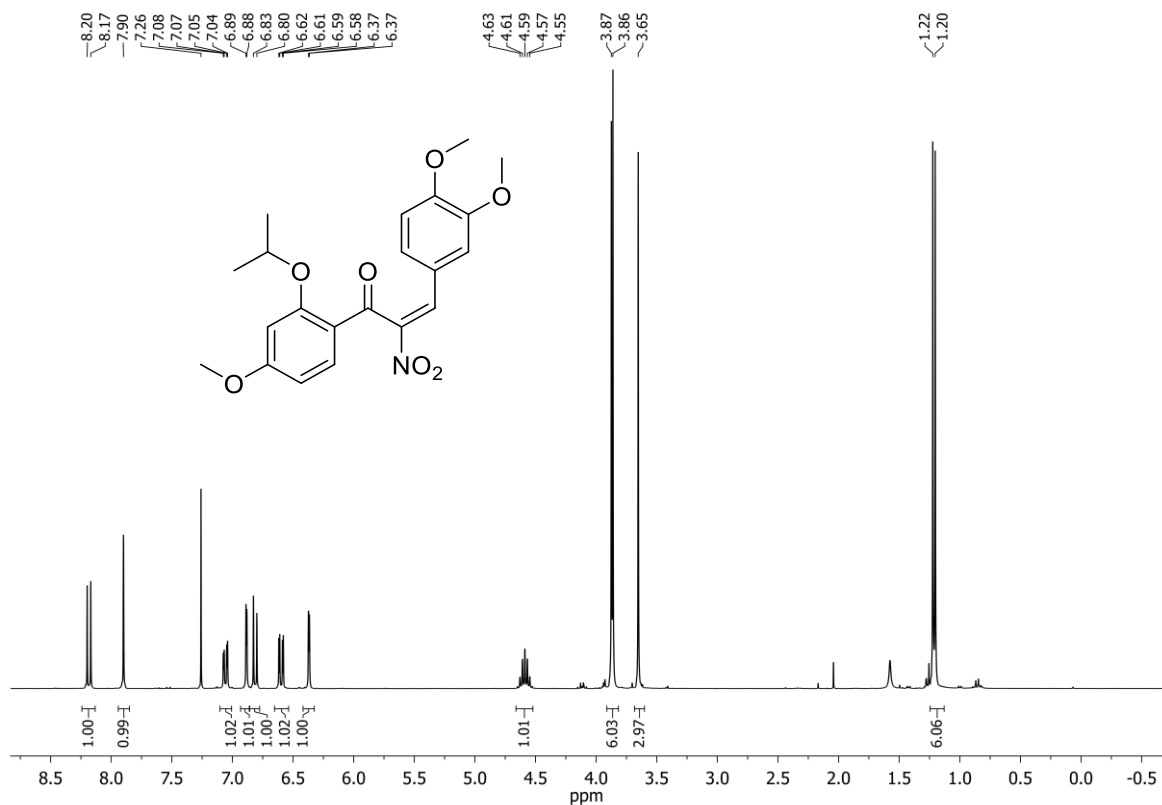
¹³C NMR:



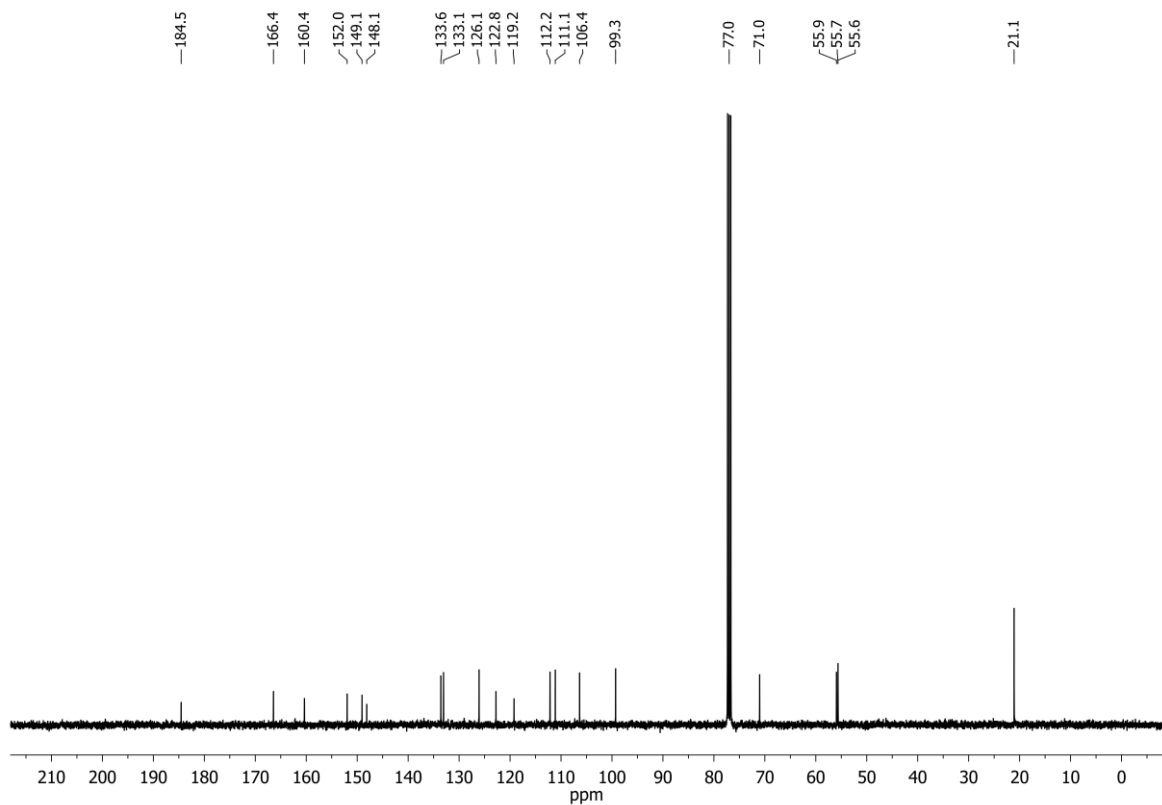
1-(2-Isopropoxy-4-methoxyphenyl)-2-nitroethan-1-one (**68**) in CDCl₃¹H-NMR:¹³C NMR:

(*E*)-3-(3,4-dimethoxyphenyl)-1-(2-isopropoxy-4-methoxyphenyl)-2-nitroprop-2-en-1-one
(**70**) in CDCl₃

¹H-NMR:

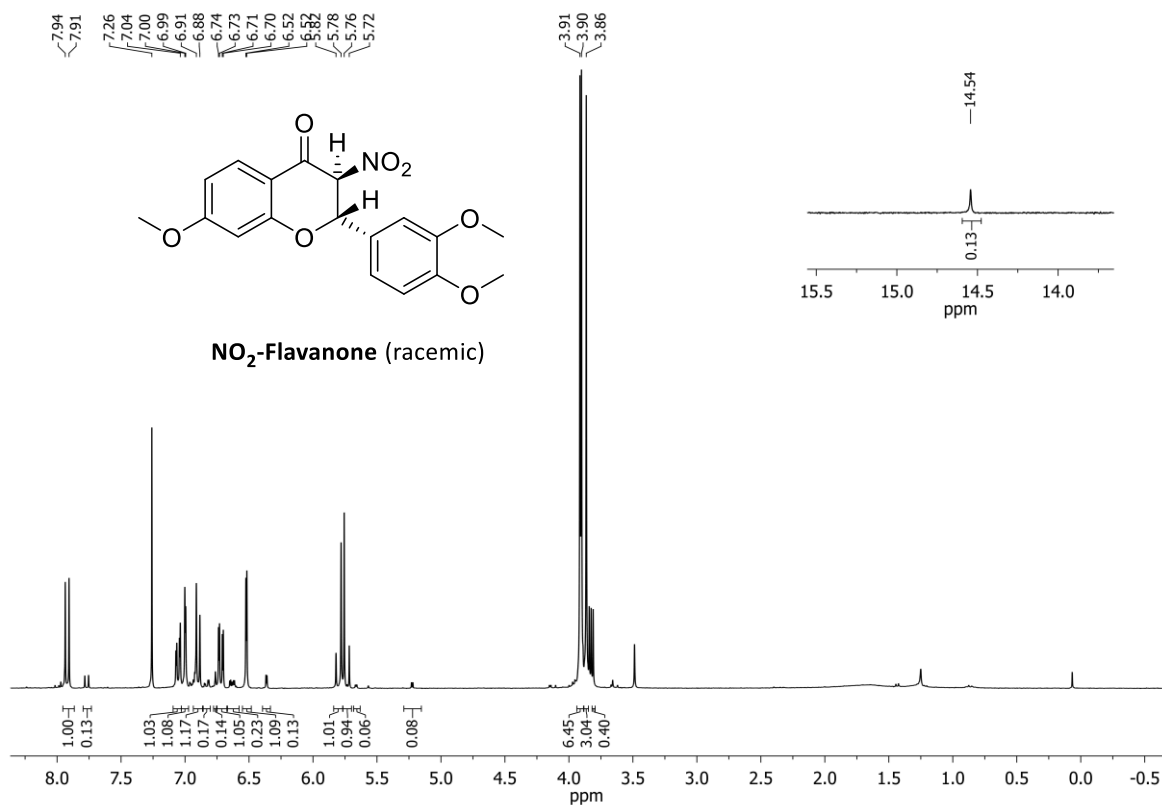


¹³C NMR:

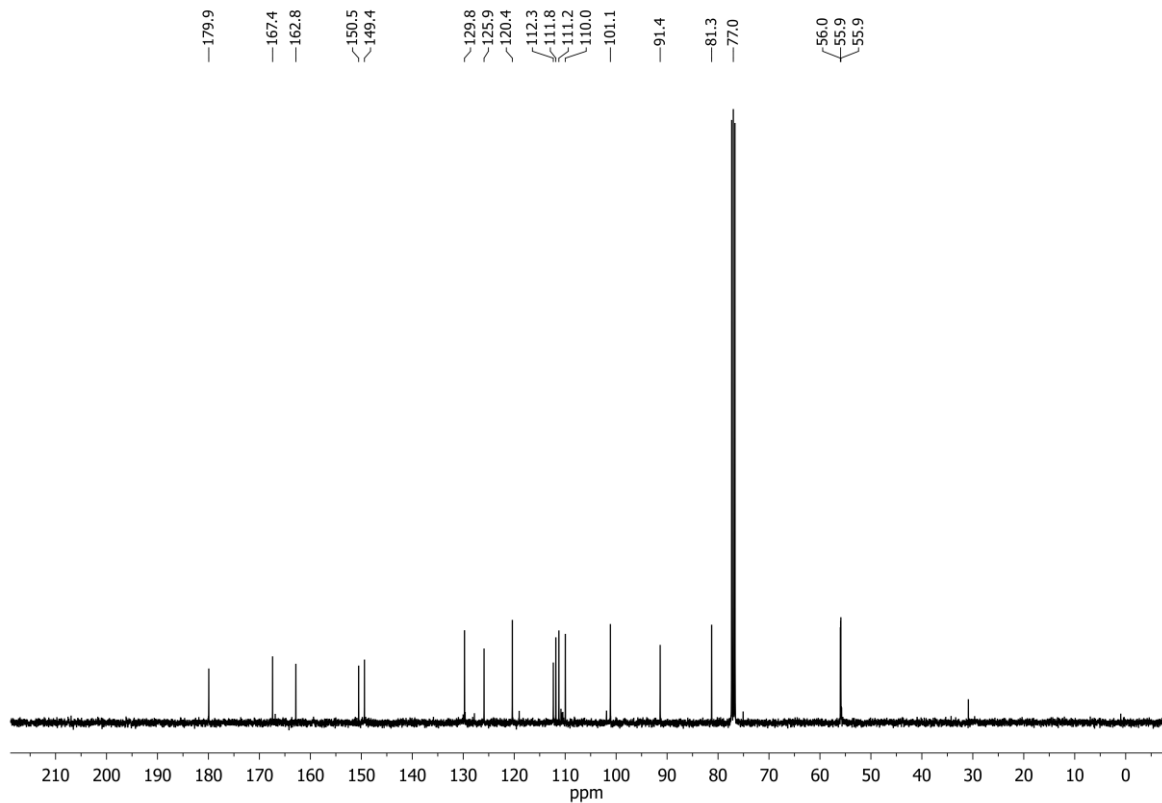


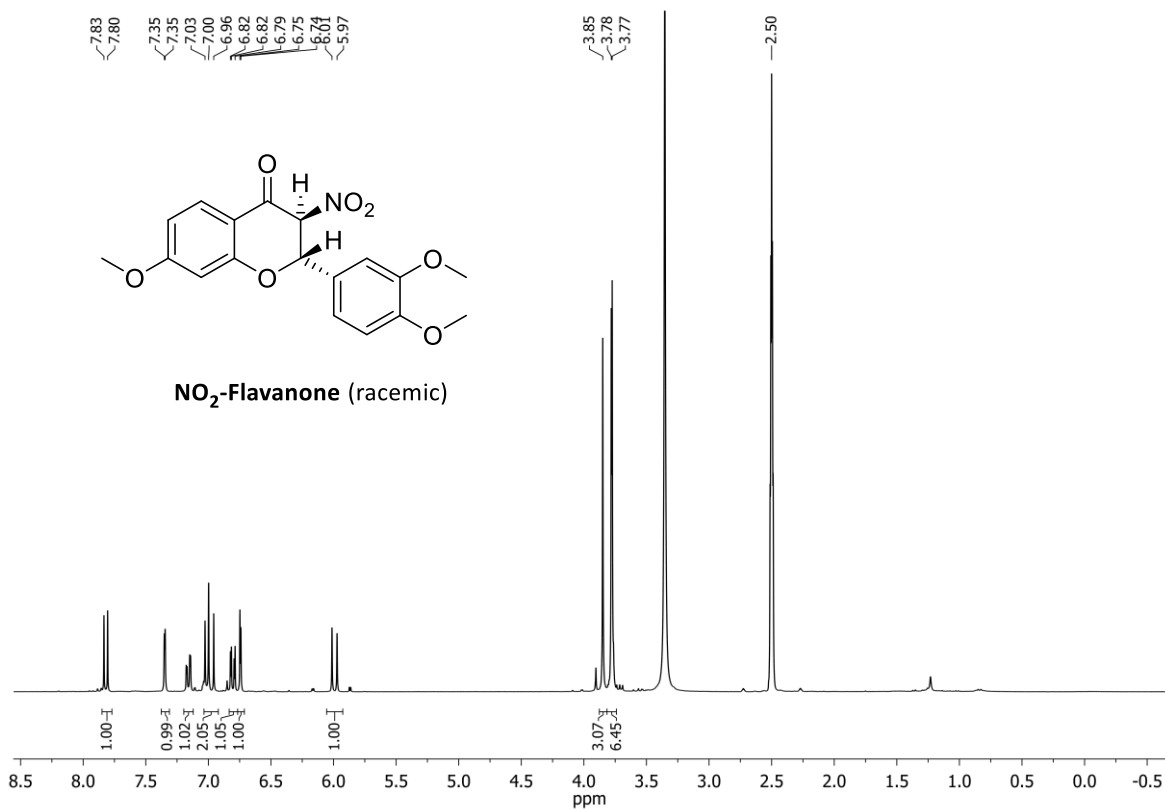
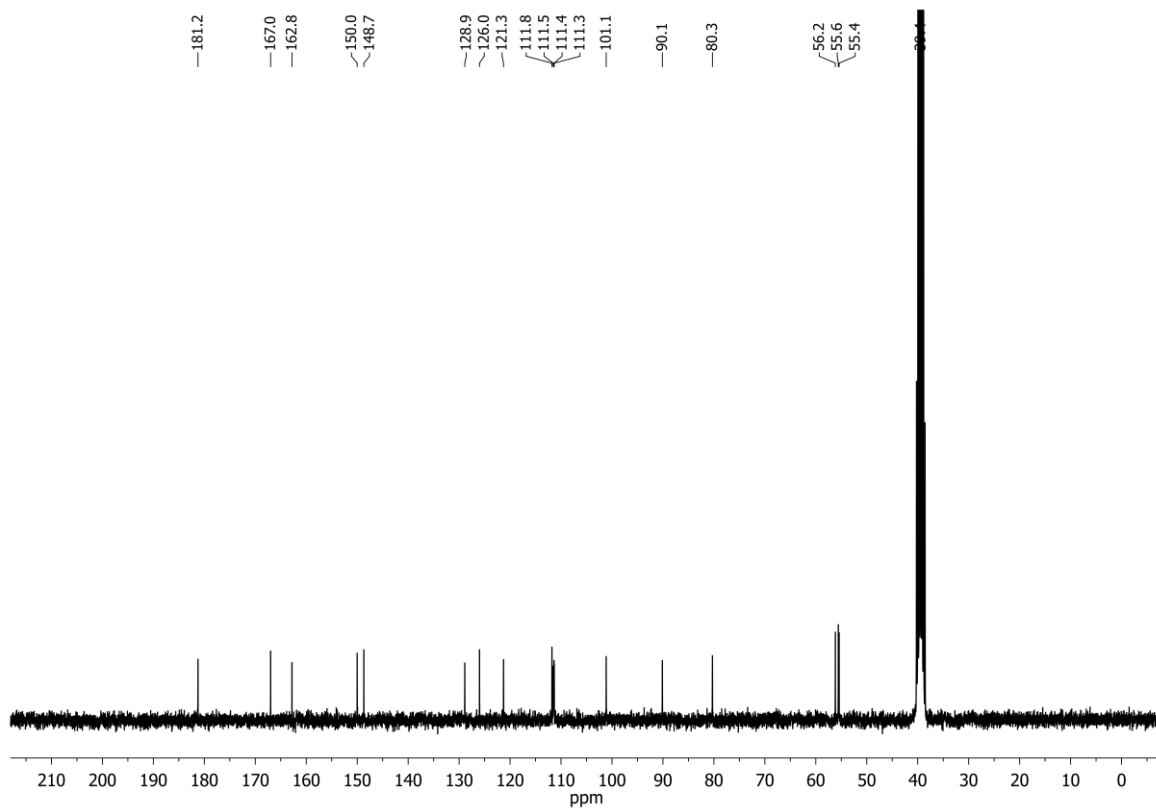
2-(3,4-Dimethoxyphenyl)-6-methoxy-3-nitrochroman-4-one (**NO₂-Flavanone**) with approximately 10% of isomer **α-NO₂-HC** in CDCl₃

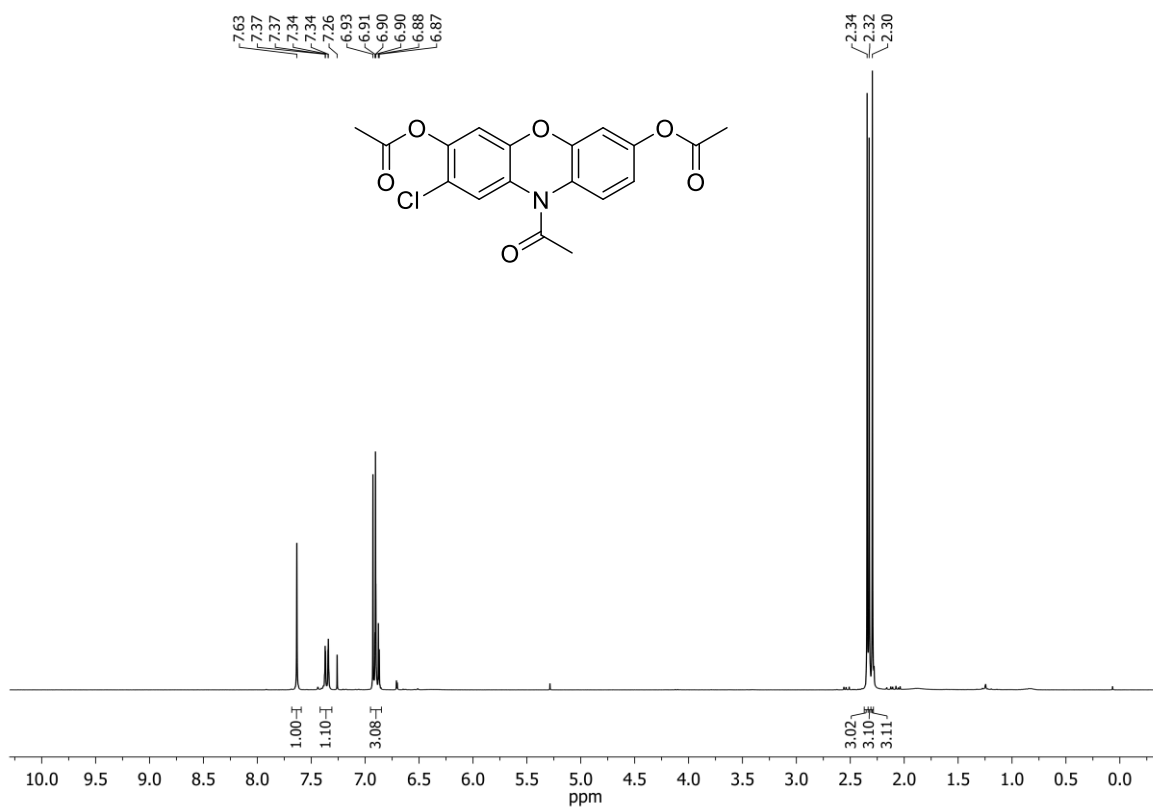
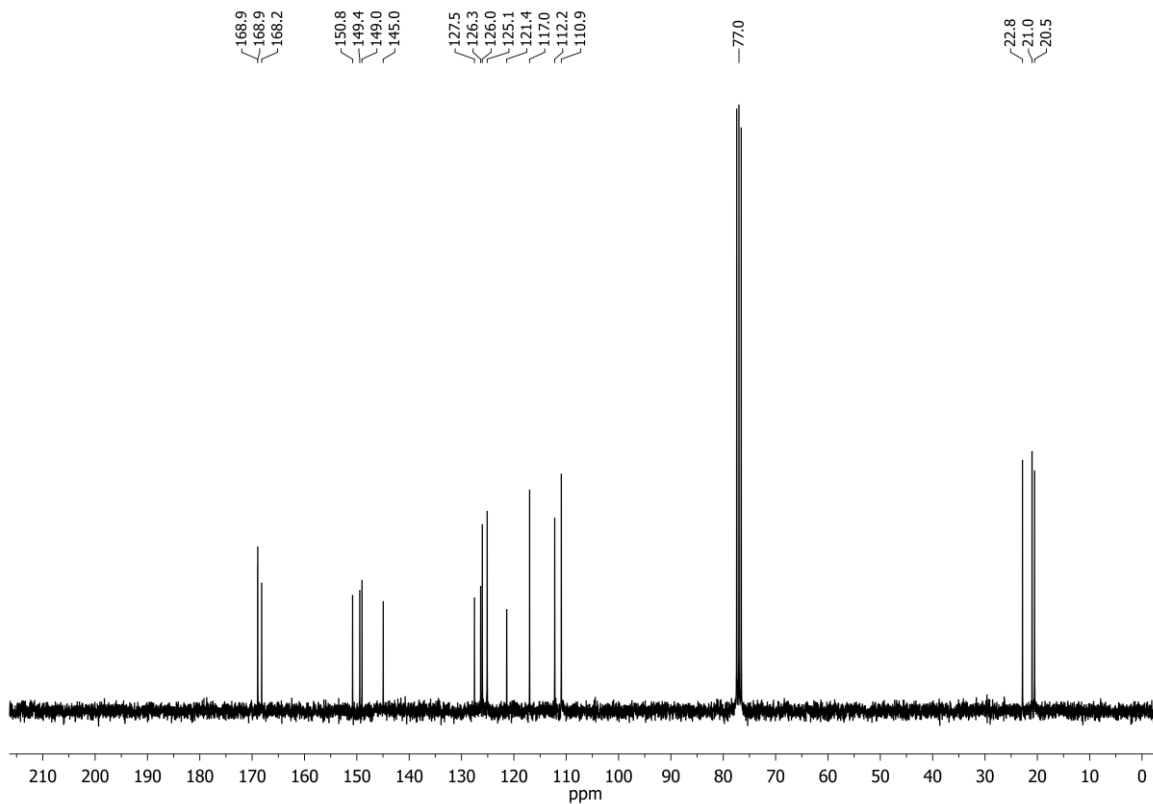
¹H-NMR:

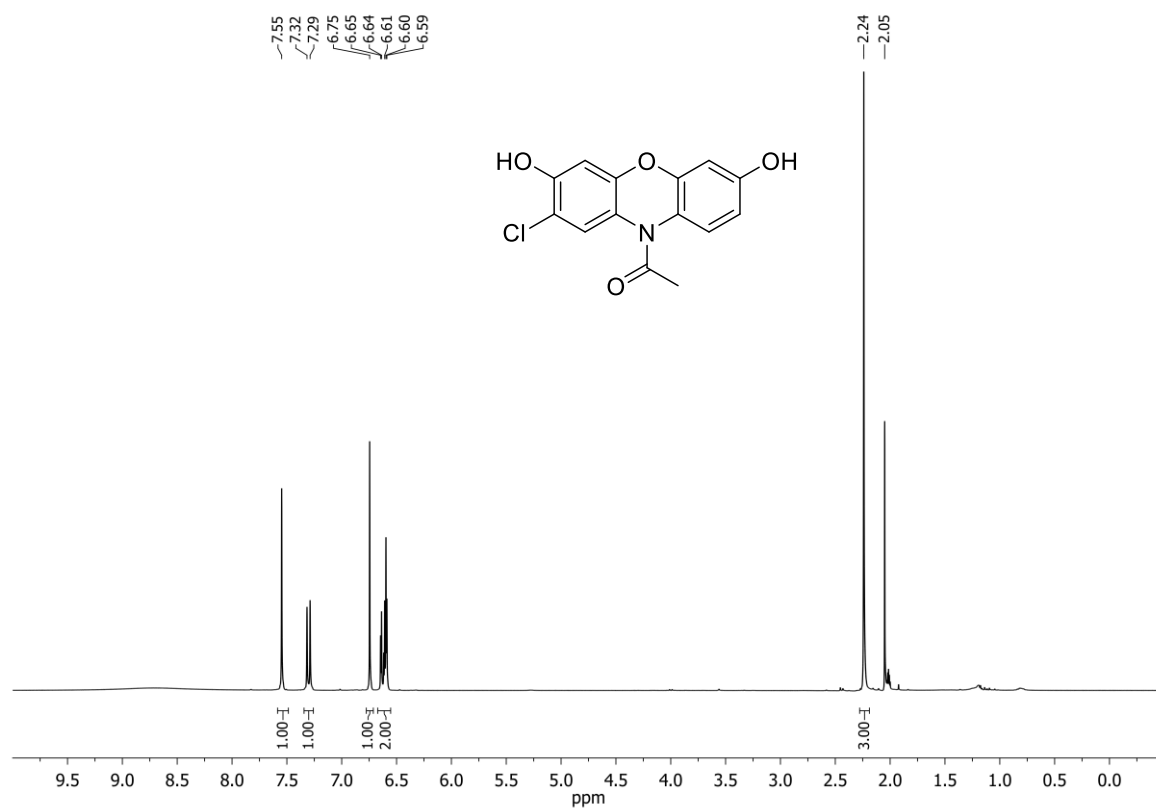
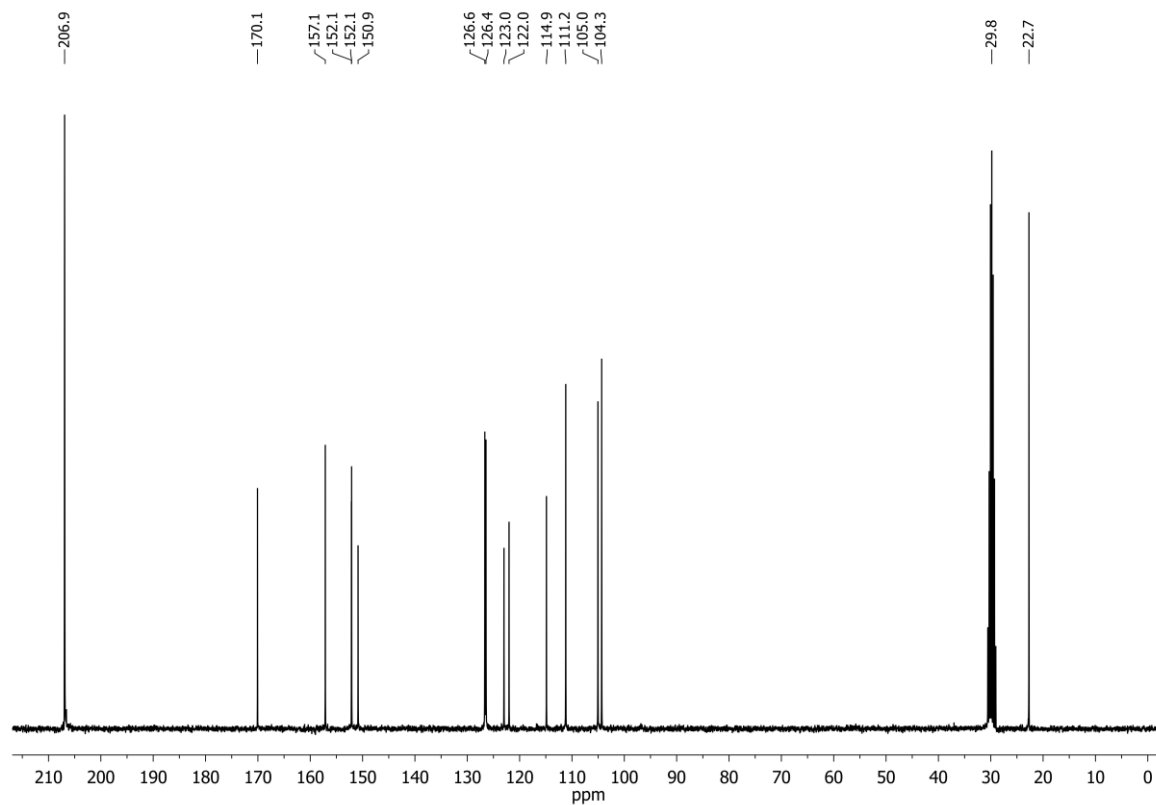


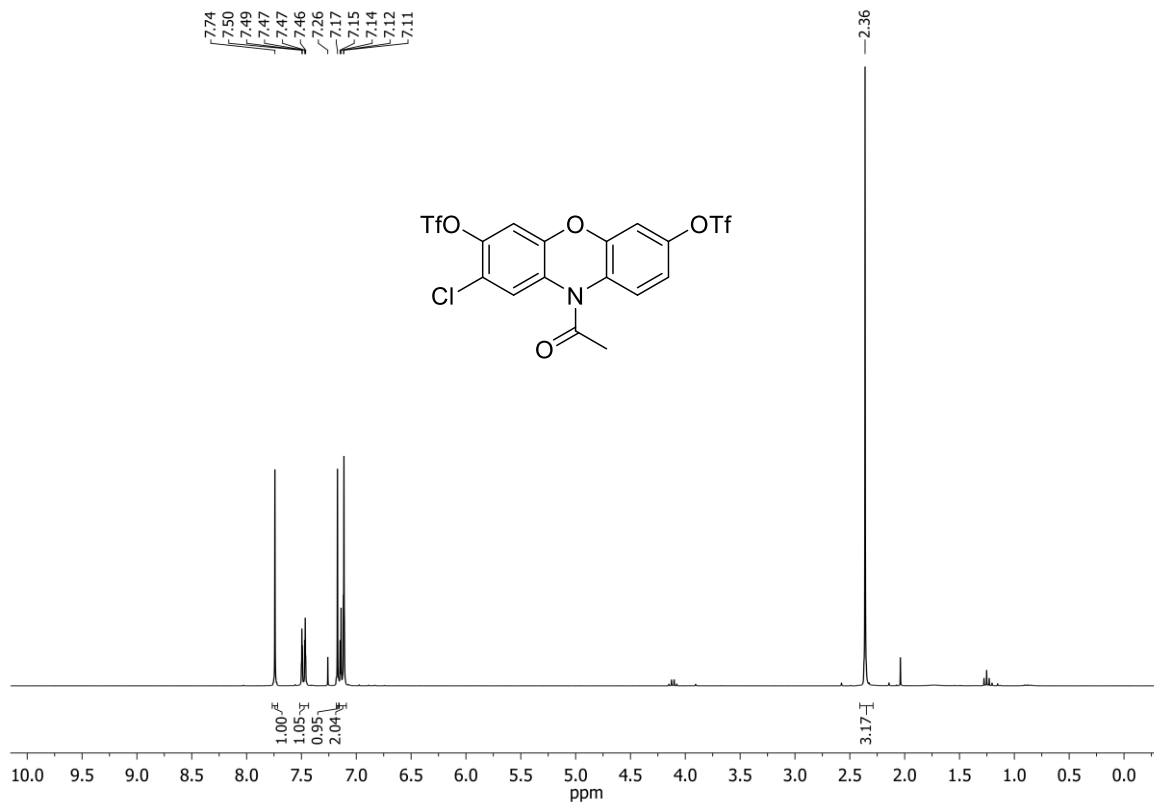
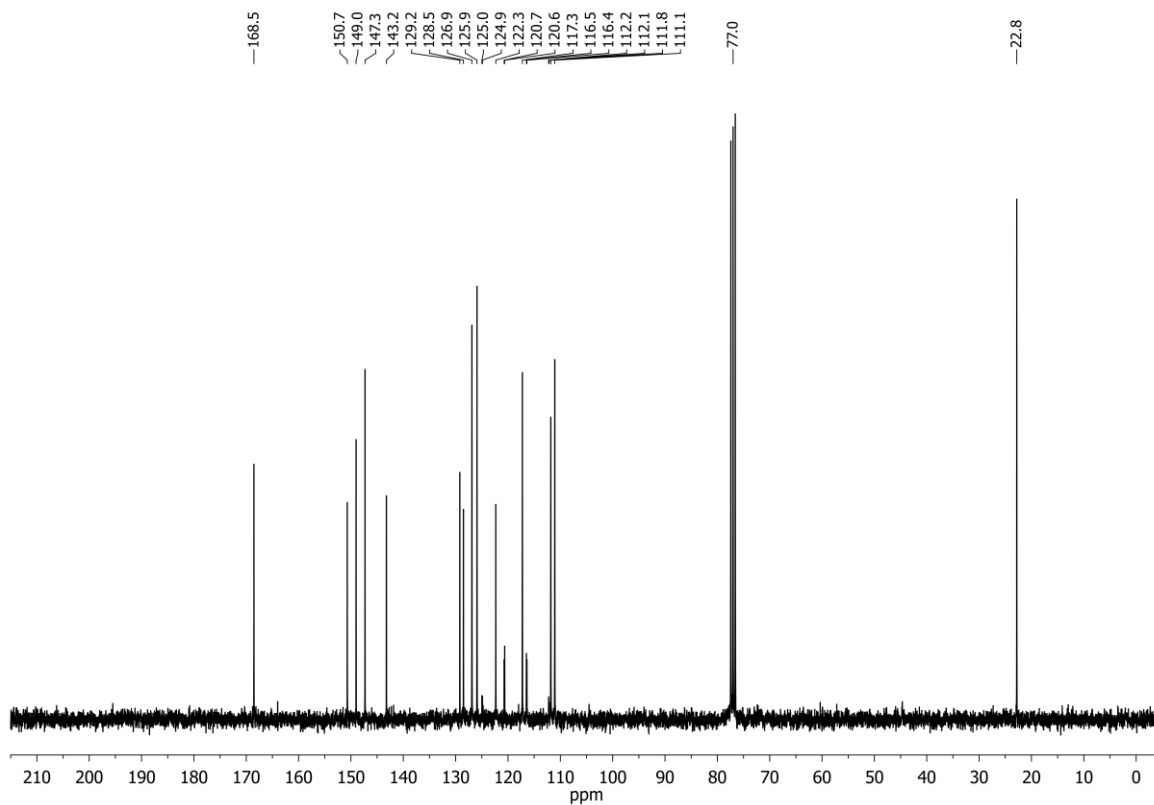
¹³C NMR:



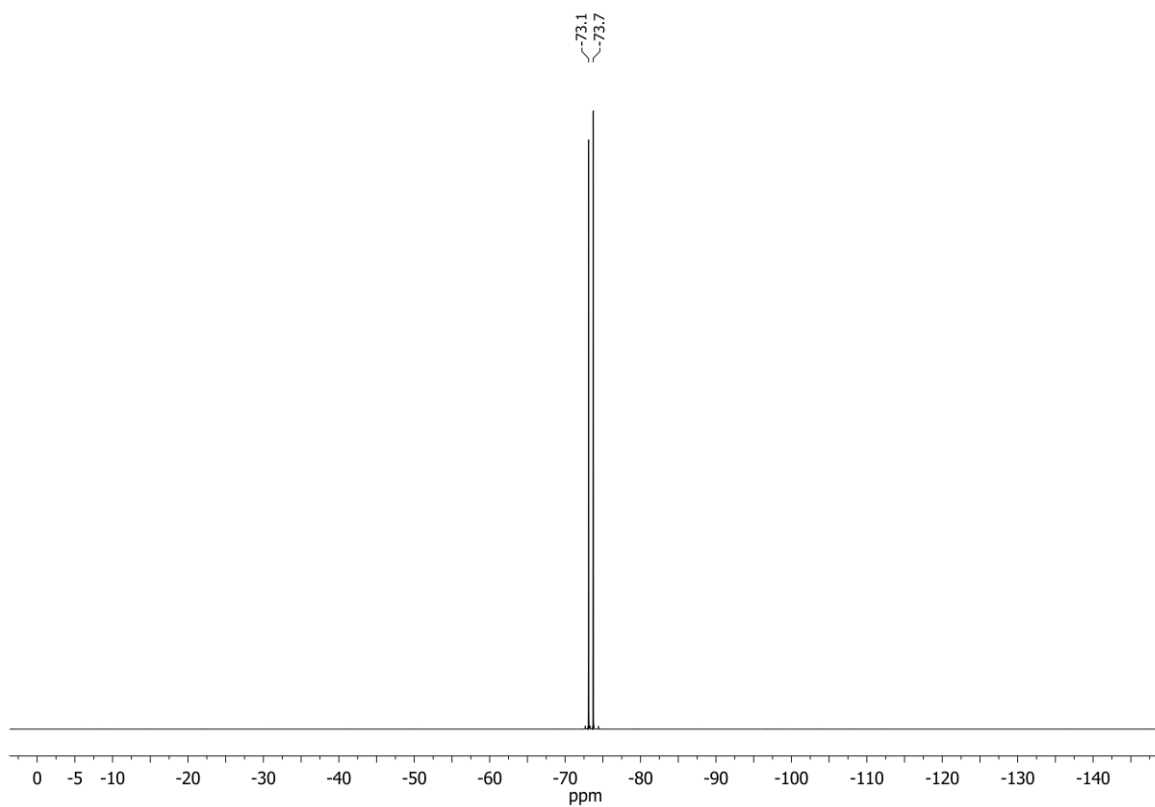
2-(3,4-Dimethoxyphenyl)-6-methoxy-3-nitrochroman-4-one (**NO₂-Flavanone**) in DMSO-d₆¹H-NMR:¹³C NMR:

10-Acetyl-8-chloro-10,10a-dihydro-3H-phenoxazine-3,7-diyl diacetate (**89**) in CDCl₃¹H-NMR:¹³C NMR:

1-(8-Chloro-3,7-dihydroxy-3,10a-dihydro-10H-phenoxazin-10-yl)ethan-1-one (**90**) in Acetone- d_6 $^1\text{H-NMR}$: $^{13}\text{C-NMR}$:

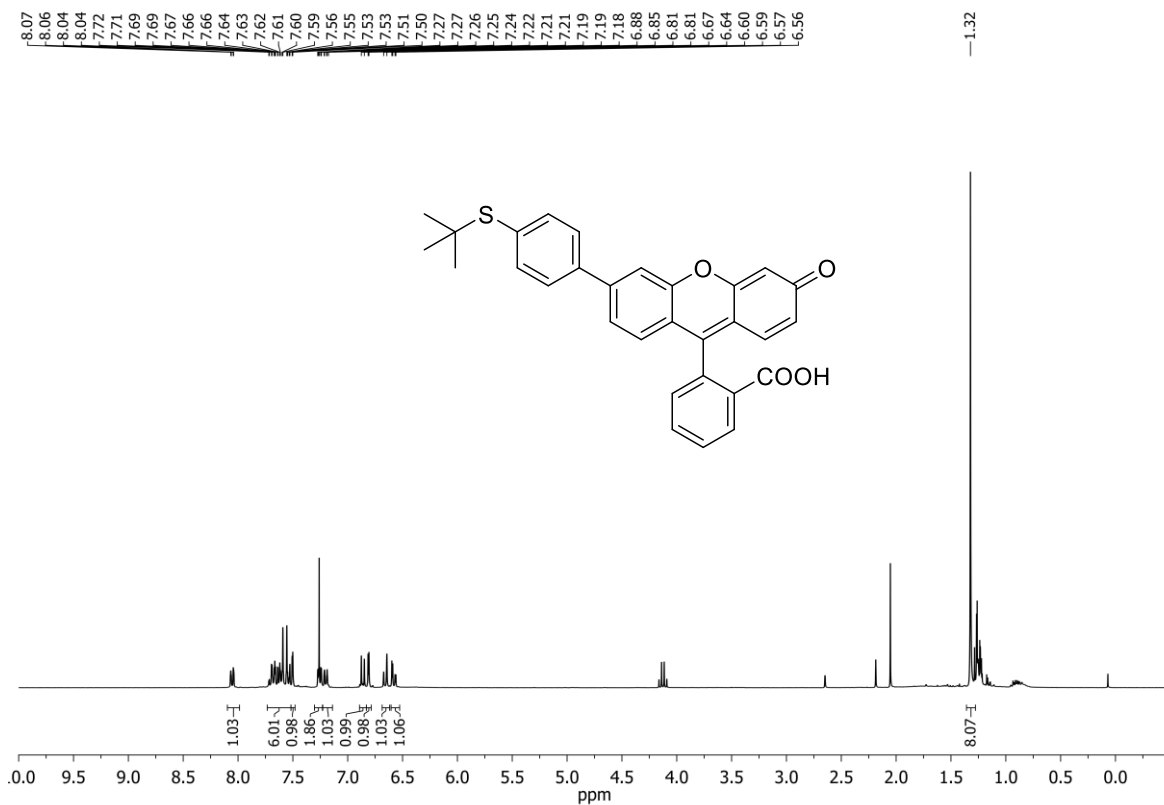
10-Acetyl-8-chloro-10,10a-dihydro-3H-phenoxazine-3,7-diyl bis(trifluoromethanesulfonate) (**92**) in CDCl₃¹H-NMR:¹³C NMR:

^{19}F -NMR:

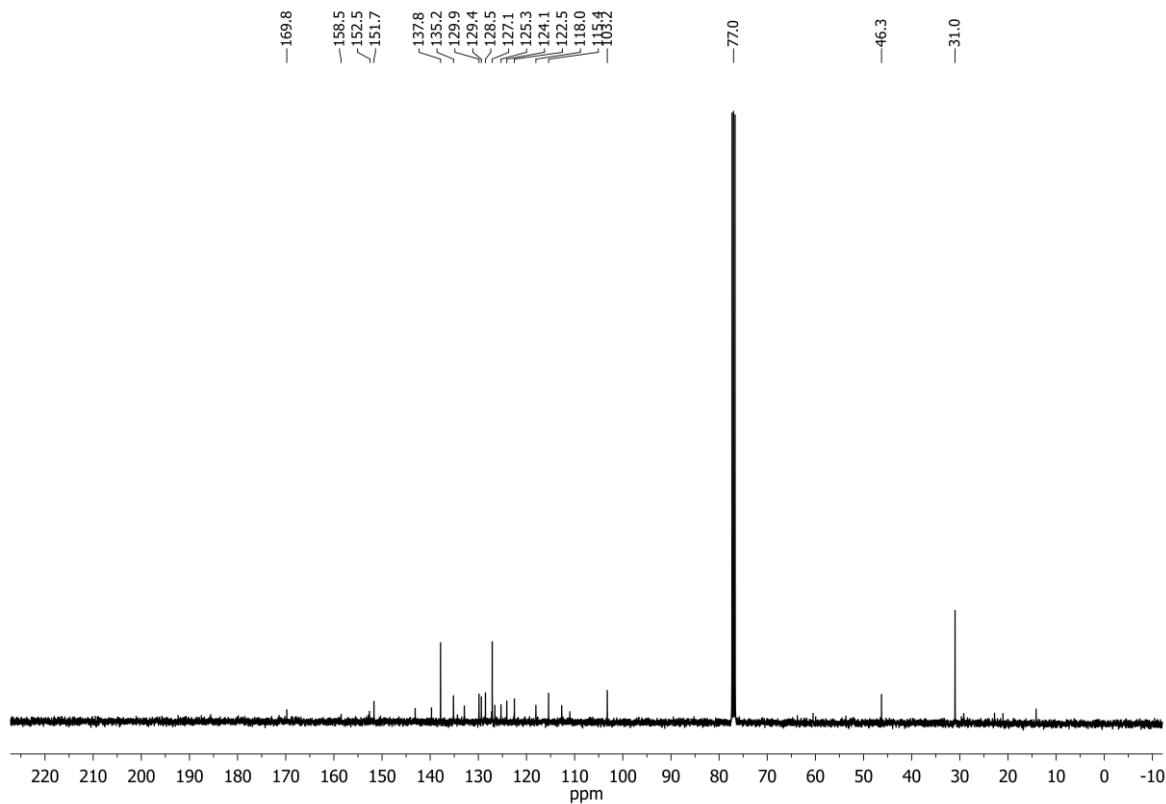


2-(6-(4-(*tert*-Butylthio)phenyl)-3-oxo-3*H*-xanthen-9-yl)benzoic acid (**99**) in CDCl₃

¹H-NMR:



¹³C NMR:



D 2 Pre-kinetic UV-Vis spectra of OXEs

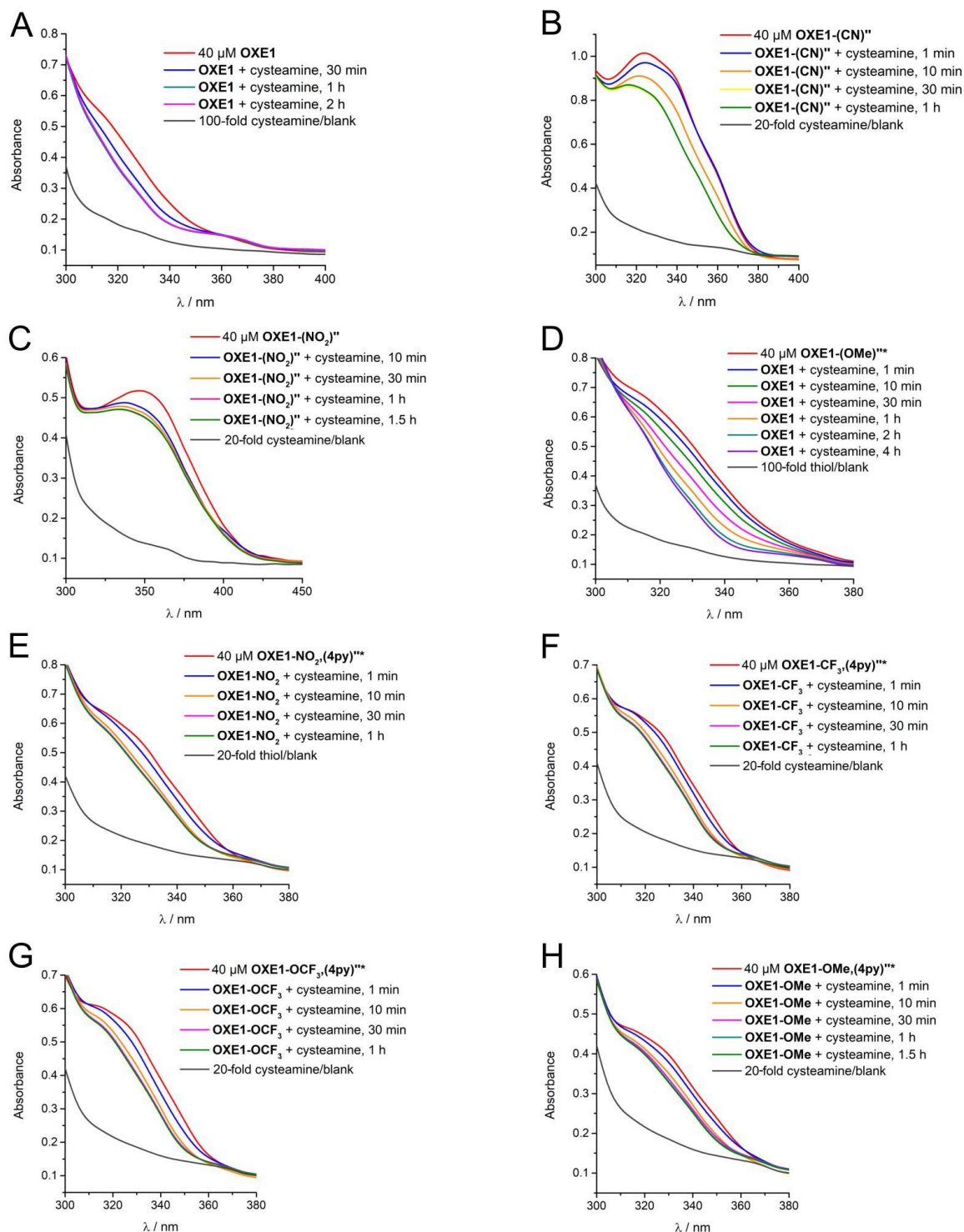


Figure 60: Pre-kinetic UV-Vis investigations: Time-dependent absorption spectra of 40 μM OXEs in 100 mM TRIS-HCl buffer pH 7.4, 2 mM EDTA/ethylene glycol 20:80 with and without cysteamine. **A:** OXE1 + 100-fold cysteamine, **B:** OXE1-(CN)** + 20-fold cysteamine, **C:** OXE1-(NO₂)** + 20-fold cysteamine, **D:** OXE1-(OMe)** + 20-fold cysteamine, * = abbreviated: OXE1; **E:** OXE1-NO₂(4py)** + 20-fold cysteamine, * = abbreviated: OXE1-NO₂; **F:** OXE1-CF₃(4py)** + 20-fold cysteamine, * = abbreviated: OXE1-CF₃; **G:** OXE1-OCF₃(4py)** + 20-fold cysteamine, * = abbreviated OXE1-OCF₃; **H:** OXE1-OMe(4py)** + 20-fold cysteamine, * = abbreviated OXE1-OMe.

Pre-kinetic investigations: Time dependent UV-Vis spectra of OXE1s

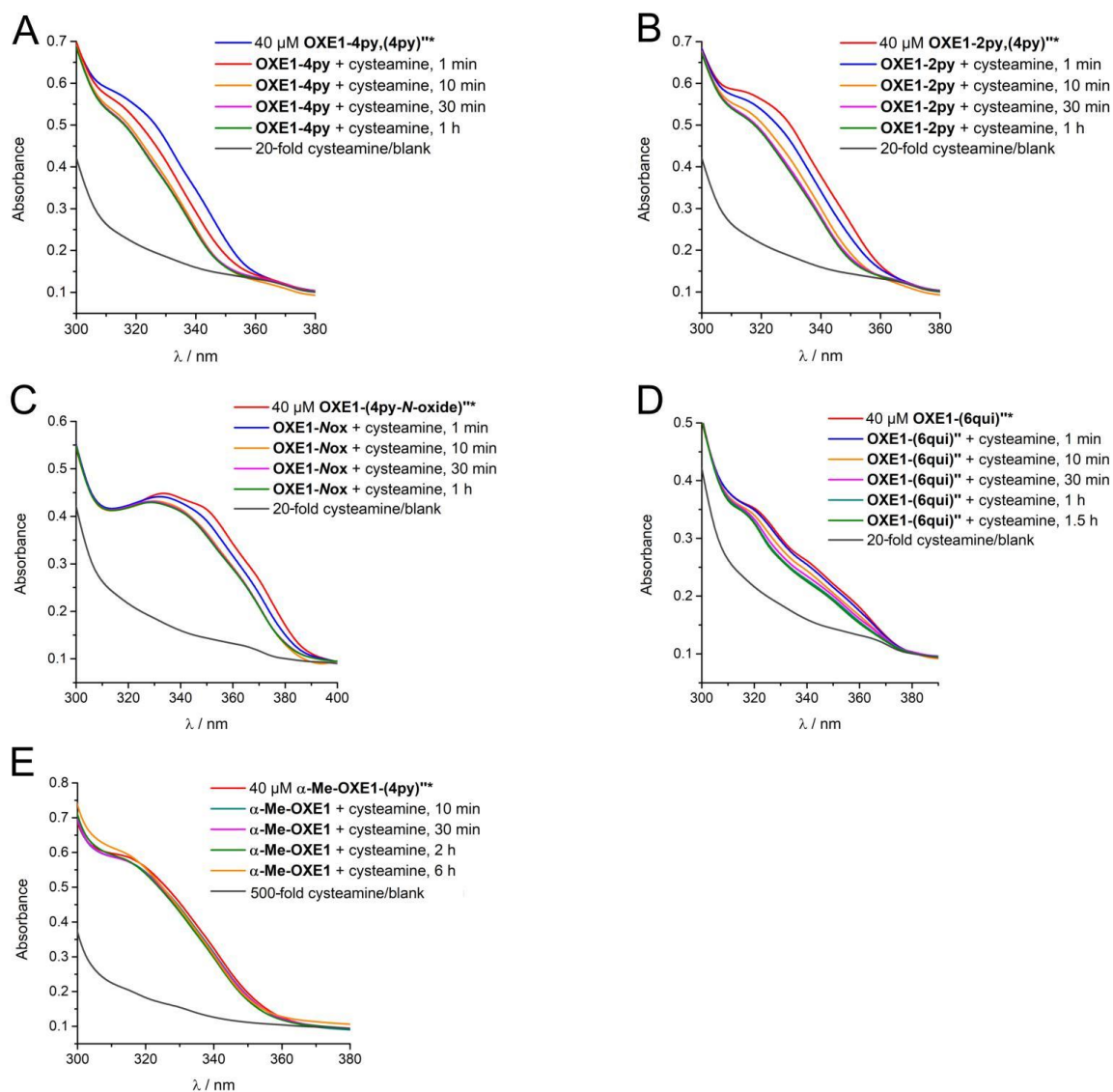


Figure 61: Pre-kinetic UV-Vis investigations: Time-dependent absorption spectra of 40 μM OXE1s in 100 mM TRIS-HCl buffer pH 7.4, 2 mM EDTA/ethylene glycol 20:80 with and without cysteamine. **A:** OXE1-4py,(4py)** + 20-fold cysteamine, * = abbreviated OXE1-4py; **B:** OXE1-2py,(4py)** + 20-fold cysteamine, * = abbreviated OXE1-2py; **C:** OXE1-(4py-N-oxide)** + 20-fold cysteamine, * = abbreviated OXE1-Nox; **D:** OXE1-(6qui)** + 20-fold cysteamine; **E:** α -Me-OXE1 + 500-fold cysteamine, * = abbreviated α -Me-OXE1.

Pre-kinetic investigations: Time dependent UV-Vis spectra of OXE2, OXE3, OXE4, OXE5s

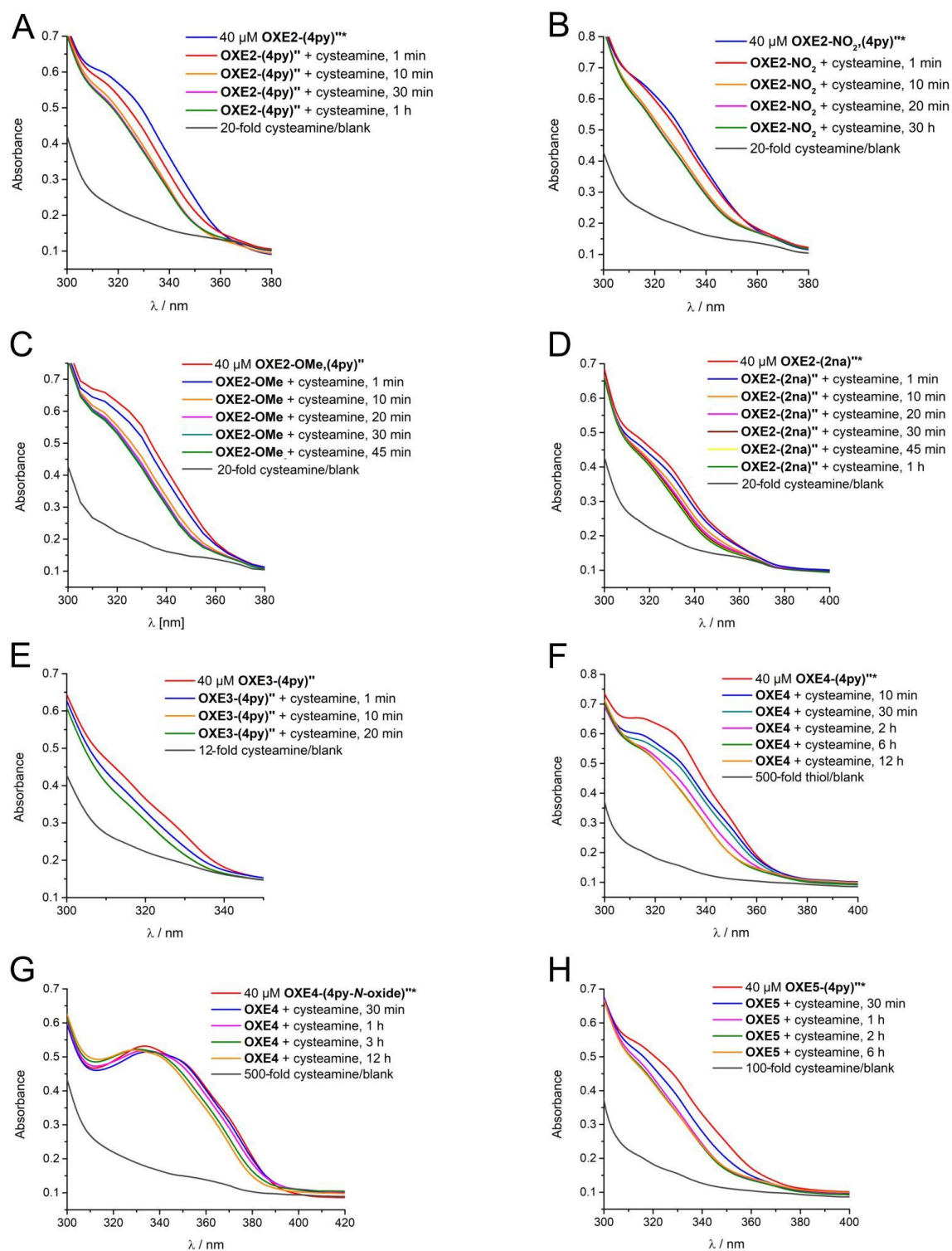


Figure 62: Pre-kinetic UV-Vis investigations: Time-dependent absorption spectra of 40 μM OXEs in 100 mM TRIS-HCl buffer pH 7.4, 2 mM EDTA/ethylene glycol 20:80 with and without cysteamine. **A:** OXE2-(4py)** + 20-fold cysteamine; **B:** OXE2-NO₂-(4py)** + 20-fold cysteamine, * = abbreviated OXE2-NO₂; **C:** OXE2-OMe-(4py)** + 20-fold cysteamine, * = abbreviated OXE2-OMe; **D:** OXE2-(2na)** + 20-fold cysteamine; **E:** OXE3-(4py)** + 20-fold cysteamine; **F:** OXE4-(4py)** + 500-fold cysteamine; **G:** OXE4-(4py-N-oxide)** + 500-fold cysteamine, * = abbreviated OXE4; **H:** OXE5-(4py)** + 100-fold cysteamine.

Pre-kinetic investigations: Time dependent UV-Vis spectra of OXE7s and OXCE

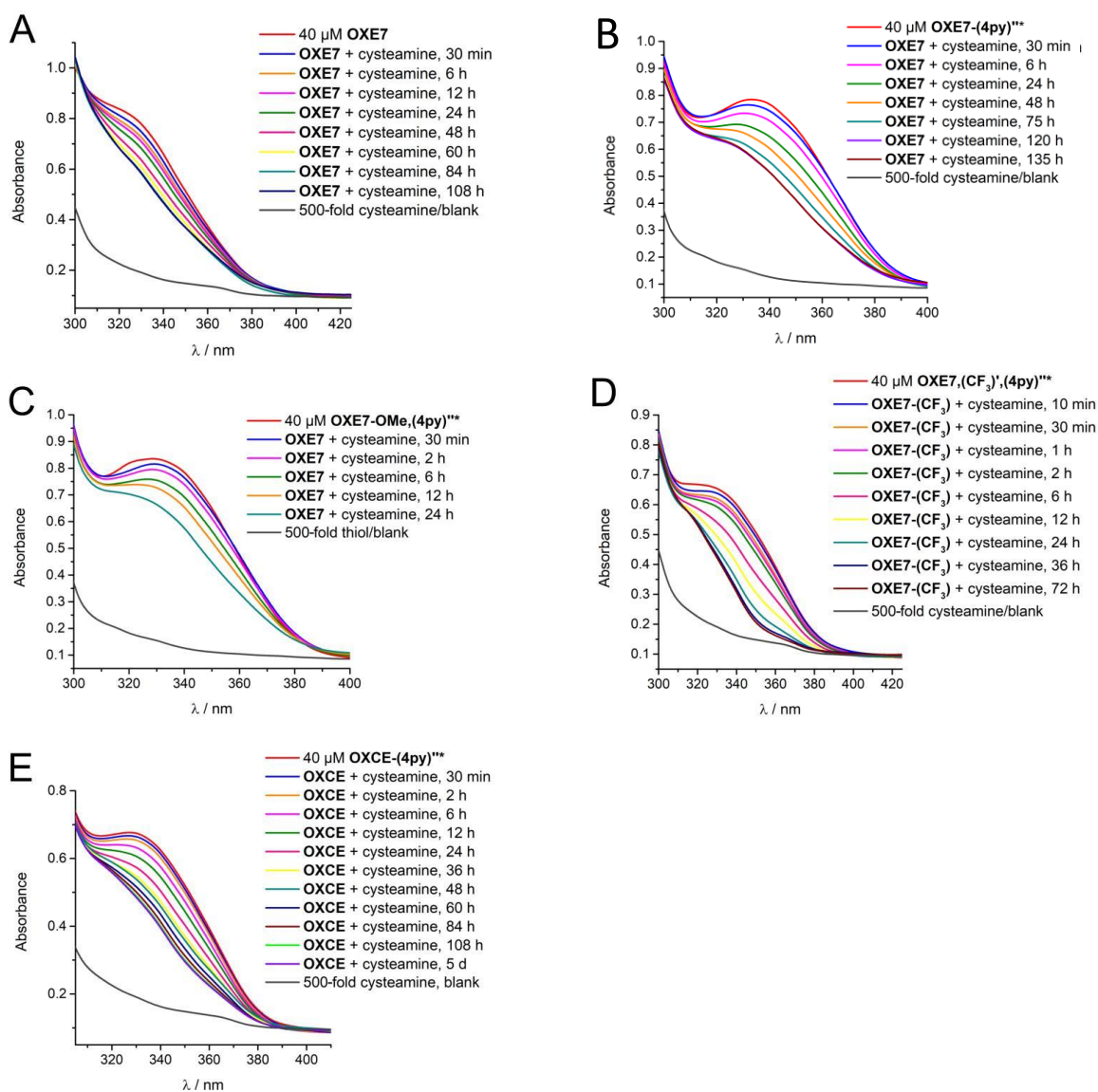


Figure 63: Pre-kinetic UV-Vis investigations: Time-dependent absorption spectra of 40 μM OXEs in 100 mM TRIS-HCl buffer pH 7.4, 2 mM EDTA/ethylene glycol 20:80 with and without cysteamine. **A:** OXE7 + 500-fold cysteamine; **B:** OXE7-(4py)** + 500-fold cysteamine, * = abbreviated OXE7; **C:** OXE7-OMe,(4py)** + 500-fold cysteamine, * = abbreviated OXE7; **D:** OXE7-(CF₃)',(4py)** + 500-fold cysteamine, * = abbreviated OXE7-CF₃; **E:** OXCE-(4py)** + 500-fold cysteamine, * = abbreviated OXCE.

Pre-kinetic investigations: Time dependent UV-Vis spectra of OXE8s

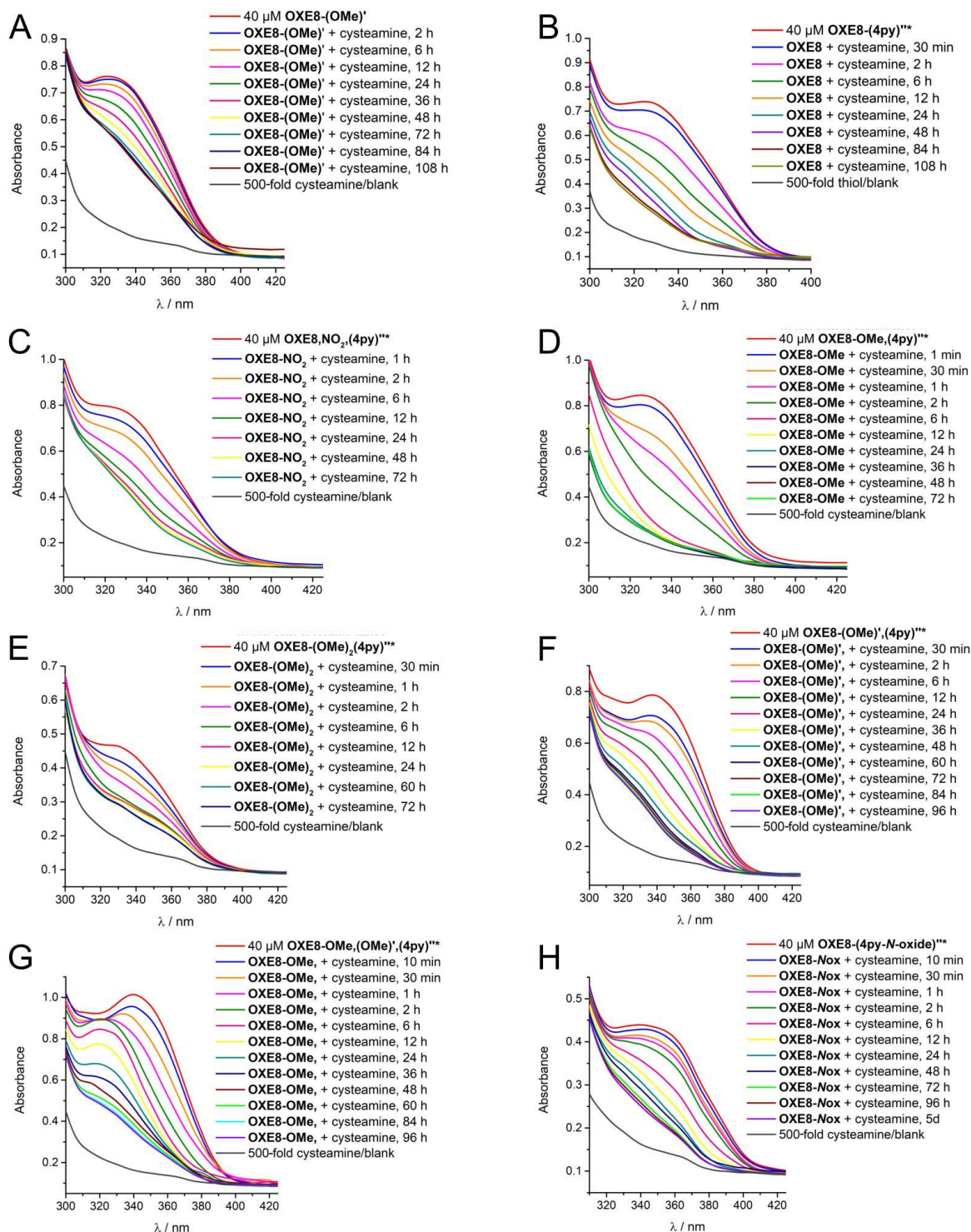


Figure 64: Pre-kinetic UV-Vis investigations: Time-dependent absorption spectra of 40 μM OXE8s in 100 mM TRIS-HCl buffer pH 7.4, 2 mM EDTA/ethylene glycol 20:80 with and without cysteamine. **A:** OXE8-(OMe)['] + 500-fold cysteamine; **B:** OXE8-(4py)^{''} + 500-fold cysteamine, * = abbreviated OXE8; **C:** OXE8-NO₂-(4py)^{''} + 500-fold cysteamine, * = abbreviated OXE8-NO₂; **D:** OXE8-OMe-(4py)^{''} + 500-fold cysteamine, * = abbreviated OXE8-OMe; **E:** OXE8-(OMe)₂-(4py)^{''} + 500-fold cysteamine, * = abbreviated OXE8-(OMe)₂; **F:** OXE8-(OMe)[']-(4py)^{''} + 500-fold cysteamine, * = abbreviated OXE8-(OMe)[']; **G:** OXE8-OMe-(OMe)[']-(4py)^{''} + 500-fold cysteamine, * = abbreviated OXE8-OMe; **H:** OXE8-(4py-N-oxide)^{''} + 500-fold cysteamine, * = abbreviated OXE8-Nox.

D 3 Additional figures for the kinetic evaluation of OXEs and OXE analogues

Decay figures of the stopped-flow assay of OXE3-(4py)" with cysteamine 100-300 fold

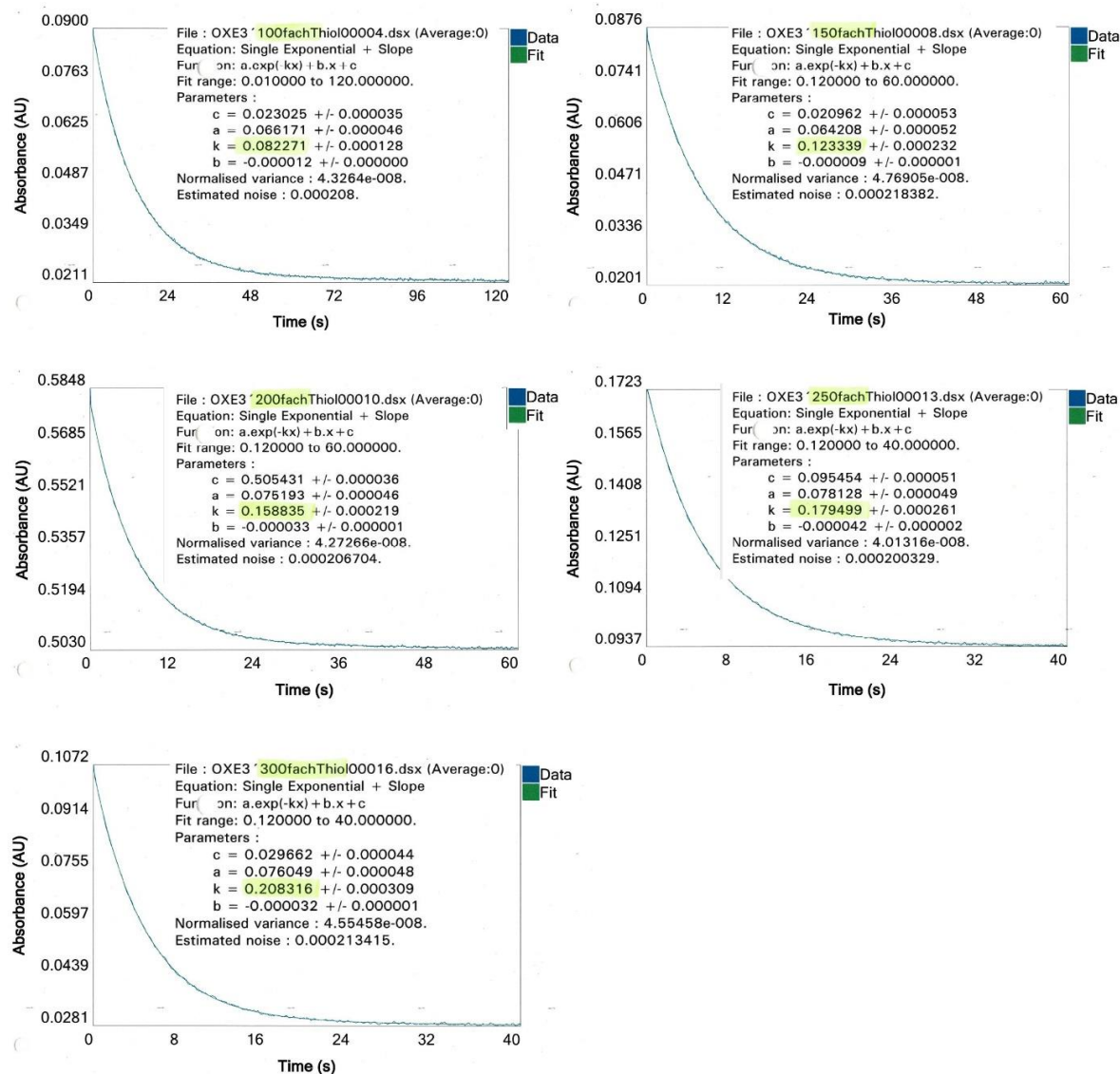


Figure 65: Representative exponential decay curves for the reaction of 40 μM OXE3-(4py)" with 100, 150, 200, 250 and 300 fold of cysteamine in 100 mM TRIS-HCl buffer pH 7.4, 2 mM EDTA/ethylene glycol 20:80. The measurement was done by stopped-flow technique. The results of the k_{obs} values are given as k values.

Decay curves from plate assay of OXE1 with cysteamine (part 1)

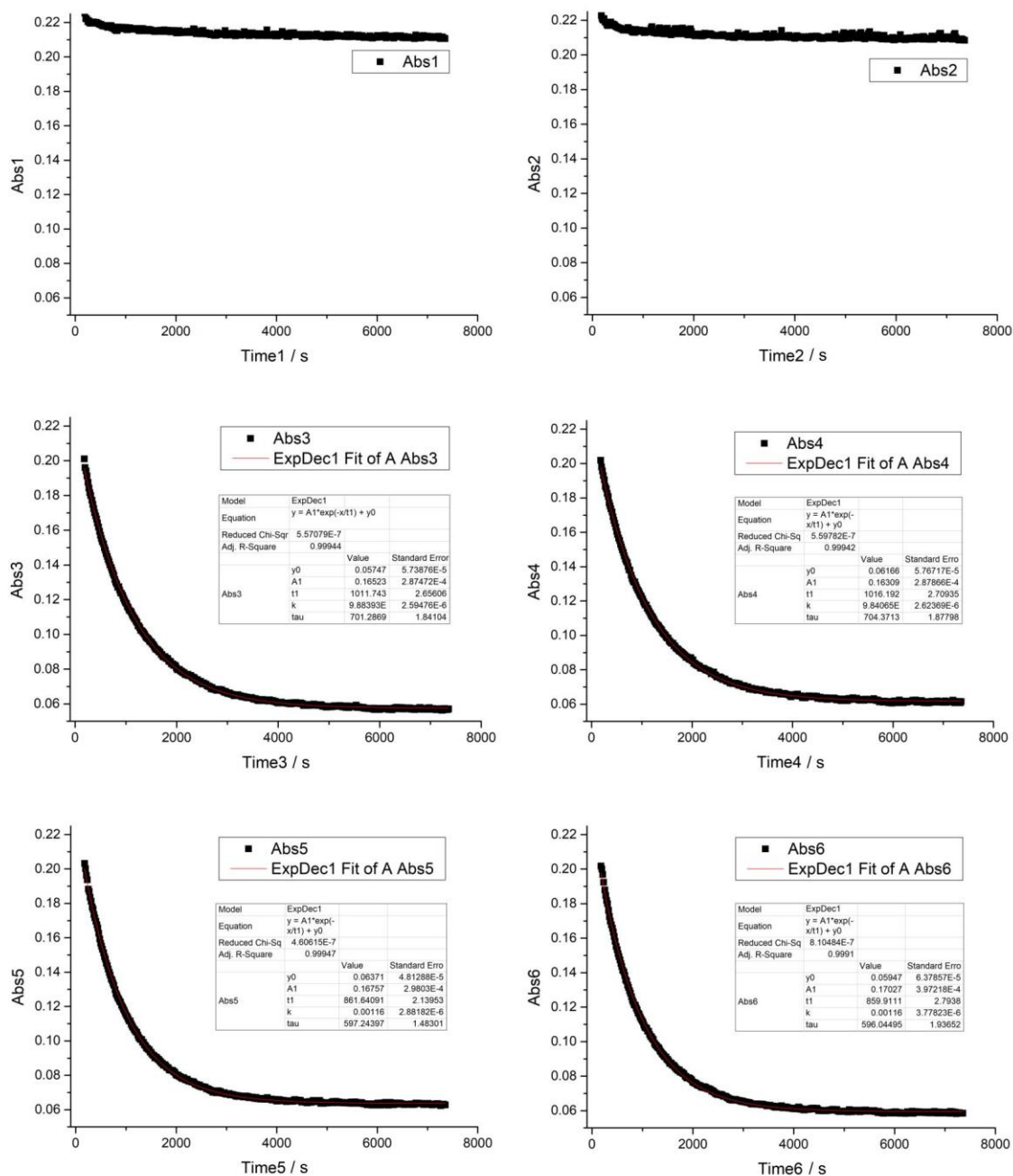


Figure 66: Representative exponential decay curves for the reaction of 40 μM OXE1 with 0, 60 and 72 fold of cysteamine at 330 nm in 100 mM TRIS-HCl buffer pH 7.4, 2 mM EDTA/ethylene glycol 20:80 (duplicates). 380 data points were gained all 18 s. The results of the $1/k_{\text{obs}}$ values are given in the little tables as t1 values.

Decay curves from plate assay of OXE1 with cysteamine (part 2)

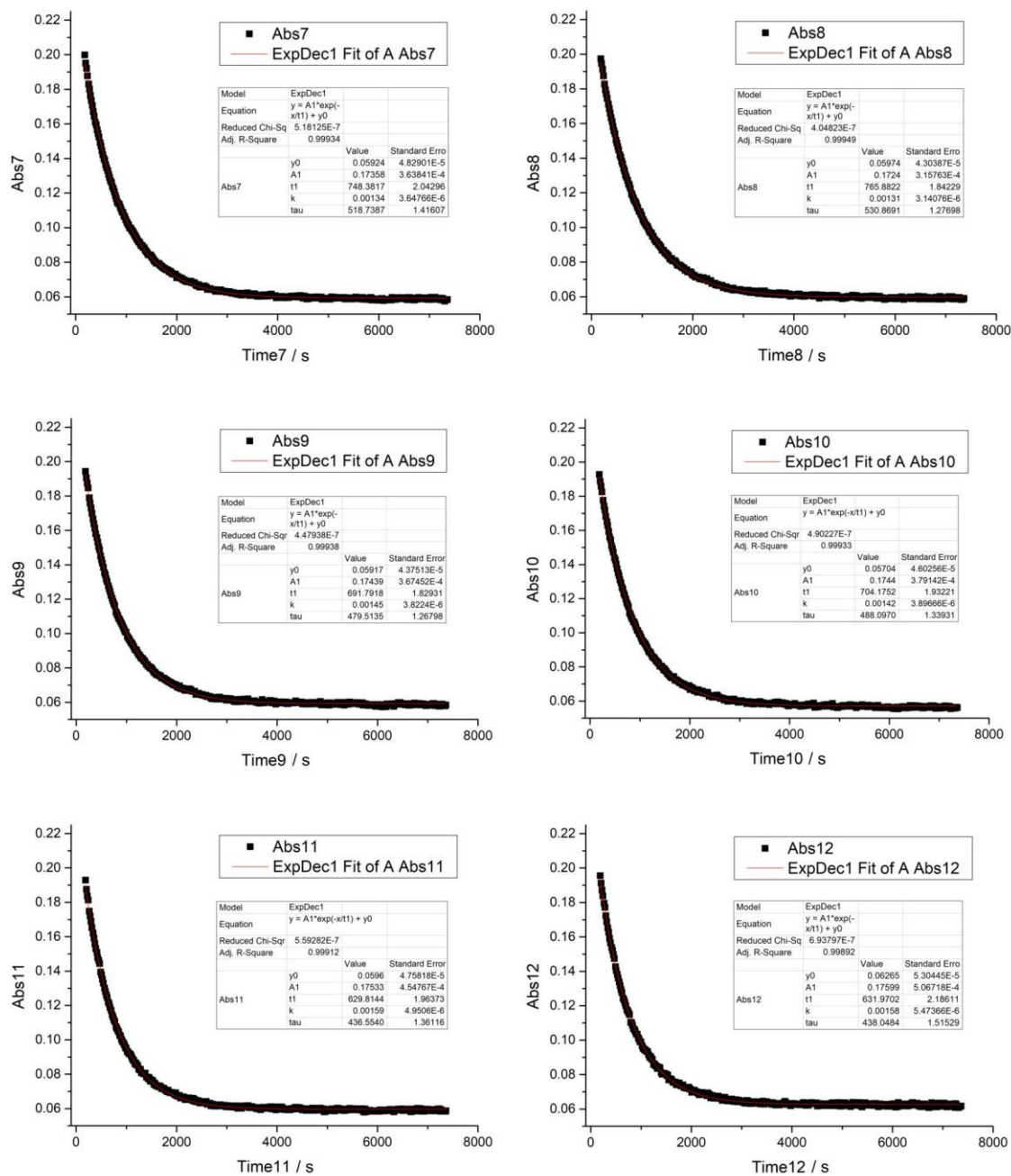


Figure 67: Representative exponential decay curves for the reaction of 40 μM OXE1 with 84, 96 and 108 fold of cysteamine at 330 nm in 100 mM TRIS-HCl buffer pH 7.4, 2 mM EDTA/ethylene glycol 20:80 (duplicates). 380 data points were gained all 18 s. The results of the $1/k_{\text{obs}}$ values are given in the little tables as t1 values.

k_2 determinations of OXE1, OXE1-(CN)^{''}, OXE1-(NO₂)^{''}, OXE1-(OMe)^{''}, OXE1-(4py)^{''} and OXE1-NO₂,(4py)^{''} with cysteamine by linear regression

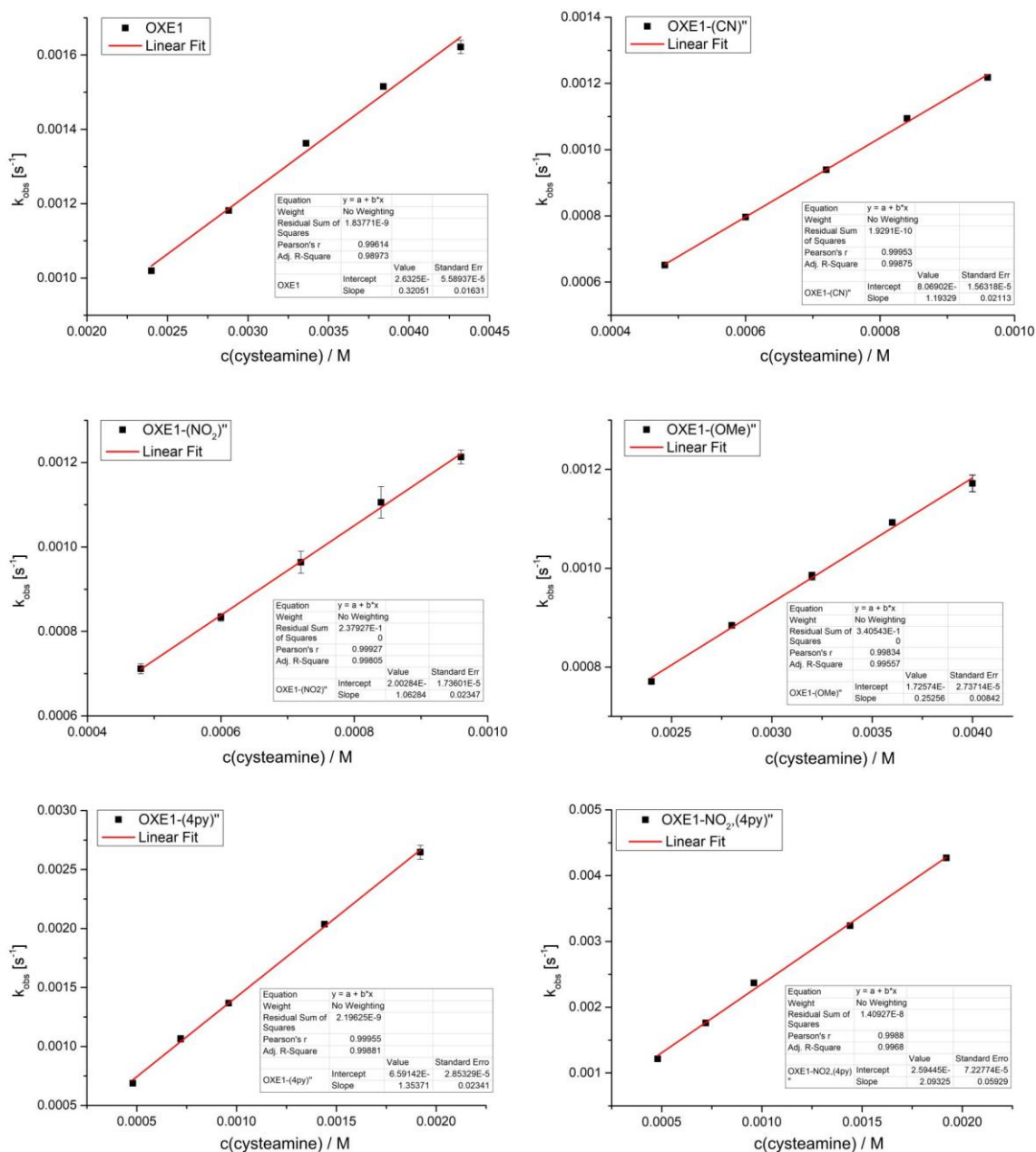


Figure 68: Representative k_2 value determinations for compounds **OXE1**, **OXE1-(CN)^{''}**, **OXE1-(NO₂)^{''}**, **OXE1-(OMe)^{''}**, **OXE1-(4py)^{''}** and **OXE1-NO₂,(4py)^{''}** with cysteamine. K_{obs} values were plotted against cysteamine concentrations and a linear fit was applied to give the corresponding k_2 values.

k_2 determinations of OXE1-CF₃,(4py)", OXE1-OCF₃,(4py)", OXE1-OMe,(4py)", OXE1-4py,(4py)", OXE1-2py,(4py)" and OXE1-(4py-N-oxide)" with cysteamine by linear regression

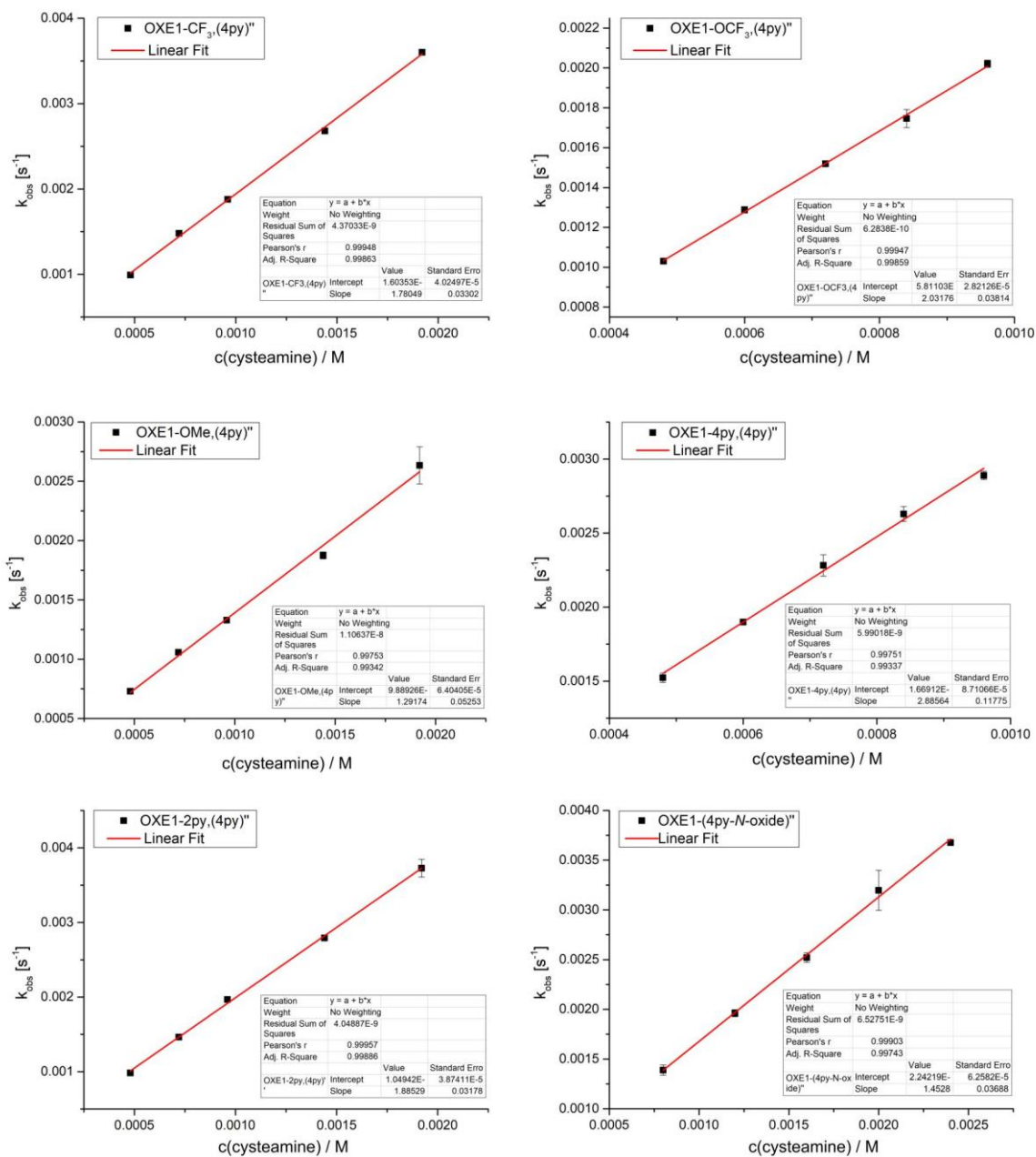


Figure 69: Representative k_2 value determinations for compounds OXE1-CF₃,(4py)", OXE1-OCF₃,(4py)", OXE1-OMe,(4py)", OXE1-4py,(4py)", OXE1-2py,(4py)" and OXE1-(4py-N-oxide)" with cysteamine. K_{obs} values were plotted against cysteamine concentrations and a linear fit was applied to give the corresponding k_2 values.

k_2 determinations of OXE1-(6qui)"', OXE2-(4py)"', OXE2-NO₂-(4py)"', OXE2-OMe-(4py)"', OXE2-(2na)"' and OXE3-(4py)"' with cysteamine by linear regression

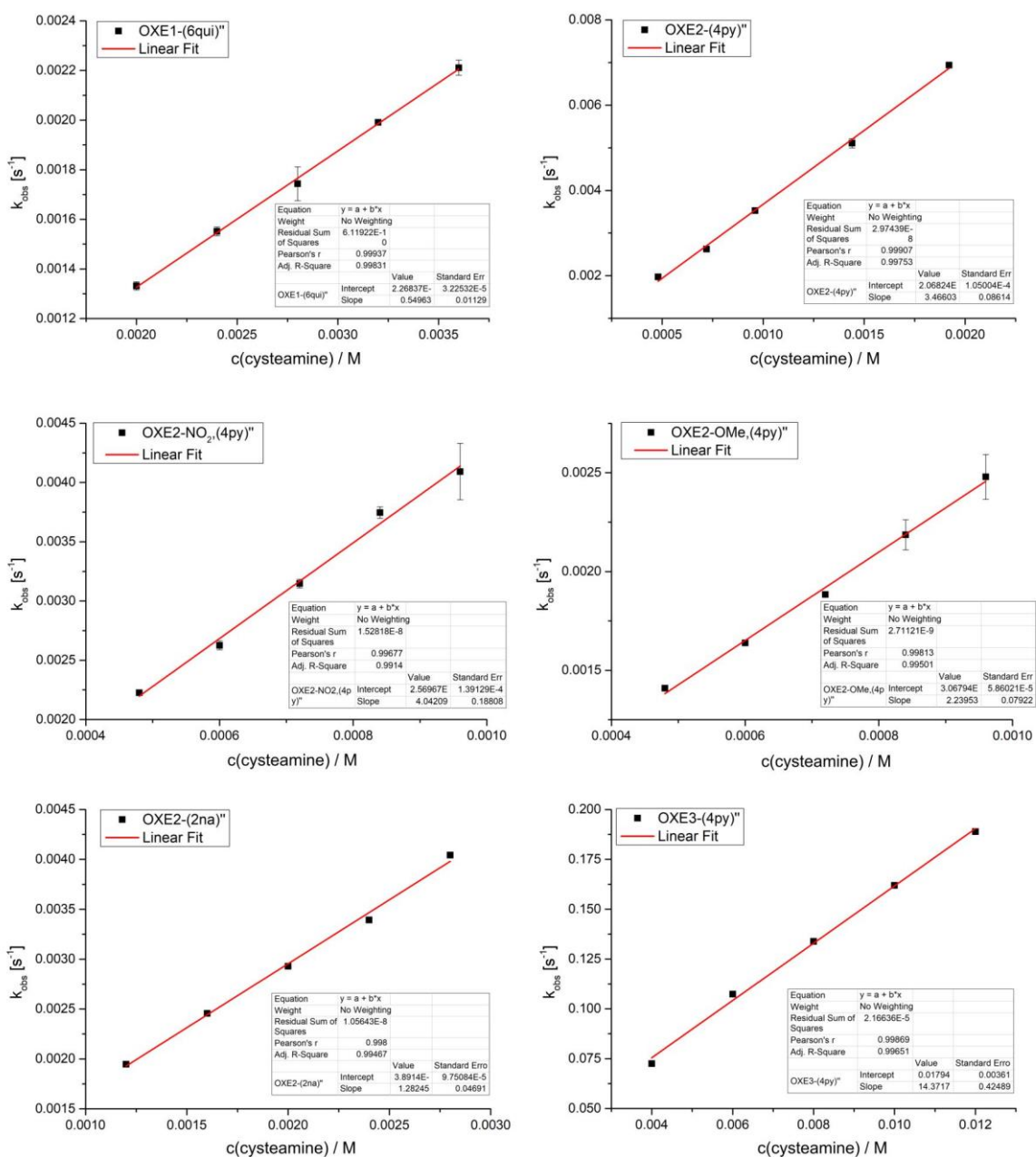


Figure 70: Representative k_2 value determinations for compounds OXE1-(6qui)"', OXE2-(4py)"', OXE2-NO₂-(4py)"', OXE2-OMe-(4py)"', OXE2-(2na)"' and OXE3-(4py)"' with cysteamine. k_{obs} values were plotted against cysteamine concentrations and a linear fit was applied to give the corresponding k_2 values.

k_2 determinations of OXE4-(4py)^{''}, OXE4-(4py-N-oxide)^{''}, OXE5-(4py)^{''}, OXE7-CF₃-(4py)^{''}, OXE8-(4py)^{''} and OXE8-NO₂-(4py)^{''} with cysteamine by linear regression

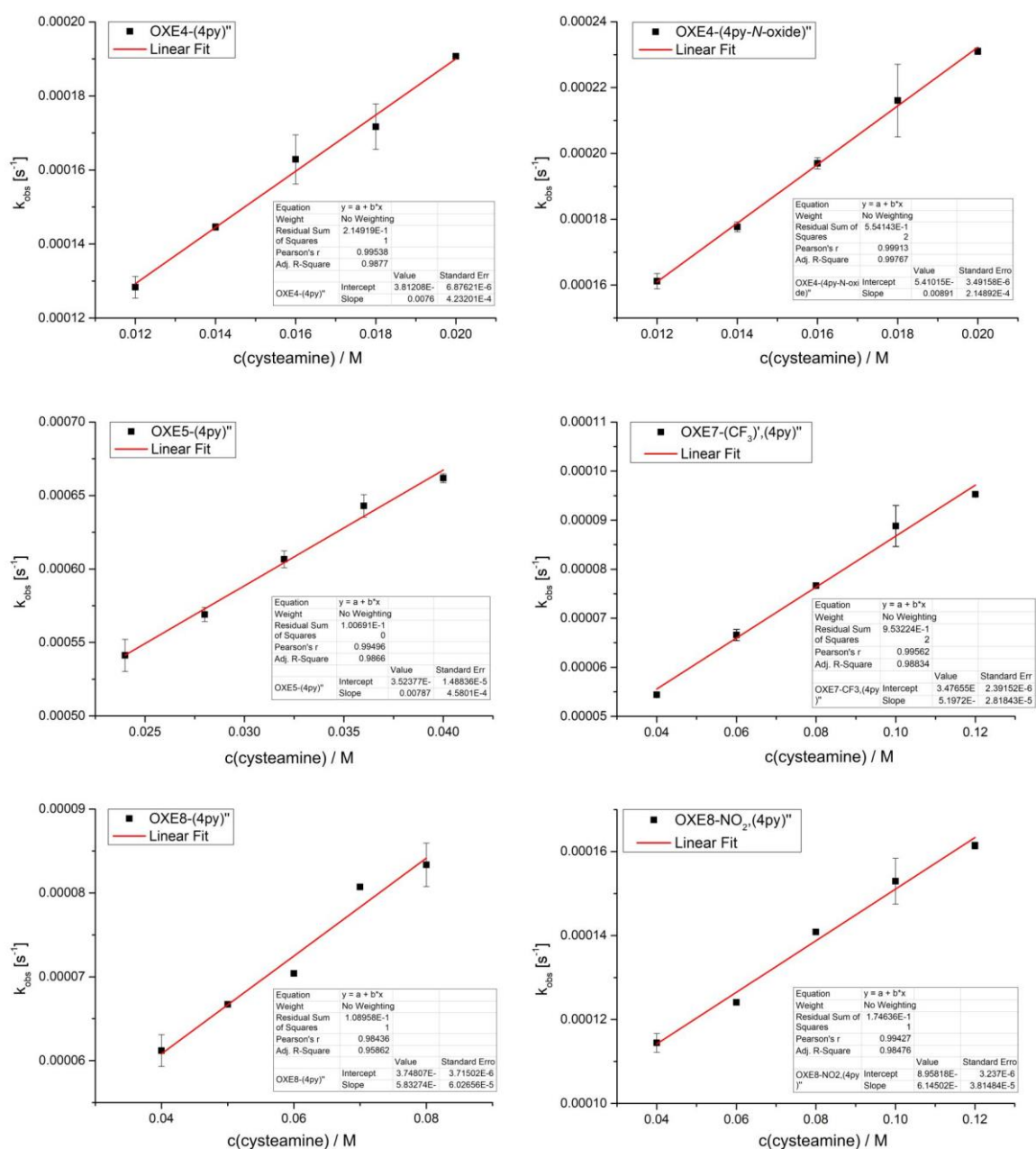


Figure 71: Representative k_2 value determinations for compounds OXE4-(4py)^{''}, OXE4-(4py-N-oxide)^{''}, OXE5-(4py)^{''}, OXE7-CF₃-(4py)^{''}, OXE8-(4py)^{''} and OXE8-NO₂-(4py)^{''} with cysteamine. k_{obs} values were plotted against cysteamine concentrations and a linear fit was applied to give the corresponding k_2 values.

k_2 determinations of OXE8-OMe,(4py)"', OXE8-(OMe)₂(4py)"', OXE8-OMe,(NO₂),(4py)"', OXE8-(OMe)',(4py)"', OXE8-OMe,(OMe)',(4py)"' and OXE8-(4py-N-oxide)"' with cysteamine by linear regression

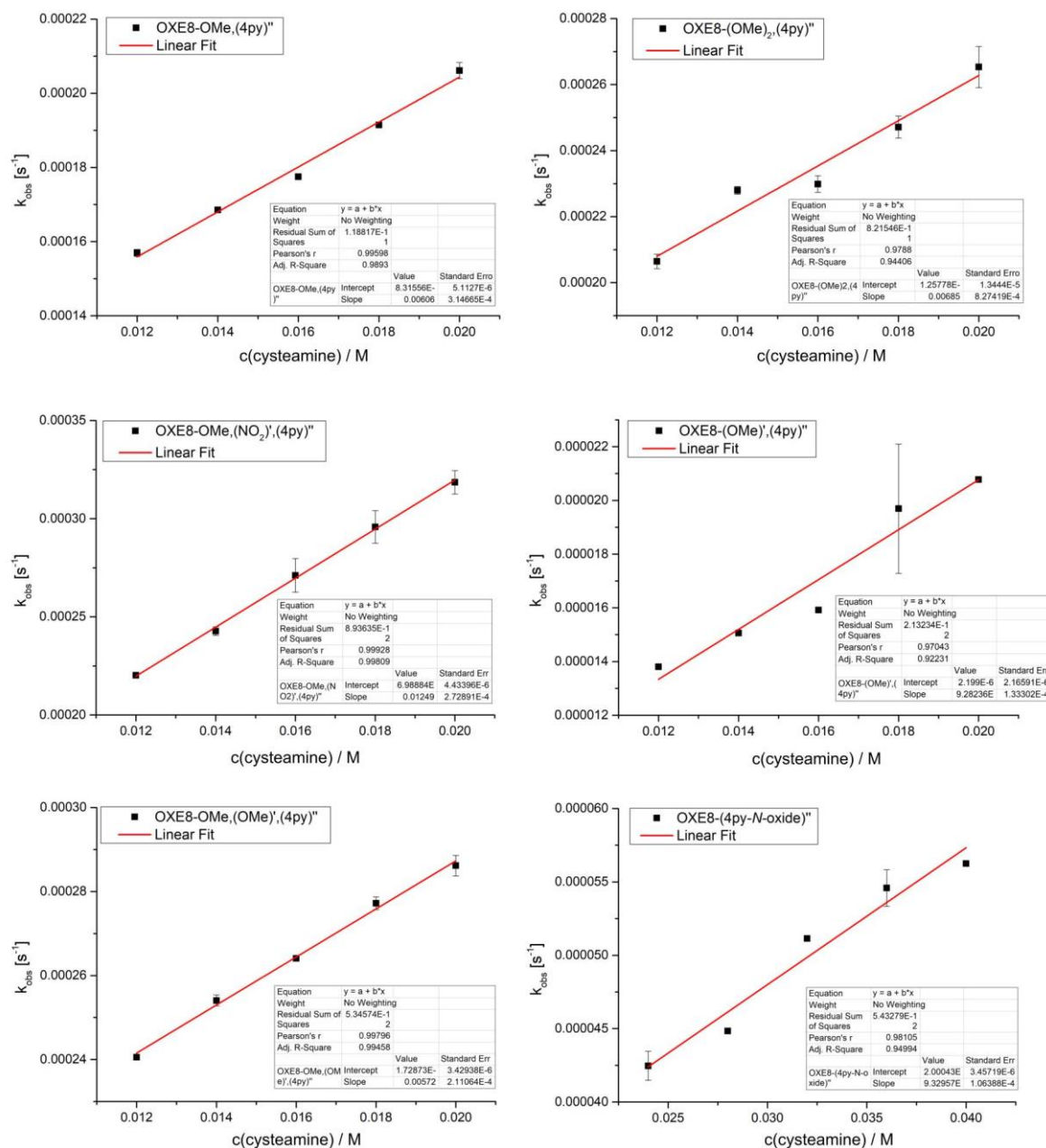


Figure 72: Representative k_2 value determinations for compounds OXE8-OMe,(4py)"', OXE8-(OMe)₂(4py)"', OXE8-OMe,(NO₂),(4py)"', OXE8-(OMe)',(4py)"', OXE8-OMe,(OMe)',(4py)"' and OXE8-(4py-N-oxide)"' with cysteamine. k_{obs} values were plotted against cysteamine concentrations and a linear fit was applied to give the corresponding k_2 values.

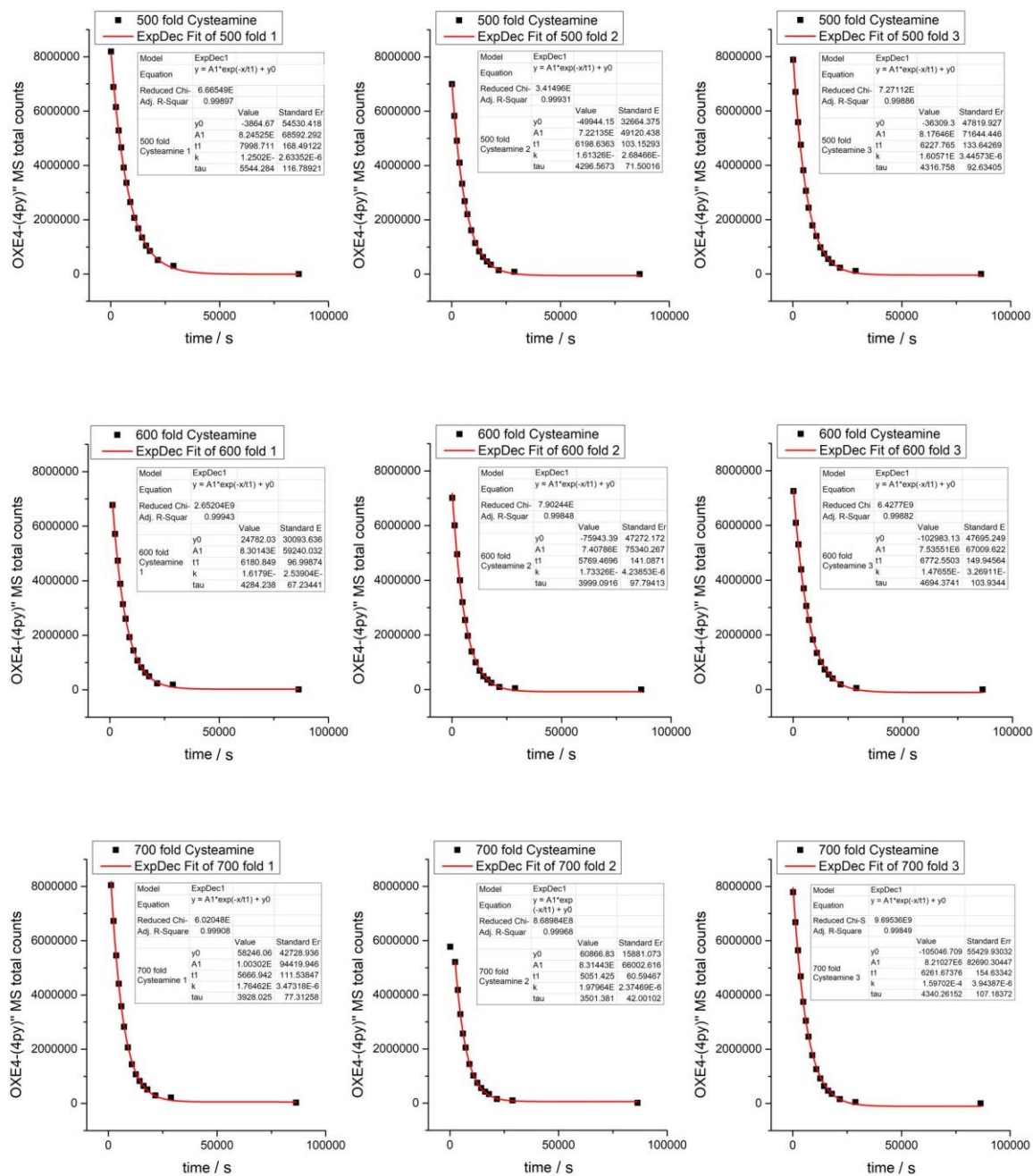
Decay curves from MS kinetic assay of OXE4-(4py)⁺ with cysteamine

Figure 73: All exponential decay curves for the reaction of 40 μM OXE4-(4py)⁺ with 500, 600 and 700 fold of cysteamine in 100 mM TRIS-HCl buffer pH 7.4, 2 mM EDTA/ethylene glycol 20:80 (triplicates). Data points were gained after 2, 20, 40, 60, 80, 100, 120 min, then 2.5, 3, 3.5, 4, 4.5, 5, 6, 8 and 24 h. In some cases, the 2 and/or 20 min data point is missing due to detection issues: no substance detectable. The results of the $1/k_{\text{obs}}$ values are given in the little tables as t1 values.

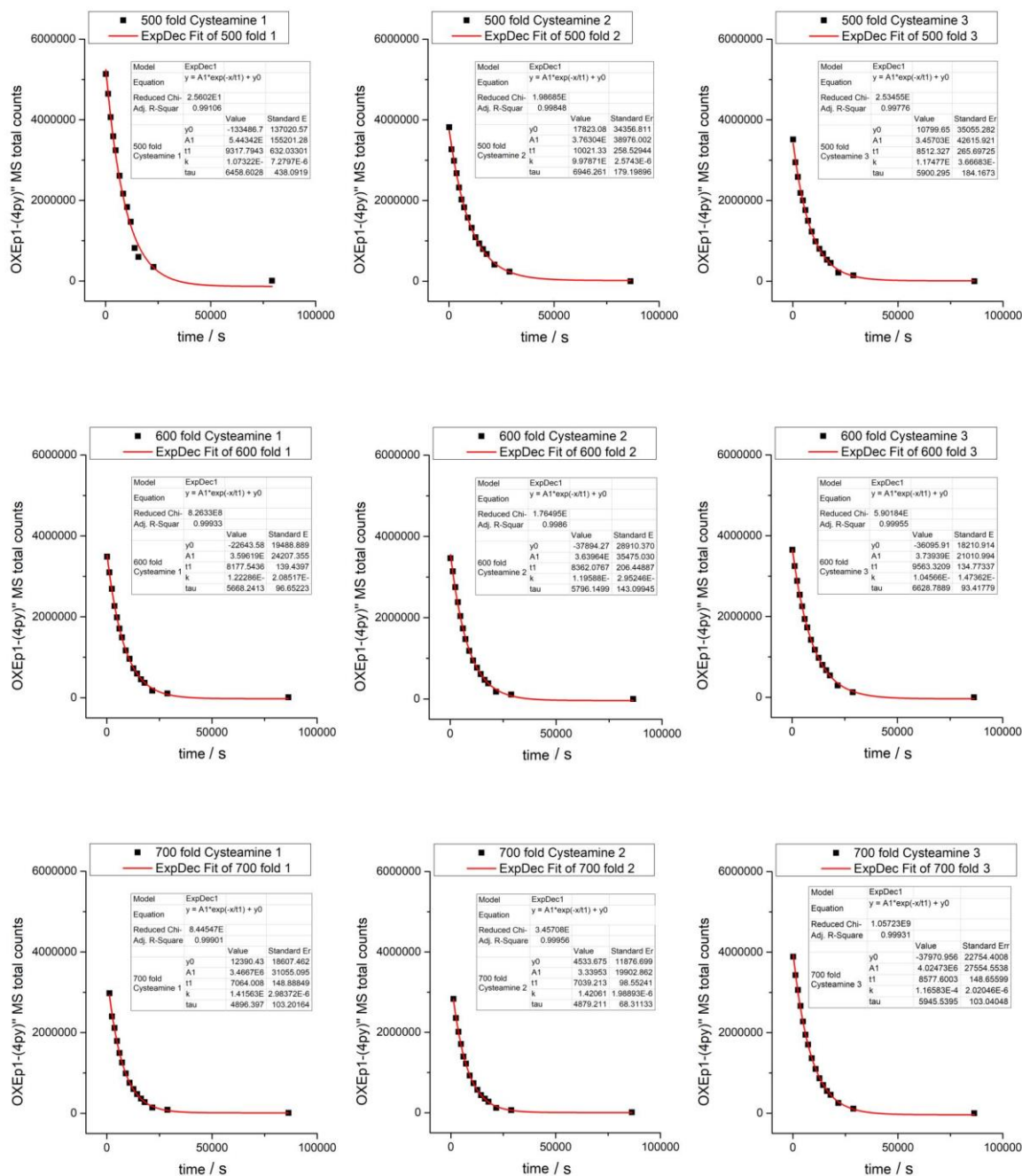
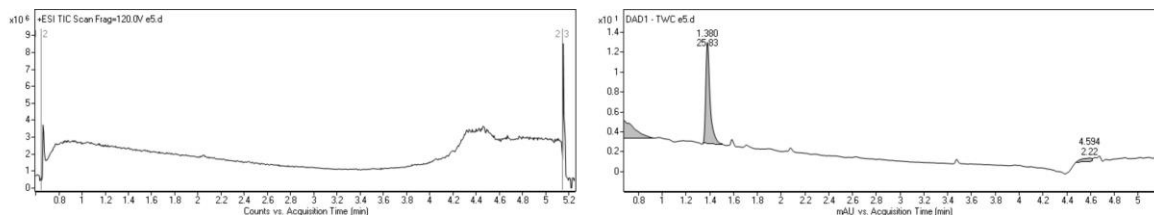
Decay curves from MS kinetic assay of OXEp1-(4py)⁺ with cysteamine

Figure 74: All exponential decay curves for the reaction of 40 μM OXEp1-(4py)⁺ with 500, 600 and 700 fold of cysteamine in 100 mM TRIS-HCl buffer pH 7.4, 2 mM EDTA/ethylene glycol 20:80 (triplicates). Data points were gained after 2, 20, 40, 60, 80, 100, 120 min, then 2.5, 3, 3.5, 4, 4.5, 5, 6, 8 and 24 h. In some cases, the 2 and/or 20 min data point is missing due to detection issues: no substance detectable. The results of the $1/k_{\text{obs}}$ values are given in the little tables as t1 values.

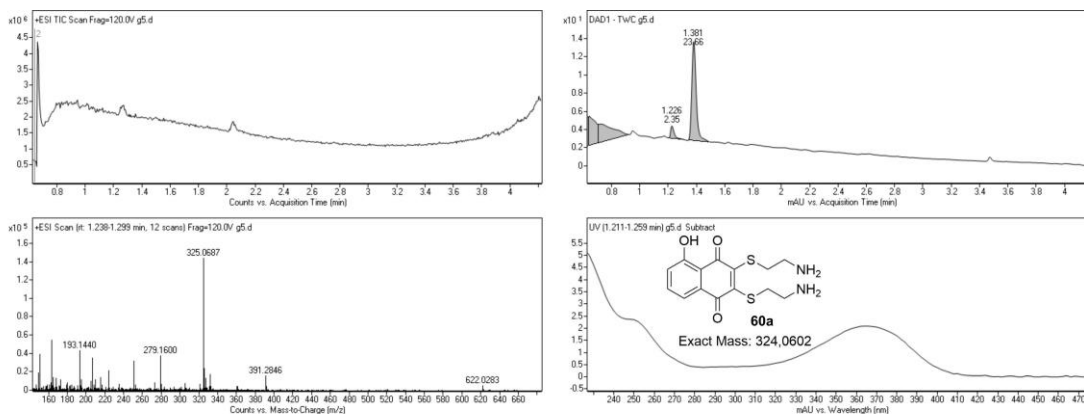
D 4 LC-MS data of juglone derivatives in kinetic assay buffer

Note: Only compounds with distinct and conclusive MS **AND** UV-Vis data were evaluated. Assay fragments and other unknown compounds which appeared only in the LC-run and/or in the UV-Vis detection with no evaluable MS data and/or no UV-Vis absorbance > 200 nm were not considered in the evaluation.

80 μ M juglon (33a) without cysteamine after 10 min – 1 h

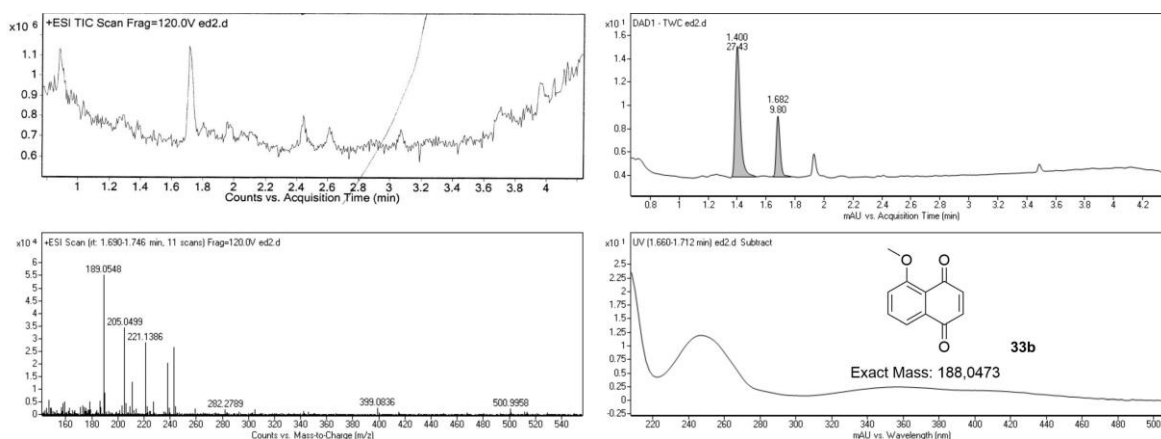


80 μ M juglon (33a) with 500-fold cysteamine after 10 min – 1 h

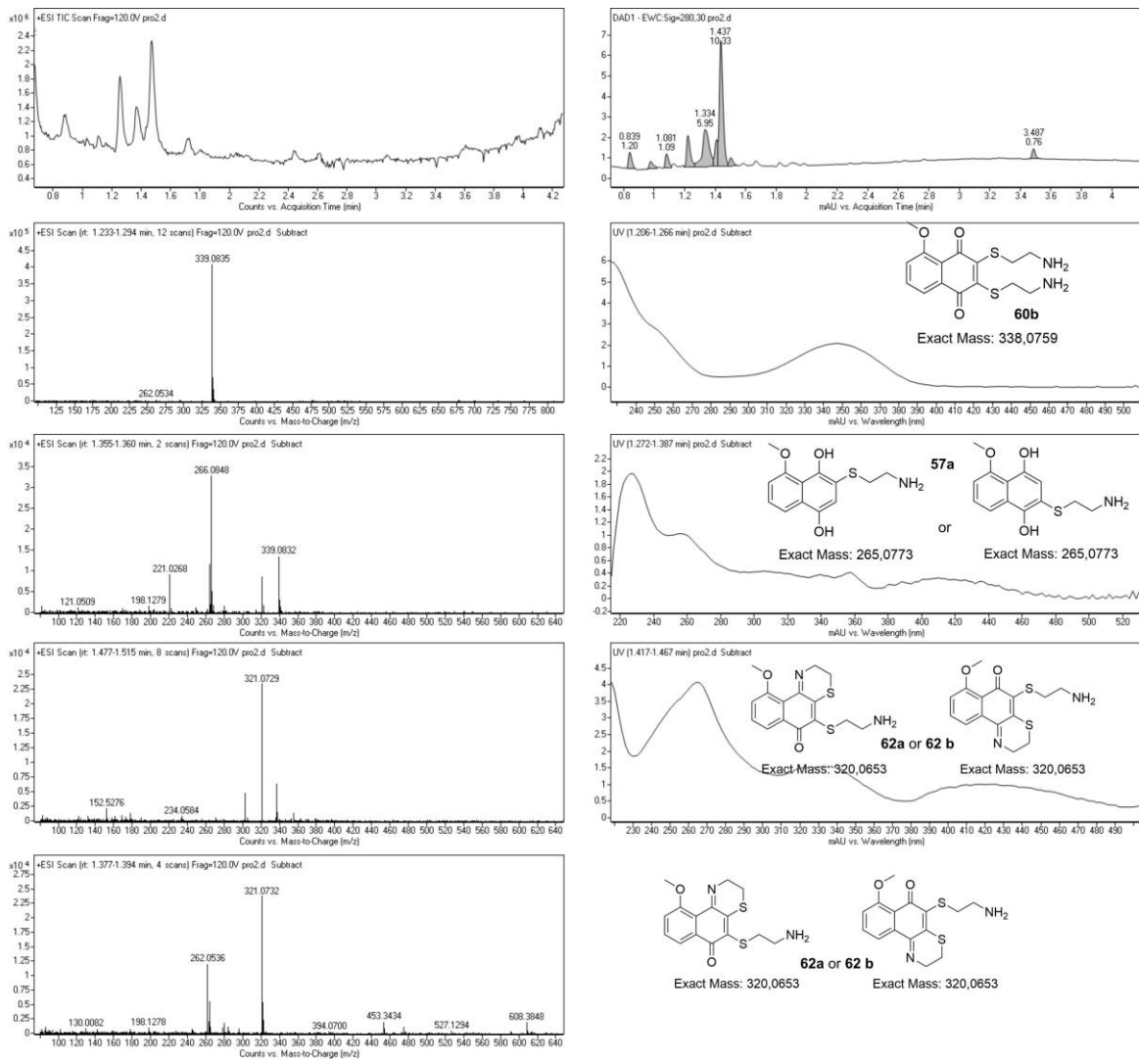


33b

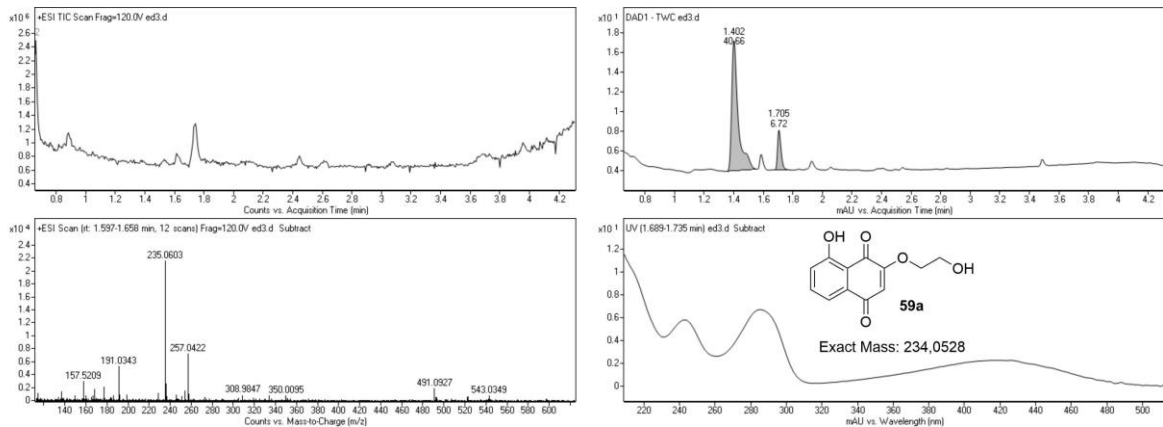
40 μ M *O*-methyljuglon (33b) without cysteamine after 3-5 h

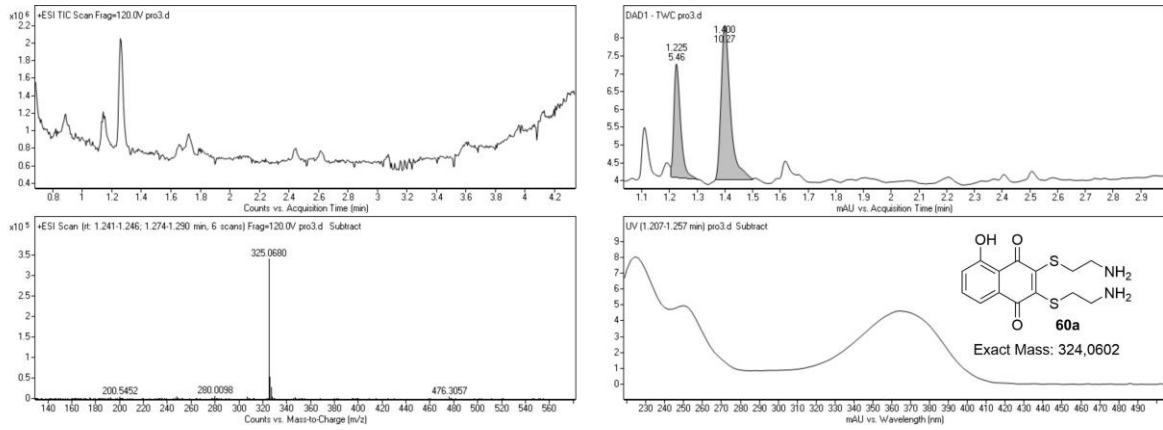
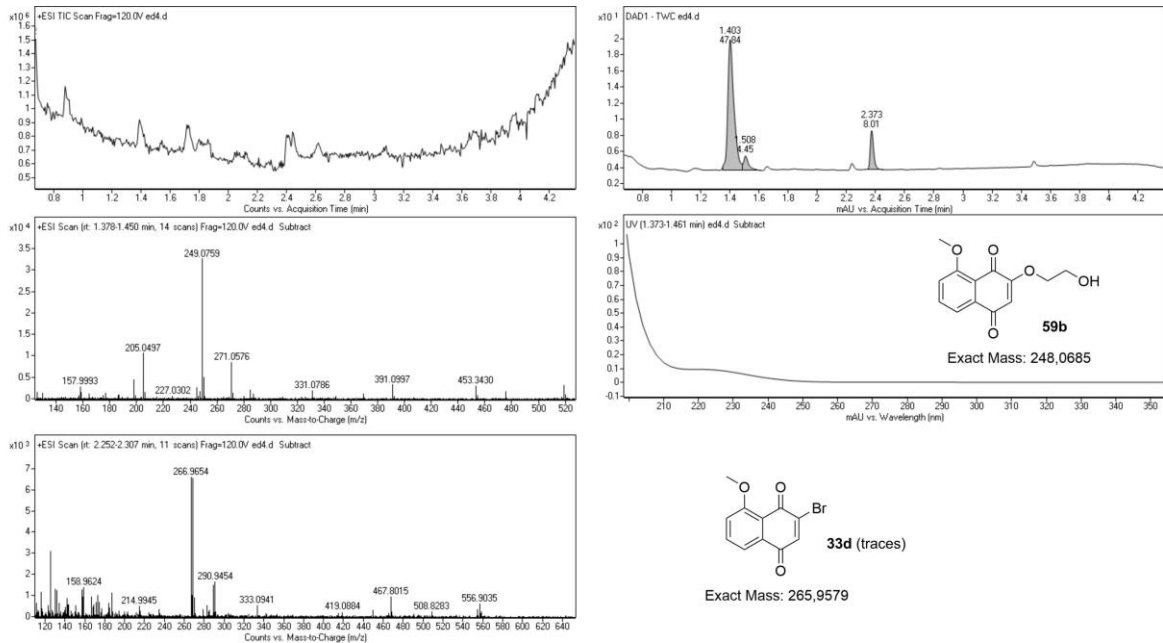


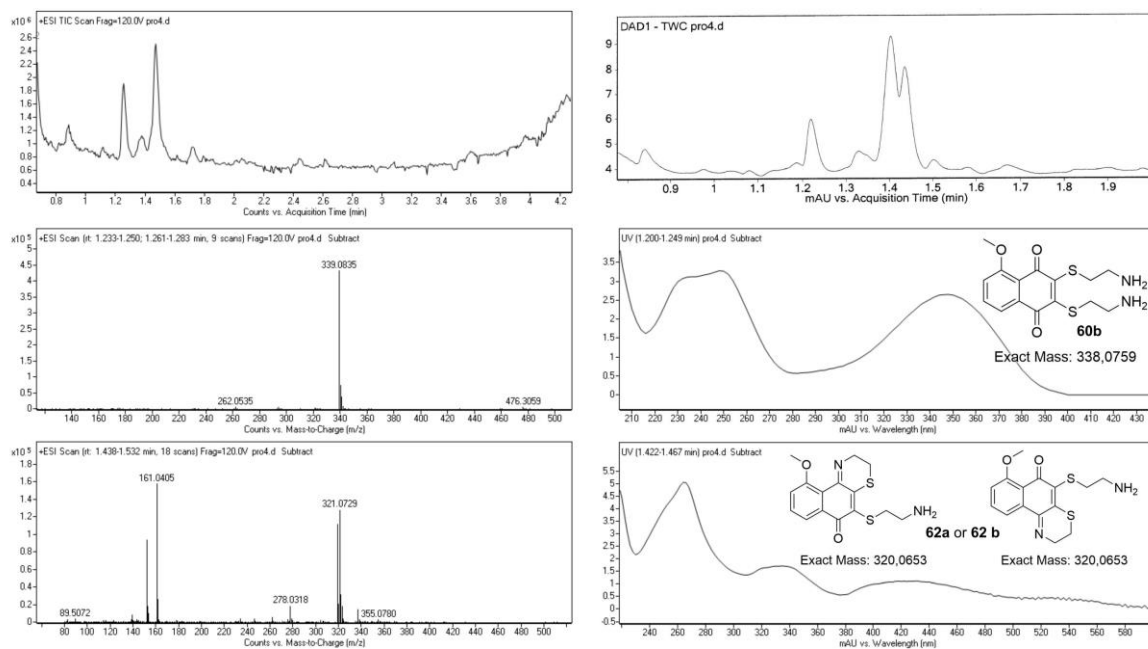
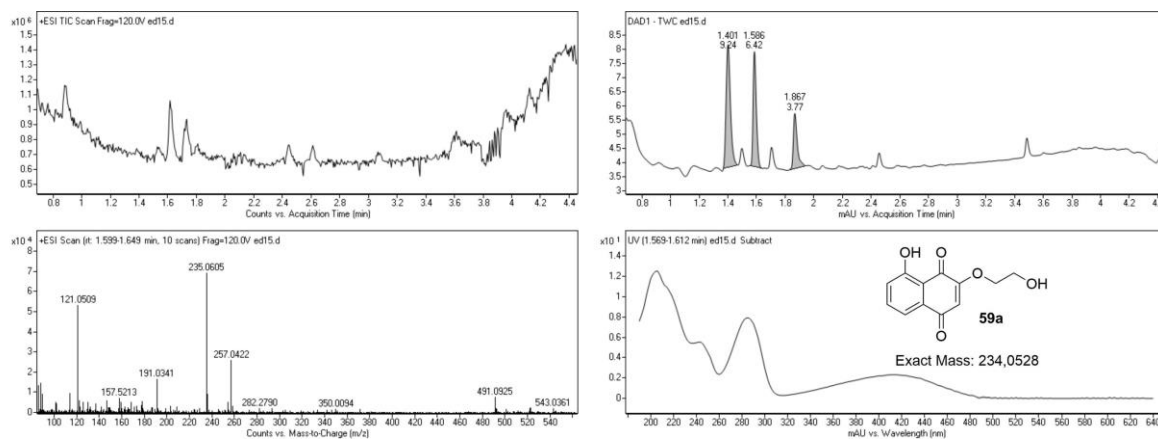
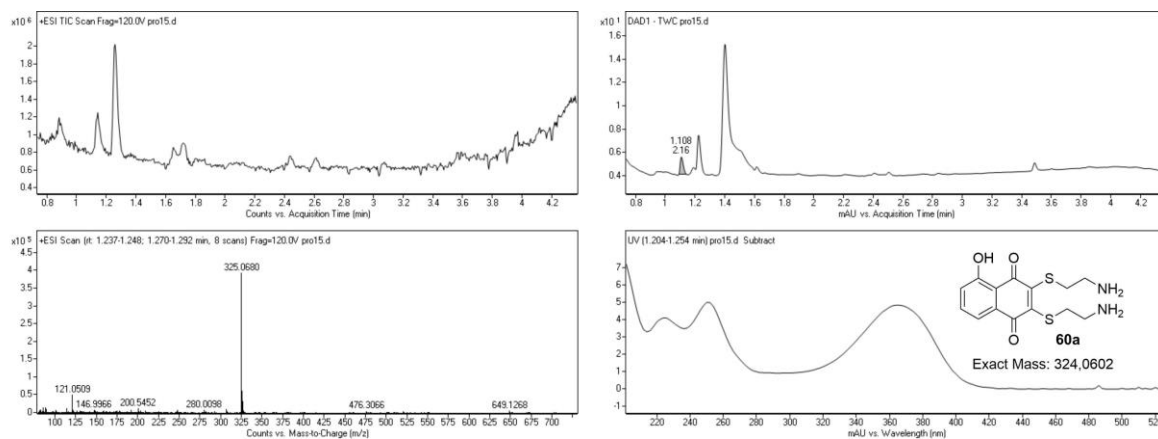
40 μ M *O*-methyljuglon (33b) with 500-fold cysteamine after 3-5 h



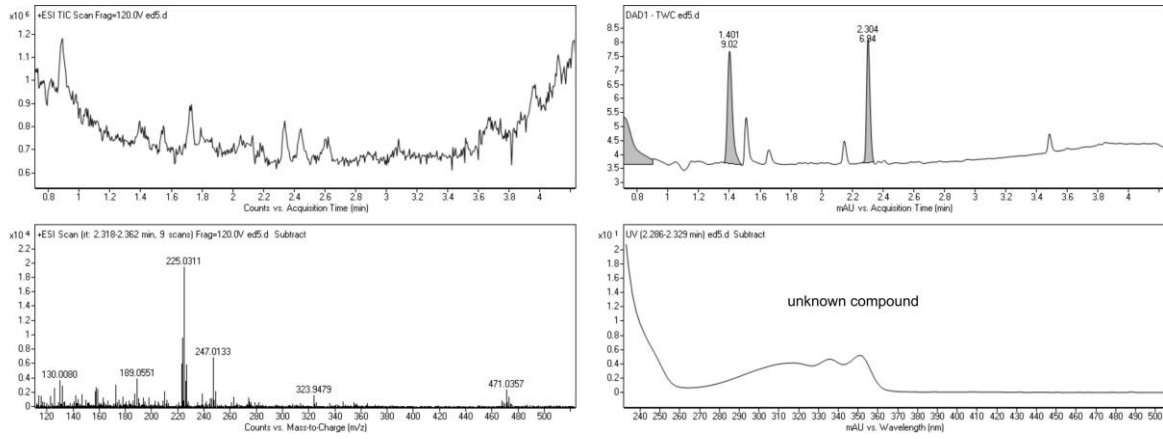
40 μ M 3-bromojuglon (33c) without cysteamine after 3-5 h



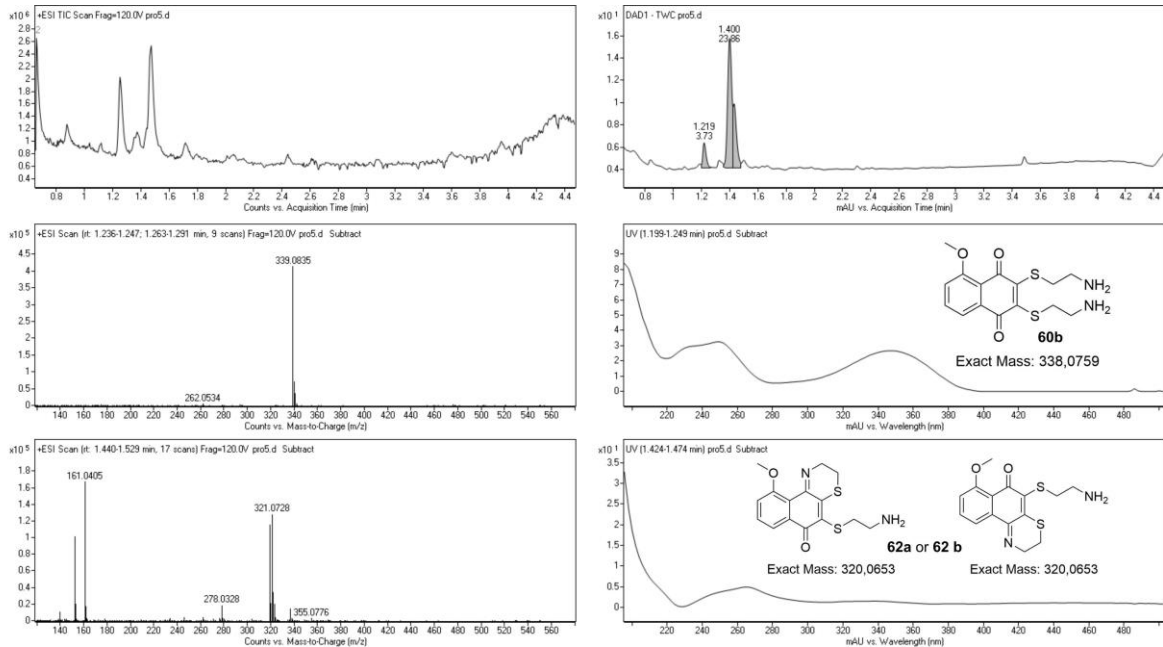
40 μ M 3-bromojuglon (33c) with 500-fold cysteamine after 3-5 h40 μ M 3-bromo-*O*-methyljuglon (33d) without cysteamine after 3-5 h

40 μ M 3-bromo-*O*-methyljuglon (33d) with 500-fold cysteamine after 3-5 h40 μ M 3-chlorojuglon (33e) without cysteamine40 μ M 3-chlorojuglon (33e) with 500-fold cysteamine after 3-5 h

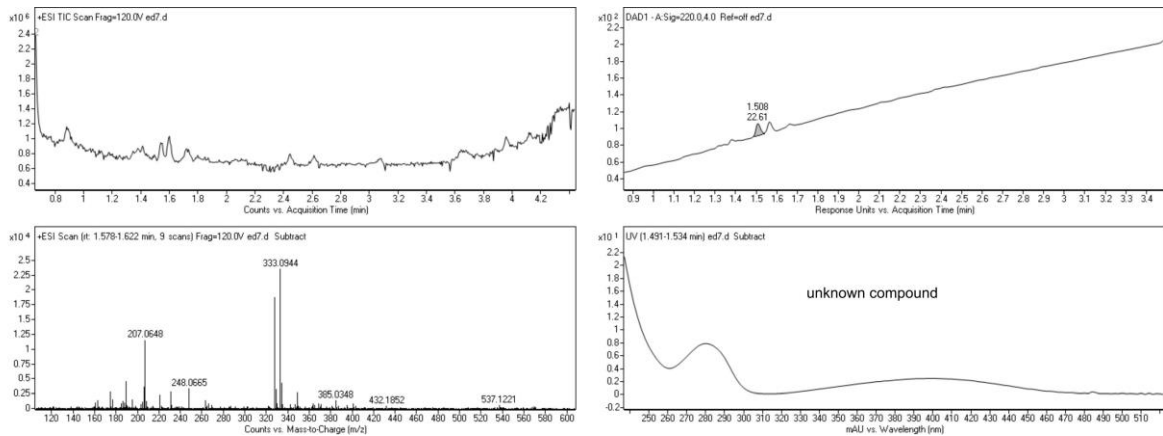
40 μ M 3-chloro-*O*-methyljuglon (33f) without cysteamine after 3-5 h



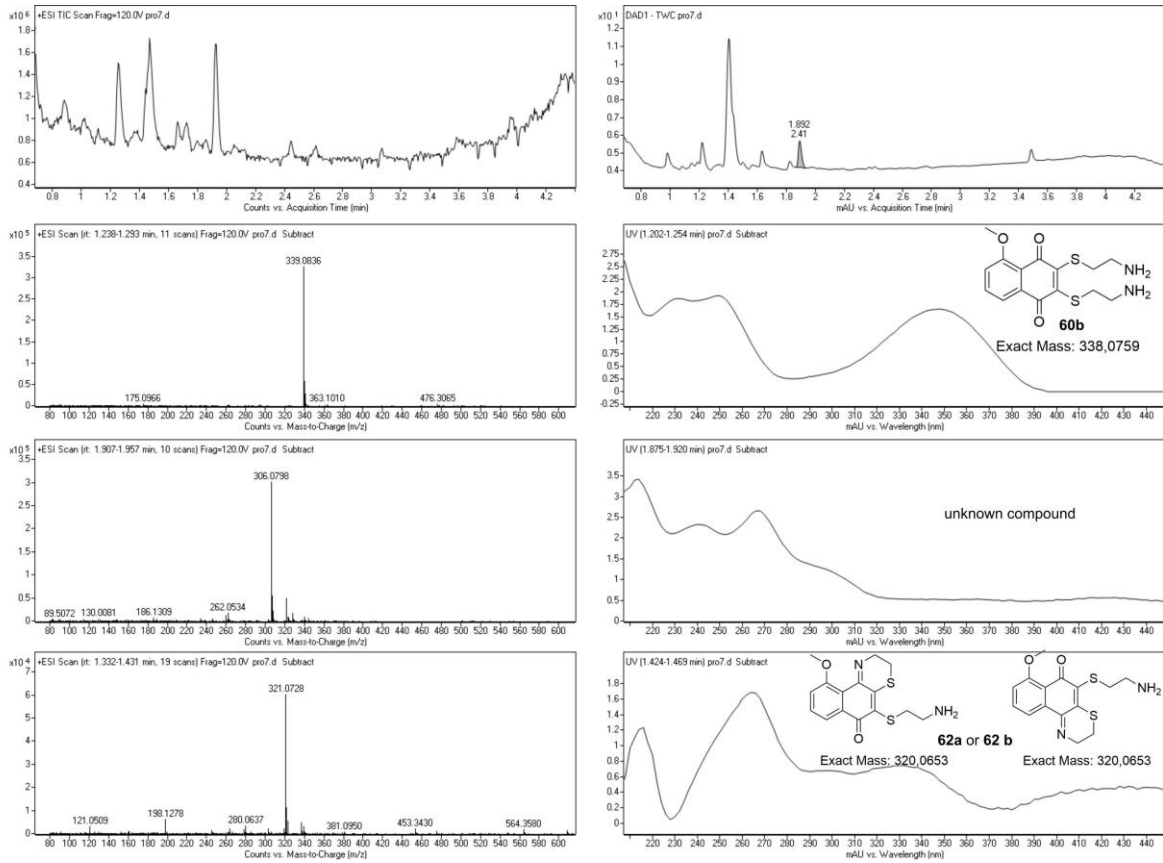
40 μ M 3-chloro-*O*-methyljuglon (33f) with 500-fold cysteamine after 3-5 h



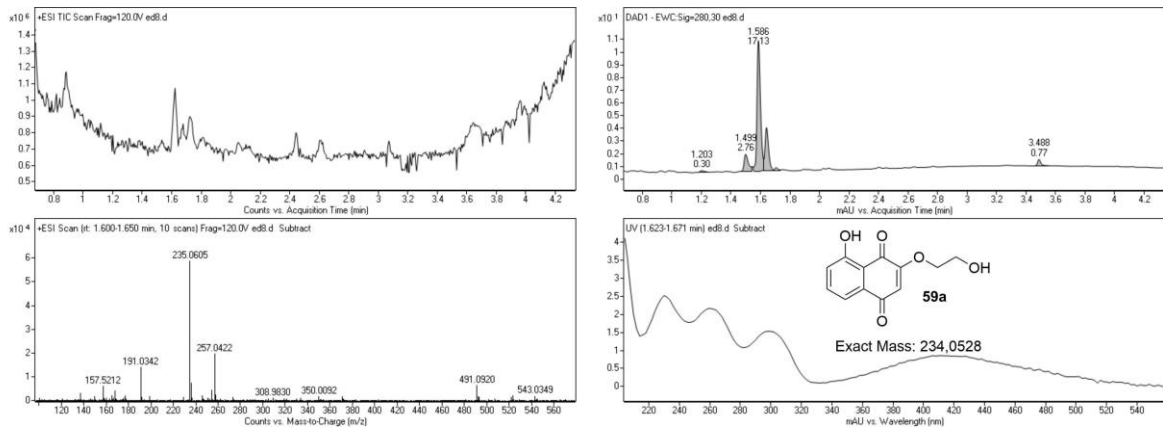
40 μ M 3-fluoro-*O*-methyljuglon (33g) without cysteamine after 3-5 h



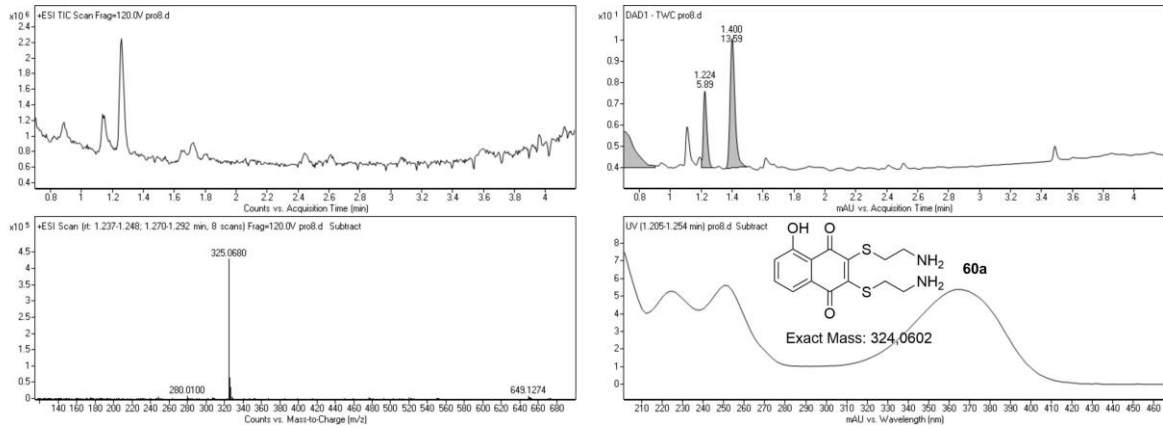
40 μ M 3-fluoro-*O*-methyljuglon (33g) with 500-fold cysteamine after 3-5 h



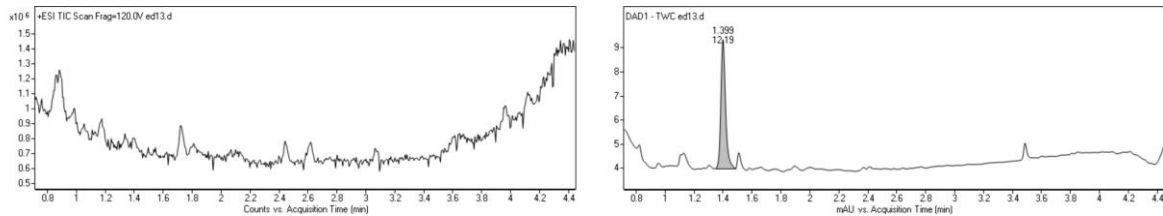
40 μ M 3-azidoguglon (33h) without cysteamine after 3-5 h



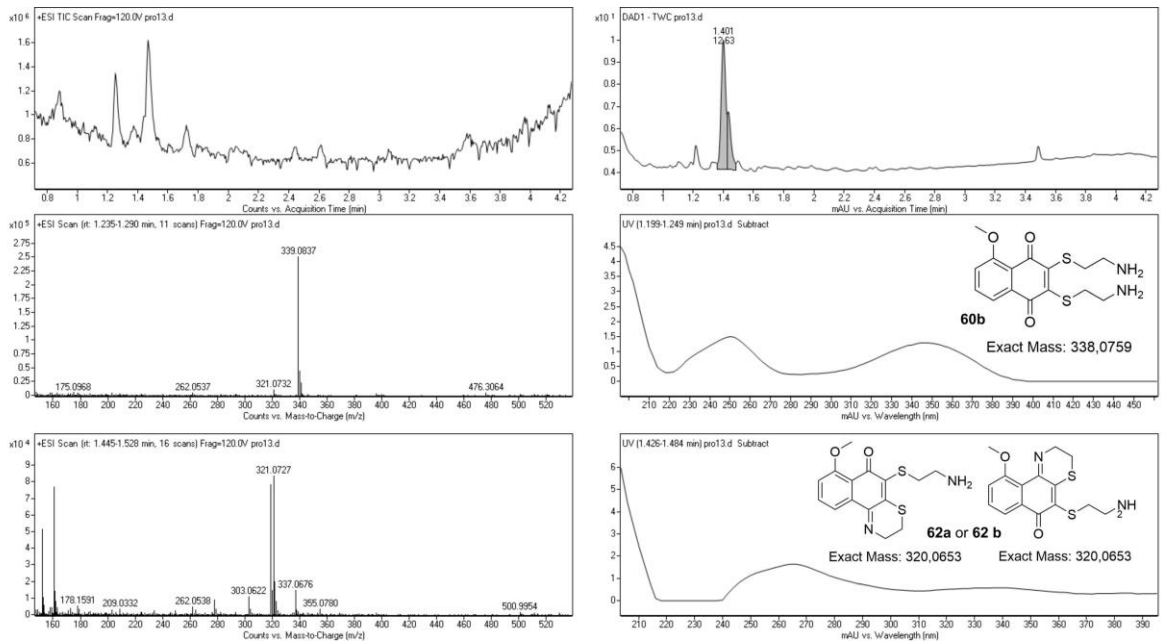
40 μ M 3-azidojuglon (33h) 500-fold cysteamine after 3-5 h



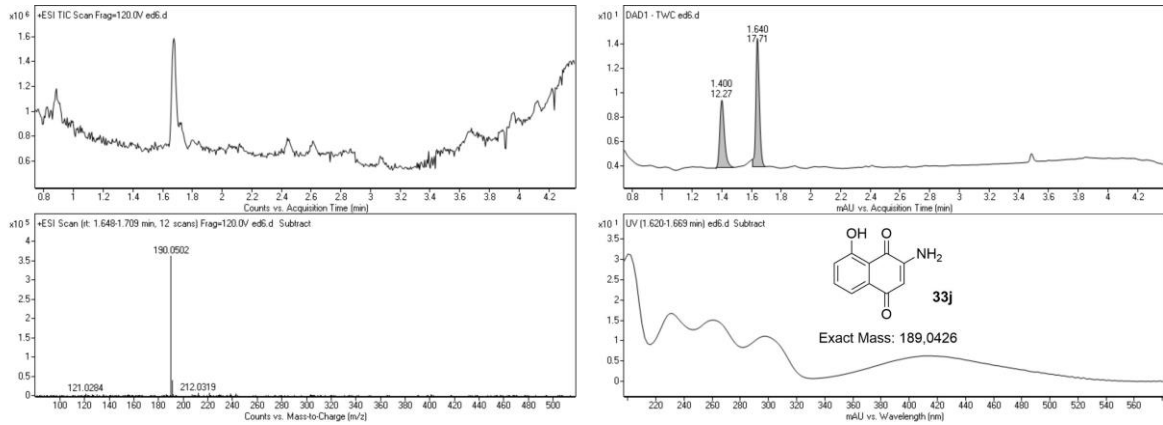
40 μ M 3-azido-O-methyljuglon (33i) without cysteamine after 3-5 h



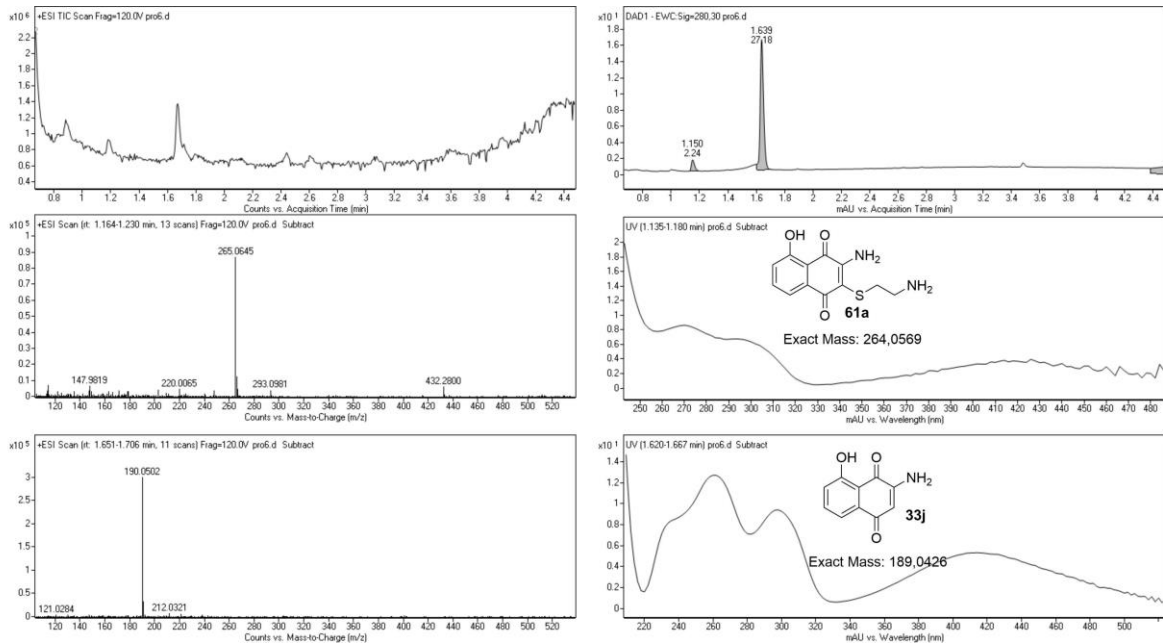
40 μ M 3-azido-O-methyljuglon (33i) with 500-fold cysteamine after 3-5 h



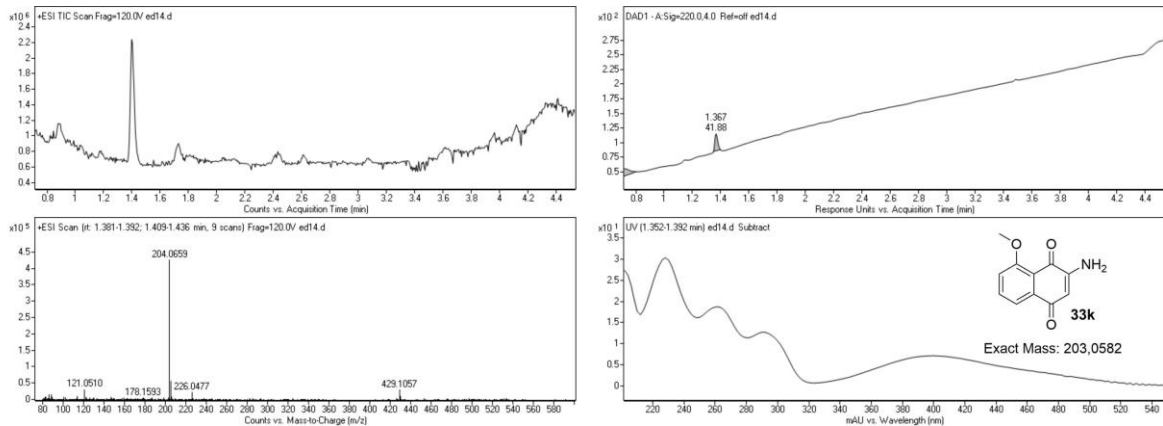
40 μ M 3-aminojuglon (33j) without cysteamine



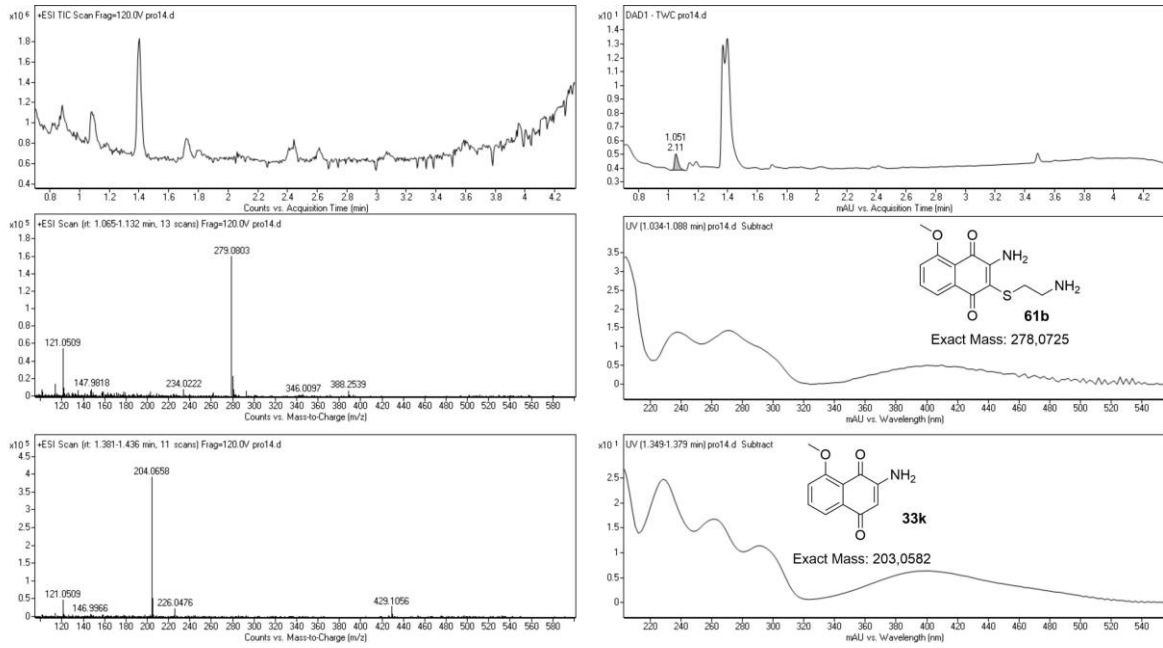
40 μ M 3-aminojuglon (33j) with 500-fold cysteamine after 3-5 h



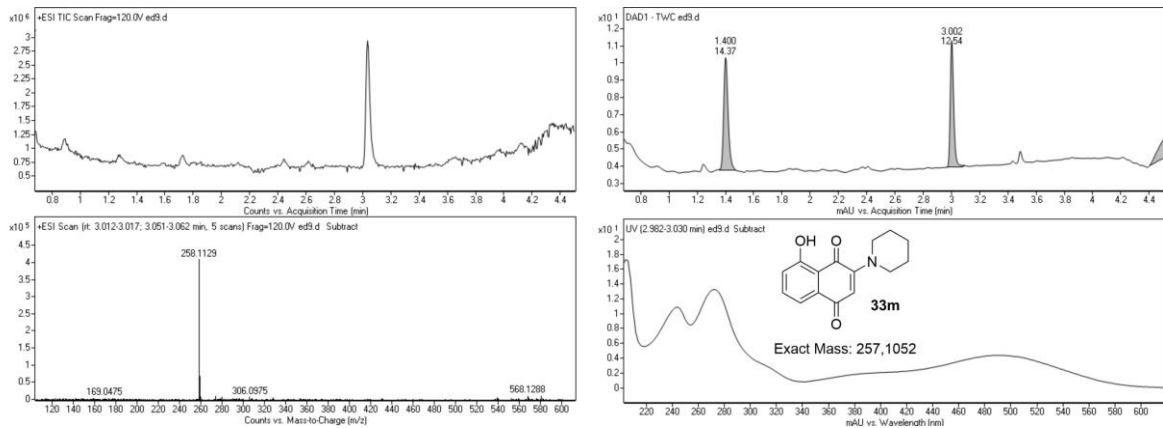
40 μ M 3-amino-O-methyljuglon (33k) without cysteamine after 3-5 h



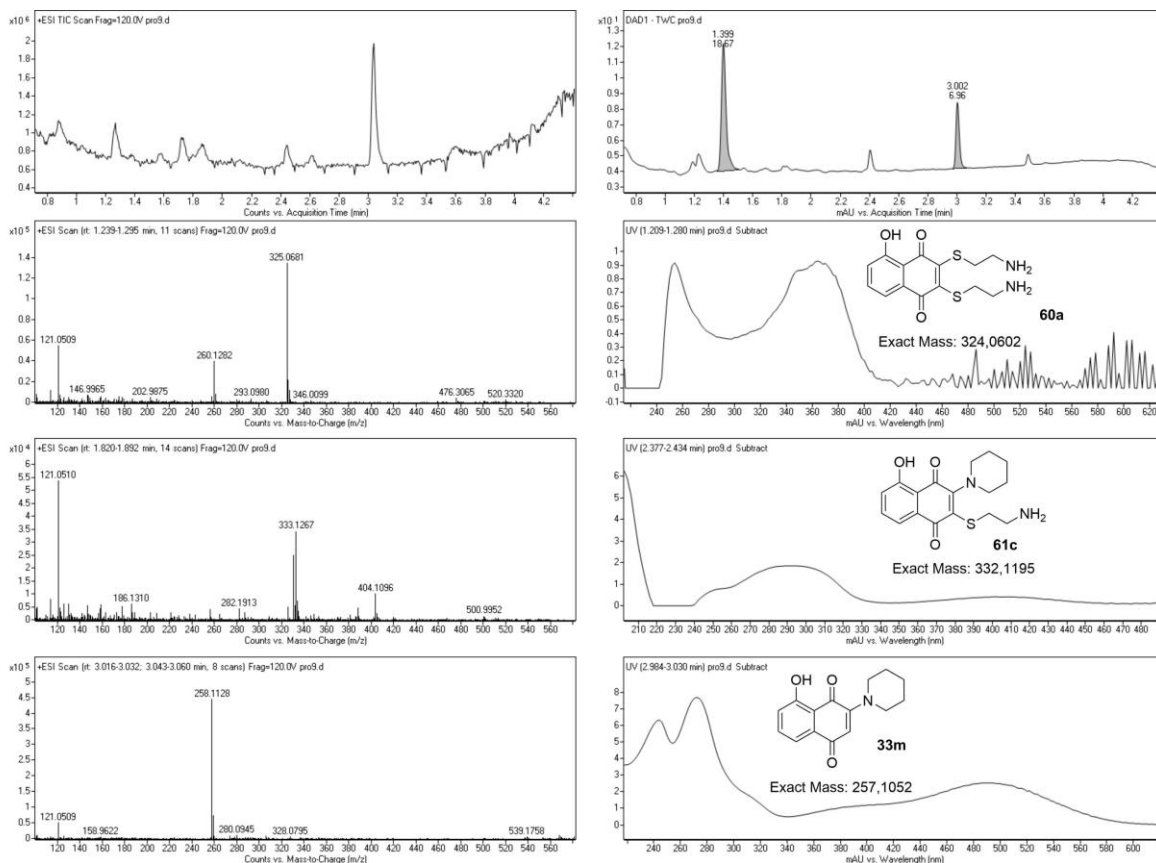
40 μ M 3-amino-*O*-methyljuglon (33k) with 500-fold cysteamine after 3-5 h



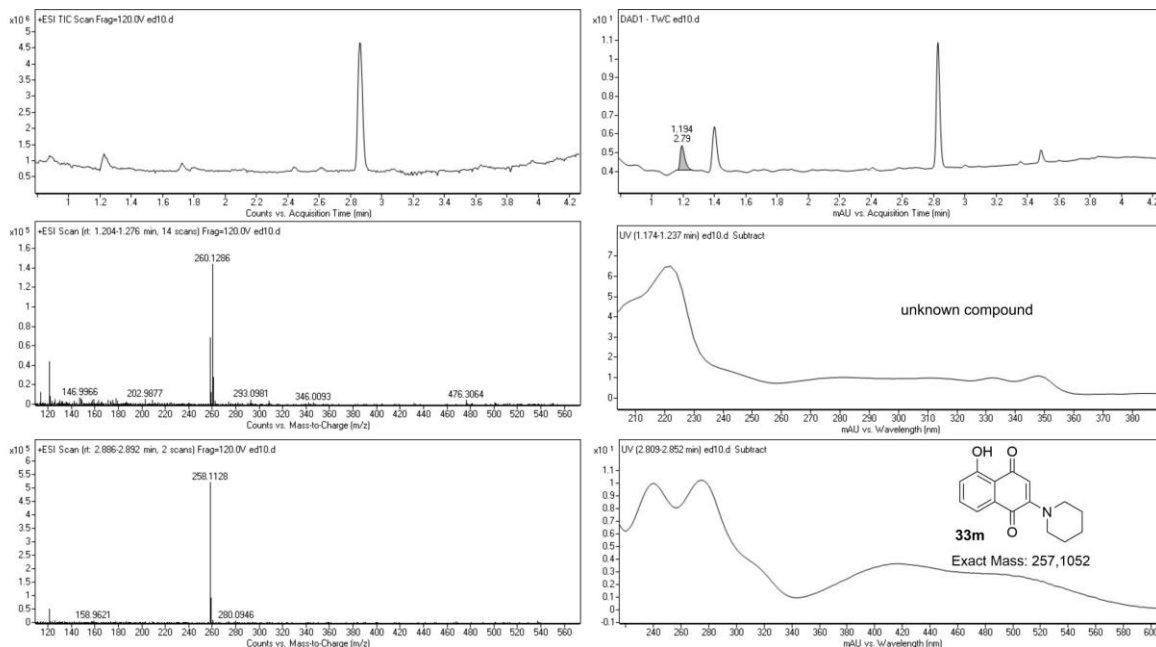
40 μ M 3-piperidinojuglon (33l) without cysteamine



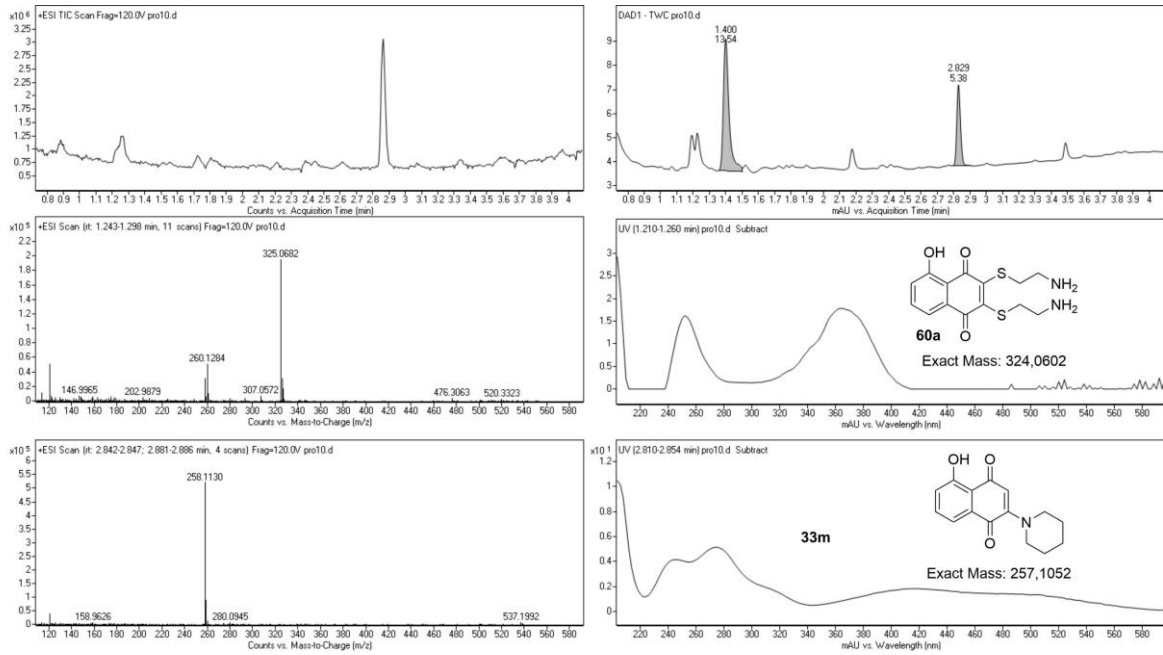
40 μ M 3-piperidinojuglon (33l) with 500-fold cysteamine after 3-5 h



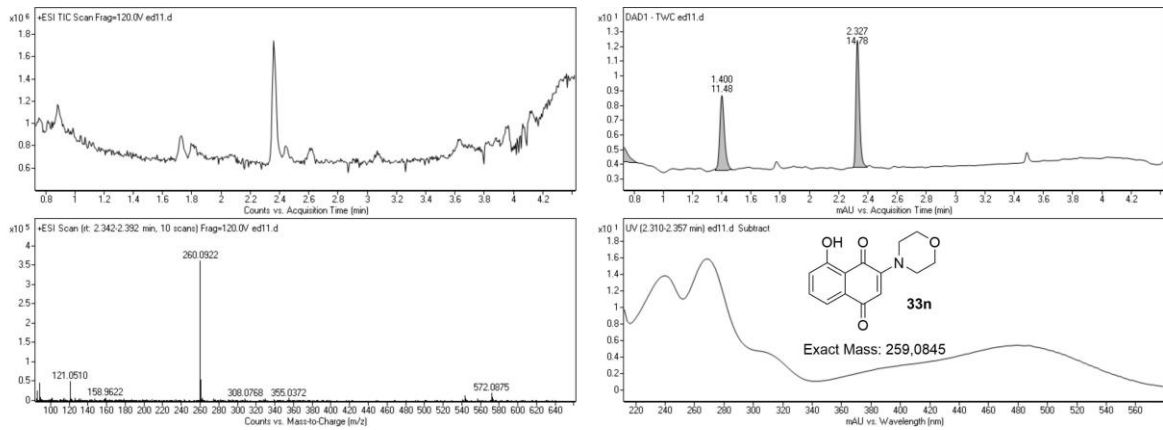
40 μ M 2-piperidinojuglon (33m) without cysteamine



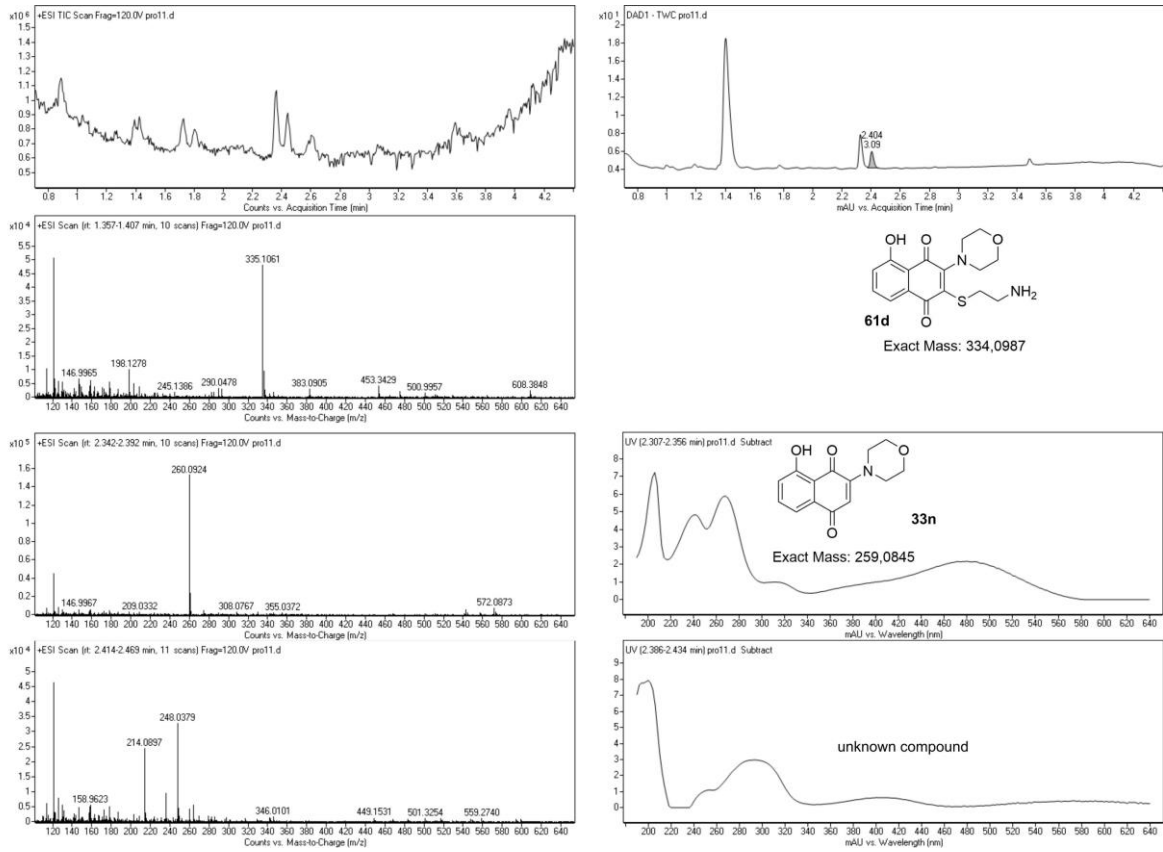
40 μ M 2-piperidinojuglon (33m) with 500-fold cysteamine after 3-5 h



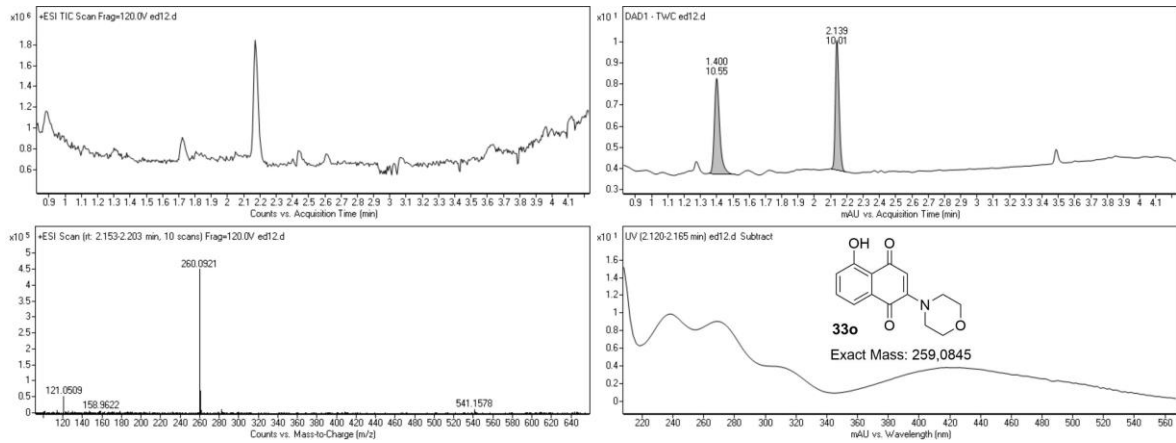
40 μ M 3-morpholinojuglon (33n) without cysteamine

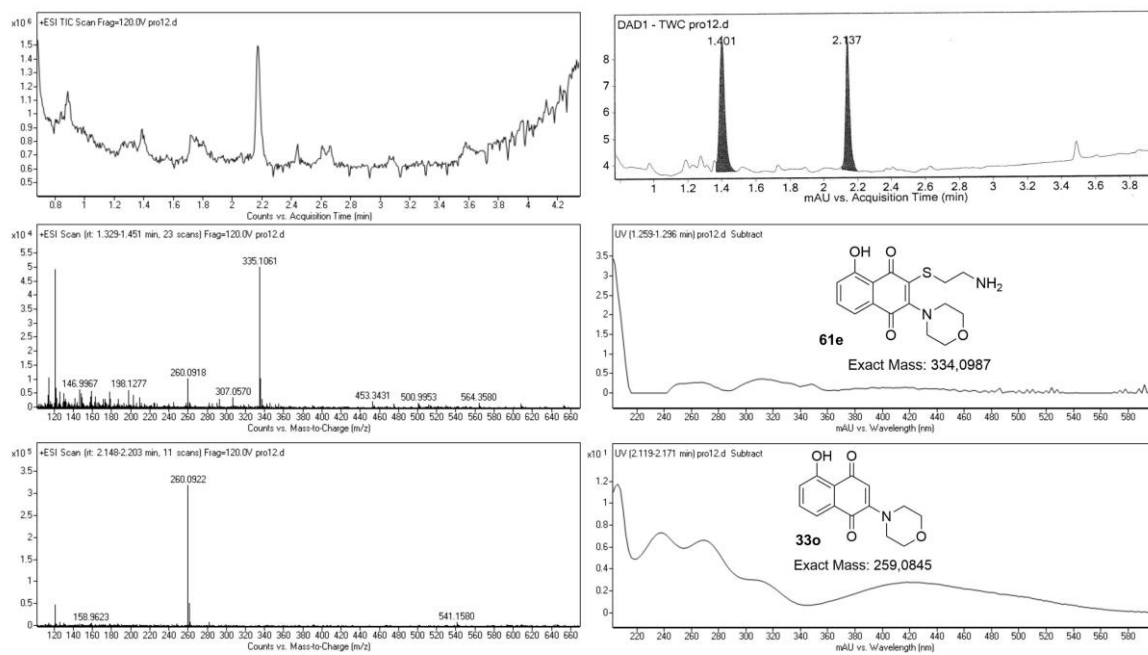


40 μ M 3-morpholinojuglon (33n) with 500-fold cysteamine after 3-5 h



40 μ M 2-morpholinojuglon (33o) without cysteamine



40 μ M 2-morpholinojuglon (33o) with 500-fold cysteamine after 3-5 h

D 5 Additional figures for protein labeling experiments

BTN3A1 B30.2: HMBPP titration experiments: 20 μ M protein with 30 μ M probe

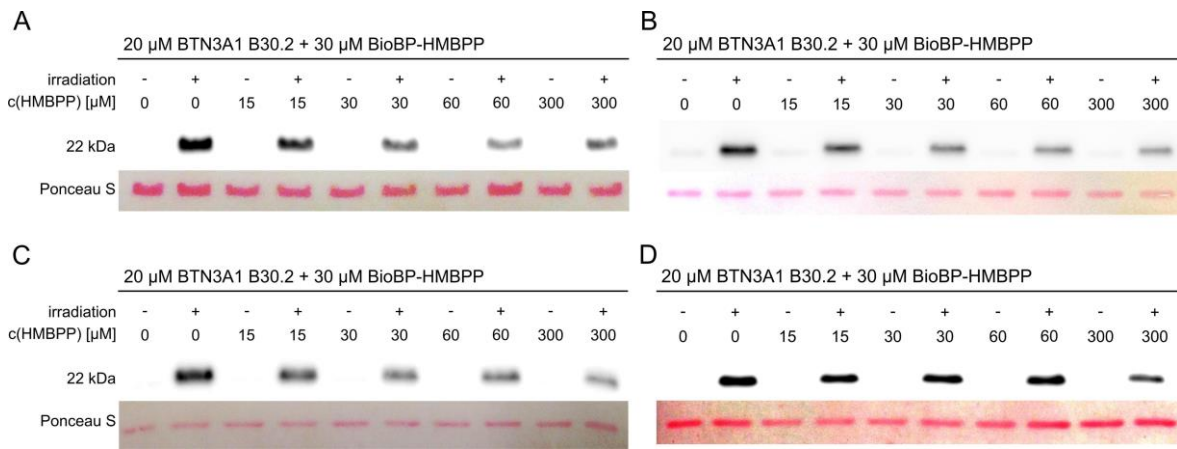


Figure 75: BTN3A1 B30.2 domain labeling with BioBP-HMBPP, competition with HMBPP. **A-D:** Four repetition experiments with 20 μ M protein and 30 μ M probe. Protein bands are stained with Ponceau S (red).

BTN3A1 B30.2: HMBPP titration experiments: 60 μ M protein with 100 μ M probe

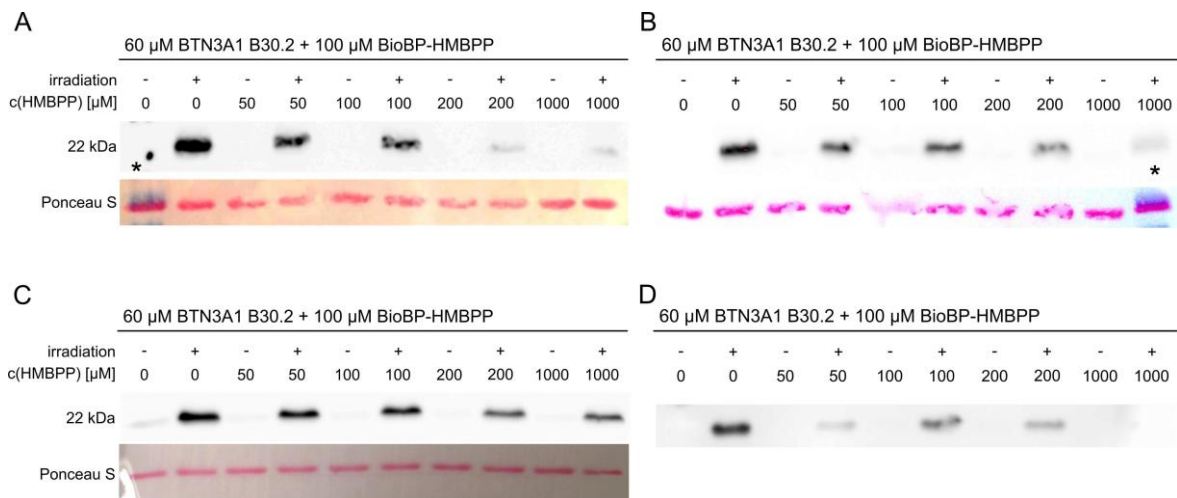


Figure 76: Labeling experiments with the wild type of the BTN3A1 B30.2 domain and BioBP-HMBPP, competition with HMBPP. **A-D:** Four experiments with 60 μ M protein and 100 μ M probe. Protein bands are stained with Ponceau S (red). * = sample contains prestained protein standard.

BSA: HMBPP titration experiments: 20 μ M protein with 30 μ M probe

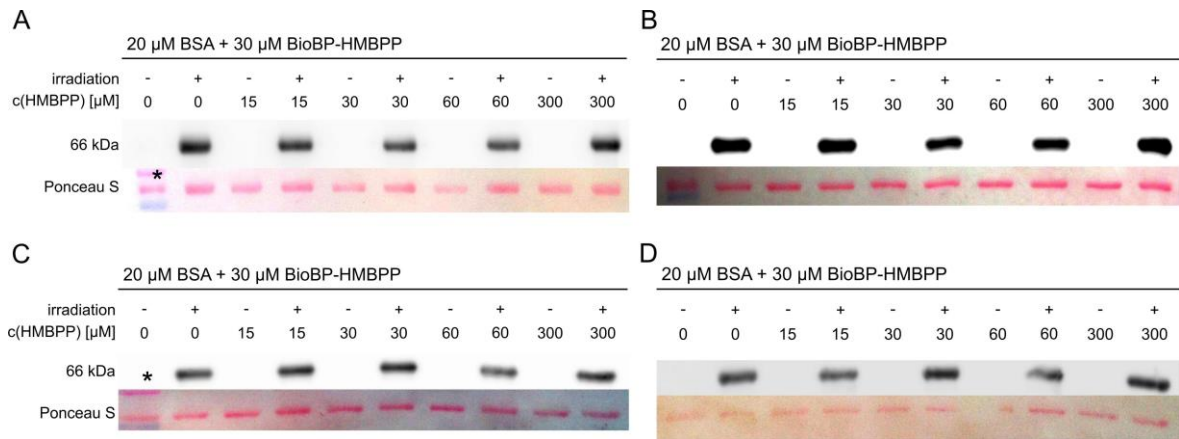


Figure 77: Labeling experiments with BSA and BioBP-HMBPP, competition with HMBPP. **A-D:** Repetition experiments with 20 μ M protein and 30 μ M probe. Protein bands are stained with Ponceau S (red). * = sample contains pre-stained protein standard.

BSA: HMBPP titration experiments: 60 μ M protein with 100 μ M probe

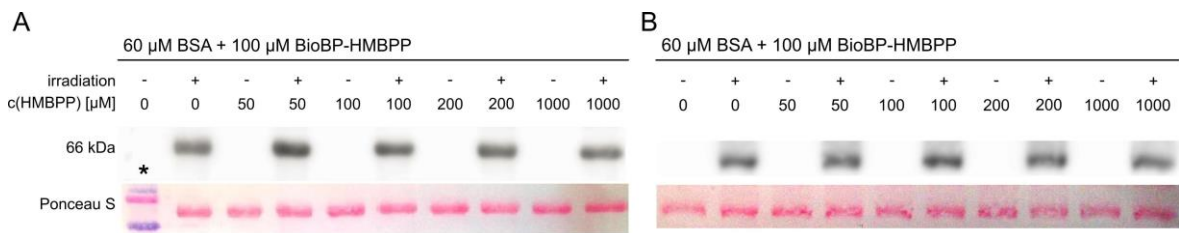


Figure 78: Labeling experiments with BSA and BioBP-HMBPP, competition with HMBPP. **A-B:** Experiments with 60 μ M protein and 100 μ M probe. Protein bands are stained with Ponceau S (red). * = sample contains pre-stained protein standard.

Charge Reversal Mutant of BTN3A1 B30.2: HMBPP titration experiment: 20 μ M protein- with 30 μ M probe

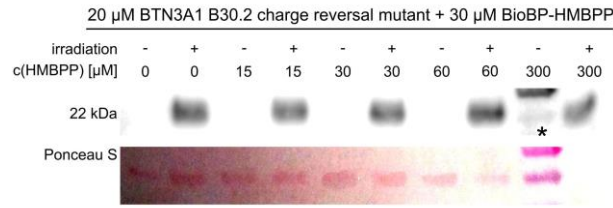


Figure 79: Labeling experiment with the BTN3A1 B30.2 charge reversal mutant and BioBP-HMBPP, competition with HMBPP, 20 μ M protein and 30 μ M probe. Protein bands are stained with Ponceau S (red). * = sample contains prestained protein standard.

Charge Reversal Mutant of BTN3A1 B30.2: HMBPP titration experiments: 60 μ M protein- with 100 μ M probe

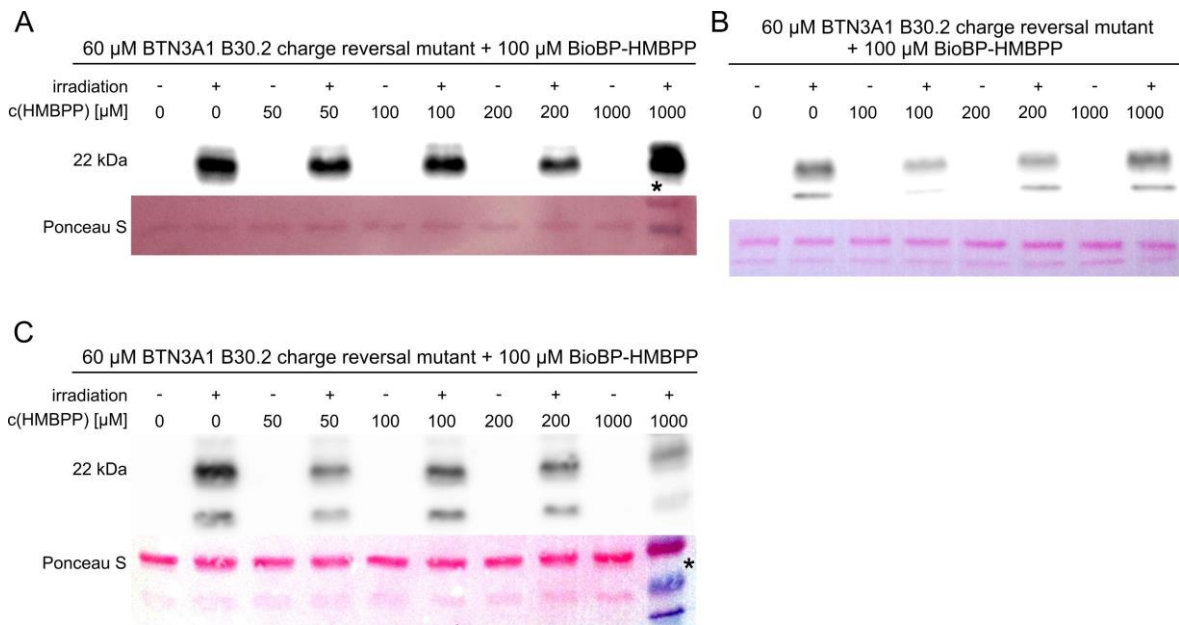


Figure 80: Labeling experiments with the BTN3A1 B30.2 charge reversal mutant and BioBP-HMBPP, competition with HMBPP. **A-C:** Three experiments with 60 μ M protein and 100 μ M probe. Protein bands are stained with Ponceau S (red). * = sample contains prestained protein standard.